Fakultät für Physik
der
Ludwig-Maximilians-Universität München

# HIGHER ORDER QCD CORRECTIONS IN EXCLUSIVE CHARMLESS $B$ DECAYS

GUIDO BELL

Oktober 2006

# HIGHER ORDER QCD CORRECTIONS IN EXCLUSIVE CHARMLESS $B$ DECAYS

vorgelegt von

## GUIDO BELL

aus
Neuwied am Rhein

München, den 31. Oktober 2006

# Abstract

We discuss exclusive charmless $B$ decays within the Standard Model of particle physics. These decays play a central role in the on-going process to constrain the parameters of the CKM matrix and to clarify the nature of CP violation. In order to exploit the rich source of data that is currently being collected at the experiments, a systematic theoretical treatment of the complicated hadronic dynamics is strongly desired. QCD Factorization represents a model-independent framework to compute hadronic matrix elements from first principles. It is based on a power expansion in $\Lambda_{\mathrm{QCD}}/m_b$ and allows for the systematic implementation of perturbative corrections.

In particular, we consider hadronic two-body decays as $B \to \pi\pi$ and perform a conceptual analysis of heavy-to-light form factors which encode the strong interaction effects in semi-leptonic decays as $B \to \pi\ell\nu$.

Concerning the hadronic decays we compute NNLO QCD corrections which are particularly important with respect to strong interaction phases and hence direct CP asymmetries. On the technical level, we perform a 2-loop calculation which is based on an automatized reduction algorithm and apply sophisticated techniques for the calculation of loop-integrals. We indeed find that the considered quantities are well-defined as predicted by QCD Factorization, which is the result of a highly complicated subtraction procedure. We present results for the imaginary part of the topological tree amplitudes and observe that the considered corrections are substantial. The calculation of the real part of the amplitudes is far more complicated and we present a preliminary result which is based on certain simplifications. Our calculation is one part of the full NNLO analysis of nonleptonic $B$ decays within QCD Factorization which is currently pursued by various groups.

In our conceptual analysis of the QCD dynamics in heavy-to-light transitions we consider form factors between non-relativistic bound states which can be addressed in perturbation theory. We perform a NLO analysis of these form factors and discuss some open questions of the general factorization formula which is obtained from the heavy-quark expansion in QCD. These include the origin and resummation of large logarithms and the non-factorization of soft and collinear effects in the so-called soft-overlap contribution. We show that the latter can be calculated in our set-up and address the issue of endpoint singularities. As a byproduct of our analysis, we calculate leading-twist light-cone distribution amplitudes for non-relativistic bound states which can be applied for the description of $B_c$ and $\eta_c$ mesons.

# Contents

# Part I

# Introduction

# Introduction

The analyses presented in this thesis rely on the *Standard Model* of particle physics [1–9] which reflects our current knowledge of three of the four known fundamental forces in nature. Electromagnetic, weak and strong interactions are described therein by a relativistic and renormalizable quantum field theory which is based on a gauge principle. The Standard Model represents an impressive theoretical achievement which successfully explains phenomena from everyday electricity to high-energetic quantum processes that are investigated at dedicated particle accelerator facilities. It is one of the best-tested theories of contemporary physics. This may be illustrated by comparing the experimentally measured value of the anomalous magnetic moment of the muon[1]

$$a_\mu^{\text{exp}} = 11\ 659\ 208.0\ (5.4)(3.3) \times 10^{-10} \tag{1}$$

with its theoretical prediction calculated within the Standard Model [10]

$$a_\mu^{\text{SM}} = 11\ 659\ 185.8\ (7.2)(3.5)(0.3) \times 10^{-10}. \tag{2}$$

Despite its tremendous success the Standard Model has its insufficiencies and is commonly believed to be incomplete. Severe constraints from electroweak precision data may be interpreted as a hint that "something unknown" happens at the TeV-scale, an energy scale that has been out of the scope of todays collider experiments. The Large Hadron Collider (LHC), which is currently being built at CERN and is scheduled to start operation in mid-2007, has particularly been designed to explore the physics at the TeV-scale. Thousands of particle physicists from all around the world are looking forward to the first data taking of the LHC, in the hope that it will help us to reveal the limitations of the Standard Model and give a first clue about the theory that lies beyond it.

Apart from these direct searches, the physical effects that are supposed to lie beyond the Standard Model (often referred to as *New Physics*) can be investigated indirectly in high-precision measurements of low-energy observables as the anomalous magnetic moment of the muon mentioned above. Every physical observable is in principle sensitive to arbitrarily high energies and thus to New Physics due to quantum effects.

---

[1]The anomalous magnetic moment of the electron can be measured even more precisely. As it is less likely to be affected by physics beyond the Standard Model, its measurement is used for the determination of one of the Standard Model parameters, namely the fine structure constant [11].

The quantitative investigation of these tiny effects represents a highly challenging task, both for experimental measurements and for theoretical calculations which have to match the experimental accuracy.

Whereas the gauge sector of the Standard Model has been tested to remarkable precision in the era of the Large Electron Positron Collider (LEP), the flavour sector is experimentally less constrained. The flavour sector contains a large number of parameters as the quark and the lepton masses or the four parameters related to the Cabibbo-Kobayashi-Maskawa (CKM) matrix [12,13] which describes the mixing of the quark mass eigenstates in weak interactions. The numerical values of these parameters are not predicted by the Standard Model but rather have to be extracted from experimental measurements before making any theoretical prediction.

The ultimate goal of $B$ physics is to precisely determine some of these parameters and to test the CKM sector of the Standard Model. The phenomenon of CP violation is of particular interest as it is related to the observed matter-antimatter asymmetry in our universe. Two CKM parameters are known to date at the percent level [14]

$$\lambda = 0.22717^{+0.00100}_{-0.00101}, \qquad A = 0.806^{+0.014}_{-0.014} \qquad (3)$$

and the remaining two parameters $\bar{\rho}$ and $\bar{\eta}$ are conveniently discussed in the context of a *unitarity triangle* which reflects the unitarity of the CKM matrix. The current status of the unitarity triangle is shown in Figure 1. The values of the parameters $\bar{\rho}$ and $\bar{\eta}$ correspond to the upper tip of the triangle which is given by [14]

$$\bar{\rho} = 0.195^{+0.022}_{-0.055}, \qquad \bar{\eta} = 0.326^{+0.027}_{-0.015}. \qquad (4)$$
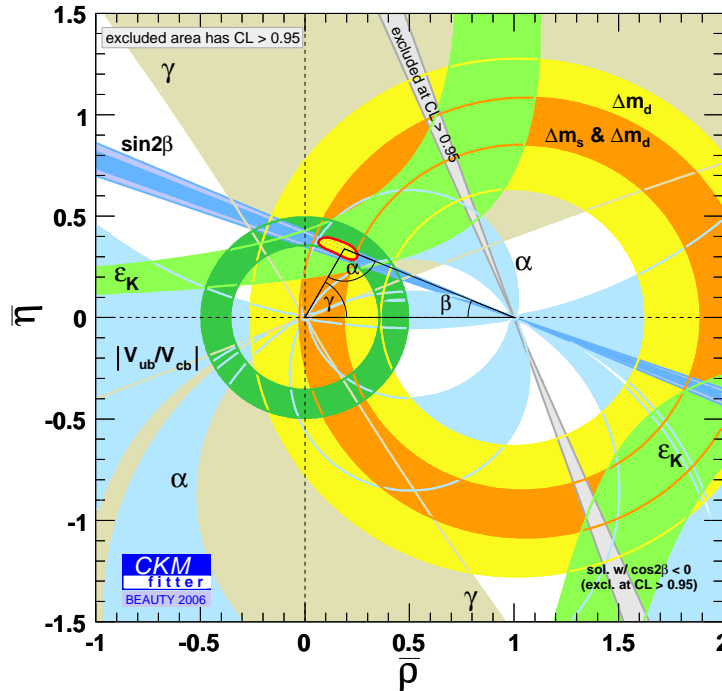


Figure 1: *Global fit of the unitarity triangle (status September 2006) [14].*

Notice that these determinations are far less accurate than the ones of $\lambda$ and $A$ and that various independent measurements of $\bar{\rho}$ and $\bar{\eta}$, which are indicated by the coloured bands in Figure 1, are all consistent with each other. The very fact that the area of the unitarity triangle is non-zero is a manifestation of CP violation.

Two dedicated $B$ factories, the BaBar experiment at SLAC and the Belle experiment at KeK, have contributed substantially to our current understanding of $B$ physics and CP violation. One of the most important milestones in their physics programme was the observation of (indirect) CP violation in the neutral $B$ system in 2001 [15,16] more than 35 years after the first observation of CP violation by James Cronin, Val Fitch and collaborators in the Kaon system [17].
Since the start of BaBar and Belle in 1999, the $B$ factories have produced $\sim 10^9$ pairs of $B$ mesons which correspond to $\sim 1$ ab$^{-1}$ of integrated luminosity. This impressive wealth of data will continuously increase until the end of their physics programme in 2010. It will then be complemented by the LHC-b experiment and future plans concerning an upgrade of the $B$ factories are already envisaged. With this ongoing experimental effort it will be possible to nicely overconstrain the unitarity triangle and to reduce the uncertainty of the parameters $\bar{\rho}$ and $\bar{\eta}$ to a few percent.

The reader may wonder why some observables as the anomalous magnetic moment of the muon can be determined with an uncertainty of better than 1 part in $10^5$ and why it is apparently so difficult to reduce the uncertainty of the CKM parameters at the percent level. One of the reasons is that the CKM parameters are related to quarks which are always affected by strong interactions[2].
In the Standard Model the strong interactions are described by a non-abelian gauge theory called *Quantum Chromo Dynamics* (QCD) [4–9]. The most important property of QCD is *asymptotic freedom*, i.e. the fact that the coupling of the quarks to the gluons becomes weak at large energy scales (cf. Figure 2). Strong interaction effects from high energies as e.g. the $Z^0$ resonance at $M_Z = 91.2$ GeV can be precisely calculated in perturbation theory as an expansion in the coupling constant $\alpha_s(M_Z) \sim 0.12$. At lower energies of order of the QCD scale $\Lambda_{\text{QCD}} \sim 0.5$ GeV, the perturbative expansion in the coupling constant breaks down and the quarks get confined into complicated colour-singlet hadrons. In our theoretical description of any hadronic process that is observed in experiment we thus have to deal with these non-perturbative effects. We may sometimes be lucky and find some observables which are almost free of these hadronic uncertainties as the "golden" $\sin 2\beta$ measurement from the $B \to J/\psi\, K_S$ decay which corresponds to the thin dark blue ray in Figure 1. As it is not always possible to find such clean observables, we have to look for sophisticated methods which allow to control the hadronic dynamics.

In this thesis we mainly deal with strong interaction effects in $B$ meson decays. The role of $B$ mesons is special as they are (apart from the $\Upsilon$-resonances) the heaviest mesons which show an extremely rich phenomenology including many interesting CP

---

[2]Even though the anomalous magnetic moment of the muon is a leptonic quantity, the main limitation in its determination also stems from small strong interaction effects.
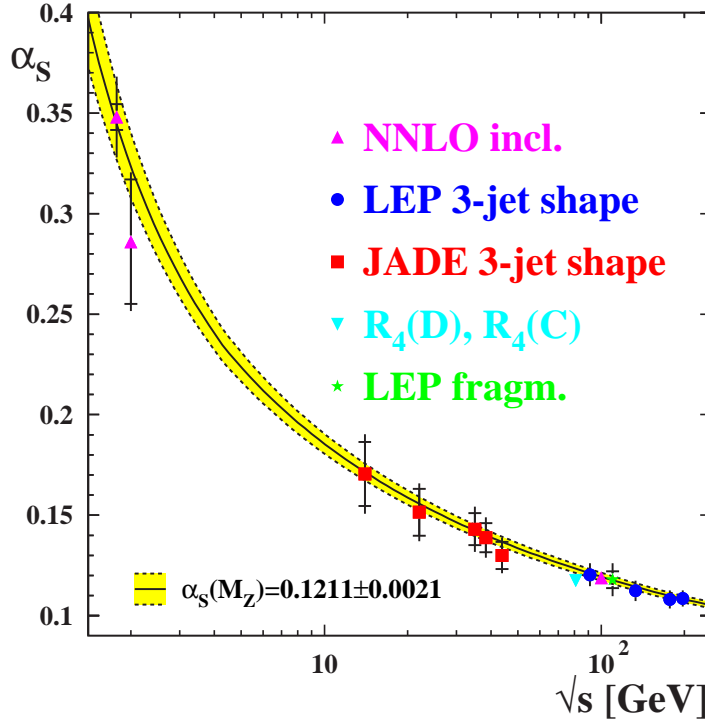
Figure 2: *Running of strong coupling constant [18].*

violating observables. Furthermore, the hadronic dynamics in $B$ meson decays turns out to be partly accessible within perturbation theory as the intrinsic mass of the $b$-quark $m_b \sim 5$ GeV corresponds to a perturbative scale with $\alpha_s(m_b) \sim 0.22$. More precisely, the weak decay of the $b$-quark is accompanied by short-distance effects and unaffected by the hadronization of the quarks which occurs at much larger time scales. The technical procedure which disentangles perturbative from non-perturbative effects is called *factorization*. For more details concerning factorization we refer to the comprehensive introduction in the first chapter of this thesis.

We in particular consider exclusive charmless decays of $B$ mesons, as $B \to \pi\pi$ or $B \to \pi\ell\nu$. These decays provide important information on the unitarity triangle, the former serve for the determination of the CKM angle $\alpha$ and the latter for the measurement of $|V_{ub}|$. The impact of these decays on the unitarity triangle from Figure 1 are reflected by the light blue band and the dark green circle, respectively. Rather than focussing on the phenomenological aspects of these decays, we examine the complicated strong interaction dynamics which is encoded in the hadronic matrix elements.

The decays considered in this thesis share the feature that the $B$ meson decays into very energetic light mesons (in the $B$ meson rest frame). The factorization of short- and long-distance QCD effects for these heavy-to-light transitions has first been worked out in the framework of *QCD Factorization* [19–21] and has later been translated into a field theoretical formulation which is called *Soft-Collinear Effective Theory* (SCET) [22–24]. We are mainly concerned with the calculation of higher

order perturbative QCD corrections, but have also a general look at the factorization properties of heavy-to-light form factors which are among the "simplest" objects for studying the QCD dynamics in $B \to \pi$ transitions.

The core of this thesis consists in a 2-loop calculation related to the hadronic two-body decay modes. Due to the complexity of the problem we split the calculation into two parts. We first compute the imaginary part of the hadronic matrix elements which is technically simpler than the real part. It is in addition of particular interest in phenomenological applications as it is related to a strong phase shift between the final state mesons which "pollutes" the interesting information about the underlying weak CKM phases. Our calculation represents one part of the full next-to-next-to-leading order (NNLO) analysis of the topological tree amplitudes within QCD Factorization. Another part of this analysis concerning (1-loop) spectator scattering has been calculated recently by various groups [25–27]. We remark that the phenomenological impact of our corrections is beyond the scope of this thesis as the full NNLO calculation (including topological penguin amplitudes) is still incomplete.

Our conceptual analysis of heavy-to-light form factors is based on a particular scenario. We consider transition form factors between non-relativistic bound states which can be addressed in perturbation theory. We perform a next-to-leading order (NLO) analysis of these form factors using the same techniques that we have developed for the aforementioned 2-loop calculation. We then compare our explicit results with the general factorization formula for heavy-to-light form factors and address some of its open questions concerning the so-called soft-overlap contribution, the issue of endpoint singularities and the resummation of large (Sudakov) logarithms. We emphasize that this analysis can be applied for the description of $B_c \to (\bar{c}c)$ transitions, although we focus on the more conceptual aspects here.

Large parts of this thesis deal with the calculation of loop-integrals. One important element in our calculation procedure is an automatized reduction algorithm which allows us to reduce the calculation of several thousands of loop-integrals to a much smaller set of so-called Master Integrals. The calculation of these Master Integrals represents the most difficult task of the entire calculation. We would like to point out that the technical difficulties that we encountered in the two considered calculations are of rather different origins. Whereas the first calculation in the $B \to \pi\pi$ context represents a highly challenging and complex 2-loop calculation, the other (1-loop) calculation related to the form factors is complicated due to the presence of various physical scales. In this case we restrict our attention to the leading power in a mass expansion which requires different techniques than for full loop-integrals. Consequently, our collection of loop-techniques that we present in the second chapter of this thesis, summarizes (almost) all of the most sophisticated techniques that have been developed so far: the method of differential equations [28,29], the formalism of harmonic polylogarithms [30], the method of expansion by regions [31], Mellin-Barnes techniques [32,33] and the method of sector decomposition [34]. Most of these techniques have rarely been applied in $B$ physics so far.

The structure of this thesis can be outlined as follows:

In the first chapter we present the theoretical background required for an analysis of exclusive charmless $B$ decays. We give a comprehensive introduction to QCD Factorization and Soft-Collinear Effective Theory and comment briefly on several alternative approaches. The remainder of this chapter is devoted to a detailed analysis of hadronic two-body decays and heavy-to-light form factors which are of particular interest in this work.

In Chapter 2 we collect the techniques that we have used in our calculations. We develop a systematic strategy which is based on an automatized reduction algorithm. As most parts of this thesis deal with the calculation of loop-integrals, we dedicate a sizeable part of Chapter 2 to the presentation of several sophisticated techniques.

Due to this structure, the second part of this thesis is free of the technical issues related to the calculation of loop-diagrams. In Chapter 3 we consider the imaginary part of the topological tree amplitudes in hadronic two-body decays. Apart from the 2-loop calculation, we address the issues of Fierz symmetry, evanescent operators, renormalization and IR subtractions. We finally obtain our results in an analytical form and conclude this chapter with a brief numerical analysis.

Chapter 4 is devoted to the real part of the topological tree amplitudes in hadronic two-body decays. The calculation follows the same lines as in Chapter 3 but is technically much more involved. So far, we have accomplished the technical part of this calculation and present some preliminary numerical results.

In our final analysis in Chapter 5 we consider heavy-to-light form factors between non-relativistic bound states. We first address the non-relativistic approximation in this context and present subsequently the NLO (1-loop) calculation of the form factors. In our conceptual analysis we investigate the origin of endpoint singularities and comment on the resummation of logarithms. We show that we can isolate (and calculate) the so-called soft-overlap contribution in our set-up and calculate leading twist light-cone distribution amplitudes of non-relativistic bound states.

We finally conclude and give an outlook on future developments. The results for all Master Integrals that appeared in our calculations from Chapter 3 - 5 as well as the explicit expressions for the NLO form factors are summarized in the appendix.

# Part II

# Formalism

# Chapter 1

# Exclusive charmless $B$ decays

In the first chapter we present the theoretical background for the description of exclusive charmless $B$ decays. As the perturbative calculations in the second part of this thesis are based on QCD Factorization and Soft-Collinear Effective Theory, we give a profound introduction to these two developments. We paid special attention to avoid unnecessary formulas in the introductory chapter in order to allow for a transparent presentation of the basic ideas behind these concepts. We comment briefly on alternative approaches to charmless $B$ decays and have a closer look at those decays which are of particular interest in the work at hand. These include hadronic two-body decays and a conceptual analysis of heavy-to-light form factors which are important ingredients in semi-leptonic and radiative $B$ decays.

## 1.1 Basic concepts

### 1.1.1 QCD Factorization

The phrase *QCD Factorization* is closely related to the theory of hadronic two-body decays of $B$ mesons. At the end of the 90s Beneke, Buchalla, Neubert and Sachrajda, to which we refer as BBNS in the following, established this novel framework which allowed for the first time for a systematic treatment of these decays in QCD [19–21]. However, QCD Factorization is a more general framework with applications covering a wide spectrum of semi-leptonic, radiative and hadronic $B$ decays.

QCD Factorization basically merged two different developments that were known at that time: the heavy quark expansion (for a review see [35]) and the theory of hard exclusive processes which is also known as collinear factorization [36,37]. In the course of the 90s much progress has been made in the understanding of heavy mesons. It has been realized that the QCD dynamics of heavy mesons simplifies substantially when it is considered in the heavy quark expansion[1] (HQE), i.e. an expansion in the ratio $\Lambda_{\mathrm{QCD}}/m_Q$ where $m_Q$ is the mass of the heavy quark. On the

---

[1]The phrase *heavy quark expansion* is often used in the literature in the context of inclusive decays. We will refer to it here more generally whenever we speak about an expansion in $\Lambda_{\mathrm{QCD}}/m_Q$.

other hand the theory of hard exclusive processes can be seen as the counterpart of deep-inelastic scattering for inclusive processes. It was developed for the description of exclusive processes with a large momentum transfer $Q^2 \gg \Lambda_{\mathrm{QCD}}^2$. Due to the large momentum transfer, the particles in these processes are very energetic and assumed to move collinear to light-cone directions which leads to important simplifications. Charmless $B$ decays naturally incorporate both of these aspects. The $B$ meson in the initial state implies a systematic description in terms of a HQE in $\Lambda_{\mathrm{QCD}}/m_b$. The final state being charmless, which means that it consists of light hadrons only, further implies that the particles in the final state are very energetic in the $B$ meson rest frame and can be described to move almost on the light-cone.

The basic idea of factorization is the attempt to disentangle physical effects from different length or momentum scales. This is a very general idea that can be applied in many different fields of physics. Concerning the dynamics of the strong interactions this strategy is particularly suited due to the asymptotic freedom of QCD. Any decay or scattering process involving hadrons is sensitive to the scale $\Lambda_{\mathrm{QCD}}$ which is responsible for the confinement of the quarks into the hadrons. As the strong coupling constant at these scales is of $\mathcal{O}(1)$, the respective effects cannot be addressed in perturbation theory and therefore we call them non-perturbative. In $B$ physics we are confronted with an additional intrinsic scale in form of the mass of the b-quark $m_b \gg \Lambda_{\mathrm{QCD}}$ which is a perturbative scale with $\alpha_s(m_b) \sim 0.22$. We see that the idea of disentangling the effects from the scales $m_b$ and $\Lambda_{\mathrm{QCD}}$ is equivalent to separating perturbative from non-perturbative effects in QCD. The predictive power of factorization lies in the fact that we can calculate the former systematically in perturbation theory whereas the latter typically give rise to universal hadronic quantities which can be obtained from other methods as lattice gauge theory or QCD sum rules or they can even be extracted from experimental data.

The essence of the QCD Factorization prediction is summarized in a factorization formula for a hadronic matrix element. The factorization formula illustrates how the perturbative and non-perturbative effects are disentangled (*factorized*). In the remainder of this section we present several examples of factorization formulas for different classes of exclusive processes. In the first two examples we sketch the situation that was known before QCD Factorization was established. The first one deals with a heavy-to-heavy transition which can be described with the help of the HQE and the second one corresponds to collinear factorization. In the last two examples we illustrate how QCD Factorization combines these two pictures. We give slightly simplified descriptions in order to concentrate on the main aspects concerning factorization. We hope that our presentation will help to understand the structure of the factorization formulas that we discuss in the following sections.

**Example 1:** $B \to D\ell\nu$

We start with the simplest example in form of exclusive $B$ decays into final states that do not contain light hadrons as e.g. $B \to D\ell\nu$. The relevant scales in these
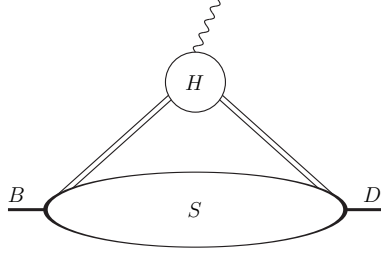
Figure 1.1: *Factorization of short- and long distance effects in heavy-to-heavy transitions. The former are contained in a coefficient function $H$, the latter in a soft-overlap contribution $S$. The double lines denote heavy quarks with $m_Q \gg \Lambda_{QCD}$.*

processes are the mass(es) of the heavy quark(s) which we simply denote by $m_Q$ and the hadronic scale $\Lambda_{QCD}$. The factorization formula for a generic hadronic matrix element of a current $\mathcal{J}$ takes the schematic form

$$\langle D|\mathcal{J}|B\rangle = H(\mu_F)\,S(\mu_F) + \mathcal{O}(\Lambda_{QCD}/m_Q). \tag{1.1}$$

The factorization formula is illustrated in Figure 1.1. We first notice that the factorization formula makes a statement about the leading power in the HQE. On the other hand it is predicted to be valid to all orders in perturbation theory. In writing (1.1), *hard* effects from the scale $m_Q$ and *soft* effects related to $\Lambda_{QCD}$ have been disentangled, the former being contained in the coefficient function $H(\mu_F)$ and the latter in a remnant matrix element which we denoted by $S(\mu_F)$. Technically, factorization is achieved with the help of a factorization scale $\mu_F$ satisfying $m_Q \gg \mu_F \gg \Lambda_{QCD}$. The effects form hard gluons with virtualities $k^2 > \mu_F^2$ are contained in $H(\mu_F)$ and those from soft gluons with $k^2 < \mu_F^2$ are absorbed into $S(\mu_F)$. As the factorization scale has been introduced artificially in the factorization formula (1.1), the dependence of the functions $H(\mu_F)$ and $S(\mu_F)$ has to cancel in their product.

As a side remark we mention that the concept presented above applies as well to the effective weak interactions in the description of low-energetic hadronic processes. These processes provide the hierarchy $M_W^2 \gg q^2$ where $M_W$ is the mass of the $W$-boson and $q^2$ is a typical momentum scale in the process. In leading power in an expansion in $q^2/M_W^2$ the hadronic matrix elements factorize similar to (1.1) into short-distance Wilson coefficients, which correspond to the $H(\mu_F)$ in our notation, and remnant matrix elements $S(\mu_F)$ which can be calculated in the Fermi theory of weak interactions. We come back to the effective weak interactions when we consider hadronic two-body decays in Section 1.2.

**Example 2:** $\pi\gamma^* \to \pi$

In a second example we consider hard exclusive processes which are not related to $B$ physics, as e.g. $\pi\gamma^* \to \pi$ where the kinematics sets a perturbative scale in form of the large momentum transfer $Q^2 \gg \Lambda_{QCD}^2$ . Because of the large momentum transfer, light-cone dynamics comes into play and the energetic light mesons can approximately be described by their two-particle quark-antiquark Fock states. Similar to what is done in deep-inelastic scattering, the quark and the antiquark can be assumed to move collinearly inside the meson and share its momentum with
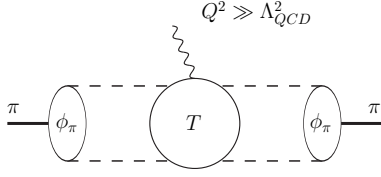
Figure 1.2: *Collinear factorization of short- and long distance effects. The former give rise to a hard-scattering kernel $T$, the latter to light-cone distribution amplitudes $\phi_\pi$. The dashed lines denote collinear quarks.*

fractions $u$ and $\bar{u} \equiv 1 - u$, respectively. The corresponding factorization formula is sketched in Figure 1.2 and reads

$$\langle \pi | \mathcal{J} | \pi \rangle = \int_0^1 du \int_0^1 dv \ \phi_\pi(v; \mu_F) \, T(v, u; \mu_F) \, \phi_\pi(u; \mu_F) + \mathcal{O}(\Lambda_{\mathrm{QCD}}^2 / Q^2). \quad (1.2)$$

Again, perturbative and non-perturbative effects are systematically disentangled in leading power. In this case the *hard* effects from the scale $Q^2$ give rise to a hard-scattering kernel $T(v, u; \mu_F)$ which depends on the momentum fractions $v$ and $u$ of the quarks in the mesons. The *collinear* effects from the scale $\Lambda_{\mathrm{QCD}}^2$ are encoded in light-cone distribution amplitudes $\phi_\pi(v; \mu_F)$ and $\phi_\pi(u; \mu_F)$ of the initial and final state particles.

Let us stress two important differences between the factorization formulas (1.1) and (1.2). First, in (1.2) there is no long-distance interaction between the initial and the final state particle at leading power. The interaction between both mesons is entirely described by the perturbative hard-scattering kernel. The non-perturbative input in form of the distribution amplitudes contains information about the structure of the participating mesons and is independent of the considered process. This is different in (1.1) where the soft matrix element depends on the overlap between the wave functions of the initial and the final state particle and therefore on the considered process. Second, in (1.1) all effects related to the large scale $m_b$ are contained in the hard coefficient function whereas the non-perturbative input corresponds to a soft matrix element of a *local* operator. The situation is more complicated in (1.2) where all effects from large virtualities $Q^2$ are encoded in the hard-scattering kernel, but the large scale still enters the non-perturbative matrix elements in form of the large energy of the mesons. The distribution amplitudes correspond to *non-local* matrix elements which are defined on the light-cone. The non-locality in position space translates into convolutions over the fractions $u$ and $v$ in momentum space as illustrated in (1.2).

**Example 3:** $B \to D\pi$

For the first example in QCD Factorization we choose exclusive $B$ decays into heavy-light final states as e.g. $B \to D\pi$. According to the two-particle kinematics in the final state, the pion is very energetic in these decays with $E_\pi = \mathcal{O}(m_b)$ in the $B$ meson rest frame. Similar to what we have seen in the last example, the pion can
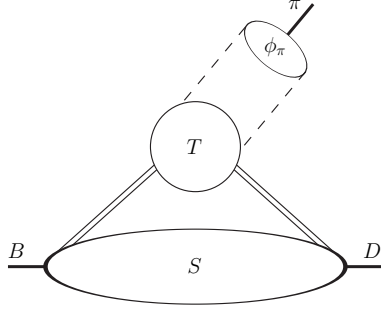
Figure 1.3: *QCD Factorization of short- and long distance effects in exclusive B decays into heavy-light final states. All related quantities have already been introduced in Figure 1.1 and 1.2.*

be described by its two particle Fock state in the collinear approximation. The factorization formula now becomes (cf. Figure 1.3)

$$\langle D\pi | \mathcal{J} | B \rangle = S(\mu_F) \int_0^1 du \; T(u; \mu_F) \, \phi_\pi(u; \mu_F) + \mathcal{O}(\Lambda_{\text{QCD}}/m_Q). \qquad (1.3)$$

The soft matrix element $S(\mu_F)$ describes the long-distance dynamics in the $B - D$ transition as in (1.1). The energetic pion enters in form of its distribution amplitude $\phi_\pi(u; \mu_F)$ and the perturbative effects are contained in a hard-scattering kernel $T(u; \mu_F)$ similar to (1.2). We see that there is no long-distance interaction between the pion and the $B - D$ system at leading power. This corresponds to the famous argument of colour transparency which states that the soft gluons cannot resolve the fast moving colour-singlet pion [38,39].

Let us make one remark concerning strong phases which are important in phenomenological applications. Strong phases arise from final state interactions, but we have just seen that the pion decouples in our example from the $B - D$ system in the heavy quark limit $m_b \to \infty$. The final state interactions are entirely encoded in the hard-scattering kernel and therefore predicted to be perturbative. We will see in Section 1.2 that a similar argument holds for the case of $B \to \pi\pi$ where the knowledge of strong phases is even more desirable.

We finally point out that the factorization formula (1.3) is restricted to the case where the $D$ meson picks up the spectator antiquark from the $B$ meson. In the opposite case when the spectator goes into the pion, factorization does not hold.

**Example 4:** $B \to \pi\ell\nu$

In the last example we finally discuss exclusive charmless $B$ decays. Here we take the decay $B \to \pi\ell\nu$ as an example which we reconsider in more detail in Section 1.3. As we deal with a three-body decay in this case, the energy of the pion depends on the invariant mass of the lepton pair. We restrict our attention to the case where the pion is very energetic in the $B$ meson rest frame with $E_\pi = \mathcal{O}(m_b)$. This is called the large recoil region which is similar to the situation in the last example. However, the factorization formula, which is illustrated in Figure 1.4, turns out to
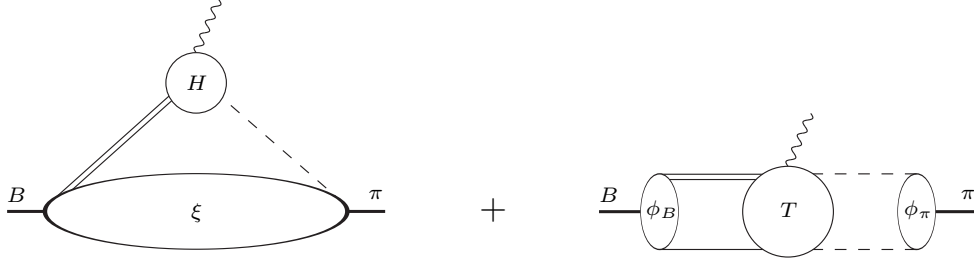
Figure 1.4: *QCD Factorization of short- and long distance effects in exclusive charmless B decays. New objects enter these decays. The first term contains a complicated overlap-contribution $\xi$ whereas the B meson distribution amplitude $\phi_B$ appears in the second one.*

be more complicated and reads

$$\langle \pi | \mathcal{J} | B \rangle \simeq H(\mu_F)\, \xi(\mu_F) + \int_0^\infty d\omega \int_0^1 du \ \phi_B(\omega; \mu_F)\, T(\omega, u; \mu_F)\, \phi_\pi(u; \mu_F). \quad (1.4)$$

It is again restricted to the leading power in $\Lambda_{\mathrm{QCD}}/m_b$ which we illustrate from now on by the symbol "$\simeq$" for brevity. The second term resembles the factorized form in (1.2). It consists of a perturbative hard-scattering kernel $T(\omega, u; \mu_F)$ convoluted with the light-cone distribution amplitudes of the pion $\phi_\pi(u; \mu_F)$ and the $B$ meson $\phi_B(\omega; \mu_F)$. Whereas the former already entered the factorization formulas in the last two examples, the appearance of the latter is new. At first sight, it might look unnatural to consider the $B$ meson on the light-cone. Nevertheless its distribution amplitude is a well-defined object, although more complicated and less understood than the one of the pion.

On the other hand the first term in (1.4) looks like the factorization formula (1.1), but again the situation is more complicated in this case. Whereas the hard effects are factorized in a coefficient functions $H(\mu_F)$, the remnant matrix element is not a soft matrix element as in (1.1). We therefore wrote $\xi(\mu_F)$ for the overlap-contribution in (1.4) which contains a highly complicated interplay of soft and collinear interactions. A deeper understanding of this overlap-contribution is the main motivation for our analysis in Chapter 5.

**Concluding remarks**

Factorization formulas within QCD Factorization are complicated because of the presence of soft and collinear effects at leading power. We have presented a simpler example in (1.3) and a more complicated one in (1.4). In general QCD Factorization does not *prove* that a factorization formula is correct. Typically, the factorization formula is shown to be valid in the lowest (non-trivial) order of the perturbative expansion and then *assumed* to hold to all orders in $\alpha_s$. It was only the development of Soft-Collinear Effective Theory which provided the necessary tools to formulate rigorous factorization proofs.

## 1.1.2   Soft-Collinear Effective Theory

The origin of Soft-Collinear Effective Theory (SCET) goes back to the beginning of this millennium. Since then SCET has sparked the interest of many physicists which led to a fast development of this field. If we focus on the publications which have contributed to the formulation of the SCET-Lagrangian, we may refer to Bauer et al. [22,23], Beneke et al. [24], Chay et al. [40] and Neubert et al. [41].

For our purposes there is no need to introduce the whole concept of SCET as only a small part of our calculations in Chapter 5 is directly related to it. However, SCET provides a deeper understanding of QCD Factorization and puts the factorization formulas onto robust grounds. We therefore give a brief introduction to SCET without going into the technical aspects.

### Preliminaries

Effective theories in general deal with the strategy that we have already discussed in the last section: the idea to disentangle the physics from different length/momentum scales. They have restricted validity up to some momentum cut-off and are designed to correctly reproduce the IR behavior of a physical process.

There are two different ways to construct an effective theory. In the *bottom-up approach* either the underlying theory, which is assumed to be valid at all momentum scales, is not known or it is not understood how to derive an effective theory from the underlying theory. It might nevertheless be possible to write down an effective theory motivated mainly by symmetry arguments and inputs from experimental observations. Chiral perturbation theory and the Standard Model of particle physics fall into this class, as we all hope that the Standard Model loses its validity above the TeV-scale. On the other hand in the *top-down approach* the effective theory can be derived directly from the underlying theory. This is case for SCET which stems from QCD.

The same is true for the effective theory which describes heavy mesons, called heavy-quark effective theory (HQET) [42,43]. We already introduced the phrases *hard* effects ($k^\mu \sim m_Q$) and *soft* effects ($k^\mu \sim \Lambda_{\mathrm{QCD}}$) in the last section, which is the appropriate characterization in this case. E.g. the gluon field is split into

$$A^\mu(x) = A_h^\mu(x) + A_s^\mu(x) \tag{1.5}$$

and the hard gluons $A_h^\mu$ and the soft gluons $A_s^\mu$ are treated as independent degrees of freedom in the effective theory. On the other hand the heavy quark field can be decomposed into its large ($\psi$) and small ($\chi$) components schematically by

$$Q(x) = \psi(x) + \chi(x) \qquad \text{with} \qquad \chi(x) = \mathcal{O}(\Lambda_{\mathrm{QCD}}/m_Q)\,\psi(x). \tag{1.6}$$

This is similar to what is done in non-relativistic theories where this procedure is called the Foldy-Wouthuysen transformation [44]. The small components of the heavy quark field and the hard gluons can then be eliminated as degrees of freedom in the effective theory with their effects encoded in coupling constants of local

operators. The effective theory is identical to QCD but benefits from the HQE at the level of the Lagrangian. It is therefore better suited for the description of heavy mesons than QCD and gives rise to the famous heavy quark symmetry [45,46] in the heavy quark limit $m_Q \to \infty$ which had a strong impact on the phenomenology of $B$ and $D$ meson decays [35].

## Complications in SCET

SCET is the effective theory for the description of energetic particles and jets. It exploits the hierarchy $E \gg \Lambda_{\mathrm{QCD}}$ and follows in principle the same strategy as outlined for HQET: introduce power counting in $\Lambda_{\mathrm{QCD}}/E$, identify relevant degrees of freedom and integrate out hard fluctuations. However, it turns out that SCET is far more complicated than HQET.

The main reason for these complications lies in the fact that SCET is a *non-local* effective theory in contrast to HQET. We do not go into the details related to this point here, but mention that this was the real challenge in the formulation of SCET. Notice that we already encountered this non-local nature of SCET in the last section in form of the light-cone distribution amplitudes as described at the end of example 2. A second complication is related to the fact that there are many different degrees of freedom in SCET. During the development of SCET the correct scaling of the collinear modes was the origin of some confusion. Later it turned out that there are two different scalings depending on the physical process under consideration. This is the reason why there are two different versions of SCET usually referred to as $\mathrm{SCET_I}$ and $\mathrm{SCET_{II}}$. Let us have a closer look at this point and at the same time introduce our notation and terminology that we use throughout this work.

## Notation and terminology

The light-cone dynamics is conveniently formulated with the help of two light-like vectors which we denote by $n_-$ and $n_+$ satisfying $n_\pm^2 = 0$ and normalized to $n_+ \cdot n_- = 2$. Any momentum can be decomposed according to its projections onto these light-cone directions and a two-dimensional transverse plane. We write

$$k^\mu = k_- \frac{n_-^\mu}{2} + k_\perp^\mu + k_+ \frac{n_+^\mu}{2} \qquad \text{with} \qquad k_\perp \cdot n_\pm = 0. \tag{1.7}$$

Notice that in our notation $k_\pm \equiv k \cdot n_\mp$. For the purpose of power counting we introduce a dimensionless parameter $\lambda$ with $\lambda^2 \equiv \Lambda_{\mathrm{QCD}}/m_b$. Scaling relations are given in the form $k \sim (k_-, k_\perp, k_+)$ where we drop factors of $m_b$ which can be restored easily by a dimensional analysis. For example, hard momenta with $p_h^\mu \sim m_b$ and soft momenta with $p_s^\mu \sim \Lambda_{\mathrm{QCD}}$ now become $p_h \sim (1,1,1)$ and $p_s \sim (\lambda^2, \lambda^2, \lambda^2)$.

In charmless $B$ decays, the energy of the fast moving light hadrons typically scales as $E \sim m_b$ in the $B$ meson rest frame (cf. the examples 3-4 in the last section). There are two possible scalings of collinear momenta given by $p_{hc} \sim (1, \lambda, \lambda^2)$ and $p_c \sim (1, \lambda^2, \lambda^4)$, the first entry reflecting the large energy in each case. These are the

| Terminology | Momentum scaling | Virtuality |
|:-----------:|:----------------:|:----------:|
| hard | $(1, 1, 1)$ | $m_b^2$ |
| hard-collinear | $(1, \lambda, \lambda^2)$ | $m_b \Lambda_{\text{QCD}}$ |
| soft | $(\lambda^2, \lambda^2, \lambda^2)$ | $\Lambda_{\text{QCD}}^2$ |
| collinear | $(1, \lambda^2, \lambda^4)$ | $\Lambda_{\text{QCD}}^2$ |

Table 1.1: *Terminology for the relevant momentum regions in charmless B decays. The momentum scaling corresponds to the light-cone decomposition $k \sim (k_-, k_\perp, k_+)$ with a dimensionless parameter $\lambda^2 \equiv \Lambda_{QCD}/m_b$, see text. We have restored the mass dimension in the respective virtualities for convenience.*

two different scalings of collinear fields that we mentioned above. The important difference lies in the respective virtualities $p_{hc}^2 \sim m_b \Lambda_{\text{QCD}} \gg p_s^2$ and $p_c^2 \sim \Lambda_{\text{QCD}}^2 \sim p_s^2$. We see that the former, to which we refer as *hard-collinear* from now on, introduce a new scale $\mu_{hc} \sim (m_b \Lambda_{\text{QCD}})^{1/2}$, whereas the latter, simply called *collinear*, are related to the hadronic scale $\Lambda_{\text{QCD}}$ as usual. The appearance of the hard-collinear scale is another complication in SCET compared to HQET. In the following we treat this intermediate scale as a perturbative scale with $\alpha_s(\mu_{hc}) \sim 0.4$

We have summarized our terminology in Table 1.1. Depending on the considered process some of these modes turn out to be irrelevant. Inclusive decays as e.g. the endpoint spectrum in $B \to X_s \gamma$ can be described with an effective theory called $\text{SCET}_{\text{I}}$ which contains hard, hard-collinear and soft modes. The invariant mass of the energetic jet is typically $M_X^2 \sim m_b \Lambda_{\text{QCD}}$ which explains the relevance of the hard-collinear modes in this case. The effective theory for exclusive decays as e.g. $B \to D\pi$ is $\text{SCET}_{\text{II}}$ containing hard, collinear and soft degrees of freedom. In this case, the virtuality of the collinear modes is related to the mass of the energetic pion with $M_\pi^2 \sim \Lambda_{\text{QCD}}^2$. Hard-collinear modes may appear in exclusive decays as well induced by soft-collinear interactions, which makes a two-step matching procedure $\text{QCD} \to \text{SCET}_{\text{I}} \to \text{SCET}_{\text{II}}$ necessary. This is the case e.g. in $B \to \pi \ell \nu$ but not in $B \to D\pi$ where these effects turn out to be power suppressed. This explains why the factorization formula for the former is much more complex than that of the latter as we have seen in the examples 3-4 in the last section.

## QCD Factorization versus SCET

What is the difference between QCD Factorization and SCET? Both frameworks provide a systematic description of QCD in the heavy quark limit $m_b \to \infty$, i.e. there is none: they are equivalent! There has been some confusion about this point in the literature. It seems as if there were different predictions from QCD Factorization and SCET in hadronic two-body decays of $B$ mesons. We stress that this is *not*

related to the underlying frameworks but to different treatments of power corrections and input parameters of two groups: BBNS and Bauer, Pirjol, Rothstein, Stewart (BPRS). Therefore, the predictions from BBNS and BPRS differ although the ones from QCD Factorization and SCET do *not*. More details concerning this issue can be found in [47–49].

From the conceptual point of view, QCD Factorization and SCET are different. QCD Factorization relies on an explicit analysis of momentum regions of Feynman diagrams. In contrast to this, SCET is a rigorous theory in the sense that it is derived from an established theory (QCD) in a well-defined expansion ($\Lambda_{\mathrm{QCD}}/E$) on the level of the Lagrangian. With the Lagrangian and the respective Feynman rules at hand, it is a convenient tool to address a large variety of inclusive and exclusive processes with applications going even beyond the domain of $B$ physics.

### 1.1.3   Alternative approaches

For completeness we give an overview of alternative approaches to exclusive charmless $B$ decays. As this section is not directly related to the remainder of this thesis, our presentation will be brief and concentrate on the most prominent methods.

**Lattice Gauge Theory**

The first method which comes into mind may be lattice field theory. In recent years there has been considerable progress concerning the reduction of its systematic uncertainties. Most importantly, a steadily increasing number of unquenched lattice calculations becomes available reducing the magnitude of its uncertainties in some cases to the percent level (in particular in ratios of hadronic quantities). For recent reviews on lattice results for heavy quark systems we refer to [50,51].
Unfortunately, lattice gauge theory can tell us very little about exclusive charmless $B$ decays. The main difficulty is related to the implementation of energetic mesons in the lattice calculations (which are usually performed in the $B$ meson rest frame). So far, there are reliable lattice results for $B$ meson decay constants and heavy-to-light form factors at small recoil which can be extrapolated to the large recoil case using dispersion relations. There are some interesting considerations to directly access the large recoil region in an approach called *moving NRQCD* [52]. However, if it will be possible to address hadronic $B$ decays on the lattice remains very challenging.

**QCD Sum Rules**

Although intrinsically limited in their accuracy, QCD sum rules have become a serious competitor to lattice gauge theory. In some sense it can even be considered as complementary to QCD Factorization since it provides important information about the non-perturbative input parameters of the latter in form of decay constants, heavy-to-light form factors (at large recoil) and light-cone distribution amplitudes. For a selection of recent Light-Cone Sum Rule (LCSR) results we refer to [53,54].

Charmless non-leptonic $B$ decays have been studied in the LCSR approach [55–58]. It should be noted that this requires a substantial extension of the standard LCSR formalism [55]. The outcome of the LCSR analysis is in good overall agreement with the QCD Factorization prediction. This technique is sometimes used to address the importance of power corrections in the QCD Factorization framework. This issue should, however, be treated with care as the essential QCD dynamics is considered at *finite* $m_b$ in this approach and the heavy-quark limit $m_b \to \infty$ is only taken at the very end of the calculation after performing the continuum subtraction. It has been pointed out in [59] that one should rather consider LCSRs *within* SCET in order to properly address distinct contributions of the QCD Factorization framework.

**Perturbative QCD**

Perturbative QCD (pQCD) [60,61], which is also known as $k_\perp$-factorization, is based on a hard-scattering approach and may at first sight look similar to QCD Factorization since decay amplitudes are expressed as convolutions of hard-scattering kernels with meson wave functions. However, pQCD does not share the same systematics as QCD Factorization and SCET and relies on the *assumption* that soft contributions to heavy-to-light form factors are suppressed by Sudakov effects (criticism concerning this point has been raised in [62]). The form factor is thus considered to be dominated by hard gluon exchange and the wave functions have to include a dependence on transverse momenta in order to avoid endpoint-singularities in the convolution integrals.
As a consequence pQCD is very different from QCD Factorization. This is reflected by a different hierarchy of various contributions to the hadronic matrix elements, different non-perturbative input quantities and by the fact that pQCD does not recover naive factorization (cf. next section) in any limit. Only recently the authors of pQCD have included next-to-leading order corrections which have simply been taken over from the QCD Factorization and SCET analyses [63,64].

**Phenomenological approaches**

Apart from these dynamical approaches there exist many ideas how to extract the interesting CKM information in exclusive charmless $B$ decays without explicitly calculating the hadronic dynamics. The basic idea is to find a suitable parametrization of the decay amplitudes and to use symmetry arguments (e.g. isospin, $SU(3)$) to derive relations between different decay processes. A sufficiently small set of unknown amplitudes is finally fitted to experimental data.
These approaches should be seen as complementary to the dynamical ones discussed above. On the one hand they require input from the dynamical approaches in order to control their own intrinsic uncertainties of e.g. $SU(3)$-breaking, on the other they can serve as a guide for the dynamical approaches and indicate where these fail to correctly reproduce the data. Rather than presenting some exemplary ideas here, we refer to a recent review about the phenomenology of $B$ decays [65].

## 1.2   Hadronic two-body decays

After this general introduction we come to the first class of exclusive $B$ decays which we consider in detail in this work: hadronic two-body decays. There is a very large variety of decay channels which fall into this class as e.g. $B \to \pi\pi$, $B \to K\pi$, $B \to \rho\rho$ or $B_s \to \pi\pi$. From the phenomenological viewpoint, we are mainly interested in the underlying weak interactions which differ among these decays due to the flavour contents of the mesons. In our analysis concerning the QCD dynamics, the only differences lie in the pseudoscalar $(P)$ or vector $(V)$ nature of the light mesons and small $SU(3)$ breaking effects. As we do not focus on the phenomenological implications of these decays here, it will be sufficient to concentrate on the $B \to \pi\pi$ channels.

### 1.2.1   Preliminaries

$B$ meson decays are mediated by weak interactions. As the typical energy and momentum scales in these decays are much smaller than the mass of the $W$-boson, we may work with an effective weak Hamiltonian which consists of a sum of local operators $Q_i$ multiplied by short-distance coefficients $C_i$ and products of CKM matrix elements $\lambda_p \equiv V_{pb}V_{pd}^*$. The effective Hamiltonian is given by

$$\mathcal{H}_{\text{eff}} = \frac{G_F}{\sqrt{2}} \sum_{p=u,c} \lambda_p \left( C_1 Q_1^p + C_2 Q_2^p + \sum_{i=3}^{6} C_i Q_i + C_8 Q_8 \right) + \text{h.c.,} \qquad (1.8)$$

where $Q_{1,2}^p$ are the left-handed current-current operators, $Q_{3-6}$ are the QCD penguin operators and $Q_8$ is the chromomagnetic dipole operator. Their explicit form reads

$$Q_1^p = (\bar{p}b)_{V-A}(\bar{d}p)_{V-A}, \qquad\qquad Q_2^p = (\bar{p}_i b_j)_{V-A}(\bar{d}_j p_i)_{V-A},$$

$$Q_3 = (\bar{d}b)_{V-A} \sum_q (\bar{q}q)_{V-A}, \qquad\qquad Q_4 = (\bar{d}_i b_j)_{V-A} \sum_q (\bar{q}_j q_i)_{V-A},$$

$$Q_5 = (\bar{d}b)_{V-A} \sum_q (\bar{q}q)_{V+A}, \qquad\qquad Q_6 = (\bar{d}_i b_j)_{V-A} \sum_q (\bar{q}_j q_i)_{V+A},$$

$$Q_8 = -\frac{g_s}{8\pi^2} m_b \, \bar{d}\sigma_{\mu\nu}(1+\gamma_5)G^{\mu\nu}b, \qquad\qquad (1.9)$$

where $(\bar{q}_1 q_2)_{V\pm A} = \bar{q}_1 \gamma_\mu(1 \pm \gamma_5)q_2$ and the sum runs over all active quark flavours in the effective theory, i.e. $q = u, d, s, c, b$. If no colour index $i, j$ is given, the two operators are assumed to be in a colour singlet state. The definition of the dipole operator $Q_8$ corresponds to the sign convention $iD_\mu = i\partial_\mu + g_s T^A A_\mu^A$.

In principle, more operators have to be taken into account. The complete set of operators contains in addition electroweak penguin operators and the electromagnetic dipole operator which are important for $B \to K\pi$ decays. As we focus on the $B \to \pi\pi$ channels here, the effects from these operators can safely be neglected.
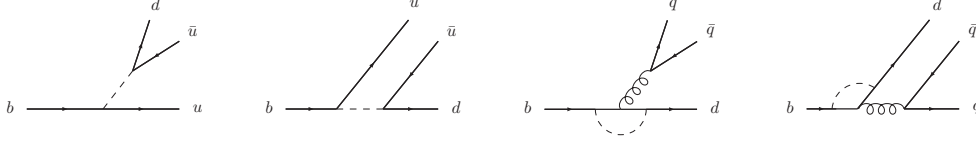
Figure 1.5: *Topological amplitudes $\alpha_{1-4}(M_1M_2)$ as introduced in [66]. The quark to the right and the spectator antiquark with flavour $\bar{q}_s$ (not drawn) form the meson $M_1$ with flavour content $[\bar{q}_s u]$, $[\bar{q}_s d]$, $[\bar{q}_s d]$ and $[\bar{q}_s q]$, respectively. The two upper lines form the meson $M_2$ with respective flavour $[\bar{u}d]$, $[\bar{u}u]$, $[\bar{q}q]$ and $[\bar{q}d]$ where $q \in \{u, d, s\}$. The flavour-singlet penguin amplitude $\alpha_3(M_1M_2)$ does not contribute to the $B \to \pi\pi$ decay amplitudes.*

For the parametrization of the $B \to \pi\pi$ decay amplitudes we follow the notation of [66]. Neglecting some smaller amplitudes related to weak annihilation, they can be written as

$$\sqrt{2}\,\langle \pi^-\pi^0|\,\mathcal{H}_{\text{eff}}\,|B^-\rangle = \lambda_u\big[\alpha_1(\pi\pi) + \alpha_2(\pi\pi)\big]\,A_{\pi\pi},$$

$$\langle \pi^+\pi^-|\,\mathcal{H}_{\text{eff}}\,|\bar{B}^0\rangle = \Big\{\lambda_u\big[\alpha_1(\pi\pi) + \alpha_4^u(\pi\pi)\big] + \lambda_c\,\alpha_4^c(\pi\pi)\Big\}\,A_{\pi\pi},$$

$$-\,\langle \pi^0\pi^0|\,\mathcal{H}_{\text{eff}}\,|\bar{B}^0\rangle = \Big\{\lambda_u\big[\alpha_2(\pi\pi) - \alpha_4^u(\pi\pi)\big] - \lambda_c\,\alpha_4^c(\pi\pi)\Big\}\,A_{\pi\pi}. \qquad (1.10)$$

The $\alpha_i(\pi\pi)$ are called topological amplitudes and are related to the flavour flows in the decays. More precisely, $\alpha_1(\pi\pi)$ is the colour-allowed tree amplitude, $\alpha_2(\pi\pi)$ is the colour-suppressed tree amplitude and $\alpha_4^p(\pi\pi)$ is the QCD penguin amplitude as illustrated in Figure 1.5. We see that $B^- \to \pi^-\pi^0$ is a pure tree decay within the approximations mentioned above. It is free of interference effects which typically introduce large uncertainties due to our poor knowledge of the weak phases and therefore particularly suited to test the QCD Factorization predictions. On the other hand $\bar{B}^0 \to \pi^0\pi^0$ is a colour-suppressed decay as can be seen in (1.10) by the absence of $\alpha_1(\pi\pi)$. Any prediction concerning this decay is expected to be accompanied by large uncertainties.

For later convenience it is useful to write the normalization of the amplitudes as

$$A_{\pi\pi} = i\,\frac{G_F}{\sqrt{2}}\,m_B^2 F_+^{B\to\pi}(0)f_\pi, \qquad (1.11)$$

where $F_+^{B\to\pi}(0)$ is a transition form factor at maximum recoil and $f_\pi$ is the pion decay constant. Their precise definitions read

$$\langle \pi^+(p')|\,\bar{u}(\not{p} - \not{p}')b\,|\bar{B}^0(p)\rangle\big|_{(p-p')^2=0} \simeq m_B^2 F_+^{B\to\pi}(0),$$

$$\langle \pi^-(q)|\,\bar{d}\gamma_\mu\gamma_5 u\,|0\rangle = -if_\pi q_\mu. \qquad (1.12)$$

As in the examples that we discussed at the beginning of this chapter, the light-cone distribution amplitudes of the pion and the $B$ meson enter the factorization formula for hadronic two-body decays. Their explicit definitions will be given in Chapter 5 (for light mesons the definition can be found in (5.39) and for the $B$ meson in (5.46)).

## 1.2.2   Factorization Formula

According to the QCD Factorization framework [19–21], the hadronic matrix elements of the operators in the effective weak Hamiltonian take the form

$$\langle M_1 M_2 | Q_i | \bar{B} \rangle \simeq m_B^2 \, F_+^{B \to M_1}(0) \, f_{M_2} \int du \; T_i^I(u) \, \phi_{M_2}(u) \tag{1.13}$$

$$+ f_B \, f_{M_1} \, f_{M_2} \int d\omega dv du \; T_i^{II}(\omega, v, u) \, \phi_B(\omega) \, \phi_{M_1}(v) \, \phi_{M_2}(u),$$

where $M_1$ denotes the light meson which picks up the spectator quark of the $\bar{B}$ meson and $M_2$ is a second light meson. The factorization formula is illustrated in Figure 1.6. Let us compare this factorization formula with the examples that we discussed in the beginning of this chapter. First, we notice that the factorization formula is again restricted to the leading power in the HQE in $\Lambda_{\mathrm{QCD}}/m_b$. Further, we have suppressed the dependence on the factorization scale $\mu_F$ for simplicity here. The perturbative information in (1.13) is encoded in the hard-scattering kernels $T^I$ and $T^{II}$ which also appeared in the examples 2-4. The same is true for the light-cone distribution amplitudes of the light mesons $\phi_{M_1}, \phi_{M_2}$ whereas the one of the $B$ meson $\phi_B$ entered the factorization formula in example 4. The distribution amplitudes always come in combination with decay constants $f_B, f_{M_1}, f_{M_2}$ which have been suppressed in Section 1.1.1 for simplicity.

The last piece in (1.13) is the heavy-to-light form factor $F_+^{B \to M_1}$ at maximum recoil. The form factor still contains perturbative *and* non-perturbative effects and therefore does not fit into the pattern that we developed in Section 1.1.1. The form factor itself can be factorized as we discuss in Section 1.3, but this is not needed here. We follow the BBNS analysis which treats the form factor as an external input with its numerical value taken from a Light-Cone QCD Sum Rule calculation.

In leading order (LO) of the perturbative expansion, the factorization formula simplifies tremendously since $T^I = \mathrm{const} + \mathcal{O}(\alpha_s)$ and $T^{II} = \mathcal{O}(\alpha_s)$. The second term
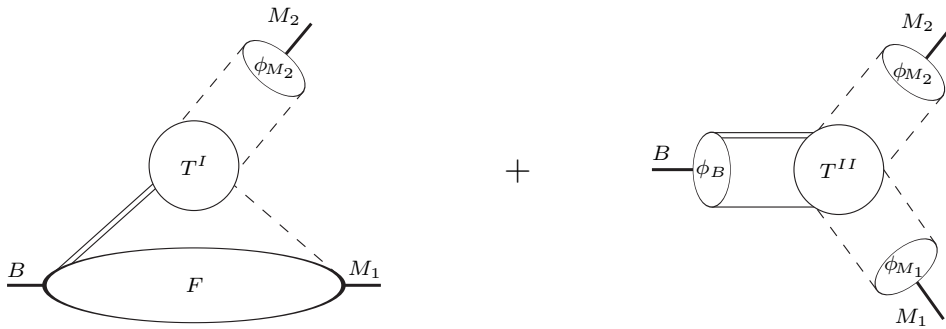


Figure 1.6: *QCD Factorization of short- and long distance effects in hadronic two-body decays. The former are contained in perturbative hard-scattering kernels $T^I$, $T^{II}$, the latter in light-cone distribution amplitudes $\phi_B$, $\phi_{M_1}$, $\phi_{M_2}$. The heavy-to-light form factor $F$ is not factorized in the BBNS approach.*

in (1.13) is thus absent in this case and the convolution in the first term simply gives the normalization of the distribution amplitude. This yields

$$\langle M_1 M_2 | Q_i | \bar{B} \rangle \sim F_+^{B \to M_1}(0) \, f_{M_2}. \tag{1.14}$$

This approximation corresponds to *naive factorization*. With naive factorization we mean that a hadronic matrix element of a local four-quark operator is split into two matrix elements of bilinear quark currents, as e.g. in

$$\langle M_1 M_2 | Q_1^u | \bar{B} \rangle \sim \langle M_1 | (\bar{u}b)_{V-A} | \bar{B} \rangle \, \langle M_2 | (\bar{d}u)_{V-A} | 0 \rangle \tag{1.15}$$

with the first matrix element on the right-hand side giving the form factor and the second one the decay constant as in (1.14). Naive factorization was used before QCD Factorization was established and gave fairly good predictions which was surprising at that time [67,68]. We now understand why this is the case: Naive factorization corresponds to the leading term in the combined expansion in $\alpha_s$ and $\Lambda_{\mathrm{QCD}}/m_b$. The fact that QCD Factorization reproduces naive factorization in this expansion is non-trivial.

One obvious problem with naive factorization is that it does not give rise to strong rescattering phases because of the lack of final state interactions. In (1.13) we see how this problem is cured in QCD Factorization. At leading power all final state interactions are encoded in the hard-scattering kernels $T^I$ and $T^{II}$. The strong phases are thus predicted to be perturbative in the QCD Factorization framework. Moreover, we just have seen that strong phases are absent in LO of the perturbative expansion. To summarize, strong phases are of $\mathcal{O}(\alpha_s)$ and $\mathcal{O}(\Lambda_{\mathrm{QCD}}/m_b)$ i.e. generically small in QCD Factorization.

We conclude this section with a comment on the factorization proof of (1.13). The explicit calculation in [19–21] showed that the factorization formula holds to $\mathcal{O}(\alpha_s)$. A recent analysis [25–27] in combination with our calculations in Chapter 3 and 4 extends this explicit proof to $\mathcal{O}(\alpha_s^2)$. So far a rigorous proof to all orders in $\alpha_s$ is still missing. For the similar (but simpler) case of $B \to D\pi$, which we introduced in example 3 of Section 1.1.1, a factorization proof has been formulated in SCET and can be found in [69]. A first step towards an all-order proof of (1.13) has been undertaken in [70].

## 1.2.3   Perturbative corrections

The power of the factorization formula (1.13) lies in the fact that it allows for a systematic calculation of perturbative corrections. They are contained in the hard-scattering kernels $T^I$ and $T^{II}$ which describe two different mechanisms to which we refer as *vertex corrections* and *spectator interactions*, respectively. Whenever the spectator antiquark in the $\bar{B}$ meson enters the perturbative subgraph, this contribution is assigned to $T^{II}$ otherwise to $T^I$. We now present the status of the perturbative calculation and identify the contributions that we address in Chapter 3 and 4.
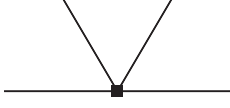
Figure 1.7: *Tree level diagram. The line to the left (right) of the vertex denotes the b quark (light quark which goes into $M_1$), the upper lines the light quark/antiquark which form $M_2$. When the spectator does not participate in the scattering, it is not drawn.*

## Tree Level

We have already anticipated in the last section that QCD Factorization reproduces naive factorization in LO of the perturbative expansion. There is only one diagram that contributes at this order which is depicted in Figure 1.7. As the spectator antiquark does not participate in this case, this corresponds to a contribution to $T^I$. We quote the result in form of the topological amplitudes introduced in (1.10)

$$\alpha_i^p(M_1 M_2) = C_i + \frac{C_{i\pm1}}{N_c} + \mathcal{O}(\alpha_s), \qquad i = 1, 2, 4 \qquad (1.16)$$

where the upper (lower) signs apply when $i$ is odd (even) and the superscript $p$ is to be omitted for $i = 1, 2$. To illustrate the phrases *colour-allowed* ($\alpha_1$) and *colour-suppressed* ($\alpha_2$), we have a look at the numerical values of the Wilson coefficients $C_1(m_b) \sim 1.1$ and $C_2(m_b) \sim -0.2$ giving $\alpha_1 \sim 1.0$ and $\alpha_2 \sim 0.2$. Notice that $\alpha_2$ is particularly small due to a cancellation in the two terms.

## Next-to-leading order

The next-to-leading order (NLO) corrections have been calculated by BBNS [19–21]. They consist in the calculation of the (naively) non-factorizable diagrams in Figure 1.8 whereas the (naively) factorizable diagrams in Figure 1.9 turn out to be irrelevant. The terminology is such that the former contain interactions between the $B - M_1$ system and $M_2$ whereas the latter do not. An explanation for the fact that only non-factorizable diagrams have to be considered in this context is relegated to
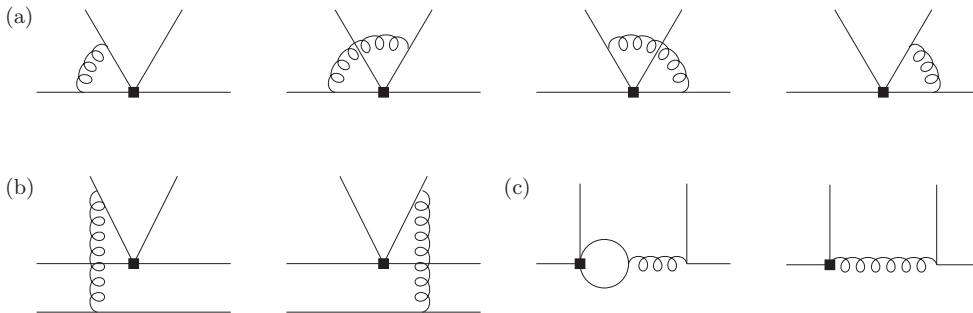


Figure 1.8: *Non-factorizable diagrams in NLO: Vertex corrections (a), hard spectator interactions (b) and penguin contractions (c). The last diagram involves an insertion of the dipole operator $Q_8$.*
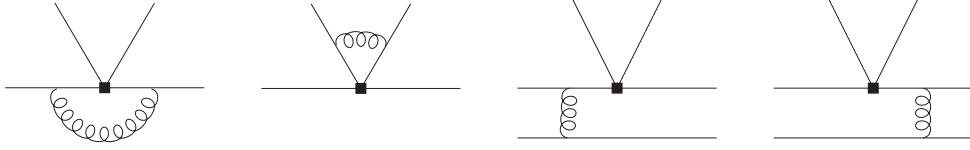
Figure 1.9: *Factorizable diagrams in NLO that need not to be calculated.*

Section 3.3.2. In addition to the vertex corrections in Figure 1.8a and the spectator interactions in Figure 1.8b, the penguin contractions in Figure 1.8c have to be taken into account for the calculation of the penguin amplitude $\alpha_4^p$. As the spectator is not involved in these diagrams, the respective contribution is again assigned to $T^I$.

At NLO the general form of the topological amplitudes $\alpha_1$, $\alpha_2$ and $\alpha_4^p$ becomes

$$\alpha_i^p(M_1 M_2) = C_i + \frac{C_{i\pm 1}}{N_c} + \frac{\alpha_s C_F}{4\pi N_c}\left[C_{i\pm 1}\, V^{(1)} + N_H\, C_{i\pm 1}\, H^{(1)} + \delta_{i4}\, P_p^{(1)}\right] + \mathcal{O}(\alpha_s^2), \tag{1.17}$$

where the functions $V^{(1)}/H^{(1)}/P_p^{(1)}$ stem from the diagrams in Figure 1.8a/b/c, respectively. They contain convolutions of the hard-scattering kernels with light-cone distribution amplitudes according to the factorization formula (1.13). The respective arguments $V^{(1)}(M_2)$, $H^{(1)}(M_1 M_2)$ and $P_p^{(1)}(M_2)$ have been suppressed in (1.17) for simplicity. The normalization of the hard spectator interactions reads

$$N_H = 4\pi^2\,\frac{f_B f_{M_1}}{N_c\, m_B \lambda_B F_+^{B\to M_1}(0)}. \tag{1.18}$$

In contrast to the remnant NLO diagrams, the spectator interactions correspond to tree level diagrams at this order which is the origin of the factor $4\pi^2$. The ratio of hadronic quantities involves the quantity $\lambda_B = \mathcal{O}(\Lambda_{\text{QCD}})$ which is related to the $B$ meson distribution amplitude (the definition can be found in (5.56)). Notice that the normalization scales as $N_H \sim 1$ in the HQE and in the large $N_c$-expansion. One might therefore expect the spectator interactions to dominate over the vertex corrections and the penguin contributions because of the factor $4\pi^2 \sim 40$. However, for realistic values of the hadronic quantities this is not the case as $N_H \sim 0.5 - 1.5$.

In the following we quote the explicit NLO results for the vertex corrections $V^{(1)}$ and the spectator interactions $H^{(1)}$. As our calculations in Chapter 3 and 4 are related to the topological tree amplitudes, the penguin contributions $P_p^{(1)}$ are not needed for our purposes (they can be found in [66]). The NLO vertex corrections can be written in the form

$$V^{(1)}(M_2) = -6\ln\frac{\mu^2}{m_b^2} - 18 + \int_0^1 du\, g(u)\, \phi_{M_2}(u). \tag{1.19}$$

The scale dependence exactly matches the one of the Wilson coefficients in the LO terms in (1.17) as desired. The function $g(u)$ is found to be

$$g(u) = \frac{3(1-2u)}{\bar{u}} \ln u - 3i\pi + \left[ 2\text{Li}_2(u) - \ln^2 u - \frac{1-3u}{\bar{u}} \ln u - 2i\pi \ln u - (u \leftrightarrow \bar{u}) \right], \tag{1.20}$$

where we wrote $\bar{u} \equiv 1 - u$. The appearance of an imaginary part in $g(u)$ is particularly interesting since it is the origin of a strong phase shift between the final state mesons. The penguin contributions $P_p^{(1)}$ are another source of an imaginary part whereas the tree-level spectator scattering gives a real contribution which reads

$$H^{(1)}(M_1 M_2) = \lambda_B \int_0^\infty d\omega \int_0^1 du \int_0^1 dv \; \frac{\phi_B(\omega)}{\omega} \frac{\phi_{M_1}(v)}{\bar{v}} \frac{\phi_{M_2}(u)}{\bar{u}}. \tag{1.21}$$

Let us make one remark concerning the typical scales of the perturbative corrections. Following our terminology in Table 1.1, the perturbative effects in $T^I$ stem from hard modes ($k^2 \sim m_b^2$) whereas $T^{II}$ contains hard as well as hard-collinear effects ($k^2 \sim \mu_{hc}^2 \sim m_b \Lambda_{\text{QCD}}$). The tree level spectator scattering in Figure 1.8b is in particular most naturally associated to the hard-collinear scale which enhances this contribution by a factor of $\alpha_s(\mu_{hc})/\alpha_s(m_b) \sim 2$ with respect to the other contributions. This issue is hidden in our notation in (1.17). A correct treatment of the perturbative scales favours a SCET analysis of the spectator interactions in order to resum large logarithms $\ln \mu/m_b$ into short-distance coefficient functions.

**Next-to-next-to-leading order**

The next-to-next-to-leading order (NNLO) calculation is to date incomplete. It has first been addressed in the so-called *large $\beta_0$-limit* in [71,72]. In this approximation, only a very small subset of NNLO diagrams has to be calculated, namely the ones with massless fermion-loops which give rise to a factor $n_f$. At the end of the calculation, the fairly motivated substitution $n_f \to -3\beta_0/2$ is made in the hope to catch the main contribution of the full calculation in this way. It must be admitted that the large $\beta_0$-limit sometimes gives a good approximation. However, whether this is the case or not can only be judged a posteriori when the full result is known. Concerning the parts of our NNLO calculation, we will answer this question in Chapter 3 and 4.
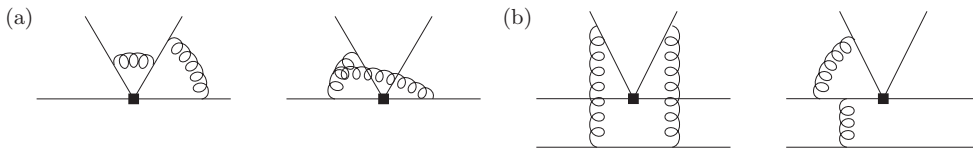


Figure 1.10: *Sample of NNLO diagrams: Vertex corrections (a) and spectator interactions (b).*

Up to the work in [73], which also considered a small and incomplete subset of NNLO diagrams, the penguin amplitude $\alpha_4^p$ has not yet been addressed. We therefore focus on the tree amplitudes in the following and disregard all diagrams with penguin contractions as well as insertions of the operators $Q_{3-6}$ and $Q_8$. We extend the general form of the tree amplitudes $\alpha_1$ and $\alpha_2$ in NNLO to

$$\alpha_i(M_1 M_2) = C_i + \frac{C_{i\pm 1}}{N_c} + \frac{\alpha_s C_F}{4\pi N_c}\left[ C_{i\pm 1}\, V^{(1)} + N_H\, C_{i\pm 1}\, H^{(1)} \right] \tag{1.22}$$

$$+ \frac{\alpha_s^2 C_F}{(4\pi)^2 N_c}\left[ C_i V_1^{(2)} + C_{i\pm 1} V_2^{(2)} + N_H\left( C_i H_1^{(2)} + C_{i\pm 1} H_2^{(2)} \right) \right] + \mathcal{O}(\alpha_s^3).$$

A first systematic study of the NNLO corrections addressed the hard spectator interactions $H_{1,2}^{(2)}$ which were calculated within SCET in [25]. A subsequent SCET calculation can be found in [26]. There is a tiny discrepancy[2] between both calculations which is claimed to be of minor numerical importance [26]. A third independent calculation of the spectator interactions in full QCD may help to resolve the origin of this discrepancy [27]. The QCD calculation consists in the computation of $\sim 50$ 1-loop diagrams as those depicted in Figure 1.10b with its main complication due to the presence of two perturbative scales $\mu_{hc}$ and $m_b$. This problem is circumvented in SCET where the two scales are systematically disentangled in the two-step matching procedure QCD $\rightarrow$ SCET$_\mathrm{I}$ $\rightarrow$ SCET$_\mathrm{II}$. Another advantage of the SCET calculation lies in the fact that the hard-collinear effects in $T^{II}$ are exactly the same as those entering the $B \rightarrow M_1$ form factor [47]. As they were already known at the 1-loop level from a different analysis [74–76], Beneke/Jäger and Kivel calculated the missing hard contributions [25,26].

No such complication arises in the calculation of the vertex corrections $V_{1,2}^{(2)}$ which we address in detail in this work. However, the vertex corrections represent a challenging 2-loop calculation including $\sim 80$ diagrams as the ones in Figure 1.10a. We divide the calculation into two parts: We first focus on the imaginary part of $V_{1,2}^{(2)}$ in Chapter 3 and calculate the real part subsequently in Chapter 4. This is done for several reasons. First of all, each part is independently well-defined and represents a lengthy calculation on its own. It is natural to focus on a simpler part of this highly demanding calculation in a first step. Second, the imaginary part enters the topological amplitudes at $\mathcal{O}(\alpha_s)$ which means that the imaginary part of $V_{1,2}^{(2)}$ has the complexity of an effective NLO calculation. Conceptual complications that arise in NNLO can therefore be relegated to our analysis in Chapter 4. Finally, the knowledge of the imaginary part is particularly important in phenomenological applications as it is the origin of a strong phase shift between the final state mesons.

One important remark is in order concerning the general form (1.22) of the tree amplitudes in NNLO. The reason for this compact form which implies $\alpha_1 \leftrightarrow \alpha_2$ by the exchange $C_1 \leftrightarrow C_2$ is related to Fierz symmetry arguments. A Fierz reordering of a four-quark operator reshuffles the contracted fields and thus the related

---

[2]The corrected version of [26] is in agreement with [25].

flavours. Notice that $\alpha_1$ and $\alpha_2$ interchange their roles under the exchange of the quark flavours $u \leftrightarrow d$ as shown in Figure 1.5. However, it is no longer obvious if Fierz symmetry is preserved in the effective theory at the level of the Wilson co-efficients. The NLO calculation showed the Fierz symmetric form (1.17) to hold and we therefore expect the same for the imaginary part of $V_{1,2}^{(2)}$ which has NLO complexity. In their SCET analysis of the spectator interactions, Beneke and Jäger paid special attention to this point and found that their result can indeed be written in the Fierz symmetric form (1.22). We have not yet solved this question for the real part of $V_{1,2}^{(2)}$ which requires a Fierz symmetric definition of evanescent operators at the 2-loop level. As a consequence, we can only give a result for the real part of the tree amplitude $\alpha_1$ in Chapter 4 but so far we cannot relate it to that of $\alpha_2$. More details concerning Fierz symmetry and evanescent operators can be found in Section 3.1.

### 1.2.4   Power corrections

The factorization formula (1.13) is exact in the formal heavy quark limit $m_b \to \infty$. Unfortunately, power corrections do not factorize in general and cannot be calculated systematically. They represent the main limitation of QCD Factorization with a generic size of $\mathcal{O}(\Lambda_{\mathrm{QCD}}/m_b) \sim 5 - 15\%$. The reader may wonder why we perform highly non-trivial NNLO calculations that are accompanied by substantial systematic uncertainties. Our ultimate goal is to look for deviations between experimental data and the QCD Factorization prediction and to address them to effects from New Physics rather than to presumably sizeable power corrections.

From our point of view QCD Factorization is nevertheless the most convincing theory to study non-leptonic $B$ decays and we should therefore reduce all uncertainties as much as possible. Calculable higher order perturbative corrections can also turn out to be sizeable and it would be erroneous to associate them with unknown power corrections. The rich phenomenology and the interplay with alternative approaches to non-leptonic $B$ decays may help us to test QCD Factorization and to get an estimate of the size of power corrections on the one hand and to focus on the interesting CP violating observables on the other. Rather than aiming at a perfect global description of all decay channels, we are convinced that we can achieve the necessary precision in selected observables. We also refer to our discussion after (1.10) in this context, concerning the question why some decay channels are better suited for a QCD Factorization prediction than others.

Obviously, it would be a significant improvement if we could get some handle about power corrections. In the remainder of this section we briefly recapitulate how BBNS implement certain classes of power corrections. The price to pay for this procedure is that their predictions become model-dependent in this way. For a model-independent analysis we refer to [77] which contains a formal classification of power corrections according to factorizable and non-factorizable operators in SCET.

## Chirally enhanced contributions

One class of power corrections, which is related to the projection on higher twist distribution amplitudes of the light mesons, appears to be enhanced by large numerical coefficients. These corrections are typically proportional to

$$r_\chi^\pi(\mu) = \frac{2m_\pi^2}{m_b(\mu)(m_u + m_d)(\mu)}, \qquad (1.23)$$

which is formally of $\mathcal{O}(\Lambda_{\mathrm{QCD}}/m_b)$ but numerically close to unity. Fortunately, an important part of this contribution, the so-called *scalar penguins*, turn out to be factorizable (at least to NLO) and can be calculated systematically within QCD Factorization. This results in an additional contribution to the penguin amplitude $\alpha_4^p$ which is currently known to NLO and can be found in [66].

In contrast to this the twist-3 projections related to the spectator interactions in Figure 1.8b do not factorize which can be seen as follows. In this case, the contributions to $\alpha_1$, $\alpha_2$ and $\alpha_4^p$ can be written as

$$\delta\alpha_i^p(M_1 M_2) = \frac{\alpha_s C_F}{4\pi N_c} \, C_{i\pm 1} \, N_H \, r_\chi^{M_1} \, \lambda_B \int_0^\infty d\omega \int_0^1 du \int_0^1 dv \, \frac{\phi_B(\omega)}{\omega} \, \frac{\phi_{m_1}(v)}{\bar{v}} \, \frac{\phi_{M_2}(u)}{u}, \qquad (1.24)$$

which involves the twist-3 distribution amplitude of the meson $M_1$ with its asymptotic form $\phi_{m_1}(v) = 1$. As it does not vanish at $v = 1$, the contribution in (1.24) is divergent which states that factorization does not hold for this power-suppressed contribution. BBNS propose a parametrization of the logarithmically divergent integral in the form

$$\int_0^1 dv \, \frac{\phi_{m1}(v)}{\bar{v}} \equiv X_H \qquad \longrightarrow \qquad X_H = \left(1 + \rho_H \, e^{i\phi_H}\right) \, \ln\frac{m_B}{\Lambda_h} \qquad (1.25)$$

as the integral is expected to be regulated by a hadronic scale $\Lambda_h = \mathcal{O}(\Lambda_{\mathrm{QCD}})$. In addition, they allow for a complex coefficient with $\rho_H = \mathcal{O}(1)$ and an arbitrary phase $\phi_H$ which might be generated due to soft rescattering effects. Notice that $X_H$ is treated to be *universal*, i.e it does not depend on the meson $M_1$ and is assumed to be the same for all topological amplitudes in (1.24). In our analysis of the tree amplitudes in Chapter 3 and 4, we adopt the BBNS treatment of non-factorizable chirally enhanced contributions.

## Weak annihilation

We briefly comment on a second class of power-suppressed effects: weak annihilation. The annihilation diagrams from Figure 1.11 turn out to be suppressed by one power in $\Lambda_{\mathrm{QCD}}/m_b$. They exhibit similar endpoint divergences as the chirally enhanced contributions and are therefore non-factorizable. In the BBNS approach, they are parameterized in analogy to (1.25) by

$$X_A = \left(1 + \rho_A \, e^{i\phi_A}\right) \, \ln\frac{m_B}{\Lambda_h}. \qquad (1.26)$$

Beneke and Neubert make a more relaxed assumption on the universality of annihilation contributions in [66] and examine a specific scenario with three different phases $\phi_A$ for the final states $PP$, $PV$ and $VV$.

Our final remark is related to recent investigations of the annihilation amplitudes. They have been considered in [78] using a new type of factorization formula which includes zero-bin subtractions in SCET$_{\mathrm{II}}$ [79]. These subtractions render the convolution integrals finite which implies that the annihilation amplitudes become calculable. We will come back to the formal aspects of this approach in Section 1.3.2 and focus on the outcome for the annihilation amplitudes here. Strong phases from annihilation are found in [78] to be of $\mathcal{O}(\alpha_s^2(\mu_{hc})\Lambda_{\mathrm{QCD}}/m_b)$ and are therefore expected to be small in qualitative agreement with predictions from a Light-Cone QCD Sum Rule analysis [58]. However, whether or not this new type of factorization formula represents a model-independent prediction for the annihilation amplitudes is still a matter of debate.
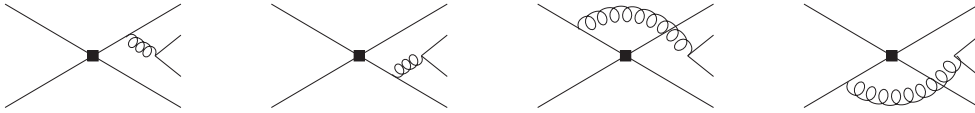


Figure 1.11: *Annihilation diagrams.*

## 1.3 Heavy-to-light form factors

Our calculation in Chapter 5 is related to an analysis of heavy-to-light form factors. These form factors encode the strong interaction effects in exclusive semi-leptonic decays (e.g. $B \to \pi \ell \nu$), hadronic two-body decays (e.g. $B \to \pi\pi$) and exclusive radiative decays (e.g. $B \to K^*\gamma$). Rather than aiming at a quantitative description, our analysis focuses on the conceptual aspects concerning factorization. Heavy-to-light form factors are among the "simplest" objects for studying the complicated QCD dynamics in exclusive charmless $B$ decays.

### 1.3.1 Factorization Formula

We concentrate on the three independent form factors in $B \to \pi$ transitions which can be defined as

$$\langle \pi(p') \,|\, \bar{q}\gamma^\mu b \,|\, \bar{B}(p)\rangle = F_+(q^2)\,(p^\mu + p'^{\,\mu}) + F_-(q^2)\,q^\mu,$$

$$\langle \pi(p') \,|\, \bar{q}\sigma^{\mu\nu}q_\nu b \,|\, \bar{B}(p)\rangle = \frac{i\,F_T(q^2)}{m_B + m_\pi}\,\left[q^2(p^\mu + p'^{\,\mu}) - (m_B^2 - m_\pi^2)\,q^\mu\right] \qquad (1.27)$$

with $q = p - p'$. We are interested in the large recoil region $q^2 \ll m_b^2$ where the pion is very energetic with $E_\pi = \mathcal{O}(m_b)$ in the $B$ meson rest frame. The factorization formula has already been introduced in example 4 at the beginning of this chapter. In a slightly different notation, it reads

$$F_i(q^2) \simeq H_i(q^2)\,\xi(q^2) + \int_0^\infty d\omega \int_0^1 du \ \phi_B(\omega)\,T_i(\omega, u; q^2)\,\phi_\pi(u), \qquad (1.28)$$

where we made the kinematical dependence on the momentum transfer explicit and suppressed the one on the factorization scale. We recapitulate its interpretation in terms of our SCET terminology from Table 1.1. The perturbative information is contained in the hard coefficient function $H_i(q^2)$ and the hard-scattering kernel $T_i(u, \omega; q^2)$; the former including hard effects ($\sim m_b^2$), the latter hard and hard-collinear effects ($\sim m_b\Lambda_{\rm QCD}$). The light-cone distribution amplitudes $\phi_B(\omega)$ and $\phi_\pi(u)$ encode soft and collinear effects, respectively, from the scale $\Lambda_{\rm QCD}$. Finally, the overlap-contribution $\xi(q^2)$ is poorly understood so far and the main subject of our analysis. The important point to notice is that the *same* function $\xi(q^2)$ enters the three $B \to \pi$ form factors (there are two other overlap functions $\xi_\parallel(q^2)$ and $\xi_\perp(q^2)$ for the seven $B \to V$ form factors). This is the basis of approximate symmetry relations between different form factors [80] which are broken by perturbative corrections and power corrections. Even if we consider the overlap-function $\xi(q^2)$ as unknown, the factorization formula (1.28) represents a useful simplification as the number of unknown hadronic quantities has been reduced from three to one (counting the distribution amplitudes as known hadronic quantities in this context as they are universal quantities that can be analyzed in different processes).

The structure of the factorization formula has first been seen to emerge in [81]. A rigorous factorization proof in SCET has been formulated later in [82–84]. The proof is usually performed in two steps, matching first QCD $\to$ SCET$_{\mathrm{I}}$ at the hard scale and subsequently SCET$_{\mathrm{I}} \to$ SCET$_{\mathrm{II}}$ at the hard-collinear scale. The two terms in (1.28) are related to two different SCET$_{\mathrm{I}}$ currents which contribute in leading power to the form factors. What remains to be shown is that one of them exhibits the symmetry properties mentioned above and that the other gives rise to a finite convolution integral of leading twist distribution amplitudes as in the second term of the factorization formula (1.28) (more details will be given in Section 5.3).

We finally remark that the overlap-contribution $\xi(q^2)$ still contains hard-collinear effects as only hard effects have been factorized in the first matching step into $H_i(q^2)$. As long as we treat the hard-collinear scale $(m_b\Lambda_{\mathrm{QCD}})^{1/2}$ as a perturbative scale, the factorization of short- and long-distance effects is thus incomplete.

## 1.3.2 Closer look at $\xi(q^2)$

We follow the notation of [83] by defining the overlap-contribution as a matrix element of a SCET$_{\mathrm{I}}$ current in the form

$$\langle \pi(p') \, | \, (\bar{\xi}_{hc}W_{hc})h_v \, | \, \bar{B}(p) \rangle \equiv 2E_\pi \, \xi(q^2), \tag{1.29}$$

where $h_v$ denote the large components of the heavy quark field satisfying $\not{v}h_v = h_v$ and $\xi_{hc}$ the ones of the hard-collinear field with $\not{n}_-\xi_{hc} = 0$. The definition of the hard-collinear Wilson line $W_{hc}$ can be found in [83].

The attempt to factorize $\xi(q^2)$ in SCET$_{\mathrm{II}}$ into light-cone distribution amplitudes leads to several complications: Sub-leading twist projections and three-particle Fock states of the $B$ meson and the pion are found to contribute at leading power. Even worse, some convolutions turn out to be divergent at the endpoints which renders the overlap-contribution incalculable similar to what we have seen in our discussion about power corrections in the context of non-leptonic decays in Section 1.2.4.

The non-factorization of soft and collinear effects in SCET$_{\mathrm{II}}$ and the related question about the correct treatment and interpretation of endpoint singularities is currently not completely understood. The problem does not only appear in energetic $B \to \pi$ transitions but also in the perturbative description of the pion form factor. In this case the soft-overlap contribution (*Feynman mechanism*) appears at sub-leading power. A solution within the effective theory approach would be a significant breakthrough on the conceptual level. Moreover, *if* the soft-overlap contribution could be expressed in terms of a few fundamental hadronic parameters, this would immediately lead to many interesting applications. This is to some extent realized in a recent approach from Manohar and Stewart [79] which we will discuss below. In any case, the problem of endpoint-divergences in SCET deserves further study which is the main motivation for our analysis in Chapter 5.

Let us briefly comment on two analyses of the overlap-contribution $\xi(q^2)$ in SCET. The first one has been performed by Neubert et al. [84] and is based on an extended formulation of $\text{SCET}_{\text{II}}$ [85] which includes additional degrees of freedom, so-called soft-collinear messenger modes, with momentum scaling $k_{sc} \sim (\lambda^2, \lambda^3, \lambda^4)$. These modes allow for a cross talk between the soft and the collinear sector of the theory as they can be exchanged between soft and collinear fields without bringing them far off-shell. Technically, these modes serve as a regulator of the divergent convolution integrals which leads to the following conclusion: If matrix elements involving messenger fields contribute at leading power to a hadronic matrix element, factorization into soft and collinear effects is spoilt.

While messenger modes provide a technical solution to calculate otherwise ill-defined quantities in perturbation theory, their physical interpretation in non-perturbative matrix elements remains obscure as virtualities with $k_{sc}^2 \sim \Lambda_{\text{QCD}}^3/m_b$ are below the confinement scale.

A second analysis of the overlap-contribution has been performed by Manohar and Stewart [79]. They propose a new type of factorization in $\text{SCET}_{\text{II}}$ which separates modes in their virtuality $k^2$ and in their rapidity $k_-$. Their method is based on a subtraction of zero-bin modes which is claimed to avoid double counting of soft and collinear modes in the effective theory. As a result a divergent convolution integral

$$\int_0^1 du \ \frac{\phi_\pi(u)}{u^2} \tag{1.30}$$

is replaced by

$$\int_0^1 du \ \frac{\phi_\pi(u)}{(u^2)_\emptyset} \equiv \int_0^1 du \ \frac{\phi_\pi(u) - u\,\phi_\pi'(0)}{u^2} + \phi_\pi'(0) \ \ln\frac{m_b}{\mu_-}, \tag{1.31}$$

where $\mu_-$ appears as the factorization scale in rapidity space. In [79] Manohar and Stewart present a factorization formula for the overlap-contribution $\xi(q^2)$ which involves leading and sub-leading twist as well as three-particle distribution amplitudes together with their derivatives at the endpoints (without the need to introduce soft-collinear messenger modes).

A still unresolved issue in this approach concerns the cancellation of the $\mu_-$ dependence which requires a more careful analysis of higher-order perturbative corrections beyond fixed-order perturbation theory. It is also to be emphasized that the quantities $\phi_\pi'(0)$, which naturally appear in this framework due to the $\emptyset$-distributions in (1.31), have to be interpreted as independent hadronic parameters since they cannot be derived from a finite number of moments of the distribution amplitude $\phi_\pi(u)$, see the argument in [59]. Unfortunately, the factorization formula loses some of its power in this way since it involves a larger number of new hadronic parameters. However, the approach from Manohar and Stewart has appeared very recently and deserves further investigations.

In our analysis in Chapter 5 we start from a different viewpoint. We consider heavy-to-light form factors between non-relativistic bound states which can be addressed in

fixed-order perturbation theory. As a consequence, all quantities in the factorization formula (1.28), in particular the overlap-contribution $\xi(q^2)$, can be calculated explicitly in our set-up. Our results shed further light on the physics of the soft-overlap contribution and also allow to address the proposals mentioned above.

# Chapter 2

# Perturbative corrections

In this chapter we address the technical aspects of the calculations that we discuss in the second part of this thesis. Most of the techniques that we present in the following have been developed within the last ten years, reflecting the steadily increasing effort in performing high precision calculations. We do not intent to give a review on multi-loop techniques but rather give a presentation from the perspective of our calculations in Chapter 3, 4 and 5 in the hope that the reader can get an idea what these calculations looked like in detail.

## 2.1 Strategy

We start with an outline of the general strategy that we have used to tackle the 1- and 2-loop calculations in Chapter 3, 4 and 5. The calculations have been performed on the basis of the computer algebra system MATHEMATICA. Unless otherwise stated, all routines have been written by ourselves. We emphasize that our algorithm is not restricted to calculations in the Standard Model. However, for calculations that are even more complex than our 2-loop calculation in Chapter 3 and 4, the efficiency of our algorithm should be improved. Our strategy consists of the following four steps:

**Step 1: Set-up for loop calculation**

We deal with up to 80 Feynman diagrams in our calculations. We first examine the kinematics of the process and calculate the colour factor of each diagram. In a 1-loop (2-loop) calculation we denote the loop momentum by $k$ $(k, l)$. The diagrams are expressed with the help of a minimal set of denominators $\mathcal{P}_i$ of propagators which we specify in each of our calculations in the second part of this thesis.

We use a general tensor decomposition to express all tensor integrals as linear combinations of scalar integrals $S_i$ multiplied by linearly independent tensors that can be formed out of the external momenta $p_i$ and the metric tensor $g$. For example in

the case of two external momenta $p_1$ and $p_2$, a 1-loop integral of rank $r = 2$ becomes

$$\int d^d k \ \frac{k^\mu k^\nu}{\mathcal{P}_1^{n_1} \dots \mathcal{P}_p^{n_p}} \ \equiv \ m^2 g^{\mu\nu} \, S_1 + p_1^\mu p_1^\nu \, S_2 + p_2^\mu p_2^\nu \, S_3 + (p_1^\mu p_2^\nu + p_1^\nu p_2^\mu) \, S_4, \quad (2.1)$$

reflecting the symmetry in $\mu \leftrightarrow \nu$ of the tensor integral which reduces the number of independent tensor structures from five to four in this example. In contrast to this a 2-loop tensor integral of rank $(r_k, r_l) = (1, 1)$ is decomposed into

$$\int d^d k \, d^d l \ \frac{k^\mu l^\nu}{\mathcal{P}_1^{n_1} \dots \mathcal{P}_p^{n_p}} \ \equiv \ m^2 g^{\mu\nu} \, S_1' + p_1^\mu p_1^\nu \, S_2' + p_2^\mu p_2^\nu \, S_3' + p_1^\mu p_2^\nu \, S_4' + p_1^\nu p_2^\mu \, S_5',$$

$$(2.2)$$

since the tensor integral has no manifest symmetry in $\mu \leftrightarrow \nu$ in this case. As the tensor decomposition becomes less trivial for higher ranks of the loop momenta, we develop a systematic decomposition in Section 2.2.

On the other hand we will see below that the reduction algorithm requires scalar projections $P_i$ of the tensor integrals as an input. In our first example from (2.1), we can form four different projections given by

$$\{P_1, P_2, P_3, P_4\} \ \equiv \ \int d^d k \ \frac{\{(kp_1)^2, (kp_1 kp_2), (kp_2)^2, (k^2)\}}{\mathcal{P}_1^{n_1} \dots \mathcal{P}_p^{n_p}}, \qquad (2.3)$$

whereas in the second example (2.2), there are five projections $P_i'$ which read

$$\{P_1', P_2', P_3', P_4', P_5'\} \ \equiv \ \int d^d k \, d^d l \ \frac{\{(kp_1)(lp_1), (kp_1)(lp_2), (kp_2)(lp_1), (kp_2)(lp_2), (kl)\}}{\mathcal{P}_1^{n_1} \dots \mathcal{P}_p^{n_p}}.$$

$$(2.4)$$

The scalar integrals $S_i$ and the projections $P_i$ are related by a linear system of equations which can be solved easily. This allows us to express each tensor integral in terms of projections $P_i$ which will be the subject of the second step.

**Step 2: Reduction to Master Integrals**

Our calculations are performed with the help of an automatized reduction algorithm which allows us to express the projections $P_i$ of the general form

$$\int d^d k \, d^d l \ \frac{\mathcal{S}_1^{m_1} \dots \mathcal{S}_s^{m_s}}{\mathcal{P}_1^{n_1} \dots \mathcal{P}_p^{n_p}} \qquad (2.5)$$

in terms of a small set of so-called Master Integrals (MIs). The $\mathcal{S}_i$ in (2.5) denote scalar products of a loop momentum with an external momentum or of two loop momenta as in the examples in (2.3) and (2.4). The reduction algorithm will be described in detail in Section 2.3. We emphasize that it makes the use of Dimensional Regularization (DR) mandatory for the calculation as anticipated by our notation writing $d$-dimensional integration measures.

Our interest to implement a reduction algorithm is threefold: First, multi-loop calculations as the one that we present in Chapter 3 and 4 are extremely complex including typically several thousands of integrals making an automatization indispensable. Second, even in less complicated 1-loop calculations as the one in Chapter 5 the algorithm is very helpful to avoid errors in the calculation as it is basically reduced to the computation of some MIs. Finally, the algorithm provides a powerful tool that can be used in the future for any kind of loop calculation as it is not based on certain Feynman rules but on particle propagators.

### Step 3: Manipulation of Dirac structures

With the loop integrations reduced to a minimal form, we consider the Dirac structures of the diagrams in the third step. We use the programme TRACER [86] for all manipulations concerning the Dirac algebra. We express all diagrams in terms of a minimal set of irreducible Dirac structures $D_i$. A generic diagram $\mathcal{D}_i$ takes the form

$$\mathcal{D}_i = \sum_{j,k} A_{ijk}(d)\, \mathrm{MI}_j\, D_k, \tag{2.6}$$

where we indicated that the coefficients $A_{ijk}$ depend on the dimension $d$. We do not go into the details concerning the reduction of the Dirac structures here as it depends on the considered calculation and represents in general only a minor problem.

The treatment of $\gamma_5$ in $d \neq 4$ dimensions requires special care. The matrix $\gamma_5$ enters our QCD calculations because of the weak vertices and/or the projection on pseudoscalar meson states. We apply the *Naive Dimensional Regularization* (NDR) scheme which treats $\gamma_5$ as a completely anticommuting object. Despite the fact that this scheme is algebraically inconsistent [87–89], it leads to correct results provided that we can avoid traces as $\mathrm{Tr}(\gamma^\mu\gamma^\nu\gamma^\rho\gamma^\sigma\gamma_5)$ [90].

### Step 4: Calculation of Master Integrals

The most difficult part finally consists in the calculation of the MIs. We have devoted Section 2.4 to this subject where we present several advanced techniques that we have found useful in our calculation. We are looking for a solution of the MIs in form of an expansion in $\varepsilon \equiv (4-d)/2$

$$\mathrm{MI}_i = \sum_j \frac{c_{ij}}{\varepsilon^j}. \tag{2.7}$$

Expanding (2.6) then determines the maximal order in the expansion of the MI that is required for the calculation. In our calculations, the expansion starts at most with double (quartic) poles due to soft and collinear IR singularities at the 1-loop (2-loop) level.

## 2.2   Decomposition of Tensor Integrals

The tensor decomposition has already been illustrated by means of a simple example in the last section. The procedure for more complicated tensor integrals is straightforward but starts to become involved for higher ranks $(r_k, r_l)$ in the 2-loop case. We therefore find it useful to present a systematic algorithm for the decomposition of 1- and 2-loop tensor integrals which can easily be extended to the multi-loop case.

**1-loop integrals**

We consider the decomposition of a 1-loop tensor integral of rank $r$

$$\int d^d k \quad \frac{k^{\mu_1} \dots k^{\mu_r}}{\mathcal{P}_1^{n_1} \dots \mathcal{P}_p^{n_p}} \tag{2.8}$$

according to $n$ external momenta $p_1, \dots, p_n$. Notice that the integral is totally symmetric under the exchange of any pair of indices $\mu_i \leftrightarrow \mu_j$.

We start with all tensors that can be formed out of $r$ external momenta $p_i$. In total there are $n^r$ tensors of this type with $\binom{n+r-1}{r}$ totally symmetric combinations. E.g. for $n = 2$ and $r = 3$ this results in $\binom{4}{3} = 4$ totally symmetric tensors which read

$$k^{\mu_1} k^{\mu_2} k^{\mu_3} \quad \rightarrow \quad p_1^{\mu_1} p_1^{\mu_2} p_1^{\mu_3}, \qquad p_1^{\mu_1} p_1^{\mu_2} p_2^{\mu_3} + p_1^{\mu_1} p_2^{\mu_2} p_1^{\mu_3} + p_2^{\mu_1} p_1^{\mu_2} p_1^{\mu_3},$$

$$p_1^{\mu_1} p_2^{\mu_2} p_2^{\mu_3} + p_2^{\mu_1} p_1^{\mu_2} p_2^{\mu_3} + p_2^{\mu_1} p_2^{\mu_2} p_1^{\mu_3}, \qquad p_2^{\mu_1} p_2^{\mu_2} p_2^{\mu_3}. \tag{2.9}$$

If $r \geq 2$, we continue with all tensors that can be formed out of $r - 2$ external momenta $p_i$ and one insertion of the metric tensor $g$. From the external momenta, we obtain $n^{r-2}$ combinations. Further, there are $\binom{r}{r-2}$ possible insertions of the metric tensor giving $\binom{r}{r-2} n^{r-2}$ tensors of this type. From these, $\binom{n+r-3}{r-2}$ are totally symmetric. In our example with $n = 2$ and $r = 3$ we thus find $\binom{2}{1} = 2$ totally symmetric tensors given by

$$k^{\mu_1} k^{\mu_2} k^{\mu_3} \quad \rightarrow \quad g^{\mu_1 \mu_2} p_1^{\mu_3} + g^{\mu_3 \mu_1} p_1^{\mu_2} + g^{\mu_2 \mu_3} p_1^{\mu_1},$$

$$g^{\mu_1 \mu_2} p_2^{\mu_3} + g^{\mu_3 \mu_1} p_2^{\mu_2} + g^{\mu_2 \mu_3} p_2^{\mu_1}. \tag{2.10}$$

The procedure continues if $r \geq 4$ with $r - 4$ external momenta $p_i$ and two insertions of the metric tensor $g$. We then find $\binom{n+r-5}{r-4}$ totally symmetric combinations etc.

We conclude that the tensor integral can be decomposed in this way according to

$$T(n; r) = \sum_{j=0}^{[r/2]} \binom{n + r - 1 - 2j}{r - 2j} \tag{2.11}$$

totally symmetric tensors where $[x]$ denotes the greatest integer less than or equal to $x$. The proof follows by complete induction, but we refrain from presenting it here. We refer to Table 2.1 for examples that are relevant in typical 1-loop calculations.

| $n \setminus r$ | 0 | 1 | 2 | 3 | 4 |
|---|---|---|---|---|---|
| 1 | 1 | 1 | 2 | 2 | 3 |
| 2 | 1 | 2 | 4 | 6 | 9 |
| 3 | 1 | 3 | 7 | 13 | 22 |

Table 2.1: *Number $T(n;r)$ of totally symmetric tensors of rank $r$ that can be formed out of $n$ external momenta and the metric tensor (relevant for the decomposition of 1-loop tensor integrals). The cases $T(2;2)$ and $T(2;3)$ have been discussed explicitly in Section 2.1 and 2.2, respectively.*

**2-loop integrals**

We come to the decomposition of a 2-loop tensor integral of rank $(r_k, r_l)$

$$\int d^d k \, d^d l \quad \frac{k^{\mu_1} \dots k^{\mu_{r_k}} \, l^{\nu_1} \dots l^{\nu_{r_l}}}{\mathcal{P}_1^{n_1} \dots \mathcal{P}_p^{n_p}} \tag{2.12}$$

according to $n$ external momenta $p_1, \dots, p_n$. In this case, the integral is totally symmetric under the exchange of any pair of indices $\mu_i \leftrightarrow \mu_j$ and $\nu_i \leftrightarrow \nu_j$.

We start with all products that can be formed out of a $r_k$-dimensional tensor with indices $\mu_1, \dots, \mu_{r_k}$ and $r_l$-dimensional tensor with $\nu_1, \dots, \nu_{r_l}$. From our analysis of 1-loop tensor integrals we conclude that we can form $T(n; r_k) \, T(n; r_l)$ tensors in this way which have the desired symmetry properties. To illustrate what we have obtained so far, we reconsider the case $n = 2$ and $(r_k, r_l) = (1, 1)$ which we introduced in Section 2.1. In this case, there are five independent tensors given by

$$k^\mu l^\nu \quad \rightarrow \quad p_1^\mu p_1^\nu, \quad p_2^\mu p_2^\nu, \quad p_1^\mu p_2^\nu, \quad p_1^\nu p_2^\mu, \quad g^{\mu\nu}, \tag{2.13}$$

whereas $T(2; 1) \, T(2; 1) = 4$ which corresponds to the first four tensors, only. We see that we have to add all contributions with metric tensors connecting the $\mu_i$ with the $\nu_j$. There are $T(n; r_k - 1) \, T(n; r_l - 1)$ combinations with one metric tensor respecting the symmetry constraint, $T(n; r_k - 2) \, T(n; r_l - 2)$ with two metric tensors etc.

We conclude that the tensor integral in (2.12) can be decomposed according to

$$T(n; r_k, r_l) = \sum_{j=0}^{\min(r_k, r_l)} T(n; r_k - j) \, T(n; r_l - j), \tag{2.14}$$

tensors respecting the symmetry in $\mu_i \leftrightarrow \mu_j$ and $\nu_i \leftrightarrow \nu_j$. We again refrain from presenting a proof and give an explicit example for illustration. Let us consider the

case $n = 2$ and $(r_k, r_l) = (2, 1)$. We find 10 independent tensors given by

$$k^{\mu_1} k^{\mu_2} l^{\nu} \quad \rightarrow \quad p_1^{\mu_1} p_1^{\mu_2} p_1^{\nu}, \qquad p_1^{\mu_1} p_1^{\mu_2} p_2^{\nu}, \qquad p_1^{\mu_1} p_2^{\mu_2} p_1^{\nu} + p_2^{\mu_1} p_1^{\mu_2} p_1^{\nu},$$

$$p_1^{\mu_1} p_2^{\mu_2} p_2^{\nu} + p_2^{\mu_1} p_1^{\mu_2} p_2^{\nu}, \qquad p_2^{\mu_1} p_2^{\mu_2} p_1^{\nu}, \qquad p_2^{\mu_1} p_2^{\mu_2} p_2^{\nu},$$

$$g^{\mu_1 \nu} p_1^{\mu_2} + g^{\mu_2 \nu} p_1^{\mu_1}, \qquad g^{\mu_1 \mu_2} p_1^{\nu},$$

$$g^{\mu_1 \nu} p_2^{\mu_2} + g^{\mu_2 \nu} p_2^{\mu_1}, \qquad g^{\mu_1 \mu_2} p_2^{\nu} \tag{2.15}$$

according to $T(2; 2, 1) = 4 \cdot 2 + 2 \cdot 1 = 10$. We refer to Table 2.2 for further examples that are relevant in typical 2-loop calculations.

| $r_k \setminus r_l$ | 0 | 1 | 2 | 3 | 4 |
|---|---|---|---|---|---|
| 0 | 1 | 1 | 2 | 2 | 3 |
| 1 | 1 | 2 | 3 | 4 | 5 |
| 2 | 2 | 3 | 6 | 7 | 10 |

| $r_k \setminus r_l$ | 0 | 1 | 2 | 3 | 4 |
|---|---|---|---|---|---|
| 0 | 1 | 2 | 4 | 6 | 9 |
| 1 | 2 | 5 | 10 | 16 | 24 |
| 2 | 4 | 10 | 21 | 34 | 52 |

Table 2.2: *Number $T(n; r_k, r_l)$ of tensors that can be formed out of $n$ external momenta and the metric tensor which are totally symmetric in the first $r_k$ and in the last $r_l$ indices. The tables correspond to $n = 1$ and $n = 2$ and are relevant for the decomposition of 2-loop tensor integrals. The cases $T(2; 1, 1)$ and $T(2; 2, 1)$ have been discussed explicitly in Section 2.1 and 2.2, respectively.*

## 2.3   Reduction to Master Integrals

The reduction algorithm is a very important element in our strategy for the calculation of higher order perturbative corrections. In principle it can be used for the reduction of any (scalar) loop integral but it reveals its full power only in the multi-loop case. To give an illustration, it served in our 2-loop calculation from Chapter 3 and 4 to express about 6.000 integrals in terms of 36 MIs which are in addition much simpler than the original integrals. Needless to say that this 2-loop calculation would have been (almost) impossible without the implementation of the reduction algorithm.

The starting point is the representation of a scalar loop integral in the form

$$\int d^d k \, d^d l \quad \frac{\mathcal{S}_1^{m_1} \dots \mathcal{S}_s^{m_s}}{\mathcal{P}_1^{n_1} \dots \mathcal{P}_p^{n_p}} \tag{2.16}$$

where the $\mathcal{S}_i$ are scalar products of a loop momentum with an external momentum or of two loop momenta. The $\mathcal{P}_i$ denote the denominators of propagators and the exponents fulfil $n_i, m_i \geq 0$. We focus on 2-loop integrals in the following with obvious simplifications (extensions) in the 1-loop (multi-loop) case. Notice that an integral can have different representations in terms of $\{\mathcal{S}, \mathcal{P}, n, m\}$ because of the freedom to shift loop momenta in DR. In fact the underlying topology, i.e. the interconnection of propagators and external momenta, uniquely defines the integral. In the following we (loosely) use the word topology in order to classify the integrals. An integral with $t$ different propagators $\mathcal{P}_i$ with $n_i > 0$ is called a $t$-topology.

### Preliminaries

We first classify the scalar products $\mathcal{S}_i$ into reducible and irreducible scalar products. The reducible scalar products can be written as linear combinations of denominators $\mathcal{P}_i$ which leads to the first simplification. This is sometimes called *Passarino-Veltman Reduction* [91] which represents a standard tool for the computation of loop integrals. Since it appears as a preliminary step in our reduction algorithm, we briefly illustrate the idea by means of a simple example.

We consider the following 5-topology

$$\int d^d k \, d^d l \quad \frac{kp}{k^2(k+p)^2(k-l)^2(l+p)^2 l^2} \quad \equiv \quad kp \; \underset{}{\longrightarrow}\hspace{-0.3em}\bigcirc\hspace{-0.3em}\underset{}{\longleftarrow} \tag{2.17}$$

where the right-hand side shows the underlying topology of the integral. We use dashed internal lines for massless propagators. The solid external line corresponds to the virtuality $p^2$ of the incoming momentum $p$ in this case. As the figure on the right-hand side reflects the denominator of the integral only, the scalar products in the numerator appear explicitly in our notation.

The scalar product turns out to be reducible in this case, as

$$kp \; = \; \frac{1}{2}\Big[(k+p)^2 - k^2 - p^2\Big] \tag{2.18}$$

which gives rise to



$$\tag{2.19}$$

Notice that the first two integrals on the right-hand side correspond to simpler 4-topologies and that the last one has a trivial numerator. Moreover, the advantage of our notation becomes obvious in (2.19) as it allows us to recognize easily that the first two integrals are topologically equivalent. This brings us to



$$\tag{2.20}$$

All reducible scalar products can be rewritten along these lines. We may therefore concentrate on integrals of the form (2.16) with irreducible scalar products in the numerator. In the 1-loop case there are $n+1$ scalar products $S_i$ which can be formed out of $n$ external momenta and the loop momentum: $\{kp_1, \ldots, kp_n, k^2\}$. For a 1-loop $t$-topology we thus find $n+1-t$ irreducible scalar products. In the 2-loop case the irreducible scalar products amount to $2n+3-t$. This implies that in our example discussed above ($n=1$, $t=5$) all scalar products $S_i$ are in fact reducible.

**Integration-by-parts identities**

The core of the reduction algorithm consists in the use of integration-by-parts (IBP) identities [92,93] which follow from the fact that surface terms vanish in DR

$$\int d^d k \, d^d l \;\; \frac{\partial}{\partial v^\mu} \, \frac{\mathcal{S}_1^{m_1} \ldots \mathcal{S}_s^{m_s}}{\mathcal{P}_1^{n_1} \ldots \mathcal{P}_p^{n_p}} \; = \; 0, \qquad v \in \{k, l\}. \tag{2.21}$$

In order to obtain scalar identities one may contract (2.21) with any loop or external momentum under the integral before performing the derivative. In the 1-loop (2-loop) case this generates $n+1$ ($2n+4$) identities from each integral.

We illustrate the use of IBP identities by means of the famous example from Chetyrkin and Tkachov [92,93]. Let us consider the integral

$$\int d^d k \, d^d l \;\; \frac{1}{k^2(k+p)^2(k-l)^2(l+p)^2 l^2} \;\; \equiv \;\; \text{} \tag{2.22}$$

which can be reduced with the help of the following IBP identity

$$\int d^d k \, d^d l \;\; \frac{\partial}{\partial k^\mu} \; (k-l)^\mu \; \frac{1}{k^2(k+p)^2(k-l)^2(l+p)^2 l^2} \; = \; 0. \tag{2.23}$$

We perform the derivatives explicitly on the integrand which leads to

$$d \quad \text{<image>} \quad - 2k \cdot (k - l) \quad \text{<image>}$$

$$- 2(k + p) \cdot (k - l) \quad \text{<image>} \quad - 2(k - l)^2 \quad \text{<image>} \quad = \quad 0 \qquad (2.24)$$

where the dotted propagators are taken to be squared. The scalar products can be reduced with the help of the Passarino-Veltman Reduction to give

$$-2k \cdot (k - l) \quad \text{<image>} \quad = \quad -2(k + p) \cdot (k - l) \quad \text{<image>}$$

$$= \quad \text{<image>} \quad - \quad \text{<image>} \quad - \quad \text{<image>}$$

$$-2(k - l)^2 \quad \text{<image>} \quad = -2 \quad \text{<image>} \qquad (2.25)$$

Combining (2.24) and (2.25) yields the famous result

$$\text{<image>} \quad = \quad \frac{2}{d - 4} \left[ \quad \text{<image>} \quad - \quad \text{<image>} \quad \right]. \qquad (2.26)$$

The original 5-topology has thus been reduced to two 4-topologies, the first of them being particulary simple as it represents a product of two 1-loop integrals.

**Lorentz-invariance identities**

It has been pointed out in [94] that similar Lorentz-invariance (LI) identities can be formulated which become important in problems with many external momenta (multi-leg integrals). The LI identities exploit the fact that the integrals in (2.16) transform as scalars under a Lorentz-transformation of the external momenta. In this way one may generate up to six identities from each integral depending on the number of external momenta.

As the LI identities are of minor importance in our calculations, we refer to [94] for a detailed description. In our applications in Chapter 3, 4 and 5, we deal with two external momenta $p, q$ which leads to one LI identity per integral given by

$$\int d^d k \, d^d l \, \left[ p \cdot q \left( p^\mu \frac{\partial}{\partial p^\mu} - q^\mu \frac{\partial}{\partial q^\mu} \right) + q^2 \, p^\mu \frac{\partial}{\partial q^\mu} - p^2 \, q^\mu \frac{\partial}{\partial p^\mu} \right] \frac{\mathcal{S}_1^{m_1} \dots \mathcal{S}_s^{m_s}}{\mathcal{P}_1^{n_1} \dots \mathcal{P}_p^{n_p}} \quad = \quad 0. \tag{2.27}$$

**Reduction algorithm**

As we have seen in our explicit example, the identities relate various integrals of the form (2.16) with different exponents $\{n, m\}$. In general each of the identities contains the so-called *seed integral* which has been used to generate the identity, simpler integrals with smaller $\{n, m\}$ and more complicated integrals with larger $\{n, m\}$. The identity is then used to reduce the most complicated integral rather than the seed integral itself.

We do not want to inspect single identities but are looking for an automatized reduction algorithm which exploits the full power of IBP and LI identities. This can be achieved in a bottom-up approach generating systematically all identities from all sub-topologies of a given integral. In the 2-loop case, we thus start with the identities from all 2-topologies, 3-topologies etc. which leads to a large set of identities which contains the integral that we are interested in beneath simpler and more complicated ones. If we were to use all unknown integrals that appear in these identities again as seed integrals, the procedure would be without end as we generate identities with more and more complicated integrals in each step. It was an important observation from Laporta that the number of identities grows faster than the number of unknown integrals in this procedure. At some point we may therefore stop the generation of new identities and solve the (apparently) over-constrained system of equations by expressing more complicated integrals in terms of simpler ones. Not all of the identities being linearly independent, some integrals finally turn out to be irreducible to which we refer as MIs.

The choice of the point where to stop the outlined procedure requires thorough experimentation. On the one hand we want the system of equations to be large enough to be sure that the remnant integrals in the reduction procedure are indeed irreducible. On the other hand the system should be as small as possible to assure an optimized realization of the reduction algorithm. Based on his own experiences Laporta proposed a "golden rule" for the choice of such a cutoff in [95] which we have found very useful.

In our calculation we typically deal with systems of equations made of several thousands equations. The solution being straight-forward, the runtime of the reduction algorithm depends strongly on the order in which the equations are solved. As a guideline for an efficient implementation we have followed the algorithm described in [95].
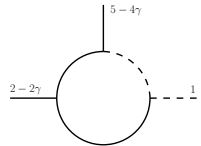
## 2.4 Calculation of Master Integrals

We now present a collection of techniques that we have used for the calculation of the MIs. This last step in our strategy from Section 2.1 represents the most difficult part of the perturbative calculation. We always intended to compute all MIs with two independent methods in order to become sure of the correctness of our results.

We illustrate the calculation techniques with two explicit examples: The first one corresponds to a 1-loop integral that appears in our calculation from Chapter 5, the second one to a 2-loop integral from Chapter 3 and 4. Albeit this section has become somewhat lengthy in this way, we think that it is instructive to present the calculation of these integrals with different methods. In both cases we have chosen simple (but non-trivial) examples which allow for a transparent presentation of the central aspects of the techniques. Despite being simple, the examples cover most of the conceptually interesting features.

**1-loop example: Definition**

In the first example we consider a 3-topology
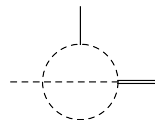
$$\int [dk] \ \frac{1}{[(mw' - mw + k)^2 - m^2][k^2 - m^2](k - mw')^2} \quad \equiv \quad \text{} \quad (2.28)$$

with $w^2 = w'^2 = 1$ and $w \cdot w' = \gamma > 1$. In our analysis in Chapter 5, we focus on the leading power in an expansion in $m/M$ where $M$ is the mass of a heavy quark and $m$ the mass of a light (non-relativistic) quark. The parameter $\gamma$ corresponds to the large boost between the rest frames of the bound states and scales as $\gamma = \mathcal{O}(M/m)$. In (2.28) we used dashed/solid internal lines for massless/massive propagators. Dashed/solid external lines denote virtualities of $\mathcal{O}(m^2)/\mathcal{O}(mM)$ which are written explicitly here as multiples of $m^2$. The normalization of the integral reads

$$[dk] \equiv \frac{\Gamma(1 - \varepsilon)}{i\pi^{d/2}} \ d^d k. \quad (2.29)$$

**2-loop example: Definition**

In the 2-loop case we consider a massless 4-topology

$$\int [dk] \, [dl] \ \frac{1}{(p - q - l)^2 (uq + l)^2 (p - q - k - l)^2 (\bar{u}q + k)^2} \quad \equiv \quad \text{} \quad (2.30)$$

with $0 \leq u \leq 1$, $\bar{u} = 1 - u$, $p^2 = 2p \cdot q = m^2$ and $q^2 = 0$. The usual $i\varepsilon$-prescription of propagators is understood. Internal dashed lines correspond to massless propagators and dashed/solid/double external lines to virtualities $0/um^2/m^2$, respectively[1].

---

[1]Notice that $m$ denotes the mass of the $b$-quark in this case, whereas the light quarks are considered massless.

### 2.4.1   Feynman Parameters

The standard method to compute loop integrals introduces Feynman parameters. As this approach is not practicable for most of our MIs, we do not describe this method here in detail. However, it turns out that our simple examples can be solved with this technique. We comment briefly on the calculations and quote their results which will serve as a reference for the other calculations.

**1-loop example: Feynman Parameters**

As we deal with a 3-topology, we introduce two Feynman parameters and obtain

$$
\raisebox{-1em}{\includegraphics{diagram}} \quad = \quad \int_0^1 dx \int_0^{1-x} dy \ \frac{-(m^2)^{-1-\varepsilon}\,\Gamma(1-\varepsilon)\,\Gamma(1+\varepsilon)}{[(5-4\gamma)x^2 + y^2 + 2(2-\gamma)xy + 4(\gamma-1)x]^{1+\varepsilon}}.
$$
(2.31)

The integral is ultraviolet (UV) and infrared (IR) finite. We focus on the leading term in the $\varepsilon$-expansion which allows us to set $\varepsilon = 0$. The integral can then be solved in a closed form in $m/M$, but we refrain from presenting the exact result since it looks rather complicated. We are only interested in the leading power of the $m/M$ expansion which takes a simple form

$$
\raisebox{-1em}{\includegraphics{diagram}} \quad \simeq \quad -\frac{1}{4\gamma m^2}\left[2\ln 2\ln\gamma + \ln^2 2 + \frac{\pi^2}{3} + \mathcal{O}(\varepsilon)\right].
$$
(2.32)

Notice that we cannot expand the integrand in (2.31) in $m/M$ before performing the parameter integrals as this would invoke IR singularities for $x \to 0$. In other words, the two expansions in $\varepsilon$ and $m/M$ do not commute with each other which complicates the extraction of the leading power.

**2-loop example: Feynman Parameters**

In this example, we introduce three Feynman parameters but one of these integrations can be done trivially. We obtain

$$
\raisebox{-1em}{\includegraphics{diagram}} \quad = \quad (m^2)^{-2\varepsilon}\,e^{2i\pi\varepsilon}\,\frac{\Gamma(2\varepsilon)\,\Gamma(1-\varepsilon)^4}{\Gamma(2-2\varepsilon)}
$$
(2.33)

$$
\int_0^1 dx \int_0^{1-x} dy \ \ x^{\varepsilon-1}(1-x-y)^{-2\varepsilon}(x+uy)^{-2\varepsilon}.
$$

The integral exhibits a double pole in $\varepsilon$ reflected by the factor $\Gamma(2\varepsilon)$ and a second singularity from $x \to 0$. The solution can be found in a closed form in $\varepsilon$ in terms of

an hypergeometric function and reads

$$
\text{\fbox{}} \;=\; (m^2)^{-2\varepsilon}\, e^{2i\pi\varepsilon}\, \frac{2\,\Gamma(-2\varepsilon)\,\Gamma(1-\varepsilon)^5}{\Gamma(2-2\varepsilon)\,\Gamma(2-3\varepsilon)} \tag{2.34}
$$

$$
\left[\Gamma(2\varepsilon)\, {}_2F_1(1,2\varepsilon;1+\varepsilon;u) - \varepsilon\Gamma(\varepsilon)^2\, u^{-\varepsilon}\bar{u}^{-\varepsilon}\right].
$$

The integral enters our calculations from Chapter 3 and 4 up to $\mathcal{O}(\varepsilon^2)$, but we restrict our attention to the first three coefficients here. Notice that the calculation of the imaginary part essentially requires one coefficient less in the $\varepsilon$-expansion. The hypergeometric function can be expanded with the help of the MATHEMATICA package HYPEXP [96] which yields

$$
\text{\fbox{}} \;=\; (m^2)^{-2\varepsilon}\, e^{2i\pi\varepsilon}\left[\frac{1}{2\varepsilon^2} + \left(\frac{5}{2} - \ln u\right)\frac{1}{\varepsilon} + \frac{19}{2} - \frac{\pi^2}{6}\right. \tag{2.35}
$$

$$
\left. + \mathrm{Li}_2(u) + \frac{1}{2}\ln^2 u + \ln u \ln \bar{u} - 5\ln u + \mathcal{O}(\varepsilon)\right].
$$

## 2.4.2 Method of Differential Equations

The method of differential equations [28,29] in combination with the formalism of harmonic polylogarithms (HPLs) [30] turned out to be extremely useful for our 2-loop calculation from Chapter 3 and 4. The method is based on the reduction algorithm that we presented in Section 2.3 and can therefore only be applied with such an algorithm at hand.

In the following we start with a general description of the method, introduce the HPLs and comment briefly on the calculation of the boundary conditions to the differential equations. Finally, we apply this method to our explicit 2-loop example. We do not use this technique in our 1-loop calculation from Chapter 5 where we focus on the extraction of the leading power in $m/M$. We therefore refrain from calculating our 1-loop example with this method.

### Solving loop-integrals with differential equations

The MIs are functions of the physical scales of the process which are given by scalar products of the external momenta and masses of the particles. In our calculations most of our MIs depend on two scales which give rise to one dimensionless ratio: $\gamma$ ($u$) in our 1-loop (2-loop) example. We therefore restrict our attention to the case that there are only two distinct scales in the process with obvious modifications for the general case. We denote the ratio of the two scales by $u$ and recall the general form (2.16) of a MI

$$
\mathrm{MI}_i(u) = \int d^d k\, d^d l \;\; \frac{\mathcal{S}_1^{m_1}\ldots\mathcal{S}_s^{m_s}}{\mathcal{P}_1^{n_1}\ldots\mathcal{P}_p^{n_p}} \tag{2.36}
$$

We perform the derivative with respect to $u$ and interchange the order of integration and derivation

$$\frac{\partial}{\partial u} \, \mathrm{MI}_i(u) = \int d^d k \, d^d l \quad \frac{\partial}{\partial u} \, \frac{\mathcal{S}_1^{m_1} \ldots \mathcal{S}_s^{m_s}}{\mathcal{P}_1^{n_1} \ldots \mathcal{P}_p^{n_p}}. \tag{2.37}$$

The right-hand side being of the same type as the IBP and LI identities in (2.21) and (2.27), this procedure again leads to a sum of various integrals with different exponents $\{n, m\}$. With the help of the reduction algorithm, these integrals can be expressed in terms of MIs which yields a differential equation of the form

$$\frac{\partial}{\partial u} \, \mathrm{MI}_i(u) = a(u; d) \, \mathrm{MI}_i(u) + \sum_{j \neq i} b_j(u; d) \, \mathrm{MI}_j(u), \tag{2.38}$$

where we indicated that the coefficients $a$ and $b_j$ depend on the dimension $d$. The inhomogeneity of the differential equation typically contains MIs of sub-topologies which are supposed to be known in a bottom-up approach. In some cases few MIs in the inhomogeneous part are of the same topology as the MI on the left hand side of (2.38) and thus unknown. Writing down the differential equations for these MIs, we find that we are left with a coupled system of linear, first order differential equations.

We are looking for a solution of the differential equation in form of an expansion

$$\mathrm{MI}_i(u) = \sum_j \frac{c_{ij}(u)}{\varepsilon^j}. \tag{2.39}$$

Expanding (2.38) then gives much simpler differential equations for the coefficients $c_{ij}$ which can be solved order by order in $\varepsilon$. The solution of the homogeneous equations is in general straight-forward. The inhomogeneous equations can then be addressed with the method of the variation of the constant. This in turn leads to indefinite integrals over the inhomogeneities which typically contain products of rational functions with logarithms or related functions as dilogarithms. With the help of the formalism of HPLs these integrations simplify substantially.

**Harmonic Polylogarithms**

The HPLs have been introduced in [30] and several extensions of the formalism have been considered in [97–99]. We briefly summarize their basic features here, focussing on the properties that are relevant for our 2-loop calculation in Chapter 3 and 4.

The HPLs, denoted by $H(\vec{m}_w; x)$, are described by a $w$-dimensional vector $\vec{m}_w$ of parameters and by its argument $x$. In their simplest form, the parameters can take the values 0 and $\pm 1$. The basic definitions of the HPLs are for weight $w = 1$

$$H(0; x) \equiv \ln x,$$

$$H(1; x) \equiv -\ln(1 - x),$$

$$H(-1; x) \equiv \ln(1 + x) \tag{2.40}$$

and for weight $w > 1$

$$H(a, \vec{m}_{w-1}; x) \equiv \int_0^x dx' \, f(a; x') \, H(\vec{m}_{w-1}; x'), \tag{2.41}$$

where the basic functions $f(a; x)$ are given by

$$f(0; x) \equiv \frac{d}{dx} H(0; x) = \frac{1}{x},$$

$$f(1; x) \equiv \frac{d}{dx} H(1; x) = \frac{1}{1 - x},$$

$$f(-1; x) \equiv \frac{d}{dx} H(-1; x) = \frac{1}{1 + x}. \tag{2.42}$$

In the case $\vec{m}_w = \vec{0}_w$, the definition in (2.41) does not apply and the HPLs read

$$H(0, \ldots, 0; x) \equiv \frac{1}{w!} \ln^w x. \tag{2.43}$$

The HPLs form a closed, linearly independent set under integrations over the basic functions $f(a; x)$ and fulfil an algebra such that a product of two HPLs of weight $w_1$ and $w_2$ gives a linear combination of HPLs of weight $w = w_1 + w_2$.

As anticipated above, the solution of the differential equation typically leads to integrals over products of rational functions with transcendental functions as logarithms or dilogarithms. More precisely, we often encounter integrals of the type

$$\int^x dx' \left\{ \frac{1}{x'}, \frac{1}{1 - x'}, \frac{1}{1 + x'} \right\} H(\vec{m}_w; x') \tag{2.44}$$

which become trivial within the formalism of HPLs as they simply correspond to an HPL of weight $w + 1$ according to (2.41). Further integrals take e.g. the form

$$\int^x dx' \left\{ 1, \frac{1}{x'^2}, \frac{1}{(1 - x')^2}, \frac{1}{(1 + x')^2} \right\} H(\vec{m}_w; x'). \tag{2.45}$$

The solution of these integrals is also straight-forward within the formalism of HPLs as an integration-by-parts relates them either to an HPL of weight $w+1$ or gives rise to a simple recurrence relation. Not surprisingly, the pattern in (2.44) and (2.45) does not apply to all integrals that we encounter in our 2-loop calculation from Chapter 3 and 4. However, a large part of this lengthy calculation can be performed along these lines.

Furthermore, the formalism of HPLs helps us to avoid the problem of "hidden zeros". Let us illustrate this point with a simple example. In our calculation we may obtain the result

$$\left[ \text{Li}_2(u) + \text{Li}_2(\bar{u}) + \ln u \ln \bar{u} - \frac{\pi^2}{6} \right] \frac{1}{\varepsilon} \tag{2.46}$$

and be surprised that it contains a singularity. A closer look reveals that it is indeed free of any singularities since (2.46) vanishes identically. This can be seen easily when we rewrite the second dilogarithm in the form

$$\mathrm{Li}_2(\bar{u}) = \frac{\pi^2}{6} - \ln u \ln \bar{u} - \mathrm{Li}_2(u). \qquad (2.47)$$

We therefore call (2.46) a "hidden zero". In complicated multi-loop calculations with HPLs of higher weight and various arguments, it might become difficult to identify "hidden zeros". In order to avoid this problem, it is important to use a formulation in terms of a minimal set of transcendental functions. The HPLs provide such a minimal set. To give an example, in our 2-loop calculation from Chapter 3 we were able to express our results in terms of the following HPLs

$$H(0; u) = \ln u,$$

$$H(1; u) = -\ln(1 - u),$$

$$H(0, 1; u) = \mathrm{Li}_2(u),$$

$$H(0, 0, 1; u) = \mathrm{Li}_3(u),$$

$$H(0, 1, 1; u) = \mathrm{S}_{1,2}(u). \qquad (2.48)$$

**Comment on boundary conditions**

A unique solution of a differential equation requires the knowledge of its boundary conditions. In the considered case the boundary conditions typically represent single-scale integrals corresponding to $u = 0, 1$. It is of crucial importance that the integral has a smooth limit at the chosen point such that setting $u = 0$ or $u = 1$ does not modify the divergence structure introduced in (2.39).

The boundary conditions can be addressed with any method presented in this section. In some cases the calculation becomes trivial as they correspond to simpler topologies which may turn out to be reducible. If so, the integral can be expressed in terms of known MIs with the help of the reduction algorithm. For the more complicated integrals this is not the case and the calculation of the boundary conditions represents sometimes the most difficult part in the computation of the MIs.

**2-loop example: Method of Differential Equations**

With the help of the reduction algorithm we derive the following differential equation

$$\frac{\partial}{\partial u} \; \text{} \; = \; \frac{1 - 2u}{2u\bar{u}} \, (d - 4) \; \text{} \; + \; \frac{3d - 8}{2u\bar{u}m^2} \; \text{} \qquad (2.49)$$

where the inhomogeneous part contains a 3-topology which is supposed to be known

$$\text{} \; = \; (m^2)^{1-2\varepsilon} \, e^{2i\pi\varepsilon} \, \frac{\Gamma(-1 + 2\varepsilon)\Gamma(1 - \varepsilon)^5}{\Gamma(3 - 3\varepsilon)}. \qquad (2.50)$$

Concerning the boundary conditions, we examine if the integral has a smooth limit for $u \to 0, 1$. From (2.33) we see that setting $u = 0$ modifies the divergence structure of the integral in the form $x^{\varepsilon-1} \to x^{-\varepsilon-1}$, whereas $u = 1$ does not. We therefore use the latter boundary condition which corresponds to a reducible topology

$$
\text{(diagram)} = \frac{3d-8}{(d-4)m^2} \quad \text{(diagram)} = (m^2)^{-2\varepsilon}\, e^{2i\pi\varepsilon} \left[ \frac{1}{2\varepsilon^2} + \frac{5}{2\varepsilon} + \frac{19}{2} + \mathcal{O}(\varepsilon) \right]
$$
(2.51)

We solve the differential equation (2.49) order by order in $\varepsilon$ with the ansatz

$$
\text{(diagram)} = (m^2)^{-2\varepsilon}\, e^{2i\pi\varepsilon} \left\{ \sum_{i=-4}^{0} c_i(u)\, \varepsilon^i + \mathcal{O}(\varepsilon) \right\}.
$$
(2.52)

Notice that the differential equation has a particular simple structure in our example because of the explicit factor $(d-4) = \mathcal{O}(\varepsilon)$. However, the non-trivial element in the solution of the differential equation consists in the integration over the inhomogeneity which can be illustrated here. In the lowest order, we simply find

$$
\frac{\partial}{\partial u}\, c_{-4}(u) = 0 \qquad \to \qquad c_{-4}(u) = \text{const}
$$
(2.53)

and the comparison with (2.51) leads to $c_{-4}(u) = 0$. The computation of $c_{-3}$ follows exactly the same lines. The first non-vanishing coefficient is $c_{-2}$ which again obeys

$$
\frac{\partial}{\partial u}\, c_{-2}(u) = 0 \qquad \to \qquad c_{-2}(u) = \text{const},
$$
(2.54)

but the boundary condition (2.51) yields $c_{-2}(u) = \frac{1}{2}$. From now on, the differential equations take a non-trivial form which perfectly fit into the formalism of HPLs

$$
\frac{\partial}{\partial u}\, c_{-1}(u) = -\frac{1}{u} \qquad \to \qquad c_{-1}(u) = -H(0; u) + \text{const.}
$$
(2.55)

The boundary condition results in $c_{-1}(u) = \frac{5}{2} - H(0; u)$. In the next step, we have

$$
\frac{\partial}{\partial u}\, c_0(u) = \left( \frac{1}{u} - \frac{1}{\bar{u}} \right) H(0; u) - \frac{5}{u}
$$

$$
\to \qquad c_0(u) = H(0, 0; u) - H(1, 0; u) - 5H(0; u) + \text{const.}
$$
(2.56)

The comparison with (2.51) gives $c_0(u) = \frac{19}{2} - \frac{\pi^2}{6} + H(0, 0; u) - H(1, 0; u) - 5H(0; u)$ which can be expressed in terms of the minimal set (2.48) with the help of

$$
H(0, 0; u) = \frac{1}{2} H(0; u)^2,
$$

$$
H(1, 0; u) = H(0; u)H(1; u) - H(0, 1; u).
$$
(2.57)

Collecting all coefficients $c_i$ and using (2.52) with (2.48), we finally reproduce our result from (2.35). It is evident that this MI has been particularly simply but it nevertheless illustrated the usefulness of the HPLs in this context.

## 2.4.3   Expansion by Momentum Regions

The method of expansion by regions [31] is one of the most powerful techniques to determine loop integrals to leading power in some small expansion parameter. We have already pointed out that the extraction of the leading power would simplify substantially if we could interchange the order of loop integration and power expansion. However, we have seen in the analysis of our 1-loop example after (2.32) that this procedure may generate artificial IR singularities which invalidates this naive approach.

We will see in this section that we *can* do so if we split the loop integration into individual momentum regions and expand the integrands in each region separately. This in turn generates artificial singularities in each region which cancel when we reconstruct the full integral as the sum over all regions. When the calculation is performed within DR, no further cutoffs are required to separate the momentum regions due to the fact that scaleless integrals vanish in DR. We now switch to our explicit 1-loop example to demonstrate how this technique works in detail.

**1-loop example: Expansion by Momentum Regions**

We first address a power-counting to the external momenta and particle masses in the problem. We adopt the SCET terminology from Table 1.1 in our example by identifying $\lambda^2 \equiv m/M$ in the non-relativistic set-up. The momentum of the spectator antiquark in the initial bound state corresponds to a soft momentum with $mw = (m, 0, m) \sim (\lambda^2, 0, \lambda^2)$ whereas the quark and antiquark in the final bound state are in a collinear configuration with $mw' = (2\gamma m, 0, m/2\gamma) \sim (1, 0, \lambda^4)$. Notice that this parametrization fulfils the conditions $w^2 = w'^2 = 1$, $w \cdot w' \simeq \gamma \sim 1/\lambda^2$ (transverse components are suppressed in the non-relativistic approach).

We want to compute the leading power in $\lambda$ of the integral

$$-\bigcirc\!\!\!-- = \int [dk] \; \frac{1}{[(mw' - mw + k)^2 - m^2][k^2 - m^2](k - mw')^2} \qquad (2.58)$$

Potential leading contributions come from hard, hard-collinear, soft and collinear momentum configurations of the particles in the loop. We may also look for contributions from soft-collinear messenger modes as discussed in Section 1.3.2. We perform a power counting of the integral in the individual momentum regions of the loop momentum $k$. This gives rise to the following pattern

$$
\begin{array}{lll}
\text{hard} & (1, 1, 1) & 0 - 0 - 0 - 0 = 0, \\[4pt]
\text{hard-collinear} & (1, \lambda, \lambda^2) & 4 - 2 - 2 - 2 = -2, \\[4pt]
\text{soft} & (\lambda^2, \lambda^2, \lambda^2) & 8 - 2 - 4 - 2 = 0, \\[4pt]
\text{collinear} & (1, \lambda^2, \lambda^4) & 8 - 2 - 4 - 4 = -2, \\[4pt]
\text{soft-collinear} & (\lambda^2, \lambda^3, \lambda^4) & 12 - 2 - 4 - 4 = 2.
\end{array}
\qquad (2.59)
$$

The first term in each region comes from the scaling of the integration measure and the other terms from the three propagators. We find a leading contribution of $\mathcal{O}(1/\lambda^2)$ which stems from the hard-collinear and the collinear momentum region.

We first address the hard-collinear region. As anticipated above, we expand the integrand in this region counting $k \sim (1, \lambda, \lambda^2)$ and do not need to introduce additional cutoffs in DR. The hard-collinear contribution becomes

$$
\simeq \frac{\Gamma(1-\varepsilon)}{2i\pi^{d/2}} \int dk_- \, dk_+ \, d^{d-2}k_\perp \quad \frac{1}{[k_+ k_- + k_\perp^2 - 2\gamma m k_+ + i\varepsilon]}
$$

$$
\frac{1}{[k_+ k_- + k_\perp^2 + 2\gamma m(k_+ - m) - m k_- + i\varepsilon][k_+ k_- + k_\perp^2 + i\varepsilon]} \quad (2.60)
$$

where we have made the $i\varepsilon$-prescription of the propagators explicit and translated the $d$-dimensional integration measure from (2.29) into light-cone coordinates. We first perform the $k_-$ integration by contour methods. As all poles lie in the upper (lower) half plane for $k_+ < 0$ ($k_+ > m$), the only non-vanishing contribution comes from $0 < k_+ < m$. In this case one of the poles lies in the upper half plane and the two others in the lower one which yields

$$
\simeq \frac{\Gamma(1-\varepsilon)}{\pi^{d/2-1}} \int_0^m dk_+ \quad \frac{k_+ - m}{m^2}
$$

$$
\int d^{d-2}k_\perp \quad \frac{1}{[k_\perp^2 - 4\gamma k_+(m - k_+)][k_\perp^2 - 2\gamma k_+(m - k_+)]}. \quad (2.61)
$$

The remnant integrations are straight-forward and give

$$
\simeq -\frac{\Gamma(1-\varepsilon)\,\Gamma(1+\varepsilon)}{m^2} \frac{1 - 2^{-\varepsilon}}{\varepsilon} \int_0^m dk_+ \, (2\gamma k_+)^{-1-\varepsilon} \, (m - k_+)^{-\varepsilon}
$$

$$
= -(2\gamma m^2)^{-1-\varepsilon} \frac{4^\varepsilon - 2^\varepsilon}{\varepsilon} \frac{\Gamma(1-\varepsilon)\,\Gamma(1+\varepsilon)\,\Gamma(1/2)\,\Gamma(-\varepsilon)}{\Gamma(1/2 - \varepsilon)}
$$

$$
= -\frac{1}{4\gamma m^2} \left[ -\frac{2\ln 2}{\varepsilon} + 2\ln 2 \ln(\gamma m^2) + 3\ln^2 2 + \mathcal{O}(\varepsilon) \right]. \quad (2.62)
$$

Now we consider the collinear region counting $k \sim (1, \lambda^2, \lambda^4)$

$$
\simeq \frac{\Gamma(1-\varepsilon)}{2i\pi^{d/2}} \int dk_- \, dk_+ \, d^{d-2}k_\perp \quad \frac{1}{[k_+ k_- + k_\perp^2 - m^2 + i\varepsilon]} \quad (2.63)
$$

$$
\frac{1}{[-m k_- - 2\gamma m^2 + i\varepsilon][k_+ k_- + k_\perp^2 - 2\gamma m k_+ - m k_-/(2\gamma) + m^2 + i\varepsilon]}
$$

We perform the $k_+$-integration with contour methods and find a contribution for $0 < k_- < 2\gamma m$. The other integrations are again straight-forward.

$$
\simeq \frac{\Gamma(1-\varepsilon)}{\pi^{d/2-1}} \int_0^{2\gamma m} dk_- \; \frac{1}{2\gamma m^2(k_- + 2\gamma m)} \; \frac{d^{d-2}k_\perp}{[k_\perp^2 - (m - k_-/(2\gamma))^2]}
$$

$$
= -\frac{\Gamma(1-\varepsilon)\,\Gamma(\varepsilon)}{2\gamma m^2} \int_0^{2\gamma m} dk_- \; (k_- + 2\gamma m)^{-1} \; (m - k_-/(2\gamma))^{-2\varepsilon}
$$

$$
= -\frac{\Gamma(1-\varepsilon)\,\Gamma(\varepsilon)}{2\gamma m^2} \; (m^2)^{-\varepsilon} \; \frac{{}_2F_1(1,1;2-2\varepsilon;-1)}{1-2\varepsilon}
$$

$$
= -\frac{1}{4\gamma m^2} \left[ \frac{2\ln 2}{\varepsilon} - 2\ln 2 \ln m^2 - 2\ln^2 2 + \frac{\pi^2}{3} + \mathcal{O}(\varepsilon) \right]. \qquad (2.64)
$$

Combining the two contributions from (2.62) and (2.64), we see that the artificial divergences that appeared in each region cancel each other. We finally reproduce our result from (2.32)

$$
+ \qquad \simeq \quad -\frac{1}{4\gamma m^2} \left[ 2\ln 2 \ln \gamma + \ln^2 2 + \frac{\pi^2}{3} + \mathcal{O}(\varepsilon) \right]. \quad (2.65)
$$

Notice that (2.62) and (2.64) determine the leading power of the integral in a closed form in $\varepsilon$ whereas we were only able to determine the first coefficient in the $\varepsilon$-expansion with the help of Feynman parameters in Section 2.4.1.

### 2.4.4 Mellin-Barnes Techniques

In the last two sections we have introduced two sophisticated techniques for the calculation of loop integrals. The first one was particularly suited for our 2-loop calculation from Chapter 3 and 4, the second one for the 1-loop calculation in Chapter 5. We now present a third method which we used in both calculations. In our 2-loop calculation we typically applied Mellin-Barnes techniques [32,33] for the calculation of the boundary conditions, i.e. for single-scale integrals. As the boundary condition in our 2-loop example is rather trivial, we present the computation of the full 2-loop integral in the following. Mellin-Barnes techniques are also a comfortable tool for the calculation of loop integrals in a power expansion as we will see in our 1-loop example below.

The method is based on the following representation

$$
\frac{1}{(X+Y)^\lambda} = \frac{1}{\Gamma(\lambda)} \; \frac{1}{2\pi i} \int_{-i\infty}^{+i\infty} dz \; \Gamma(\lambda+z)\,\Gamma(-z) \; Y^z \, X^{-z-\lambda}, \qquad (2.66)
$$

where the contour separates *left poles* from *right poles* (we specify the meaning of this phrases in our examples) and $z$ is called a Mellin-Barnes parameter. We see that (2.66) basically converts a sum into a product at the cost of a contour integration.

We typically introduce Feynman parameter first and use the Mellin-Barnes representation (2.66) to simplify the corresponding integrations. With all integrations over Feynman parameters done, we examine the analytical properties of the integrand and perform the Mellin-Barnes integrations with contour methods. This leads to infinite sums over residues which often represent the main obstacle in this approach.

**2-loop example: Mellin-Barnes Techniques**

We first address our 2-loop integral from (2.30). The starting point is equation (2.33) which we rewrite with the help of the substitution $x = st$, $y = \bar{s}t$ with the usual bar-notation understood. This yields

$$
= (m^2)^{-2\varepsilon} \, e^{2i\pi\varepsilon} \, \frac{\Gamma(2\varepsilon)\,\Gamma(1-\varepsilon)^4}{\Gamma(2-2\varepsilon)} \int_0^1 ds \int_0^1 dt \; s^{\varepsilon-1}\, t^{-\varepsilon}\, \bar{t}^{-2\varepsilon}\, (s+u\bar{s})^{-2\varepsilon} \tag{2.67}
$$

We introduce one Mellin-Barnes parameter to split the last factor into a product. The integrations over the Feynman parameters give rise to $\Gamma$-functions and we obtain

$$
= (m^2)^{-2\varepsilon} \, e^{2i\pi\varepsilon} \, \frac{\Gamma(1-\varepsilon)^4}{(1-2\varepsilon)\,\Gamma(2-3\varepsilon)} \tag{2.68}
$$

$$
\frac{1}{2\pi i} \int_{\mathcal{C}} dz \quad \Gamma(2\varepsilon+z)\,\Gamma(1+z)\,\Gamma(-\varepsilon-z)\,\Gamma(-z)\, u^z.
$$

The integrand has simple poles which we classify into *left poles* which stem from $\Gamma(\ldots + z)$ and *right poles* from $\Gamma(\ldots - z)$. We find

left poles:  $\quad z = -2\varepsilon,\, -1-2\varepsilon,\, -2-2\varepsilon,\, \ldots \qquad z = -1,\, -2,\, -3,\, \ldots$

right poles:  $\quad z = -\varepsilon,\, 1-\varepsilon,\, 2-\varepsilon,\, \ldots \qquad\qquad z = 0,\, 1,\, 2,\, \ldots \tag{2.69}$

The contour $\mathcal{C}$ separates these two types of poles. Notice that we cannot simply set $\varepsilon = 0$ as this would glue left and right poles together at $z = 0$. There is no such problem for $0 < \varepsilon < 1$; let us take $\varepsilon = 1/2$ for the moment. We see that we can choose the contour $\mathcal{C}$ as a straight line in this case (cf. Figure 2.1a). For $\varepsilon \to 0$ the contour is deformed into $\mathcal{C}'$ as shown in Figure 2.1b. Alternatively, we may stick to the contour $\mathcal{C}$ and add the contributions from the poles that crossed the straight line for $\varepsilon \to 0$ explicitly. The crucial point is that all singularities of the integral stem from such contour crossings. In our example we pick up the pole for $z = -2\varepsilon$ and may safely set $\varepsilon = 0$ in the remnant contour integral which results in

$$
= (m^2)^{-2\varepsilon} \, e^{2i\pi\varepsilon} \, \frac{\Gamma(1-\varepsilon)^4}{(1-2\varepsilon)\,\Gamma(2-3\varepsilon)} \Big[ \Gamma(1-2\varepsilon)\Gamma(\varepsilon)\Gamma(2\varepsilon)u^{-2\varepsilon}
$$

$$
+ \frac{1}{2\pi i} \int_{-3/4-i\infty}^{-3/4+i\infty} dz \; \Big( \Gamma(z)\,\Gamma(1+z)\,\Gamma(-z)^2\, u^z + \mathcal{O}(\varepsilon) \Big) \Big] \tag{2.70}
$$
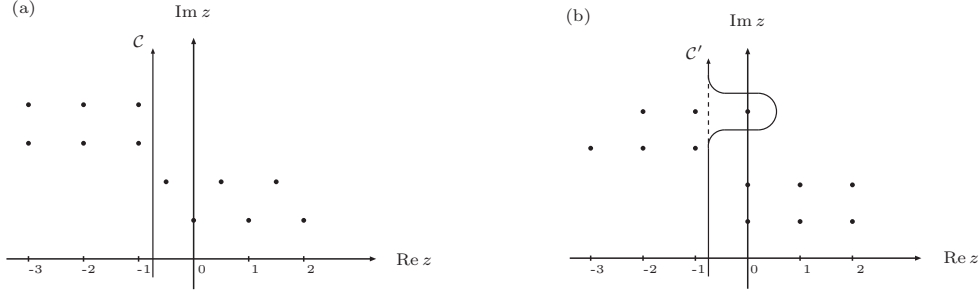
Figure 2.1: *Possible integration contours in (2.68) that separate left poles from right poles. The figures show the position of the poles for $\varepsilon = 1/2$ (a) and $\varepsilon = 0$ (b). All poles lie on the real axis, but we have assigned a positive imaginary part for illustrative reasons.*

We close the contour to the left and sum the infinite residues from $z = -1, -2, -3, \ldots$

$$\frac{1}{2\pi i} \int_{-3/4-i\infty}^{-3/4+i\infty} dz \ \ \Gamma(z)\,\Gamma(1+z)\,\Gamma(-z)^2\,u^z \ = \ \sum_{n=1}^{\infty} \frac{-(1+n\ln u)}{n^2 u^n} \tag{2.71}$$

$$= \ \mathrm{Li}_2(u) + \ln u \ln \bar{u} - \frac{1}{2}\ln^2 u - \frac{\pi^2}{3}.$$

The expansion of (2.70) in $\varepsilon$ yields together with (2.71) our result from (2.35).

## 1-loop example: Mellin-Barnes Techniques

In our 1-loop example we start from (2.31) and perform the substitution $x = st$, $y = \bar{s}t$ as in the last example

$$\text{(diagram)} \ = \ \int_0^1 ds \int_0^1 dt \ \frac{-(m^2)^{-1-\varepsilon}\,\Gamma(1-\varepsilon)\,\Gamma(1+\varepsilon)\,t^{-\varepsilon}}{[t + 2s(2\bar{t} + t\bar{s})(\gamma - 1)]^{1+\varepsilon}}. \tag{2.72}$$

We introduce two Mellin-Barnes parameters in this case to obtain standard integrations over Feynman parameters in terms of $\Gamma$-functions. We find

$$\text{(diagram)} \ = \ -(m^2)^{-1-\varepsilon}\,\frac{\Gamma(1-\varepsilon)}{\Gamma(1-2\varepsilon)}\,\frac{1}{2\pi i}\int_{\mathcal{C}_z} dz \ \Gamma(1+\varepsilon+z)\,\Gamma(1+z)\,2^{2z}(\gamma-1)^z$$

$$\frac{1}{2\pi i}\int_{\mathcal{C}_w} dw \ 2^{-w}\,\frac{\Gamma(w-z)\,\Gamma(-w)\,\Gamma(w-2\varepsilon-z)\,\Gamma(1+z-w)\,\Gamma(1+w)}{\Gamma(2+z+w)}. \tag{2.73}$$

The contours separate left poles from right poles if the arguments of the $\Gamma$-functions are positive. This can be achieved by integrating along straight lines with $w_0 = -1/2$

and $z_0 = -3/4$ for $\varepsilon = 0$ (we already know that the integral is finite and set $\varepsilon = 0$ in the following). The poles in $w$ can be classified according to

left poles: $\qquad w = z, \, -1 + z, \, -2 + z, \, \dots \qquad w = -1, \, -2, \, -3, \, \dots$

right poles: $\qquad w = 1 + z, \, 2 + z, \, 3 + z \, \dots \qquad w = 0, \, 1 \, 2, \, \dots$ $\qquad$ (2.74)

We close the contour to the right and find

$$\frac{1}{2\pi i} \int_{\mathcal{C}_w} dw \; 2^{-w} \frac{\Gamma(w - z)^2 \, \Gamma(-w) \, \Gamma(1 + z - w) \, \Gamma(1 + w)}{\Gamma(2 + z + w)}$$

$$= \sum_{n=0}^{\infty} (-1)^n \left[ 2^{-n} \frac{\Gamma(n - z)^2 \, \Gamma(1 - n + z)}{\Gamma(2 + n + z)} \right.$$

$$\left. + 2^{-n-1-z} \frac{\Gamma(-1 - n - z) \, \Gamma(2 + n + z) \, \Gamma(n + 1)}{\Gamma(3 + n + 2z)} \right]$$

$$= 2(1 + z) \, \Gamma(-1 - z)^2 \, {}_2F_1(1, 2 + 2z; 2 + z; -1)$$

$$- 2^{-1-z} \frac{\Gamma(1 - z) \, \Gamma(z)}{\Gamma(2 + 2z)} \left[ \psi(1 + z) - \psi(3/2 + z) \right] \qquad (2.75)$$

where $\psi(z)$ is the digamma function given by $\psi(z) \equiv \Gamma'(z)/\Gamma(z)$. So far our computation has been exact in $m/M$. The important point to notice is that the remnant contour integral has poles for $z \in \mathbf{Z}$. If we close the contour to the left, *the leading contribution in $m/M$ stems from a single pole at $z = -1$* because of the explicit factor $(\gamma - 1)^z \sim \gamma^z$ in (2.73). This yields



$$\simeq \; -\frac{1}{4\gamma m^2} \left[ 2 \ln 2 \ln \gamma + \ln^2 2 + \frac{\pi^2}{3} + \mathcal{O}(\varepsilon) \right] \qquad (2.76)$$

in agreement with (2.32). We see that the Mellin-Barnes technique is particularly suited to compute the subleading contributions in $m/M$ which stem from subsequent poles in $z$ in our example.

## 2.4.5 Sector Decomposition

Let us summarize what we have obtained so far. Concerning our 1-loop calculation from Chapter 5, we presented two analytical methods for the calculation of the MIs: the method of expansion by regions and Mellin-Barnes techniques. The comparison between these two independent calculations is extremely helpful to avoid errors in this part of the calculation. So far, we have found only one method for our 2-loop calculation from Chapter 3 and 4: the method of differential equations in combination with Mellin-Barnes techniques for the calculation of the boundary conditions. A second independent method would also be very helpful in this case.

We use a numerical method, the method of sector decomposition [34], in order to check our analytical results of the 2-loop integrals from Chapter 3 and 4. We refrain from presenting this technique here in detail as we will only use it as an (important) check. The basic idea corresponds to a decomposition procedure of Feynman parameter integrals which systematically disentangles overlapping IR divergences. These divergences can then be isolated with the help of an adequate subtraction procedure. At this step the MI is given in form of a Laurent expansion in $\varepsilon$ with coefficients that correspond to *regular* parameter integrals that can be evaluated numerically.

The power of the considered algorithm lies in the fact that it can easily be automatized and be applied, at least in principle, for any multi-loop integral. Its numerical precision is mainly limited by the potential presence of thresholds in the parameter integrals. The obtained precision therefore varies strongly in our applications between 1 part in $10^2$-$10^8$ depending on the considered integral. This situation could, however, be improved by performing the numerical integrations with more efficient routines.

# Part III

# Applications

# Chapter 3

# Hadronic two-body decays I: Imaginary part

In the second part of this thesis we consider several perturbative calculations in the framework of QCD Factorization. We first compute the imaginary part of the NNLO vertex corrections in charmless hadronic two-body decays as e.g. $B \to \pi\pi$ (the real part will be considered in Chapter 4). The results presented in this chapter will be published in [100].

The outline of this chapter is as follows: We first introduce a new operator basis of the effective Hamiltonian which is particularly suited for multi-loop calculations. We then present some details of the 2-loop calculation following our strategy from Section 2.1. As the factorization formula reveals a rather complicated divergence structure at NNLO, we elaborate the subsequent UV and IR subtractions in some detail. The imaginary part of the topological tree amplitudes is finally obtained in an analytic form. We conclude with a brief analysis of the numerical impact of the NNLO vertex corrections.

## 3.1   Change of operator basis

In view of the calculation of topological tree amplitudes, we restrict our attention to the current-current operators $Q_{1,2}$ of the effective weak Hamiltonian (1.8). Due to the fact that we work within Dimensional Regularization (DR), we also have to consider *evanescent operators* [90,101,102]. These non-physical operators vanish in $d = 4$ dimensions but contribute at intermediate steps of the calculation in $d \neq 4$ dimensions. We have emphasized in Section 1.2.3 that the imaginary part considered here has effectively NLO complexity. We will indeed see that the calculation of the imaginary part only requires 1-loop evanescent operators (2-loop evanescent operators will contribute to the real part which we consider in Chapter 4). For our

purposes the complete operator basis is thus given by

$$\tilde{Q}_1 = [\bar{u}\gamma^\mu L\, b]\ [\bar{d}\gamma_\mu\, L\, u]\,,$$

$$\tilde{Q}_2 = [\bar{u}_i\gamma^\mu L\, b_j]\ [\bar{d}_j\gamma_\mu\, L\, u_i]\,,$$

$$\tilde{E}_1 = [\bar{u}\gamma^\mu\gamma^\nu\gamma^\rho L\, b]\ [\bar{d}\gamma_\mu\gamma_\nu\gamma_\rho\, L\, u] - (16 - 4\varepsilon)\,\tilde{Q}_1,$$

$$\tilde{E}_2 = [\bar{u}_i\gamma^\mu\gamma^\nu\gamma^\rho L\, b_j]\ [\bar{d}_j\gamma_\mu\gamma_\nu\gamma_\rho\, L\, u_i] - (16 - 4\varepsilon)\,\tilde{Q}_2, \qquad (3.1)$$

with $L \equiv 1 - \gamma_5$. We refer to this basis as the (standard) QCDF basis for convenience and denote the corresponding Wilson coefficients and operators with a tilde.

It has been argued by Chetyrkin, Misiak and Münz (CMM) that one should use a different operator basis in order to perform multi-loop calculations [103]. Although the deeper reason is related to the penguin operators which we do not consider here, we prefer to introduce the CMM basis in view of future extensions of our work. The CMM basis allows to consistently use DR with a naive anticommuting $\gamma_5$ to all orders in perturbation theory. In the CMM basis the current-current operators and corresponding 1-loop evanescent operators read (denoted with a hat)

$$\hat{Q}_1 = \left[\bar{u}\gamma^\mu L\, T^A b\right]\ \left[\bar{d}\gamma_\mu\, L\, T^A u\right]\,,$$

$$\hat{Q}_2 = [\bar{u}\gamma^\mu L\, b]\ [\bar{d}\gamma_\mu\, L\, u]\,,$$

$$\hat{E}_1 = \left[\bar{u}\gamma^\mu\gamma^\nu\gamma^\rho L\, T^A b\right]\ \left[\bar{d}\gamma_\mu\gamma_\nu\gamma_\rho\, L\, T^A u\right] - 16\,\hat{Q}_1,$$

$$\hat{E}_2 = [\bar{u}\gamma^\mu\gamma^\nu\gamma^\rho L\, b]\ [\bar{d}\gamma_\mu\gamma_\nu\gamma_\rho\, L\, u] - 16\,\hat{Q}_2. \qquad (3.2)$$

Comparing (3.1) and (3.2) we observe two differences: First, the two bases use different colour structures which is a rather trivial point. More importantly, they contain slightly different definitions of evanescent operators which we will examine now in detail.

The issue is related to Fierz symmetry. We will see below that the definition of evanescent operators in the CMM basis explicitly breaks Fierz symmetry which relates the two diagrams in Figure 3.1. This can be seen by considering the UV part



Figure 3.1: *Generic 1-loop diagram with different contractions of fields in a four-quark operator $Q_i$. The two insertions are related by a Fierz reordering, see text ($\alpha, \beta, \gamma, \delta$ are spinor indices).*

of the left diagram which involves the following combination of Dirac matrices

$$\left(\gamma^\mu L\gamma^\nu\gamma^\rho\right)_{\alpha\beta}\left(\gamma_\rho\gamma_\nu\gamma_\mu L\right)_{\gamma\delta} = -\left(\gamma^\mu\gamma^\nu\gamma^\rho L\right)_{\alpha\beta}\left(\gamma_\mu\gamma_\nu\gamma_\rho L\right)_{\gamma\delta} + (6d-4)\left(\gamma^\mu L\right)_{\alpha\beta}\left(\gamma_\mu L\right)_{\gamma\delta} \tag{3.3}$$

which we reshuffled into a more convenient form using an anticommuting $\gamma_5$. On the other hand the right diagram gives

$$\left(\gamma^\rho\gamma^\nu\gamma^\mu L\gamma_\nu\gamma_\rho\right)_{\gamma\beta}\left(\gamma_\mu L\right)_{\alpha\delta} = (d-2)^2\left(\gamma^\mu L\right)_{\gamma\beta}\left(\gamma_\mu L\right)_{\alpha\delta} \overset{\text{Fierz}}{=} (d-2)^2\left(\gamma^\mu L\right)_{\alpha\beta}\left(\gamma_\mu L\right)_{\gamma\delta}, \tag{3.4}$$

where we have performed a Fierz reordering in the second step. If we now *impose* Fierz symmetry, the expressions (3.3) and (3.4) have to be equal and we arrive at

$$\left(\gamma^\mu\gamma^\nu\gamma^\rho L\right)_{\alpha\beta}\left(\gamma_\mu\gamma_\nu\gamma_\rho L\right)_{\gamma\delta} = (16 - 4\varepsilon - 4\varepsilon^2)\left(\gamma^\mu L\right)_{\alpha\beta}\left(\gamma_\mu L\right)_{\gamma\delta} \tag{3.5}$$

If we look at the remnant 1-loop diagrams we find that (3.5) is in fact the only constraint from Fierz symmetry. In NLO the terms of $\mathcal{O}(\varepsilon^2)$ do not contribute as the loop-integrals have at most $1/\varepsilon$ (UV) divergences. They can therefore simply be neglected here (we stress that this will be different in our analysis in Chapter 4). We conclude that the QCDF basis from (3.1) is Fierz symmetric whereas the CMM basis from (3.2) is *not*. In other words, the freedom in the definition of evanescent operators has been used in the QCDF basis to properly adjust the $\varepsilon$-terms into a Fierz symmetric form.

Why do we care about Fierz symmetry? In the considered calculation the contraction depicted in the left diagram from Figure 3.1 is related to the colour-allowed tree amplitude $(\alpha_1)$, whereas the one from the right diagram leads to the colour-suppressed tree amplitude $(\alpha_2)$. On the technical level these two possible insertions of a four-quark operator correspond to two completely different calculations. It would be very tedious if we had to perform both calculations explicitly, in particular in the considered 2-loop case. We have pointed out in Section 1.2.3 that $\alpha_1$ and $\alpha_2$ can naturally be related by Fierz symmetry. For this, it is of crucial importance that we *preserve* Fierz symmetry when we work in the effective theory which factorizes the amplitudes into Wilson coefficients and matrix elements within DR. As we have argued above, this is indeed the case in the QCDF basis which allows us to *derive* $\alpha_2$ from $\alpha_1$ by simply interchanging $\tilde{C}_1 \leftrightarrow \tilde{C}_2$.

We conclude that the CMM basis is the appropriate choice for a 2-loop calculation whereas the QCDF basis provides a short-cut for the derivation of the colour-suppressed amplitude. We therefore propose the following strategy for the calculation of the NNLO vertex corrections: We perform the explicit 2-loop calculation in the CMM basis using the first type of insertion in the left diagram from Figure 3.1. In this way we obtain $\alpha_1(\hat{C}_i)$. We then transform this expression into the QCDF basis which yields $\alpha_1(\tilde{C}_i)$ and finally apply Fierz symmetry arguments to derive $\alpha_2(\tilde{C}_i)$ from $\alpha_1(\tilde{C}_i)$ under the exchange $\tilde{C}_1 \leftrightarrow \tilde{C}_2$.

## 3.2 2-loop calculation

In this section we present a brief overview of the technical aspects of the considered 2-loop calculation. Herein, we follow the systematics of our strategy from Section 2.1.

**Step 1: Set-up for loop calculation**

We will see explicitly in Section 3.3.2 that we may restrict our attention to (naively) non-factorizable diagrams, similar to what we have seen in the NLO analysis from Section 1.2.3. These diagrams contain at least one gluon which connects the two currents in the left diagram of Figure 3.1. The full set of 2-loop diagrams to be considered here is depicted in Figure 3.2, but only about half of these diagrams give rise to an imaginary part. It is an easy task to identify this subset of diagrams as the generation of an imaginary part is always related to final state interactions.

The colour factors of the 2-loop diagrams from Figure 3.2 can be found in Table 3.1. The diagrams can be written in terms of the following denominators of propagators

$$
\begin{aligned}
&\mathcal{P}_1 = (p - q - k)^2\,, &&\mathcal{P}_{13} = (p + k)^2 - m^2, \\
&\mathcal{P}_2 = (p - q - l)^2\,, &&\mathcal{P}_{14} = (p + l)^2 - m^2, \\
&\mathcal{P}_3 = (uq + k)^2\,, &&\mathcal{P}_{15} = (p + k + l)^2 - m^2, \\
&\mathcal{P}_4 = (uq + l)^2\,, &&\mathcal{P}_{16} = (uq + k + l)^2\,, \\
&\mathcal{P}_5 = (\bar{u}q + k)^2\,, &&\mathcal{P}_{17} = (\bar{u}q + k + l)^2\,, \\
&\mathcal{P}_6 = (\bar{u}q + l)^2\,, &&\mathcal{P}_{18} = (p + k - l)^2 - m^2, \\
&\mathcal{P}_7 = k^2, &&\mathcal{P}_{19} = (p - q + k - l)^2\,, \\
&\mathcal{P}_8 = l^2, &&\mathcal{P}_{20} = (p - q + k)^2\,, \\
&\mathcal{P}_9 = (k - l)^2\,, &&\mathcal{P}_{21} = (uq - l)^2\,, \\
&\mathcal{P}_{10} = (uq + k - l)^2\,, &&\mathcal{P}_{22} = (k - l)^2 - z_f^2 m^2, \\
&\mathcal{P}_{11} = (\bar{u}q + k - l)^2\,, &&\mathcal{P}_{23} = l^2 - z_f^2 m^2, \\
&\mathcal{P}_{12} = (p - q - k - l)^2\,, &&\text{(3.6)}
\end{aligned}
$$

where $p$ denotes the momentum of the $b$-quark (with mass $m \equiv m_b$), $p - q$ the one of the quark to the right of the weak vertex and the quark/antiquark of the emitted meson have $uq/\bar{u}q$, respectively. The on-shell kinematics is reflected by $q^2 = 0$ and $p^2 = 2p \cdot q = m^2$. The variable $z_f = m_f/m_b$ is related to the diagrams with a closed fermion loop. For massless quarks in the loop we simply have $z_q = 0$, for an internal b-quark $z_b = 1$ and for the case of a charm quark we write $z \equiv z_c = m_c/m_b$.
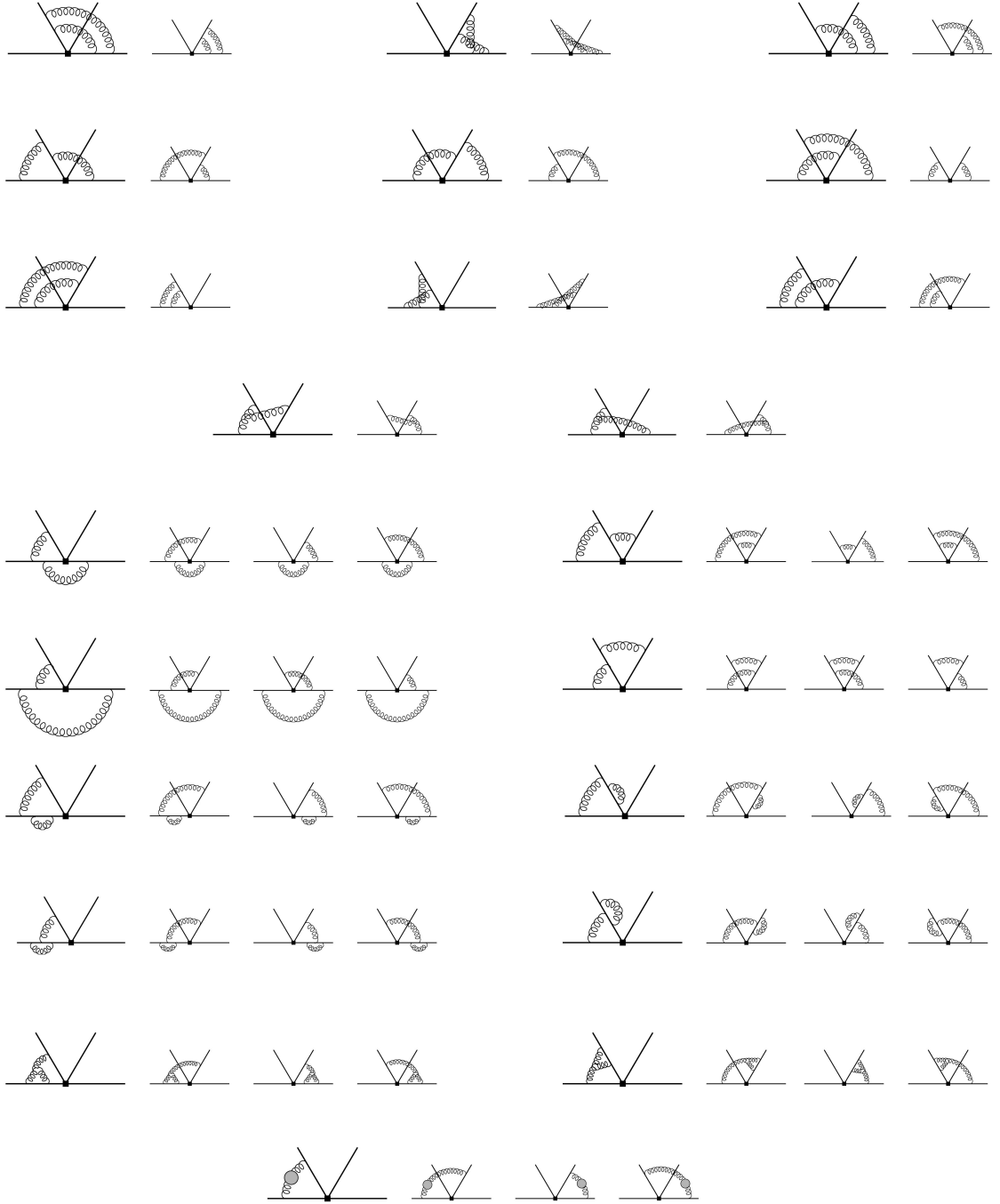
Figure 3.2: *Full set of non-factorizable 2-loop diagrams. In each diagram the fermion line to the left of the four-quark vertex denotes the massive b quark, all other quarks are massless. The bubble in the last four diagrams represents the 1-loop gluon self-energy. Only diagrams with final state interactions, i.e. with at least one gluon connecting the line to the right of the vertex with one of the upper lines, give rise to an imaginary part.*

| Operator | $\hat{Q}_1$ | $\hat{Q}_2$ |
|----------|-------------|-------------|
| line 1-3 (L) | $C_F^2 - \frac{C_F N_c}{2}$ | $\frac{C_F}{2}$ |
| line 1-3 (S) | $C_F^2 - \frac{C_F N_c}{4}$ | $\frac{C_F}{2}$ |
| line 6-7 | $\frac{C_F^2}{2}$ | $0$ |
| line 5,8 | $\frac{C_F^2}{2} - \frac{C_F N_c}{4}$ | $0$ |
| line 4,9 | $\frac{C_F N_c}{4}$ | $0$ |
| line 10 (A) | $\frac{C_F}{4}$ | $0$ |
| line 10 (NA) | $-\frac{C_F N_c}{2}$ | $0$ |

Table 3.1: *Colour factors of the diagrams in Figure 3.2. With "L" and "S" we refer to the large and small figures, with "A" and "NA" to abelian and non-abelian diagrams. The normalization is chosen such that the tree diagram from Figure 1.7 gives $N_c$ for $\hat{Q}_2$.*
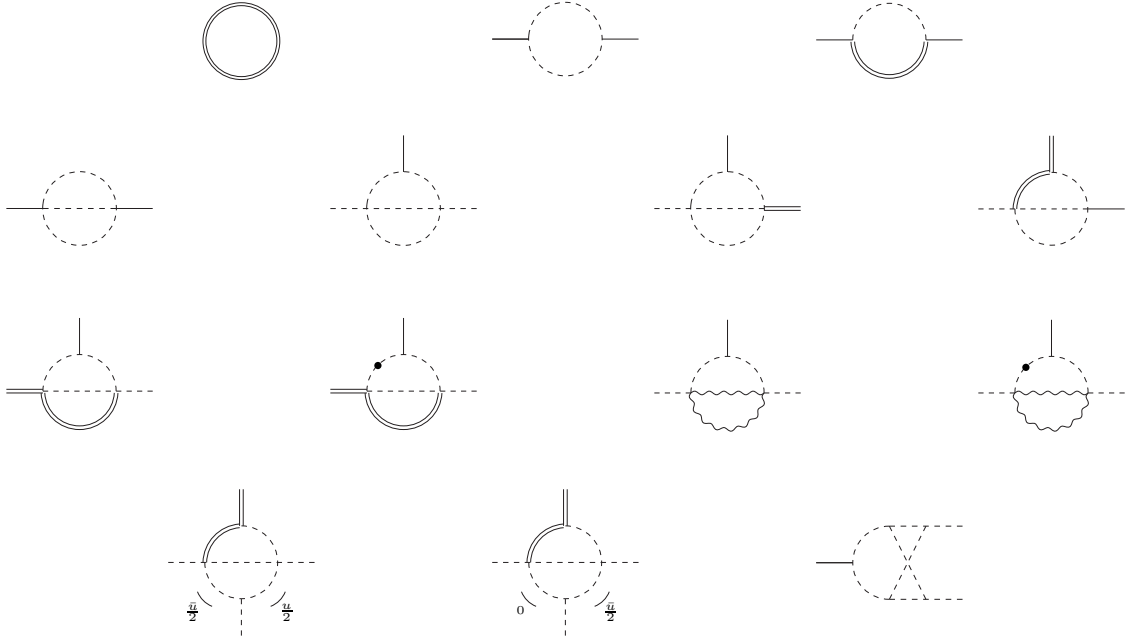


Figure 3.3: *Scalar Master Integrals that appear in our calculation. We use dashed lines for massless propagators and double (wavy) lines for the ones with mass $m$ ($z_f m$). Dashed/solid/double external lines correspond to virtualities $0/um^2/m^2$, respectively. Dotted propagators are taken to be squared.*

## Step 2: Reduction to Master Integrals

The reduction algorithm represents an indispensable tool for the considered calculation. It enables us to express all diagrams from Figure 3.2 as linear combinations of MIs which are multiplied by some Dirac structures. As the coefficients in these linear combinations are real, we may extract the imaginary part of a diagram at the level of the MIs which is a much simpler task than for the full diagrams. The calculation of the imaginary part involves 14 MIs which are depicted in Figure 3.3.

## Step 3: Manipulation of Dirac structures

We do not perform the bound state projections at this level of the calculation as this would yield unwanted traces with $\gamma_5$. We instead treat the two currents independently and make use of the equations of motion for the on-shell quarks in order to simplify the Dirac structures. In this way we end up with three irreducible structures which are given by

$$[\bar{u}\gamma^\mu L\, b]\ \left[\bar{d}\gamma_\mu\, L\, u\right],$$

$$[\bar{u}\gamma^\mu\gamma^\nu\gamma^\rho L\, b]\ \left[\bar{d}\gamma_\mu\gamma_\nu\gamma_\rho\, L\, u\right],$$

$$[\bar{u}\gamma^\mu\gamma^\nu\gamma^\rho\gamma^\sigma\gamma^\tau L\, b]\ \left[\bar{d}\gamma_\mu\gamma_\nu\gamma_\rho\gamma_\sigma\gamma_\tau\, L\, u\right]. \tag{3.7}$$

The second structure gives rise to 1-loop evanescent operators according to (3.2). As the last structure only enters in the finite piece of the considered calculation, it can simply be evaluated in $d = 4$ dimensions without the need to introduce 2-loop evanescent operators.

## Step 4: Calculation of Master Integrals

Some MIs in Figure 3.3 can be solved easily with the help of Feynman parameters. This direct approach could be improved with the help of the MATHEMATICA package HYPEXP [96] which allows to expand a special class of hyper-geometric functions to arbitrary order in $\varepsilon$. However, as discussed in detail in Section 2.4, wide parts of the 2-loop calculation were performed with the help of the method of differential equations in combination with the formalism of Harmonic Polylogarithms (HPLs). We further applied Mellin-Barnes techniques for the calculation of the boundary conditions to the differential equations. Apart from the two MIs with an internal charm quark (wavy line), we were able to express all MIs with the help of a minimal set of five HPLs given in (2.48).

The situation is more complicated for the MIs with an internal charm quark which introduces a new scale to the problem. However, a closer look reveals that these MIs depend on two physical scales only, namely $um_b^2$ and $m_c^2 \equiv z^2 m_b^2$. The MIs can then be solved within the formalism of HPLs in terms of the ratio $\xi \equiv z^2/u$ if we allow for more complicated arguments of the HPLs as $\eta \equiv \frac{1}{2}\left(1 - \sqrt{1 + 4\xi}\right)$. As an independent check of our results we evaluated the MIs numerically using the method of sector decomposition. The results of the MIs can be found in Appendix A.1.

## 3.3    Renormalization and IR subtractions

So far we have computed the (unrenormalized) matrix elements

$$\langle \hat{Q}_{1,2} \rangle \equiv \langle M_1 M_2 | \hat{Q}_{1,2} | \bar{B} \rangle \tag{3.8}$$

to NNLO in perturbation theory (without spectator scattering). These matrix elements are UV and IR divergent. In this section we discuss adequate subtractions which will lead to a finite result for the NNLO vertex corrections.

### 3.3.1    Renormalization

The renormalization procedure involves standard QCD counterterms, which amount to the calculation of various 1-loop diagrams as the ones depicted in Figure 3.4, as well as counterterms from the effective Hamiltonian. We write the renormalized matrix elements as

$$\langle \hat{Q}_i \rangle_{\text{ren}} = Z_\psi \, \hat{Z}_{ij} \, \langle \hat{Q}_j \rangle_{\text{bare}}, \tag{3.9}$$

where $Z_\psi = Z_b^{1/2} Z_q^{3/2}$ contains the wave-function renormalization factors of the massive b-quark $Z_b$ and the massless quarks $Z_q$, whereas $\hat{Z}$ is the operator renormalization matrix in the effective theory. We introduce the following notation for the perturbative expansions of these quantities

$$\langle \hat{Q}_i \rangle_{\text{ren/bare}} = \sum_{k=0}^{\infty} \left( \frac{\alpha_s}{4\pi} \right)^k \langle \hat{Q}_i \rangle_{\text{ren/bare}}^{(k)},$$

$$Z_\psi = 1 + \sum_{k=1}^{\infty} \left( \frac{\alpha_s}{4\pi} \right)^k Z_\psi^{(k)}, \qquad \hat{Z}_{ij} = \delta_{ij} + \sum_{k=1}^{\infty} \left( \frac{\alpha_s}{4\pi} \right)^k \hat{Z}_{ij}^{(k)} \tag{3.10}$$

and rewrite (3.9) in perturbation theory up to NNLO which yields

$$\langle \hat{Q}_i \rangle_{\text{ren}}^{(0)} = \langle \hat{Q}_i \rangle_{\text{bare}}^{(0)},$$

$$\langle \hat{Q}_i \rangle_{\text{ren}}^{(1)} = \langle \hat{Q}_i \rangle_{\text{bare}}^{(1)} + \left[ \hat{Z}_{ij}^{(1)} + Z_\psi^{(1)} \delta_{ij} \right] \langle \hat{Q}_j \rangle_{\text{bare}}^{(0)}, \tag{3.11}$$

$$\langle \hat{Q}_i \rangle_{\text{ren}}^{(2)} = \langle \hat{Q}_i \rangle_{\text{bare}}^{(2)} + \left[ \hat{Z}_{ij}^{(1)} + Z_\psi^{(1)} \delta_{ij} \right] \langle \hat{Q}_j \rangle_{\text{bare}}^{(1)} + \left[ \hat{Z}_{ij}^{(2)} + Z_\psi^{(1)} \hat{Z}_{ij}^{(1)} + Z_\psi^{(2)} \delta_{ij} \right] \langle \hat{Q}_j \rangle_{\text{bare}}^{(0)}.$$

The full calculation thus requires the operator renormalization matrices $\hat{Z}^{(1,2)}$. For the calculation of the imaginary part, the terms proportional to the tree level matrix
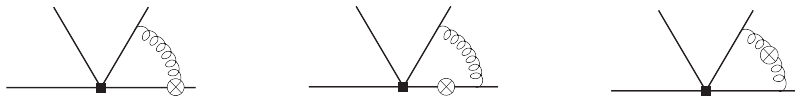


Figure 3.4: *Sample of counterterm diagrams.*

elements do not contribute and $\hat{Z}^{(2)}$ drops out in (3.11) as expected for an effective NLO calculation.

Mass and wave function renormalization are found to be higher order effects. For the renormalization of the coupling constant we use

$$Z_g = 1 - \frac{\alpha_s}{4\pi\varepsilon}\left(\frac{11}{6}N_c - \frac{1}{3}n_f\right) + \mathcal{O}(\alpha_s^2). \tag{3.12}$$

The 1-loop renormalization matrix $\hat{Z}^{(1)}$ can be found e.g. in [104] and reads

$$\hat{Z}^{(1)} = \begin{pmatrix} -2 & \frac{4}{3} & \frac{5}{12} & \frac{2}{9} \\ 6 & 0 & 1 & 0 \end{pmatrix}\frac{1}{\varepsilon}, \tag{3.13}$$

where the two lines correspond to the basis of physical operators $\{\hat{Q}_1, \hat{Q}_2\}$ and the four columns to the extended basis $\{\hat{Q}_1, \hat{Q}_2, \hat{E}_1, \hat{E}_2\}$ including the mixing of the non-physical evanescent operators into the physical ones.

### 3.3.2 Factorization in NNLO

In this section it will be convenient to introduce the following short-hand notation for the factorization formula (1.13)

$$\langle\hat{Q}_i\rangle_{\mathrm{ren}} = F \cdot T_i \otimes \Phi + \ldots \tag{3.14}$$

where $F$ denotes the $B \to M_1$ form factor, $T_i$ the hard-scattering kernels and $\Phi$ the product of the decay constant $f_{M_2}$ and the distribution amplitude $\phi_{M_2}$. The convolution in (1.13) has been represented by the symbol $\otimes$ and the ellipses contain the terms from spectator scattering which we disregard in the following.

Formally, we may introduce the perturbative expansions

$$F = \sum_{k=0}^{\infty}\left(\frac{\alpha_s}{4\pi}\right)^k F^{(k)}, \qquad T_i = \sum_{k=0}^{\infty}\left(\frac{\alpha_s}{4\pi}\right)^k T_i^{(k)}, \qquad \Phi = \sum_{k=0}^{\infty}\left(\frac{\alpha_s}{4\pi}\right)^k \Phi^{(k)}. \tag{3.15}$$

Up to NNLO the expansion of (3.14) yields

$$\langle\hat{Q}_i\rangle_{\mathrm{ren}}^{(0)} = F^{(0)} \cdot T_i^{(0)} \otimes \Phi^{(0)},$$

$$\langle\hat{Q}_i\rangle_{\mathrm{ren}}^{(1)} = F^{(0)} \cdot T_i^{(1)} \otimes \Phi^{(0)} + F^{(1)} \cdot T_i^{(0)} \otimes \Phi^{(0)} + F^{(0)} \cdot T_i^{(0)} \otimes \Phi^{(1)},$$

$$\langle\hat{Q}_i\rangle_{\mathrm{ren}}^{(2)} = F^{(0)} \cdot T_i^{(2)} \otimes \Phi^{(0)} + F^{(1)} \cdot T_i^{(1)} \otimes \Phi^{(0)} + F^{(0)} \cdot T_i^{(1)} \otimes \Phi^{(1)}$$

$$+ F^{(2)} \cdot T_i^{(0)} \otimes \Phi^{(0)} + F^{(1)} \cdot T_i^{(0)} \otimes \Phi^{(1)} + F^{(0)} \cdot T_i^{(0)} \otimes \Phi^{(2)}. \tag{3.16}$$

In LO the comparison of (3.11) and (3.16) gives the trivial relation

$$\langle\hat{Q}_i\rangle^{(0)} \equiv \langle\hat{Q}_i\rangle_{\mathrm{bare}}^{(0)} = F^{(0)} \cdot T_i^{(0)} \otimes \Phi^{(0)} \tag{3.17}$$

which states that $T_i^{(0)}$ can be computed from the tree level diagram in Figure 1.7. In order to address higher order terms we split the bare matrix elements into contributions from (naively) factorizable (f) and non-factorizable (nf) diagrams

$$\langle \hat{Q}_i \rangle_{\text{bare}}^{(k)} \equiv \langle \hat{Q}_i \rangle_{\text{f}}^{(k)} + \langle \hat{Q}_i \rangle_{\text{nf}}^{(k)}. \tag{3.18}$$

In NLO the corresponding diagrams have been shown in Figure 1.9 and Figure 1.8, respectively. To this order (3.11) and (3.16) lead to

$$\langle \hat{Q}_i \rangle_{\text{f}}^{(1)} + \langle \hat{Q}_i \rangle_{\text{nf}}^{(1)} + \left[ \hat{Z}_{ij}^{(1)} + Z_\psi^{(1)} \delta_{ij} \right] \langle \hat{Q}_j \rangle^{(0)}$$
$$= F^{(0)} \cdot T_i^{(1)} \otimes \Phi^{(0)} + F^{(1)} \cdot T_i^{(0)} \otimes \Phi^{(0)} + F^{(0)} \cdot T_i^{(0)} \otimes \Phi^{(1)}. \tag{3.19}$$

which splits into

$$\langle \hat{Q}_i \rangle_{\text{nf}}^{(1)} + \hat{Z}_{ij}^{(1)} \langle \hat{Q}_j \rangle^{(0)} = F^{(0)} \cdot T_i^{(1)} \otimes \Phi^{(0)} \tag{3.20}$$

for the calculation of the NLO kernels $T_i^{(1)}$ and

$$\langle \hat{Q}_i \rangle_{\text{f}}^{(1)} + Z_\psi^{(1)} \langle \hat{Q}_i \rangle^{(0)} = F^{(1)} \cdot T_i^{(0)} \otimes \Phi^{(0)} + F^{(0)} \cdot T_i^{(0)} \otimes \Phi^{(1)}, \tag{3.21}$$

which shows that the factorizable diagrams and the wave-function renormalization are absorbed by the form factor and wave function corrections $F^{(1)}$ and $\Phi^{(1)}$.

This suggests in NNLO the following structure

$$\langle \hat{Q}_i \rangle_{\text{f}}^{(2)} + Z_\psi^{(1)} \langle \hat{Q}_i \rangle_{\text{f}}^{(1)} + Z_\psi^{(2)} \langle \hat{Q}_i \rangle^{(0)}$$
$$= F^{(2)} \cdot T_i^{(0)} \otimes \Phi^{(0)} + F^{(1)} \cdot T_i^{(0)} \otimes \Phi^{(1)} + F^{(0)} \cdot T_i^{(0)} \otimes \Phi^{(2)}. \tag{3.22}$$

These terms are thus irrelevant for the calculation of the NNLO kernels $T_i^{(2)}$ which justifies that we could restrict our attention to the non-factorizable 2-loop diagrams from Figure 3.2. In NNLO the remaining terms from (3.11) and (3.16) contain non-trivial IR subtractions

$$\langle \hat{Q}_i \rangle_{\text{nf}}^{(2)} + Z_\psi^{(1)} \langle \hat{Q}_i \rangle_{\text{nf}}^{(1)} + \hat{Z}_{ij}^{(1)} \left[ \langle \hat{Q}_j \rangle_{\text{nf}}^{(1)} + \langle \hat{Q}_j \rangle_{\text{f}}^{(1)} \right] + \left[ \hat{Z}_{ij}^{(2)} + Z_\psi^{(1)} \hat{Z}_{ij}^{(1)} \right] \langle \hat{Q}_j \rangle^{(0)}$$
$$= F^{(0)} \cdot T_i^{(2)} \otimes \Phi^{(0)} + F^{(1)} \cdot T_i^{(1)} \otimes \Phi^{(0)} + F^{(0)} \cdot T_i^{(1)} \otimes \Phi^{(1)}. \tag{3.23}$$

This equation can be simplified further when we make the wave function renormalization factors in the form factor and the distribution amplitude explicit

$$F = Z_b^{1/2} Z_q^{1/2} F_{\text{amp}}, \qquad \Phi = Z_q \Phi_{\text{amp}}. \tag{3.24}$$

Notice that the resulting amputated form factor $F_{\text{amp}}$ and wave function $\Phi_{\text{amp}}$ contain UV divergences by construction. We recall that $Z_\psi = Z_b^{1/2} Z_q^{3/2}$ and find

$$F^{(1)} \cdot T_i^{(1)} \otimes \Phi^{(0)} + F^{(0)} \cdot T_i^{(1)} \otimes \Phi^{(1)}$$
$$= F_{\text{amp}}^{(1)} \cdot T_i^{(1)} \otimes \Phi^{(0)} + F^{(0)} \cdot T_i^{(1)} \otimes \Phi_{\text{amp}}^{(1)} + Z_\psi^{(1)} F^{(0)} \cdot T_i^{(1)} \otimes \Phi^{(0)}. \tag{3.25}$$

Combining (3.23) with (3.25) and (3.20), we arrive at the Master Formula for the calculation of the hard-scattering kernels $T_i^{(2)}$ in NNLO

$$\langle \hat{Q}_i \rangle_{\mathrm{nf}}^{(2)} + \hat{Z}_{ij}^{(1)} \left[ \langle \hat{Q}_j \rangle_{\mathrm{nf}}^{(1)} + \langle \hat{Q}_j \rangle_{\mathrm{f}}^{(1)} \right] + \hat{Z}_{ij}^{(2)} \langle \hat{Q}_j \rangle^{(0)}$$

$$= F^{(0)} \cdot T_i^{(2)} \otimes \Phi^{(0)} + F_{\mathrm{amp}}^{(1)} \cdot T_i^{(1)} \otimes \Phi^{(0)} + F^{(0)} \cdot T_i^{(1)} \otimes \Phi_{\mathrm{amp}}^{(1)}. \qquad (3.26)$$

The 2-loop matrix elements on the left-hand side of (3.26) have been considered in Section 3.2 and the 1-loop renormalization matrix has been given in (4.4). The 1-loop matrix elements of the non-factorizable diagrams involve the calculation of the diagrams in Figure 1.8a. The tree level matrix elements as well as the 1-loop matrix elements of the factorizable diagrams from Figure 1.9 can be disregarded here as they do not give rise to an imaginary part. Hence, the only missing pieces for the calculation of the imaginary part of the NNLO kernels $T_i^{(2)}$ are the IR subtractions on the right-hand side of (3.26) which we consider in the following section.

### 3.3.3 IR subtractions

Let us first address the NLO kernels $T_i^{(1)}$ which can be determined from equation (3.20). The renormalization in the evanescent sector implies that the left hand side of (3.20) is free of contributions from evanescent operators up to the *finite order* $\varepsilon^0$. However, as the NLO kernels enter (3.26) in combination with the form factor correction $F^{(1)}$ which contains double (soft and collinear) IR divergences, the NLO kernels are required here up to $\mathcal{O}(\varepsilon^2)$. Concerning the subleading terms of $\mathcal{O}(\varepsilon)$, the evanescent operators do not drop out on the left hand side of (3.20) and we therefore have to extend the factorization formula on the right hand side to include these evanescent structures as well. Schematically,

$$\langle \hat{Q}_i \rangle_{\mathrm{nf}}^{(1)} + \hat{Z}_{ij}^{(1)} \langle \hat{Q}_j \rangle^{(0)} = F^{(0)} \cdot T_i^{(1)} \otimes \Phi^{(0)} + F_E^{(0)} \cdot T_{i,E}^{(1)} \otimes \Phi_E^{(0)} \qquad (3.27)$$

with a kernel $T_{i,E}^{(1)} = \mathcal{O}(1)$ and an evanescent matrix element $F_E^{(0)} \Phi_E^{(0)} = \mathcal{O}(\varepsilon)$. Similarly, the right hand side of (3.26) has to be modified to include these evanescent structures.

From the calculation of the 1-loop diagrams in Figure 1.8a, we find that the NLO kernels vanish in the colour-singlet case, $T_2^{(1)} = T_{2,E}^{(1)} = 0$, whereas the imaginary part of the colour-octet kernels is given by

$$\frac{1}{\pi} \operatorname{Im} T_1^{(1)}(u) = \frac{C_F}{2N_c} \Bigg\{ (-3 - 2\ln u + 2\ln \bar{u}) \left( 1 + \varepsilon L + \frac{1}{2}\varepsilon^2 L^2 \right)$$

$$- (11 - 3\ln \bar{u} - \ln^2 u + \ln^2 \bar{u}) \left( \varepsilon + \varepsilon^2 L \right)$$

$$+ \left[ \frac{3\pi^2}{4} - 26 + \left( 2 + \frac{\pi^2}{2} \right) \ln u + \left( 9 - \frac{\pi^2}{2} \right) \ln \bar{u} \right.$$

$$\left. - \frac{3}{2}\ln^2 \bar{u} - \frac{1}{3} \left( \ln^3 u - \ln^3 \bar{u} \right) \right] \varepsilon^2 + \mathcal{O}(\varepsilon^3) \Bigg\},$$

$$\frac{1}{\pi} \operatorname{Im} T_{1,E}^{(1)}(u) = -\frac{C_F}{4N_c} \left\{ 1 + \varepsilon L + \left( \frac{8}{3} - \frac{1}{2} \ln u - \frac{1}{2} \ln \bar{u} \right) \varepsilon + \mathcal{O}(\varepsilon^2) \right\}, \qquad (3.28)$$

where $L \equiv \ln \mu^2/m_b^2$ and we recall that $\bar{u} \equiv 1 - u$.

**Form factor subtractions**

We now address the form factor corrections which require the calculation of the diagram in Figure 3.5 (for on-shell quarks) and its counterterm. According to the definition of $F_{\text{amp}}$ in (3.24), we do not have to consider the wave function renormalization of the quark fields here.

We again have to compute the corrections for physical and evanescent operators. Concerning the physical operators with Dirac structure $[\gamma^\mu L] [\gamma_\mu L]$ the counterterm is found to vanish and we get

$$F_{\text{amp}}^{(1)} \Phi^{(0)} = -C_F \left( \frac{e^{\gamma_E} \mu^2}{m_b^2} \right)^\varepsilon \Gamma(\varepsilon) \frac{1 - \varepsilon + 2\varepsilon^2}{\varepsilon(1 - 2\varepsilon)} F^{(0)} \Phi^{(0)} \qquad (3.29)$$

reflecting the $1/\varepsilon^2$–singularities mentioned at the beginning of this section. On the other hand, the evanescent operators with $[\gamma^\mu \gamma^\nu \gamma^\rho L] [\gamma_\mu \gamma_\nu \gamma_\rho L] - 16[\gamma^\mu L] [\gamma_\mu L]$ yield a contribution proportional to the evanescent *and* the physical operators. We find a non-vanishing contribution from the counterterm diagram in this case and obtain

$$F_{\text{amp,E}}^{(1)} \Phi_E^{(0)} = C_F \left[ \left( \frac{e^{\gamma_E} \mu^2}{m_b^2} \right)^\varepsilon \Gamma(\varepsilon) \frac{24\varepsilon(1 + \varepsilon)}{(1 - \varepsilon)^2} - 24 \right] F^{(0)} \Phi^{(0)}$$

$$- C_F \left( \frac{e^{\gamma_E} \mu^2}{m_b^2} \right)^\varepsilon \Gamma(\varepsilon) \frac{1 - 3\varepsilon + \varepsilon^2 + 3\varepsilon^3 + 2\varepsilon^4}{\varepsilon(1 - 2\varepsilon)(1 - \varepsilon)^2} F_E^{(0)} \Phi_E^{(0)}. \qquad (3.30)$$

The first subtraction term in (3.26) then follows from combining the form factor corrections in (3.29) and (3.30) with the NLO kernels in (3.28). We emphasize that the corrections related to the evanescent operators do *not* induce a contribution to the physical NNLO kernel $T_1^{(2)}$ in this case since

$$\frac{1}{\pi} F_{\text{amp,E}}^{(1)} \operatorname{Im} T_{1,E}^{(1)} \Phi_E^{(0)} \quad \rightarrow \quad \left[ \mathcal{O}(\varepsilon) \right] F^{(0)} \Phi^{(0)}. \qquad (3.31)$$

**Wave function subtractions**

Concerning the wave function corrections we are left with the calculation of the diagrams in Figure 3.6 for collinear and on-shell partons with momenta $uq$ and $\bar{u}q$.
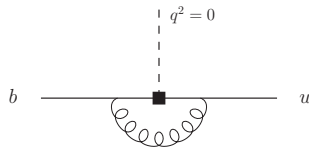


Figure 3.5: *1-loop contribution to the form factor correction $F_{amp}^{(1)}$.*
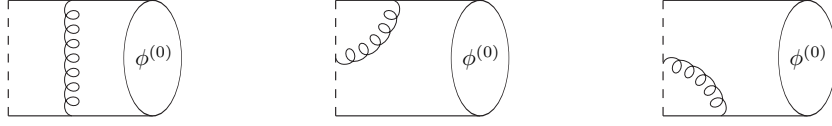
Figure 3.6: *1-loop contributions to the wave function correction $\Phi_{amp}^{(1)}$. The dashed line indicates the Wilson-line connecting the quark and antiquark fields.*

However, as in our set-up $q^2 = 0$ all these diagrams vanish due to scaleless integrals in DR. We conclude that the wave function corrections are determined entirely by the counterterms. We compute these counterterms by calculating the diagrams from Figure 3.6 with an off-shell regularization prescription in order to isolate the UV-divergences. The counterterm for the physical operators is found to be

$$F^{(0)} \, \Phi_{\text{amp}}^{(1)}(u) = -\frac{2C_F}{\varepsilon} \int_0^1 dw \, V(u,w) \, F^{(0)} \, \Phi^{(0)}(w) \tag{3.32}$$

with the familiar Efremov-Radyushkin-Brodsky-Lepage (ERBL) kernel [36,37]

$$V(u,w) = \left[ \theta(w-u)\frac{u}{w}\left(1 + \frac{1}{w-u}\right) + \theta(u-w)\frac{\bar{u}}{\bar{w}}\left(1 + \frac{1}{\bar{w}-\bar{u}}\right) \right]_+ \tag{3.33}$$

where the plus-distribution is defined as $[f(u,w)]_+ = f(u,w) - \delta(u-w)\int_0^1 dv \, f(v,w)$. For the evanescent operators we obtain

$$F_E^{(0)} \, \Phi_{\text{amp,E}}^{(1)}(u) = -\frac{2C_F}{\varepsilon} \int_0^1 dw \left[ 24\varepsilon \, V_E(u,w) \, F^{(0)} \, \Phi^{(0)}(w) + V(u,w) \, F_E^{(0)} \, \Phi_E^{(0)}(w) \right] \tag{3.34}$$

where $V_E(u,w)$ denotes the spin-dependent part of the ERBL kernel given by

$$V_E(u,w) = \theta(w-u)\frac{u}{w} + \theta(u-w)\frac{\bar{u}}{\bar{w}} \tag{3.35}$$

Notice that the evanescent operators *do* induce a finite contribution to the physical kernel $T_1^{(2)}$ in this case as the convolution with the corresponding NLO kernel implies

$$\frac{1}{\pi} \, F_E^{(0)} \, \text{Im} \, T_{1,E}^{(1)} \, \Phi_{\text{amp,E}}^{(1)} \quad \rightarrow \quad \left[ \frac{6C_F^2}{N_c} + \mathcal{O}(\varepsilon) \right] F^{(0)} \, \Phi^{(0)}. \tag{3.36}$$

We finally quote the result for the convolution with the physical NLO kernel

$$\begin{aligned}
\frac{1}{\pi} \, F^{(0)} \, \text{Im} \, T_1^{(1)} \, \Phi_{\text{amp}}^{(1)} = \frac{C_F^2}{N_c} &\left\{ \left[ \frac{\pi^2}{3} + \frac{\ln u}{\bar{u}} - \frac{\ln \bar{u}}{u} + \ln^2 u - 2\ln u \ln \bar{u} - \ln^2 \bar{u} - 4\text{Li}_2(u) \right] \right. \\
&\left( \frac{1}{\varepsilon} + L \right) + \frac{\pi^2}{2} - \frac{15}{4} - 2\zeta_3 + \frac{5u-4}{2}\left( \frac{\ln u}{\bar{u}} + \frac{\ln \bar{u}}{u} \right) - \frac{\pi^2}{3}\ln \bar{u} \\
&- 3\text{Li}_2(u) - \frac{1}{2\bar{u}}\ln^2 u + \frac{1-3u}{2u}\ln^2 \bar{u} - \frac{2}{3}\ln^3 u + \ln^2 u \ln \bar{u} \\
&\left. + \frac{2}{3}\ln^3 \bar{u} + 2\ln \bar{u}\,\text{Li}_2(u) + 2\text{Li}_3(u) + 2\text{S}_{1,2}(u) + \mathcal{O}(\varepsilon) \right\} F^{(0)} \, \Phi^{(0)}
\end{aligned} \tag{3.37}$$

## 3.4　Tree amplitudes in NNLO

The NNLO kernels $T_i^{(2)}$ can now be determined from the Master Formula (3.26). We indeed observe that all UV and IR singularities cancel in the NNLO kernels which provides a very important and highly non-trivial cross-check of the calculation[1]. In analogy to Section 1.2.3, we quote our results in terms of the tree amplitudes $\alpha_{1,2}$.

### 3.4.1　$\alpha_1$ in CMM basis

The procedure outlined so far leads to the colour-allowed tree amplitude in the CMM operator basis from (3.2). We write

$$\alpha_1(M_1 M_2) = \hat{C}_2 + \frac{\alpha_s}{4\pi} \frac{C_F}{2N_c} \left[ \hat{C}_1 \hat{V}^{(1)} + \frac{\alpha_s}{4\pi} \left( \hat{C}_1 \hat{V}_1^{(2)} + \hat{C}_2 \hat{V}_2^{(2)} \right) + \mathcal{O}(\alpha_s^2) \right] + \dots \tag{3.38}$$

where the ellipses denote the terms from spectator scattering which are irrelevant for our purposes. In the CMM basis, the imaginary part of the vertex corrections $\hat{V}^{(1,2)}$ can be written in the form

$$\frac{1}{\pi} \operatorname{Im} \hat{V}^{(1)} \equiv \int_0^1 du\, g_1(u)\, \phi_{M_2}(u),$$

$$\frac{1}{\pi} \operatorname{Im} \hat{V}_1^{(2)} \equiv \int_0^1 du\, \left\{ \left[ \left( \frac{29}{3} N_c - \frac{2}{3} n_f \right) g_1(u) + C_F\, h_1(u) \right] \ln \frac{\mu^2}{m_b^2} \right.$$

$$\left. + C_F\, h_2(u) + N_c\, h_3(u) + (n_f - 2)\, h_4(u; 0) + h_4(u; z) + h_4(u; 1) \right\} \phi_{M_2}(u),$$

$$\frac{1}{\pi} \operatorname{Im} \hat{V}_2^{(2)} \equiv \int_0^1 du\, \left\{ -6\, g_1(u) \ln \frac{\mu^2}{m_b^2} + h_0(u) \right\} \phi_{M_2}(u). \tag{3.39}$$

We stress that these quantities do *not* correspond to the $V^{(1,2)}$ from (1.22) which will be given in the following section after the transformation to the QCDF basis. In writing (3.39), we have made the dependence on the renormalization scale explicit and we have disentangled contributions that belong to different colour structures. The function $h_4(u; z_f)$ stems from diagrams with a closed fermion loop and depends on the mass of the internal quark through $z_f = m_f/m_b$. We write $z \equiv z_c = m_c/m_b$ for simplicity.

In NLO we find

$$g_1(u) = -3 - 2\ln u + 2\ln \bar{u}. \tag{3.40}$$

---

[1]As we do not distinguish between UV and IR singularities in our calculation, we cannot verify their cancellation independently. However, the aforementioned renormalization and IR subtraction procedure can be organized in a way that allows to control the cancellation of the leading poles in several intermediate steps of the calculation.

The NNLO kernels were so far unknown. They are found in this work to be

$$h_0(u) = \left[\frac{155}{4} + 4\zeta_3 + 4\text{Li}_3(u) - 4\text{S}_{1,2}(u) - 12\ln u\,\text{Li}_2(u) + \frac{4}{3}\ln^3 u - 6\ln^2 u\ln\bar{u}\right.$$

$$+ \frac{2-u^2}{\bar{u}}\text{Li}_2(u) - \frac{5-3u+3u^2-2u^3}{2\bar{u}}\ln^2 u + \frac{3-2u^4}{2u\bar{u}}\ln u\ln\bar{u}$$

$$\left.- \left(\frac{4-11u+2u^2}{\bar{u}} + \frac{4\pi^2}{3}\right)\ln u - \frac{(5+6u^2-12u^4)\pi^2}{24u\bar{u}} + (u\leftrightarrow\bar{u})\right]$$

$$+ \left[\frac{3-u+7u^2}{2\bar{u}}\ln^2 u - \frac{11-10u^2}{4u\bar{u}}\text{Li}_2(u) + \frac{1-14u^2}{4\bar{u}}\ln u\ln\bar{u}\right.$$

$$\left.+ \frac{46-51u}{\bar{u}}\ln u - \frac{(41-42u^2)\pi^2}{24\bar{u}} - (u\leftrightarrow\bar{u})\right],$$

$$h_1(u) = 36 + \left[2\ln^2 u - 4\text{Li}_2(u) + \frac{2(13-12u)}{1-u}\ln u - (u\leftrightarrow\bar{u})\right],$$

$$h_2(u) = \left[79 + 32\zeta_3 - 16\text{Li}_3(u) - 32\text{S}_{1,2}(u) + \frac{8}{3}\ln^3 u + \frac{2(4-u^2)}{\bar{u}}\text{Li}_2(u)\right.$$

$$- \frac{13-9u+6u^2-4u^3}{2\bar{u}}\ln^2 u + \frac{17-6u^2-8u^4}{4u\bar{u}}\ln u\ln\bar{u}$$

$$\left.- 2\left(\frac{5-11u+2u^2}{\bar{u}} + \frac{4\pi^2}{3}\right)\ln u - \frac{(1+14u^2-8u^4)\pi^2}{8u\bar{u}} + (u\leftrightarrow\bar{u})\right]$$

$$+ \left[4\text{Li}_3(u) + 4\text{S}_{1,2}(u) - \frac{2}{3}\ln^3 u + 2\ln^2 u\ln\bar{u} - \frac{9-14u^2}{u\bar{u}}\text{Li}_2(u)\right.$$

$$+ \frac{13-11u+14u^2}{2\bar{u}}\ln^2 u + \frac{5-7u^2}{\bar{u}}\ln u\ln\bar{u}$$

$$\left.+ 4\left(\frac{24-23u}{\bar{u}} + \frac{\pi^2}{3}\right)\ln u - \frac{(26-21u^2)\pi^2}{6\bar{u}} - (u\leftrightarrow\bar{u})\right],$$

$$h_3(u) = \left[-\frac{1379}{24} - 12\zeta_3 + 6\text{Li}_3(u) + 12\text{S}_{1,2}(u) - \ln^3 u - \frac{4-u^2}{\bar{u}}\text{Li}_2(u)\right.$$

$$+ \frac{9-2u+6u^2-4u^3}{4\bar{u}}\ln^2 u - \frac{7+4u^2-4u^4}{4u\bar{u}}\ln u\ln\bar{u}$$

$$\left.+ \left(\frac{41-66u+8u^2}{4\bar{u}} + \pi^2\right)\ln u + \frac{(1+6u^2-4u^4)\pi^2}{8u\bar{u}} + (u\leftrightarrow\bar{u})\right]$$

$$+ \left[-2\text{Li}_3(u) + 4\text{S}_{1,2}(u) + 4\ln u\,\text{Li}_2(u) + \frac{1}{3}\ln^3 u + \frac{15-26u^2}{4u\bar{u}}\text{Li}_2(u)\right.$$

$$+ \frac{11-14u-42u^2}{12\bar{u}}\ln^2 u - \frac{11-14u^2}{4\bar{u}}\ln u\ln\bar{u}$$

$$- \left( \frac{2165 - 2156u}{36\bar{u}} - \frac{\pi^2}{3} \right) \ln u + \frac{(53 - 42u^2)\pi^2}{24\bar{u}} - (u \leftrightarrow \bar{u}) \Bigg],$$

$$h_4(u; z) = \left[ \frac{17}{6} + \frac{7\xi}{\bar{u}} - 2\xi^2 \ln^2 \frac{x_1}{x_2} + 2\Big((1 + 4\xi)x_1 + (1 + 6\xi)x_2\Big) \ln x_1 - 4\xi\, x_1 \ln x_2 \right.$$

$$+ \left( \frac{\xi}{\bar{u}} - 2(1 + 4\xi)x_2 \right) \ln z^2 + \Big((1 + 2\xi)x_1 + (1 + 6\xi)x_2\Big) \ln u + (u \leftrightarrow \bar{u}) \Bigg]$$

$$+ \left[ \frac{94z^2}{9\bar{u}} - \frac{2(1 - 3\xi^2)}{3} \ln^2 \frac{x_1}{x_2} - \frac{2[(6 + 29\xi + 20\xi^2)x_1 + (29 + 38\xi)\xi\, x_2]}{9\xi} \ln x_1 \right.$$

$$- \frac{4(1 - 3\xi^2)}{3\xi} x_1 \ln x_2 + \frac{2u\bar{u}(6 + 29\xi + 20\xi^2)x_2 + (1 - 2u)(6\bar{u} - u\xi^2)}{9u\bar{u}\xi} \ln z^2$$

$$- \frac{4}{3} \ln u \ln z^2 - \frac{(12 + 29\xi + 2\xi^2)x_1 + (29 + 38\xi)\xi\, x_2}{9\xi} \ln u - (u \leftrightarrow \bar{u}) \Bigg].$$

$$(3.41)$$

The last kernel $h_4(u; z)$ has been given in terms of

$$x_1 \equiv \frac{1}{2} \left( \sqrt{1 + 4\xi} - 1 \right), \qquad x_2 \equiv \frac{1}{2} \left( \sqrt{1 + 4\xi} + 1 \right), \qquad \xi \equiv \frac{z^2}{u}. \qquad (3.42)$$

In the massless limit $h_4(u; z)$ simply becomes

$$h_4(u; 0) = \frac{17}{3} - \frac{2}{3} \ln^2 u + \frac{2}{3} \ln^2 \bar{u} + \frac{20}{9} \ln u - \frac{38}{9} \ln \bar{u}. \qquad (3.43)$$

### 3.4.2　$\alpha_1$ and $\alpha_2$ in QCDF basis

We now perform the transformation of the colour-allowed tree amplitude $\alpha_1$ into the QCDF operator basis from (3.1). As discussed in Section 3.1, manifest Fierz symmetry in the QCDF basis allows us to derive the colour-suppressed amplitude $\alpha_2$ directly from $\alpha_1$ under the exchange $\tilde{C}_1 \leftrightarrow \tilde{C}_2$.

The colour-allowed tree amplitude has been given in the CMM basis in (3.38) and in the QCDF basis in (1.22). If we focus on the imaginary part and disregard contributions from spectator scattering, these relations become

$$\frac{1}{\pi} \operatorname{Im} \alpha_1 \big|_V = \frac{\alpha_s C_F}{4\pi\, N_c} \frac{1}{\pi} \operatorname{Im} \left[ \frac{1}{2} \hat{C}_1\, \hat{V}^{(1)} + \frac{\alpha_s}{4\pi} \left( \frac{1}{2} \hat{C}_1\, \hat{V}_1^{(2)} + \frac{1}{2} \hat{C}_2\, \hat{V}_2^{(2)} \right) + \mathcal{O}(\alpha_s^2) \right]$$

$$= \frac{\alpha_s C_F}{4\pi\, N_c} \frac{1}{\pi} \operatorname{Im} \left[ \tilde{C}_2\, V^{(1)} + \frac{\alpha_s}{4\pi} \left( \tilde{C}_1\, V_1^{(2)} + \tilde{C}_2\, V_2^{(2)} \right) + \mathcal{O}(\alpha_s^2) \right]. \qquad (3.44)$$

In order to compute $V^{(1,2)}$, we need the relation between the Wilson coefficients in the CMM basis $\hat{C}_{1,2}$ and the ones in the QCDF basis $\tilde{C}_{1,2}$ to NLL approximation.

The Wilson coefficients can be found e.g. in [103], where the transformation between both bases has been studied in detail. From this, we derive

$$\hat{C}_1 = 2\tilde{C}_2 + \frac{\alpha_s}{4\pi}\left(4\tilde{C}_1 + \frac{14}{3}\tilde{C}_2\right) + \mathcal{O}(\alpha_s^2),$$

$$\hat{C}_2 = \tilde{C}_1 + \frac{1}{3}\tilde{C}_2 + \mathcal{O}(\alpha_s). \tag{3.45}$$

Combining (3.44), (3.45) and (3.39) we obtain

$$\frac{1}{\pi}\,\mathrm{Im}\,V^{(1)} = \frac{1}{\pi}\,\mathrm{Im}\,\hat{V}^{(1)}$$

$$= \int_0^1 du\; g_1(u)\,\phi_{M_2}(u),$$

$$\frac{1}{\pi}\,\mathrm{Im}\,V_1^{(2)} = \frac{1}{\pi}\,\mathrm{Im}\left[\frac{1}{2}\,\hat{V}_2^{(2)} + 2\,\hat{V}^{(1)}\right]$$

$$= \int_0^1 du\left\{-3\,g_1(u)\ln\frac{\mu^2}{m_b^2} + 2\,g_1(u) + \frac{1}{2}\,h_0(u)\right\}\phi_{M_2}(u),$$

$$\frac{1}{\pi}\,\mathrm{Im}\,V_2^{(2)} = \frac{1}{\pi}\,\mathrm{Im}\left[\hat{V}_1^{(2)} + \frac{1}{6}\,\hat{V}_2^{(2)} + \frac{7}{3}\,\hat{V}^{(1)}\right]$$

$$= \int_0^1 du\left\{\left[\left(28 - \frac{2}{3}n_f\right)g_1(u) + \frac{4}{3}h_1(u)\right]\ln\frac{\mu^2}{m_b^2} + \frac{7}{3}\,g_1(u) + \frac{1}{6}\,h_0(u)\right.$$

$$\left. + \frac{4}{3}\,h_2(u) + 3\,h_3(u) + (n_f - 2)\,h_4(u;0) + h_4(u;z) + h_4(u;1)\right\}\phi_{M_2}(u). \tag{3.46}$$

Notice that these expressions determine the vertex corrections for the colour-allowed amplitude $\alpha_1$ *and* the colour-suppressed amplitude $\alpha_2$ according to (1.22). The equations in (3.46) represent the central result of our analysis. The expression for $V^{(1)}$ is in agreement with (1.19), whereas the expressions for $V_{1,2}^{(2)}$ are new. The kernels $g_1$ and $h_{0-4}$ can be found in (3.40) and (3.41). The terms proportional to $n_f$ have already been considered in the analysis of the large $\beta_0$-limit in [71,72]. Our results are in agreement with these findings.

### 3.4.3   Convolution with distribution amplitude

The NNLO vertex corrections have been given in (3.46) as convolutions of hard-scattering kernels with the light-cone distribution amplitude of the meson $M_2$. We may explicitly perform the convolution integrals by expanding the distribution amplitude into the eigenfunctions of the 1-loop evolution kernel

$$\phi_{M_2}(u) = 6u\bar{u}\left[1 + \sum_{n=1}^{\infty} a_n^{M_2}\, C_n^{(3/2)}(2u - 1)\right], \tag{3.47}$$

where $a_n^{M_2}$ and $C_n^{(3/2)}$ are the Gegenbauer moments and polynomials, respectively. It is convenient to truncate this expansion at $n = 2$. The convolution integrals with the kernels $g_1$ and $h_{0-3}$ from (3.40) and (3.41) then give

$$\int_0^1 du\, g_1(u)\, \phi_{M_2}(u) = -3 - 3\, a_1^{M_2},$$

$$\int_0^1 du\, h_0(u)\, \phi_{M_2}(u) = \frac{1333}{12} + \frac{47\pi^2}{45} - 16\zeta_3 + \left(\frac{15}{4} + \frac{23\pi^2}{5}\right) a_1^{M_2}$$
$$- \left(\frac{173}{30} + \frac{18\pi^2}{35}\right) a_2^{M_2},$$

$$\int_0^1 du\, h_1(u)\, \phi_{M_2}(u) = 36 + 28\, a_1^{M_2},$$

$$\int_0^1 du\, h_2(u)\, \phi_{M_2}(u) = \frac{1369}{6} + \frac{139\pi^2}{45} - 32\zeta_3 - \left(\frac{17}{6} - \frac{51\pi^2}{5}\right) a_1^{M_2}$$
$$- \left(\frac{103}{15} + \frac{71\pi^2}{35}\right) a_2^{M_2},$$

$$\int_0^1 du\, h_3(u)\, \phi_{M_2}(u) = -\frac{481}{3} + \frac{7\pi^2}{30} + 12\zeta_3 - \left(\frac{643}{12} + \frac{11\pi^2}{10}\right) a_1^{M_2}$$
$$- \left(\frac{1531}{80} - \frac{169\pi^2}{70}\right) a_2^{M_2}. \tag{3.48}$$

The convolution with $h_4(u; z)$ from (3.41) can also be performed analytically

$$H_4(z) \equiv \int_0^1 du\, h_4(u; z)\, \phi_{M_2}(u)$$
$$= \frac{22}{3} + 148z^2 - 96z^4 F(z) - 36z^4 \ln^2 \frac{y_1}{y_2}$$
$$- 2\left[1 - (2y_1 + 1)(1 + 22z^2)\right] \ln \frac{y_1}{y_2} - 4\ln y_2$$
$$+ \left(7 + 164z^2 + 180z^4 + 144z^6 - 288z^4 F(z) + 12z^4(3 + 16z^2 + 12z^4) \ln^2 \frac{y_1}{y_2}\right.$$
$$\left. - 2\left[1 - (2y_1 + 1)(1 + 22z^2 + 84z^4 + 72z^6)\right] \ln \frac{y_1}{y_2} - 4\ln y_2\right) a_1^{M_2}$$
$$+ \left(\frac{3}{5} + 244z^2 + \frac{148}{3}z^4 - 640z^6 - 960z^8 + 24z^4(1 - 30z^4 - 40z^6) \ln^2 \frac{y_1}{y_2}\right.$$
$$\left. - 576z^4 F(z) + 8z^2(2y_1 + 1)(6 + 11z^2 - 70z^4 - 120z^6) \ln \frac{y_1}{y_2}\right) a_2^{M_2}, \tag{3.49}$$

where we defined

$$y_1 \equiv \frac{1}{2}\left(\sqrt{1+4z^2}-1\right), \qquad y_2 \equiv \frac{1}{2}\left(\sqrt{1+4z^2}+1\right),$$

$$F(z) \equiv \mathrm{Li}_3(-y_1) - \mathrm{S}_{1,2}(-y_1) - \ln y_1 \mathrm{Li}_2(-y_1) + \frac{1}{2}\ln y_1 \ln^2 y_2 - \frac{1}{12}\ln^3 z^2 + \zeta_3. \tag{3.50}$$

In the massless limit the function $H_4(z)$ simply becomes

$$H_4(0) = \frac{22}{3} + 7a_1^{M_2} + \frac{3}{5}a_2^{M_2}. \tag{3.51}$$

The finiteness of all convolution integrals in (3.48) and (3.49) completes the explicit factorization proof of the imaginary part of the NNLO vertex corrections.

We summarize our results for the vertex corrections in the considered representation of the light-cone distribution amplitude of the emitted meson $M_2$

$$\frac{1}{\pi}\,\mathrm{Im}\,V^{(1)} = -3 - 3a_1^{M_2},$$

$$\frac{1}{\pi}\,\mathrm{Im}\,V_1^{(2)} = 9\left(1 + a_1^{M_2}\right)\ln\frac{\mu^2}{m_b^2} + \frac{1189}{24} + \frac{47\pi^2}{90} - 8\zeta_3 - \left(\frac{33}{8} - \frac{23\pi^2}{10}\right)a_1^{M_2}$$

$$- \left(\frac{173}{60} + \frac{9\pi^2}{35}\right)a_2^{M_2},$$

$$\frac{1}{\pi}\,\mathrm{Im}\,V_2^{(2)} = -\left(26 + \frac{110}{3}a_1^{M_2}\right)\ln\frac{\mu^2}{m_b^2} - \frac{10315}{72} + \frac{674\pi^2}{135} - \frac{28}{3}\zeta_3$$

$$- \left(\frac{10793}{72} - \frac{166\pi^2}{15}\right)a_1^{M_2} - \left(\frac{3155}{48} - \frac{187\pi^2}{42}\right)a_2^{M_2} + H_4(z) + H_4(1), \tag{3.52}$$

with $H_4(z)$ given in (3.49). In order to illustrate the relative importance of the individual contributions, we set $\mu = m_b$ and $z = m_c/m_b = 0.3$ which yields

$$\mathrm{Im}\,V^{(1)} = -9.425 - 9.43a_1^{M_2},$$

$$\mathrm{Im}\,V_1^{(2)} = 141.621 + 58.36\,a_1^{M_2} - 17.03\,a_2^{M_2},$$

$$\mathrm{Im}\,V_2^{(2)} = -317.940 - 115.62\,a_1^{M_2} - 68.31\,a_2^{M_2}. \tag{3.53}$$

We find large coefficients for the NNLO vertex corrections and expect only a minor impact of the higher Gegenbauer moments (in particular in the symmetric case with $a_1^{M_2} = 0$). Notice that all contributions add constructively in $\alpha_{1,2}$ due to the relative signs of the accompanying Wilson coefficients. In the case of $\alpha_1$ the contribution from $V_1^{(2)}$ is found to exceed the formally leading contribution $V^{(1)}$ due to the fact that the latter is multiplied by the small Wilson coefficient $\tilde{C}_2$. For $\alpha_2$ the impact of the NNLO vertex corrections is also substantial, roughly saying they amount to a 50% correction. A more detailed numerical analysis including the contributions from spectator scattering will be given in the following section.

## 3.5    Numerical analysis

We conclude this chapter with a brief numerical analysis (an extended version will be
given in [100]). We first consider the vertex corrections solely without the spectator
scattering contributions which have been computed recently in [25,26]. These will be
added in the second part of our analysis which will lead us to the full NNLO result
for the imaginary part of the topological tree amplitudes in QCD Factorization.

### 3.5.1    Vertex corrections

We come back to the question if the large $\beta_0$-limit considered in [71,72] represents
a good approximation for the imaginary part of the NNLO vertex corrections. For
illustration, we introduce two functions $\zeta_i(u)$ defined by

$$\alpha_1\big|_V \equiv \int_0^1 du \ \zeta_i(u). \tag{3.54}$$

The $\zeta_i(u)$ correspond to a combination of Wilson coefficients and hard-scattering
kernels multiplied by the distribution amplitude of the emitted meson $M_2$. The
imaginary part of the functions $\zeta_i(u)$ are shown in Figure 3.7 with the asymptotic
form of the distribution amplitude, for simplicity.

As we have stated at the end of the last section, we find that the NNLO corrections
add constructively to the NLO results. They provide the dominant contribution
to the imaginary part of $\alpha_1$ and a substantial contribution to the one of $\alpha_2$. We
further see that the large $\beta_0$-limit is a good approximation in the case of $\alpha_2$ but
not for $\alpha_1$. This can be traced back to the fact that the imaginary part of $V_2^{(2)}$ is
reproduced well in this approximation whereas the one of $V_1^{(2)}$, which provides the
most important contribution to $\alpha_1$, is missed completely.

Concerning the scale dependence we recall that the imaginary part has only NLO
complexity at the considered order in perturbation theory. We therefore use the
2-loop expression for the running coupling constant ($n_f = 5$, $\Lambda_{\overline{\text{MS}}}^{(5)} = 0.225$ GeV) and
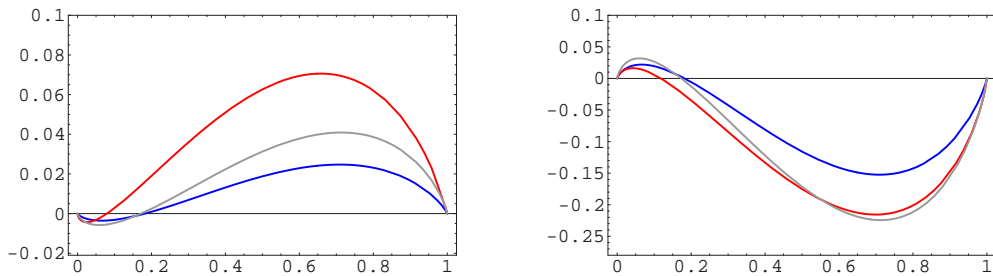


Figure 3.7: *Imaginary part of $\zeta_1(u)$ and $\zeta_2(u)$ as introduced in (3.54). The
graphs show the 1-loop vertex corrections (blue), the large $\beta_0$-approximation
(gray) and our new results including the 2-loop vertex corrections (red) for
$\mu = m_b$ (with asymptotic distribution amplitude).*
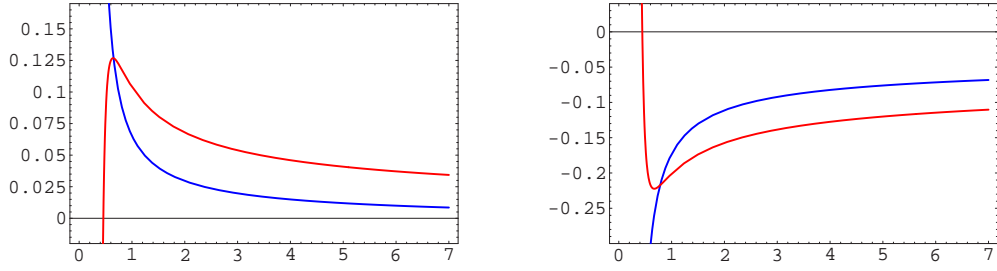
Figure 3.8: *Renormalization scale dependence of the imaginary part of $\alpha_1$ and $\alpha_2$ (without spectator scattering). Blue: NLO result. Red: NNLO result.*

consider the Wilson coefficients in NLL approximation which we take from [105]. Contrary to the second Gegenbauer moment, the first moment would also be required in NLL approximation as it enters the expression for $V^{(1)}$ in (3.52). However, in the following analysis we focus on the $B \to \pi\pi$ decays where the first moment is absent and we only implement the LL evolution of the second moment which is given by

$$a_2^{M_2}(\mu) = \left(\frac{\alpha_s(\mu)}{\alpha_s(\mu_0)}\right)^{-\gamma_2/2\beta_0} a_2^{M_2}(\mu_0), \qquad \gamma_2 = -\frac{100}{9}. \tag{3.55}$$

The scale dependence of the imaginary part of $\alpha_{1,2}$ is shown in Figure 3.8. We observe only a minor reduction of the scale dependence if we vary the scale between $m_b/2 \sim 2.4\,\text{GeV}$ and $2m_b \sim 9.6\,\text{GeV}$, in particular for $\alpha_1$ where the NNLO correction dominates over the NLO result.

### 3.5.2 Full NNLO result

We finally combine our results with the spectator scattering contributions from [25]. One remark is in order concerning the scale dependence of the spectator term. The respective kernel $T^{II}$ receives hard and hard-collinear contributions which are encoded in a hard coefficient function and a jet function, respectively (notice that the hard coefficient function represents the only source for an imaginary part). In the following discussion we simply evaluate all quantities related to the hard coefficient function at the hard scale $\mu_h$ and all other quantities at the hard-collinear scale $\mu_{hc}$ (this corresponds to equation (58) of [25] with $U_\parallel(\mu_h, \mu_{hc}) = 1$). A more sophisticated treatment of the scale issues in the spectator term is relegated to [100].

Our input parameters for the $B \to \pi\pi$ amplitudes are summarized in Table 3.2. They correspond to the values from previous analysis in QCD Factorization [25,66] with updated values for the form factor and the Gegenbauer moment based on recent LCSR analyses [53,54]. In order to estimate unknown perturbative corrections we vary the hard scale in the range $\mu_h = 4.8^{+4.8}_{-2.4}\,\text{GeV}$ and the hard-collinear scale independently between $\mu_{hc} = 1.5^{+0.7}_{-0.5}\,\text{GeV}$.

| Parameter | Value | Parameter | Value |
|-----------|-------|-----------|-------|
| $\Lambda_{\overline{\text{MS}}}^{(5)}$ | 0.225 | $f_B$ | $0.2 \pm 0.03$ |
| $m_b$ | 4.8 | $F_+^{B \to \pi}(0)$ | $0.26 \pm 0.04$ |
| $m_c$ | $1.3 \pm 0.2$ | $\lambda_B$ | $0.35 \pm 0.15$ |
| $f_\pi$ | 0.131 | $a_2^\pi(1\text{GeV})$ | $0.2 \pm 0.2$ |

Table 3.2: *Theoretical input parameters (in units of GeV or dimensionless).*

The complete NNLO result for the imaginary part of the topological tree amplitude is found to be

$$\text{Im}\,\alpha_1(\pi\pi) = \left.0.012\right|_{V^{(1)}} + \left.0.031\right|_{V^{(2)}} - \left.0.019\right|_{H^{(2)}}$$

$$= 0.025 \pm 0.021,$$

$$\text{Im}\,\alpha_2(\pi\pi) = \left.-0.077\right|_{V^{(1)}} - \left.0.052\right|_{V^{(2)}} + \left.0.031\right|_{H^{(2)}}$$

$$= -0.098 \pm 0.035, \tag{3.56}$$

where we disentangled the contributions from $V^{(1)}$, $V^{(2)}$ and $H^{(2)}$ according to (1.22). In the case of $\alpha_1$ the NNLO corrections exceed the NLO result which can be explained by the fact that the latter is multiplied by the small Wilson coefficient $\tilde{C}_2$. In both cases the individual NNLO corrections are found to be sizeable, but we observe a large cancellation in their sum. The NNLO vertex corrections considered in this work turn out to dominate over the spectator terms resulting in a moderate additive contribution to the NLO (BBNS) result.

The uncertainties quoted in (3.56) stem from the variation of the parameters shown in Table 3.3. As the dominant sources we identify the hadronic parameters $\lambda_B$ and $a_2^\pi$. Moreover, the sensitivity to the renormalization scale remains sizeable at NNLO as we have mentioned at the end of the last section. We finally emphasize that we have not yet assigned an error estimate to unknown power corrections which will be included in [100].

| | $\mu_h$ | $\mu_{hc}$ | $m_c$ | $f_B$ | $F_+^{B\pi}$ | $\lambda_B$ | $a_2^\pi$ |
|---|---------|-----------|-------|-------|-------------|-------------|-----------|
| $\alpha_1$ | 0.011 | 0.006 | 0.000 | 0.003 | 0.003 | 0.014 | 0.008 |
| $\alpha_2$ | 0.019 | 0.009 | 0.000 | 0.005 | 0.006 | 0.023 | 0.013 |

Table 3.3: *Uncertainties in our predictions of the imaginary part of $\alpha_1(\pi\pi)$ and $\alpha_2(\pi\pi)$ from the scale variation and the input parameters in Table 3.2.*

# Chapter 4

# Hadronic two-body decays II: Real part

The calculation of the real part of the NNLO vertex corrections in hadronic two-body decays proceeds along the same lines as the one of the imaginary part which we presented in the previous chapter. However, we will see below that the calculation of the real part is far more complicated involving many additional MIs and the full NNLO complexity concerning e.g. the issue of renormalization and the treatment of evanescent operators.

In this chapter we present a preliminary result for the real part of the colour-allowed tree amplitude $\alpha_1$ (in the CMM operator basis). Similar to what we have seen in the previous chapter, the colour-suppressed tree amplitude $\alpha_2$ can then be derived from $\alpha_1$ after the transformation into a Fierz-symmetric operator basis (which we called QCDF basis in Chapter 3). In NNLO we thus have to extend the basis from (3.1) to include 2-loop evanescent operators with an appropriate definition of $\varepsilon$- and $\varepsilon^2$-terms which guarantees manifest Fierz symmetry in this operator basis. As we have not yet worked out the details of this last step, we refer to [106] for the analysis of the colour-suppressed tree amplitude.

## 4.1   2-loop calculation

The 2-loop calculation will be performed in the CMM operator basis (cf. Section 3.1). Apart from the operators in (3.2), we have to take into account 2-loop evanescent operators which are defined by

$$\hat{E}_1' = \left[\bar{u}\gamma^\mu\gamma^\nu\gamma^\rho\gamma^\sigma\gamma^\tau L\, T^A b\right]\, \left[\bar{d}\gamma_\mu\gamma_\nu\gamma_\rho\gamma_\sigma\gamma_\tau L\, T^A u\right] - 20\hat{E}_1 - 256\,\hat{Q}_1,$$

$$\hat{E}_2' = \left[\bar{u}\gamma^\mu\gamma^\nu\gamma^\rho\gamma^\sigma\gamma^\tau L\, b\right]\, \left[\bar{d}\gamma_\mu\gamma_\nu\gamma_\rho\gamma_\sigma\gamma_\tau L\, u\right] - 20\hat{E}_2 - 256\,\hat{Q}_2. \tag{4.1}$$

We turn to a brief characterization of the considered 2-loop calculation following our recipe from Section 2.1.

**Step 1: Set-up for loop calculation**

In contrast to the calculation of the imaginary part from Chapter 3, we now have to consider the whole set of non-factorizable 2-loop diagrams from Figure 3.2. Notice that the most complicated diagrams only enter the calculation of the real part. Whereas the diagrams that we considered for the calculation of the imaginary part contained at most one massive ($b$-quark) propagator, we now have to deal with up to three massive propagators.

**Step 2: Reduction to Master Integrals**

The fact that the diagrams involve between 0-3 massive propagators immediately leads to many distinct topologies and a large number of MIs. In addition to the 14 MIs from Figure 3.3, we find 22 (real) MIs which are shown in Figure 4.1. We further remark that our MATHEMATICA implementation of the reduction algorithm hardly succeeds to reduce the most complicated diagrams of the considered calculation within a reasonable amount of CPU time.

**Step 3: Manipulation of Dirac structures**

Concerning the irreducible Dirac structures we find the same set (3.7) as in the calculation of the imaginary part. In contrast to our analysis from Chapter 3, the last structure now enters the divergent piece of the calculation giving rise to 2-loop evanescent operators according to (4.1).
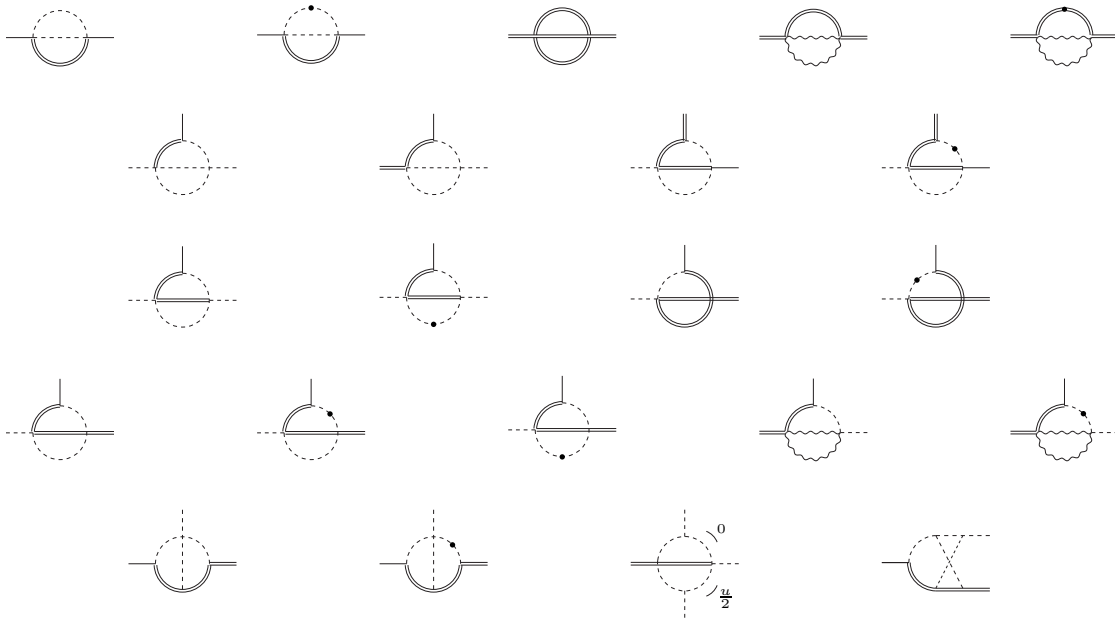


Figure 4.1: *Additional Master Integrals that have to be considered for the calculation of the real part of the NNLO vertex corrections. For details cf. Figure 3.3.*

**Step 4: Calculation of Master Integrals**

In the last step of the calculation it becomes obvious that the analysis of the real part of the NNLO vertex corrections is much more complex than the one of the imaginary part. We now have to calculate the real parts of the MIs from Figure 3.3 as well as the MIs from Figure 4.1, in general up to five orders in the $\varepsilon$-expansion. In order to tackle this highly challenging task we applied the same techniques as in our calculation from Chapter 3. It turns out that almost all MIs can be expressed in terms of the set (2.48) supplemented by the following HPLs of weight $w = 4$

$$H(0, 0, 0, 1; u) = \text{Li}_4(u),$$

$$H(0, 0, 1, 1; u) = \text{S}_{2,2}(u),$$

$$H(0, 1, 1, 1; u) = \text{S}_{1,3}(u). \tag{4.2}$$

Unfortunately, some MIs with two and three massive propagators do not fit into this pattern. We further have to include HPLs related to the parameter $-1$ and to the argument $u - 1$, cf. (A.43) – (A.53). Still, we find two functions which we could not express in terms of Nielsen polylogarithms: $H(0, -1, 0, 1; u)$ and $\mathcal{A}(u)$ from (A.49)[1].

Similar to what we have seen in Chapter 3, the situation is more complicated for the MIs which stem from the diagrams with a closed fermion loop. So far we have not yet calculated these MIs with a massive internal quark (wavy lines), i.e. we work in an approximation which treats all quarks in these loops as massless. We stress that this is certainly inconsistent for an internal $b$-quark with respect to the remainder of the calculation. However, we expect that this will only have a minor impact on our (preliminary) result. A consistent treatment of these diagrams is relegated to [106]. The analytical results for all other MIs can be found in Appendix A.2.

## 4.2 Renormalization and IR subtractions

We have shown in detail in Section 3.3 how to perform appropriate UV and IR subtractions in order to extract the NNLO kernels $T_i^{(2)}$ from the hadronic matrix elements. The essence is summarized in the Master Formula (3.26). We briefly address the issues that go beyond our analysis of the imaginary part from Chapter 3.

### 4.2.1 Renormalization

The renormalization of the $b$-quark mass becomes relevant in the considered calculation. We treat the $b$-quark in the on-shell scheme according to

$$Z_m(m) = 1 - \frac{\alpha_s C_F}{4\pi} \left( \frac{\mu^2 e^{\gamma_E}}{m^2} \right)^{\varepsilon} \Gamma(\varepsilon) \frac{3 - 2\varepsilon}{1 - 2\varepsilon} + \mathcal{O}(\alpha_s^2). \tag{4.3}$$

---

[1]The appearance of the function $\mathcal{A}(u)$ seems to be an artefact of our calculation, i.e. of our special choice of the MIs. Though it enters two of our MIs from Figure 4.1, it drops out in their sum in the respective Feynman diagrams and is therefore irrelevant for our purposes.

Due to the full NNLO complexity, we require the 2-loop renormalization matrix $\hat{Z}^{(2)}$ which we take from [104]

$$
\hat{Z}^{(2)} = \begin{pmatrix} \frac{41}{3} & -\frac{58}{9} & -\frac{125}{36} & -\frac{73}{54} & \frac{19}{96} & \frac{5}{108} \\ -29 & 4 & -\frac{73}{12} & 0 & \frac{5}{24} & \frac{1}{9} \end{pmatrix} \frac{1}{\varepsilon^2}
$$
$$
+ \begin{pmatrix} \frac{317}{36} & -\frac{515}{54} & \frac{4493}{864} & -\frac{49}{648} & \frac{1}{384} & -\frac{35}{864} \\ \frac{349}{12} & 3 & \frac{1031}{144} & \frac{8}{9} & -\frac{35}{192} & -\frac{7}{72} \end{pmatrix} \frac{1}{\varepsilon}, \tag{4.4}
$$

where the two lines correspond to the physical operators $\{\hat{Q}_1, \hat{Q}_2\}$ and the columns to the extended operator basis $\{\hat{Q}_1, \hat{Q}_2, \hat{E}_1, \hat{E}_2, \hat{E}'_1, \hat{E}'_2\}$ including evanescent operators.

## 4.2.2   IR subtractions

In order to perform the IR subtractions from the right hand side of (3.26), we must compute the real parts of the NLO kernels $T_i^{(1)}$ to $\mathcal{O}(\varepsilon^2)$. The kernels vanish in the colour-singlet case $T_2^{(1)} = T_{2,E}^{(1)} = 0$, whereas the colour-octet kernels are found to be

$$
\mathrm{Re}\, T_1^{(1)}(u) = \frac{C_F}{2N_c}\left\{ \left( -6L + t_0(u)\right)\left(1 + \varepsilon L + \frac{1}{2}\varepsilon^2 L^2\right) \right.
$$
$$
+ \left(3L^2 + t_1(u)\right)\left(\varepsilon + \varepsilon^2 L\right)
$$
$$
\left. + \left(-L^3 + t_2(u)\right)\varepsilon^2 + \mathcal{O}(\varepsilon^3)\right\},
$$
$$
\mathrm{Re}\, T_{1,E}^{(1)}(u) = -\frac{C_F}{4N_c}\left\{ \left(2L + t_{E,0}(u)\right)\left(1 + \varepsilon L\right) \right.
$$
$$
\left. + \left(-L^2 + t_{E,1}(u)\right)\varepsilon + \mathcal{O}(\varepsilon^2)\right\}, \tag{4.5}
$$

with $L \equiv \ln \mu^2/m_b^2$ and

$$
t_0(u) = 4\mathrm{Li}_2(u) - \ln^2 u + 2\ln u \ln \bar{u} + \ln^2 \bar{u} + (2 - 3u)\left(\frac{\ln u}{\bar{u}} - \frac{\ln \bar{u}}{u}\right) - \frac{\pi^2}{3} - 22,
$$

$$
t_1(u) = -2\mathrm{Li}_3(u) - 2\mathrm{S}_{1,2}(u) - 2\ln \bar{u}\,\mathrm{Li}_2(u) + \ln^3 u - 2\ln^2 u \ln \bar{u} + \ln u \ln^2 \bar{u} - \ln^3 \bar{u}
$$
$$
+ \frac{2 - 3u^2}{u\bar{u}}\mathrm{Li}_2(u) - \frac{2 - 3u}{\bar{u}}\left(\ln^2 u - \ln u \ln \bar{u}\right) + \frac{6 - 11u + 2\bar{u}\pi^2}{\bar{u}}\ln u
$$
$$
+ \frac{4 - 3u}{2u}\ln^2 \bar{u} - \frac{18 - 33u + 5u\pi^2}{3u}\ln \bar{u} + \frac{(7 - 6u)\pi^2}{6\bar{u}} + 2\zeta_3 - 52,
$$

$$
t_2(u) = 10\mathrm{Li}_4(u) - 8\mathrm{S}_{2,2}(u) + 10\mathrm{S}_{1,3}(u) - 8\ln \bar{u}\,\mathrm{Li}_3(u) + 10\ln \bar{u}\,\mathrm{S}_{1,2}(u) - \frac{7}{12}\ln^4 u
$$

$$+ 5 \ln^2 \bar{u} \, \mathrm{Li}_2(u) + \frac{4}{3} \ln^3 u \ln \bar{u} - \ln^2 u \ln^2 \bar{u} + \frac{1}{3} \ln u \ln^3 \bar{u} + \frac{7}{12} \ln^4 \bar{u}$$

$$+ \frac{2 - 6u + 6u^2}{u\bar{u}} \mathrm{Li}_3(u) - \frac{4 - 6u + 3u^2}{u\bar{u}} \Big( \mathrm{S}_{1,2}(u) + \ln \bar{u} \, \mathrm{Li}_2(u) \Big) - \frac{8 - 3u}{6u} \ln^3 \bar{u}$$

$$+ \frac{2 - 3u}{6\bar{u}} \Big( 4 \ln^3 u - 6 \ln^2 u \ln \bar{u} + 3 \ln u \ln^2 \bar{u} \Big) - \frac{60(1 - 2u) + 17\bar{u}\pi^2}{12\bar{u}} \ln^2 u$$

$$+ \frac{3(6 - 4u - 7u^2) + u\bar{u}\pi^2}{3u\bar{u}} \mathrm{Li}_2(u) + \frac{24 - 54u + 5\bar{u}\pi^2}{6\bar{u}} \ln u \ln \bar{u} + \frac{(29 - 24u)\pi^2}{6\bar{u}}$$

$$+ \frac{6(12 - 13u) + 7u\pi^2}{12u} \ln^2 \bar{u} + \frac{24(7 - 13u) + (10 - 15u)\pi^2}{12\bar{u}} \ln u - \frac{23\pi^4}{180}$$

$$- \frac{24\bar{u}(7 - 13u) + (2 + 23u - 27u^2)\pi^2 + 24u\bar{u}\zeta_3}{12u\bar{u}} \ln \bar{u} + \frac{10 - 11u}{\bar{u}} \zeta_3 - 112,$$

$$t_{E,0}(u) = - \frac{1 - 2u}{2} \Big( \frac{\ln u}{\bar{u}} - \frac{\ln \bar{u}}{u} \Big) + \frac{16}{3},$$

$$t_{E,1}(u) = - \frac{1 - 2u}{2u\bar{u}} \mathrm{Li}_2(u) + \frac{1 - 3u}{4\bar{u}} \ln^2 u + \frac{u}{2\bar{u}} \ln u \ln \bar{u} - \frac{2 - 3u}{4u} \ln^2 \bar{u}$$

$$- \frac{4(1 - 2u)}{3} \Big( \frac{\ln u}{\bar{u}} - \frac{\ln \bar{u}}{u} \Big) - \frac{(6 - 5u)\pi^2}{12\bar{u}} + 12. \tag{4.6}$$

In combination with the form factor corrections from (3.29) and (3.30), this determines the first subtraction term in (3.26). In the second subtraction we require the convolution of the NLO kernels with the wave function corrections from (3.32) and (3.34). We find

$$F^{(0)} \, \mathrm{Re} \, T_1^{(1)} \, \Phi_{\mathrm{amp}}^{(1)} \;=\; \frac{C_F^2}{N_c} \Big\{ t_3(u) \Big( \frac{1}{\varepsilon} + L \Big) + t_4(u) + \mathcal{O}(\varepsilon) \Big\} F^{(0)} \, \Phi^{(0)},$$

$$F_E^{(0)} \, \mathrm{Re} \, T_{1,E}^{(1)} \, \Phi_{\mathrm{amp,E}}^{(1)} \;\to\; \frac{C_F^2}{N_c} \Big\{ 12L + t_{E,2}(u) + \mathcal{O}(\varepsilon) \Big\} F^{(0)} \, \Phi^{(0)}, \tag{4.7}$$

where

$$t_3(u) = 4\mathrm{Li}_3(u) + 4\mathrm{S}_{1,2}(u) - 4 \ln u \, \mathrm{Li}_2(u) + \frac{2}{3} \ln^3 u - 2 \ln^2 u \ln \bar{u} - \frac{2}{3} \ln^3 \bar{u} - \frac{\mathrm{Li}_2(u)}{u\bar{u}}$$

$$- \frac{1 - 3u}{2u\bar{u}} \Big( u \ln^2 u + 2\bar{u} \ln u \ln \bar{u} - \bar{u} \ln^2 \bar{u} \Big) - \frac{3}{2u} \ln \bar{u} + \frac{(4 - 3u)\pi^2}{6\bar{u}} - \frac{15}{2} - 4\zeta_3,$$

$$t_4(u) = 12\mathrm{Li}_4(u) - 20\mathrm{S}_{2,2}(u) + 12\mathrm{S}_{1,3}(u) - 8\Big( \ln u + \ln \bar{u} \Big) \mathrm{Li}_3(u) + 12 \ln u \mathrm{S}_{1,2}(u)$$

$$+ 4 \ln \bar{u} \, \mathrm{S}_{1,2}(u) + \Big( 4 \ln^2 u + 4 \ln u \ln \bar{u} + 2 \ln^2 \bar{u} \Big) \mathrm{Li}_2(u) - \frac{3}{4} \ln^4 u + \frac{7}{3} \ln^3 u \ln \bar{u}$$

$$- \frac{1}{2} \ln^2 u \ln^2 \bar{u} - \frac{1}{3} \ln u \ln^3 \bar{u} + \frac{3}{4} \ln^4 \bar{u} - \frac{4 - 11u + 3u^2}{u\bar{u}} \mathrm{Li}_3(u) + \frac{5 - 12u}{6\bar{u}} \ln^3 u$$

$$+ \frac{1 + u - 3u^2}{u\bar{u}} S_{1,2}(u) + \frac{2 - 10u + 6u^2}{u\bar{u}} \ln u \, \mathrm{Li}_2(u) - \frac{1 - 5u + 3u^2}{u\bar{u}} \ln \bar{u} \, \mathrm{Li}_2(u)$$

$$+ \frac{2 - 10u + 9u^2}{2u\bar{u}} \ln^2 u \ln \bar{u} - \frac{1 - 2u}{2u\bar{u}} \ln u \ln^2 \bar{u} - \frac{5 - 6u}{6u} \ln^3 \bar{u}$$

$$- \frac{18 - 24u + 15u^2 - 10u\bar{u}\pi^2}{3u\bar{u}} \mathrm{Li}_2(u) - \frac{16 - 27u + 4\bar{u}\pi^2}{4\bar{u}} \ln^2 u$$

$$- \frac{6 - 36u + 27u^2 - 4u\bar{u}\pi^2}{2u\bar{u}} \ln u \ln \bar{u} + \frac{3(14 - 17u) + 8u\pi^2}{12u} \ln^2 \bar{u}$$

$$+ \frac{8 - 15u - 4\pi^2 - 48\bar{u}\zeta_3}{4\bar{u}} \ln u + \frac{3(2 - 3u)}{\bar{u}} \zeta_3 - \frac{23\pi^4}{60} + \frac{(23 - 17u)\pi^2}{12\bar{u}}$$

$$- \frac{81 - 126u + 45u^2 - (14 - 22u + 6u^2)\pi^2 - 192u\bar{u}\zeta_3}{12u\bar{u}} \ln \bar{u} - \frac{137}{4},$$

$$t_{E,2}(u) = - \frac{6(1 - 2u)}{u\bar{u}} \mathrm{Li}_2(u) - \frac{6}{u} \ln u \ln \bar{u} - 6 \ln u - 6 \ln \bar{u} - \frac{\pi^2}{\bar{u}} + 50. \qquad (4.8)$$

## 4.3  Tree amplitudes in NNLO

The NNLO kernels $T_i^{(2)}$ follow from (3.26) and are indeed found to be free of UV and IR singularities. We emphasize that this provides a very powerful check of our calculation which involves the cancellation of poles up to $1/\varepsilon^4$ ($1/\varepsilon^3$) for the calculation of the real (imaginary) part.

### 4.3.1   $\alpha_1$ in CMM basis

We now present preliminary results for the real parts of the NNLO vertex corrections. Our results are still preliminary in the sense that the calculation is not yet complete (massive fermion loops are still missing) and we have not yet performed numerical checks of all MIs. In analogy to (3.39) we write

$$\operatorname{Re}\hat{V}^{(1)} \equiv \int_0^1 du \left\{ -6\ln\frac{\mu^2}{m_b^2} + g_2(u) \right\} \phi_{M_2}(u),$$

$$\operatorname{Re}\hat{V}_1^{(2)} \equiv \int_0^1 du \left\{ \left(36 C_F - 29 N_c + 2 n_f\right) \ln^2\frac{\mu^2}{m_b^2} \right.$$

$$+ \left[ \left(\frac{29}{3} N_c - \frac{2}{3} n_f\right) g_2(u) - \frac{91}{6} N_c - \frac{10}{3} n_f + C_F\, h_6(u) \right] \ln\frac{\mu^2}{m_b^2}$$

$$\left. + C_F\, h_7(u) + N_c\, h_8(u) + (n_f - 2)\, h_9(u;0) + h_9(u;z) + h_9(u;1) \right\} \phi_{M_2}(u),$$

$$\operatorname{Re}\hat{V}_2^{(2)} \equiv \int_0^1 du \left\{ 18\ln^2\frac{\mu^2}{m_b^2} + \left(21 - 6\, g_2(u)\right)\ln\frac{\mu^2}{m_b^2} + h_5(u) \right\} \phi_{M_2}(u). \tag{4.9}$$

The NLO kernel is found to be

$$g_2(u) = -22 + \frac{3(1-2u)}{\bar{u}}\ln u + \left[ 2\operatorname{Li}_2(u) - \ln^2 u - \frac{1-3u}{\bar{u}}\ln u - (u \to \bar{u}) \right]. \tag{4.10}$$

Concerning the NNLO kernels $h_{5-9}$ we do not quote the expressions for $h_5$, $h_7$ and $h_8$ here, as they are extremely complicated and we have not yet expressed them in terms of a minimal set of HPLs. On the other hand, the expressions for $h_6$ and for $h_9$ (in the massless case) are much simpler and given by

$$h_6(u) = \left[ \frac{327}{2} - \frac{3(1-2u)}{2\bar{u}}\ln^2 u + \frac{3(1-2u^2)}{2u\bar{u}}\ln u \ln\bar{u} - \frac{3(13-24u)}{2\bar{u}}\ln u \right.$$

$$\left. + \frac{(1-2u^2)\pi^2}{4u\bar{u}} + (u \leftrightarrow \bar{u}) \right]$$

$$+ \left[ 8\operatorname{Li}_3(u) - 8\ln u \operatorname{Li}_2(u) + \frac{4}{3}\ln^3 u - 4\ln^2 u \ln\bar{u} - \frac{13-24u^2}{u\bar{u}}\operatorname{Li}_2(u) \right.$$

$$\left. + \frac{25-24u}{2\bar{u}}\ln^2 u + \frac{13}{\bar{u}}\ln u \ln\bar{u} - \frac{9}{2\bar{u}}\ln u - \frac{11\pi^2}{6\bar{u}} - (u \leftrightarrow \bar{u}) \right],$$

$$h_9(u;0) = \left[\frac{125}{12} + \frac{\mathrm{Li}_2(u)}{\bar{u}} + \frac{1-3u}{2\bar{u}}\ln^2 u + \frac{1+u}{2\bar{u}}\ln u \ln \bar{u} - \frac{17(1-2u)}{6\bar{u}}\ln u\right.$$

$$\left. - \frac{(1+u)\pi^2}{12\bar{u}} + (u \leftrightarrow \bar{u})\right]$$

$$+ \left[\frac{4}{3}\mathrm{Li}_3(u) - \frac{2}{3}\ln^3 u + \frac{4}{3}\ln^2 u \ln \bar{u} - \frac{32-29u}{9\bar{u}}\mathrm{Li}_2(u) + \frac{35-29u}{18\bar{u}}\ln^2 u\right.$$

$$\left. - \frac{1}{3\bar{u}}\ln u \ln \bar{u} - \frac{13+24\bar{u}\pi^2}{18\bar{u}}\ln u + \frac{\pi^2}{18\bar{u}} - (u \leftrightarrow \bar{u})\right]. \qquad (4.11)$$

## 4.3.2  Convolution with distribution amplitude

We now perform the convolution integrals by expressing the distribution amplitude of the emitted meson $M_2$ in terms of its Gegenbauer expansion (3.47). We obtain analytical results for the convolutions with the kernels $g_2$, $h_6$ and $h_9$

$$\int_0^1 du\, g_2(u)\, \phi_{M_2}(u) = -\frac{45}{2} + \frac{11}{2}a_1^{M_2} - \frac{21}{20}a_2^{M_2}$$

$$\int_0^1 du\, h_6(u)\, \phi_{M_2}(u) = 348 - \frac{154}{3}a_1^{M_2} + \frac{329}{40}a_2^{M_2}$$

$$\int_0^1 du\, h_9(u;0)\, \phi_{M_2}(u) = \frac{493}{18} - \frac{2\pi^2}{3} - \left(\frac{40}{3} + 2\pi^2\right)a_1^{M_2} + \left(\frac{8059}{600} - \pi^2\right)a_2^{M_2},$$
$$(4.12)$$

and computed the remaining convolution integrals numerically

$$\int_0^1 du\, h_5(u)\, \phi_{M_2}(u) = 322 - 213\, a_1^{M_2} + 3.8\, a_2^{M_2}$$

$$\int_0^1 du\, h_7(u)\, \phi_{M_2}(u) = 731 - 348\, a_1^{M_2} - a_2^{M_2}$$

$$\int_0^1 du\, h_8(u)\, \phi_{M_2}(u) = -409 + 412\, a_1^{M_2} - 32\, a_2^{M_2}. \qquad (4.13)$$

The cancellation of all singularities and the finiteness of all convolution integrals completes the explicit factorization proof of the NNLO vertex corrections.

We finally collect all contributions and illustrate the relative importance of the individual vertex corrections setting $\mu = m_b$

$$\mathrm{Re}\,\hat{V}^{(1)} = -22.5 + 5.5\, a_1^{M_2} - 1.1\, a_2^{M_2},$$

$$\mathrm{Re}\,\hat{V}_1^{(2)} = -148 + 606\, a_1^{M_2} - 80\, a_2^{M_2},$$

$$\mathrm{Re}\,\hat{V}_2^{(2)} = 322 - 213\, a_1^{M_2} + 3.8\, a_2^{M_2}. \qquad (4.14)$$

### 4.3.3  Preliminary numerical result

We conclude this chapter with the presentation of a numerical result for the real part of the NNLO vertex corrections. We stress again that this corresponds to a preliminary result which treats the $c$-quark and the $b$-quark in the closed fermion loops as massless quarks. If we reconsider our results for the imaginary part in this approximation, we find deviations of $\sim 5\%$ of the individual NNLO contributions. As the NNLO terms are subleading for the real part of the colour-allowed tree amplitude, we expect that this approximation will have only a minor impact here.

Our preliminary result for the real part of the NNLO vertex corrections reads

$$\begin{aligned} \mathrm{Re}\,\alpha_1(\pi\pi) = & \quad 1.01\big|_{V^{(0)}} + 0.03\big|_{V^{(1)}} + 0.03\big|_{V^{(2)}} \\ = & \quad 1.06, \end{aligned} \qquad (4.15)$$

where we have used Wilson coefficients in NLL approximation for simplicity (they are indeed known to the required NNLL accuracy and can be found in [107]). As expected, the contribution is of minor importance in absolute terms. However, the NNLO corrections are found to be as important as the NLO terms which are numerically suppressed by the small Wilson coefficient. Interestingly, the vertex corrections add again constructively and, as can be seen in comparison with the results from [25], come again with the opposite of the spectator interactions.

The colour-suppressed tree amplitude $\alpha_2(\pi\pi)$ is phenomenologically more interesting as the respective QCD Factorization prediction is rather low for a satisfactory description of the experimental data. In order to derive the NNLO result for $\alpha_2$ we still have to solve some conceptual aspects concerning a Fierz-symmetric definition of (2-loop) evanescent operators. We therefore relegate the discussion of the colour-suppressed tree amplitude to [106].

# Chapter 5

# Heavy-to-light form factors for non-relativistic bound states

In this chapter we investigate transition form factors between non-relativistic QCD bound states at large recoil energy. Assuming the decaying quark to be much heavier than its decay product, the relativistic dynamics can be treated according to the factorization formula (1.28) for heavy-to-light form factors obtained from the HQE in QCD. In contrast to the $B \to \pi$ transition, the form factors can be calculated entirely in perturbation theory in the non-relativistic approximation which allows for an explicit analysis of the factorization formula. We perform a NLO calculation based on the methods that we developed in Chapter 2 and look for an interpretation of the results from the viewpoint of QCD Factorization.

The basic idea of this work has already been presented in [108]. We emphasize that the formalism which we develop in this chapter can be applied for $B_c \to (\bar{c}c)$ transitions as all these particles can be considered approximatively as non-relativistic bound states. Notice that we treat the charm quark as a light quark in this case, $m_c \ll m_b$. We will adopt this terminology throughout this chapter although we consider this analysis rather as a toy model for the $B \to \pi$ transition. A phenomenological study of various $B_c$ decays in QCD Factorization will be given in [109].

## 5.1 Non-relativistic approximation

The wave function for a non-relativistic (NR) bound state of a quark and an antiquark with respective masses $m_1$ and $m_2$ can be obtained from the resummation



Figure 5.1: *Resummation of potential gluons into a non-relativistic Coulomb wave-function (details of the resummation can be found e.g. in [110]).*

of NR (*potential*) gluon exchange as sketched in Figure 5.1. The solution of the corresponding Schrödinger equation with Coulomb potential yields

$$\psi_{\rm C}(\vec{p}) \propto \frac{\kappa^{5/2}}{(\kappa^2 + \vec{p}^2)^2}, \tag{5.1}$$

where $\kappa = m_r \alpha_s C_F$ and $m_r = m_1 m_2/(m_1 + m_2)$ is the reduced mass. The normalization of the wave function gives the (non-relativistic) meson decay constant

$$f_{\rm NR} = \frac{2\sqrt{N_c}}{\pi} \frac{\kappa^{3/2}}{(m_1 + m_2)^{1/2}}. \tag{5.2}$$

In this approximation, the $B_c$ meson is entirely dominated by the two-particle Fock state built from a bottom quark with mass $M \equiv m_b$ and a charm antiquark with mass $m \equiv m_c$. Consequently to first approximation in the NR expansion, the $B_c$ meson consists of a quark with momentum $Mw_\mu$ and an antiquark with momentum $mw_\mu$, where $w_\mu$ is the four-velocity of the $B_c$ meson ($w^2 = 1$). The spinor degrees of freedom for the $B_c$ meson in the initial state are represented by the Dirac projector $\mathcal{P}_H = \frac{1}{2}(1 + \slashed{w})\gamma_5$.

Similarly, a pseudoscalar $\eta_c$ meson is interpreted as a $c\bar{c}$ bound state where both constituents have approximately equal momenta $mw'_\mu$, where $w'_\mu$ is the four-velocity of the $\eta_c$ meson ($w'^2 = 1$). The Dirac projector of the $\eta_c$ meson in the final state is given by $\mathcal{P}_L = \frac{1}{2}(1 - \slashed{w}')\gamma_5$.

In the following we consider heavy-to-light transitions at large recoil energy assuming $M \gg m$ and working in leading power of the HQE in $m/M$. The QCD dynamics is then described by the SCET degrees of freedom from Table 1.1, where we identify the typical hadronic scale with the mass of the $\eta_c$ meson $M_\eta \simeq 2m = \mathcal{O}(m)$ in the NR approach. The relevant scales in the process are thus given by

$$\mu_h \sim M \quad \gg \quad \mu_{hc} \sim \sqrt{Mm} \quad \gg \quad \mu_{s,c} \sim m \quad \gg \quad \mu_{\rm NR} \sim mv, \tag{5.3}$$

where the NR scale refers to the virtuality of the potential gluons from Figure 5.1 and $v \ll 1$ is a NR velocity. Notice that all relativistic scales are perturbative in our set-up as $M, m \gg \Lambda_{\rm QCD}$. The relativistic dynamics in the heavy-to-light transition can therefore be analyzed in perturbation theory.

The momentum transfer can be approximated as

$$q^2 = (M_B w - M_\eta w')^2 \simeq M^2 - 4Mm \, w \cdot w' \tag{5.4}$$

which implies a large relativistic boost

$$\gamma \equiv w \cdot w' = \frac{M^2 - q^2}{4Mm} = \mathcal{O}(M/m) \tag{5.5}$$

for large recoil energies with $M^2 - q^2 = \mathcal{O}(M^2)$.

## 5.2 Perturbative calculation

For simplicity, we focus on the $B_c \to \eta_c$ transition and consider the form factors $F_+(q^2)$, $F_-(q^2)$ and $F_T(q^2)$ which can be defined in analogy to (1.27). According to the general discussion for heavy-to-light decays at large recoil, we have to consider hard, hard-collinear, collinear and soft gluon exchange in order to describe the relativistic dynamics of the transition form factors, while the non-relativistic modes are contained in the bound state wave functions of the initial and final state mesons.

### 5.2.1 Tree level

We have to require at least one relativistic gluon exchange in the large recoil case in order to rearrange the quark-antiquark pair in the final state into a NR configuration. Consequently, the diagrams from Figure 5.2 contribute in LO of the perturbative expansion which imply the exchange of a hard-collinear gluon with virtualiy

$$(mw - mw')^2 \simeq -2\gamma m^2 = \mathcal{O}(Mm). \tag{5.6}$$

The result for the form factors at LO becomes

$$\frac{F_+^{\mathrm{LO}}}{1 + 2s} = -\frac{F_-^{\mathrm{LO}}}{2s} = \frac{F_T^{\mathrm{LO}}}{2s} = \frac{f_M^{\mathrm{NR}} f_m^{\mathrm{NR}}}{N_c} \frac{\pi \alpha_s C_F}{\gamma m^2}, \tag{5.7}$$

where $f_M^{\mathrm{NR}}$ and $f_m^{\mathrm{NR}}$ are the non-relativistic decay constants of the initial and final state mesons respectively and we defined

$$s \equiv \frac{M}{4\gamma m} = \frac{M^2}{M^2 - q^2} = \mathcal{O}(1) \tag{5.8}$$

with $s = 1$ at maximum recoil $q^2 = 0$.

From (5.2), we read off that the decay constants scale as $f_M^{\mathrm{NR}} \sim (mv)^{3/2} M^{-1/2}$ and $f_m^{\mathrm{NR}} \sim mv^{3/2}$ in the combined NR and HQE. We find that the form factors scale as

$$F_i^{\mathrm{LO}}(q^2) \sim \alpha_s v^3 \left(\frac{m}{M}\right)^{3/2} \tag{5.9}$$

in agreement with the expected scaling $F_i(q^2) \sim M^{-3/2}$ from the general discussion for heavy-to-light form factors at large recoil [81].
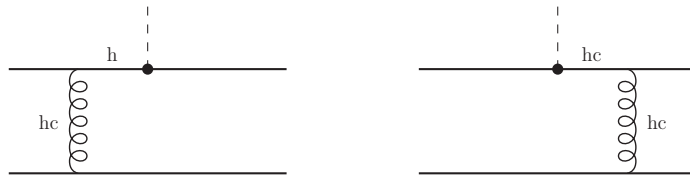


Figure 5.2: *Tree level diagrams. The dot denotes the weak vertex mediating the heavy-to-light transition, the lower line the light spectator antiquark. NR gluons from the bound state wave functions are not drawn.*

## 5.2.2    1-loop calculation

The tree level results derived above do not give rise to endpoint singularities as the wave functions of the non-relativistic bound states have vanishing support at the endpoints. For a deeper understanding of the factorization formula we therefore have to consider the NLO contributions. We will see below that our NLO calculation indeed reveals the full complexity of the factorization formula. We now switch to the technical part of the calculation and evaluate the corresponding 1-loop diagrams following our strategy from Section 2.1.

**Step 1: Set-up for loop calculation**

At NLO the form factors receive contributions from various 1-loop diagrams as shown in Figure 5.3. The corresponding colour factors are summarized in Table 5.1. All diagrams from Figure 5.3 can be expressed in terms of the following denominators of particle propagators

$$\mathcal{P}_1 = (Mw + mw - k)^2 - M^2, \qquad \mathcal{P}_8 = (Mw + mw - mw' - k)^2 - M^2,$$

$$\mathcal{P}_2 = (Mw - mw' + k)^2 - M^2, \qquad \mathcal{P}_9 = (Mw - k)^2 - M^2,$$

$$\mathcal{P}_3 = (2mw' - k)^2 - m^2, \qquad \mathcal{P}_{10} = (2mw' - mw - k)^2 - m^2,$$

$$\mathcal{P}_4 = (mw' - mw + k)^2 - m^2, \qquad \mathcal{P}_{11} = (mw' - k)^2 - m^2,$$

$$\mathcal{P}_5 = k^2 - m^2, \qquad \mathcal{P}_{12} = k^2,$$

$$\mathcal{P}_6 = (mw - k)^2, \qquad \mathcal{P}_{13} = (mw - k)^2 - m^2,$$

$$\mathcal{P}_7 = (mw' - k)^2, \qquad \mathcal{P}_{14} = (2mw' - k)^2. \qquad (5.10)$$

**Step 2: Reduction to Master Integrals**

The reduction procedure is not as efficient in this calculation as it was in the 2-loop calculation from Chapter 3 and 4. However, we were able to express about 200 scalar integrals in terms of 23 MIs which are summarized in Figure 5.4. The number of MIs is comparably high in this calculation due to the fact that we deal with three different types of propagators (with masses $0, m, M$) and four external momenta (two of them linearly independent $w, w'$).

**Step 3: Manipulation of Dirac structures**

We project onto the NR bound states with the help of the projectors $\mathcal{P}_H$ and $\mathcal{P}_L$ which we specified in Section 5.1. The flavour singlet diagrams in the last two lines of Figure 5.3 require special care as they involve traces like $\text{Tr}(\gamma^\mu \gamma^\nu \gamma^\rho \gamma^\sigma \gamma_5)$ which may invalidate the treatment of an anticommuting $\gamma_5$ within DR. However, the flavour singlet diagrams turn out to give finite contributions and the traces can safely be calculated in $d = 4$ dimensions.
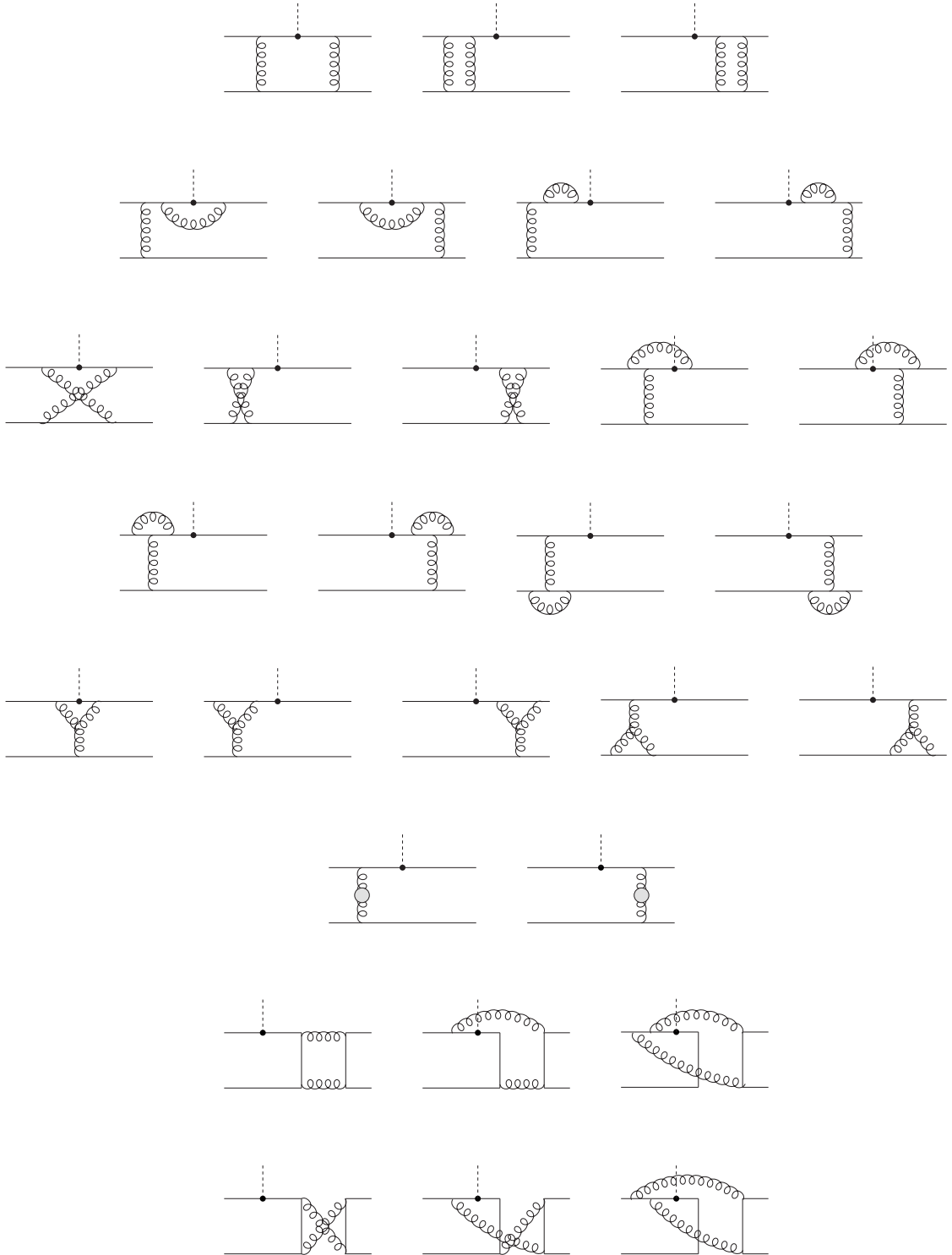
Figure 5.3: *NLO diagrams. The bubble in the diagrams from the sixth line represents the 1-loop gluon self-energy. The diagrams from the last two lines contribute to flavour singlet final states only.*

| Diagram | line 1-2 | line 3-4 | line 5 | line 6 | line 7-8 |
|---------|----------|----------|--------|--------|----------|
| Colour | $C_F^2$ | $C_F^2 - \frac{C_F N}{2}$ | $\frac{C_F N}{2}$ | $C_F$ | $\frac{C_F}{2}$ |

Table 5.1: *Colour factors of the diagrams in Figure 5.3. The normalization is chosen such that the tree diagrams from Figure 5.2 give $C_F$.*
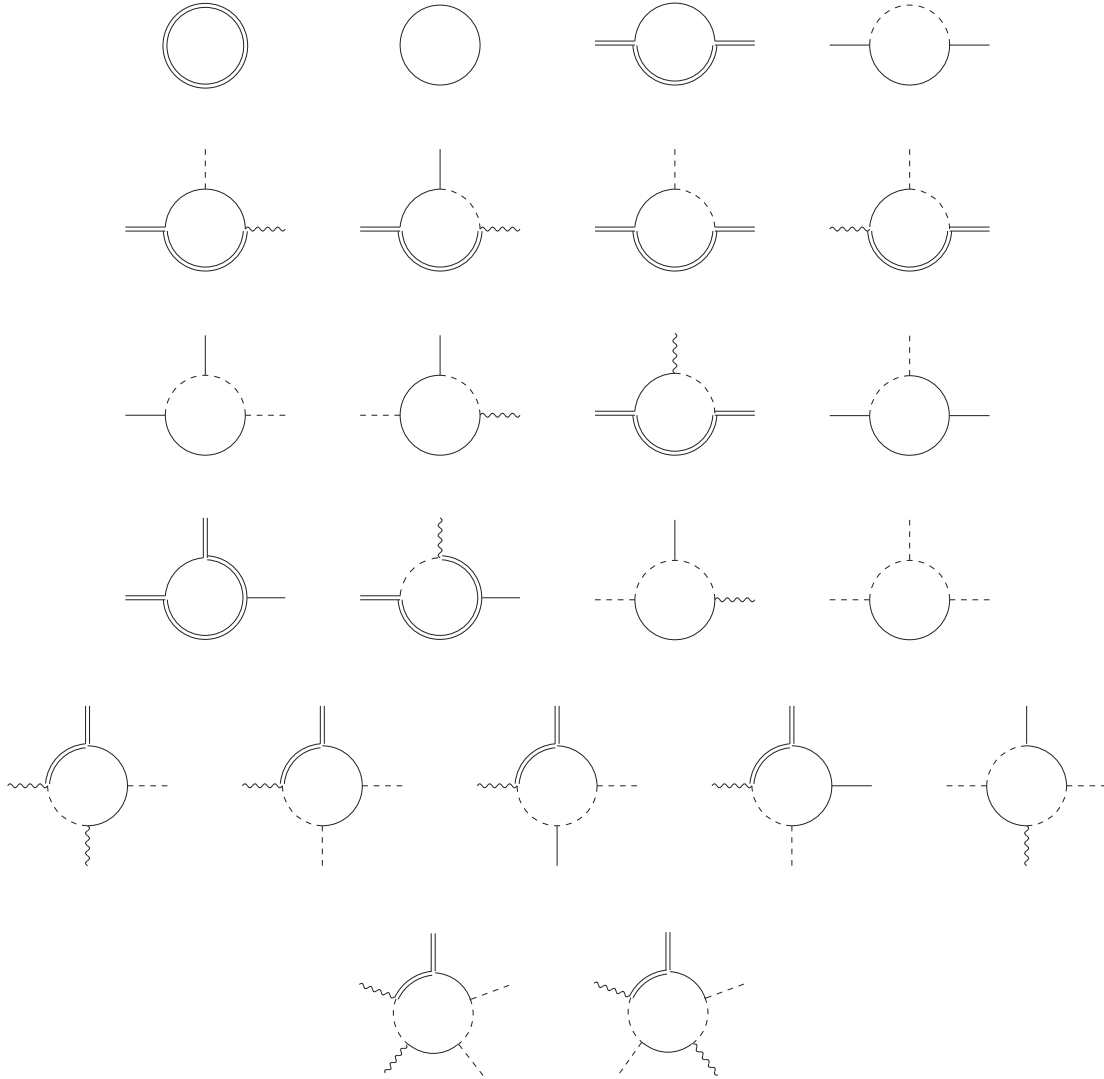


Figure 5.4: *Scalar Master Integrals that appear in the 1-loop calculation. We use dashed/solid/double internal lines for propagators with masses $0/m/M$, respectively. Double/solid/dashed/wavy external lines correspond to hard/hard-collinear/collinear/soft external momenta. Notice that we refrain from associating all external scalar products to the MIs in this case. The figures therefore do not define the MIs unambiguously in our representation (for the explicit definitions of the MIs we refer to Appendix A.3).*

**Step 4: Calculation of Master Integrals**

Though most of the MIs in Figure 5.4 correspond to apparently simple 1-loop 3-topologies, the calculation is non-trivial due to the fact that the integrals involve several distinct scales and many massive propagators. The calculation simplifies as we only require the leading power in $m/M$ of the MIs which we extract using the method of regions and Mellin-Barnes techniques as described in detail in Section 2.4. The analytical results of the MIs can be found in Appendix A.3.

### 5.2.3  Form factors in NLO

In NLO we have to take into account the 1-loop diagrams from Figure 5.3 as well as standard (tree-level) counterterm diagrams like the ones depicted in Figure 5.5. We use $\overline{\text{MS}}$-scheme renormalization constants

$$Z_g = 1 - \frac{\alpha_s}{4\pi\varepsilon}\left(\frac{11}{6}N_c - \frac{1}{3}n_f\right) + \mathcal{O}(\alpha_s^2),$$

$$Z_A = 1 - \frac{\alpha_s}{4\pi\varepsilon}\left(\frac{2}{3}n_f - \frac{5}{3}N_c\right) + \mathcal{O}(\alpha_s^2) \tag{5.11}$$

for the coupling constant and the gluon field, respectively. The (non-relativistic) quark fields are conveniently treated in the on-shell scheme with

$$Z_q(m) = 1 - \frac{\alpha_s C_F}{4\pi}\left(\frac{1}{\varepsilon} + \frac{2}{\varepsilon_{\text{IR}}} + 3\ln\frac{\mu^2}{m^2} + 4\right) + \mathcal{O}(\alpha_s^2),$$

$$Z_m(m) = 1 - \frac{\alpha_s C_F}{4\pi}\left(\frac{3}{\varepsilon} + 3\ln\frac{\mu^2}{m^2} + 4\right) + \mathcal{O}(\alpha_s^2), \tag{5.12}$$

where we indicated that the wave function renormalization constant contains IR divergences. The renormalization of the weak vertex involves the Z-factor of the heavy-to-light current $\bar{q}\,\Gamma\,Q$ which is given by

$$Z_\Gamma = 1 + \frac{\alpha_s C_F}{4\pi\varepsilon} + \mathcal{O}(\alpha_s^2) \qquad \text{for} \qquad \Gamma = \sigma^{\mu\nu}, \tag{5.13}$$

whereas $Z_\Gamma = 1$ for the conserved vector current with $\Gamma = \gamma^\mu$.

Adding up all diagrams and counterterms at NLO, all UV and IR divergences cancel in the form factors as expected. Our explicit NLO results are summarized in
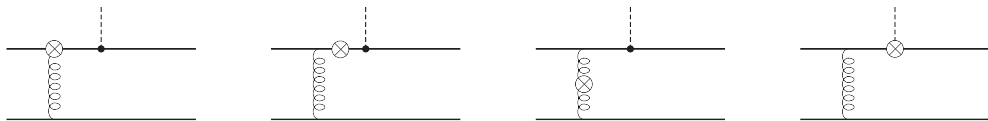


Figure 5.5: *Sample of counterterm diagrams.*
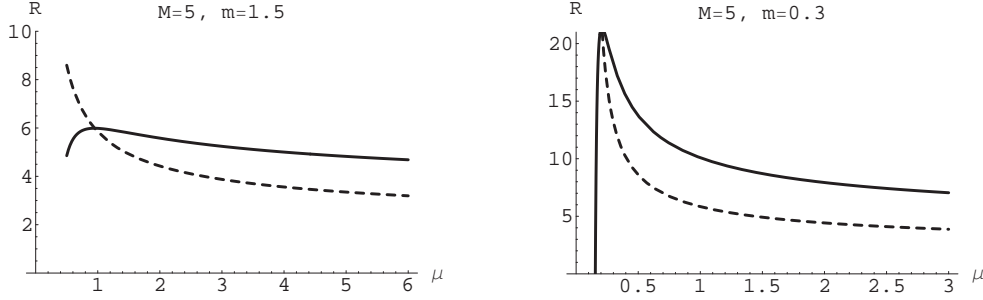
Figure 5.6: *Renormalization-scale dependence of the ratio R for different choices of quark masses. The solid (dashed) line denotes the NLO (LO) result. Left: Realistic case relevant for the $B_c \to \eta_c$ transition. Right: Toy example for the $B \to \pi$ transition.*

Appendix B. Let us quote the result for the form factor $F_+(q^2)$ at maximum recoil $q^2 = 0$ here to illustrate the structure of the NLO contributions. We find

$$
F_+^{\mathrm{NLO}}(0) = \frac{f_M^{\mathrm{NR}} f_m^{\mathrm{NR}}}{N_c} \frac{12\pi\alpha_s(\mu)C_F}{Mm} \left\{ 1 + \frac{\alpha_s(\mu)}{4\pi} \left[ \left( \frac{11}{3}N_c - \frac{2}{3}n_f \right) \ln \frac{2\mu^2}{mM} - \frac{10}{9}n_f + \mathcal{S}_+ \right.\right.
$$
$$
+ C_F \left( \frac{1}{2} \ln^2 \frac{M}{m} + \frac{35 - 20\ln 2}{6} \ln \frac{M}{m} + \frac{2}{3} \ln^2 2 + 3\ln 2 + \frac{7\pi^2}{9} - \frac{103}{6} \right)
$$
$$
\left.\left. + N_c \left( -\frac{1}{6} \ln^2 \frac{M}{m} + \frac{1 + \ln 2}{3} \ln \frac{M}{m} + \frac{1}{3} \ln^2 2 - \frac{4}{3} \ln 2 - \frac{5\pi^2}{36} + \frac{73}{9} \right) \right] \right\}
$$
$$
\tag{5.14}
$$

where $M$ and $m$ are to be considered as pole masses. In (5.14) we isolated the contribution from the flavour singlet diagrams which is given by $\mathcal{S}_+ = 1/3 \ln(M/4m)$.

We now investigate the residual renormalization-scale dependence of $F_+^{\mathrm{NLO}}(0)$. For illustration we will use two sets of quark masses with

set 1 :     $M = 5\,\mathrm{GeV}$,     $m = 1.5\,\mathrm{GeV}$,     $\mu_{hc} = \sqrt{Mm} \simeq 2.7\,\mathrm{GeV}$,

set 2 :     $M = 5\,\mathrm{GeV}$,     $m = 0.3\,\mathrm{GeV}$,     $\mu_{hc} = \sqrt{Mm} \simeq 1.2\,\mathrm{GeV}$     (5.15)

which correspond to the physical decay $B_c \to \eta_c$ and a toy model for the $B \to \pi$ transition, respectively (in the second case we thus drop the singlet contribution). We use 1-loop running of $\alpha_s$ with $n_f = 4$ and $\alpha_s(5\,\mathrm{GeV}) = 0.2$ and study the ratio

$$
R = \frac{Mm}{f_M^{\mathrm{NR}} f_m^{\mathrm{NR}}} \, F_+(0). \tag{5.16}
$$

The result is illustrated in Figure 5.6. In both cases we observe a significant enhancement from the NLO contribution. For the $B_c \to \eta_c$ case (set 1) the enhancement of the tree level result at the hard-collinear scale is about 35%. We find a substantial improvement of the scale dependence from about 40% at LO to 20% at NLO if

we vary $\mu$ between the soft scale $m$ and the hard scale $M$. The hierarchy of scales $M \gg m$ is not too large in this case, such that the formally large logarithms $\ln M/m$ do not spoil the convergence of the perturbation series too badly.

In the toy case for the $B \to \pi$ form factor (set 2), the soft scale $m$ is close to the QCD scale $\Lambda_{\text{QCD}}$ and consequently the convergence of the perturbative expansion breaks down at small scales. The theoretical error due to the renormalization scale is not under control in this case. From the conceptual viewpoint we are particularly interested in the structure and resummation of the formally large logarithms $\ln M/m$ in the $B \to \pi$ case where they should be counted as $\alpha_s \ln M/m \sim 1$. We therefore examine the origin of these logarithms in the subsequent section in detail.

## 5.3  Factorization Formula

We now come to the interpretation of our explicit NLO calculation in terms of the factorization formula for heavy-to-light form factors at large recoil energy

$$F_i(q^2) \simeq H_i(q^2)\, \xi(q^2) + \int_0^\infty d\omega \int_0^1 du \ \phi_B(\omega)\, T_i(u,\omega;q^2)\, \phi_\eta(u). \qquad (5.17)$$

We start with a closer look at the factorization formula following [76]. The two terms in (5.17) are associated to the matrix elements of two distinct $\text{SCET}_\text{I}$ operator structures, the so-called $A$-type and $B$-type operators (cf. (1.29) for notation)

$$J_A = (\bar\xi_{hc} W_{hc})\, h_v,$$

$$J_B = (\bar\xi_{hc} W_{hc})\, (W_{hc}^\dagger i \slashed{D}_{\perp hc} W_{hc})\, h_v. \qquad (5.18)$$

The matrix element of the operator $J_A$ defines the form factor $\xi(q^2)$ and the $H_i(q^2)$ denote the corresponding matching coefficients from QCD to $\text{SCET}_\text{I}$ which include the contributions from hard momentum fluctuations. The operator $J_B$ defines a non-local form factor $\Xi(\tau;q^2)$ with short-distance coefficients $C_i(q^2;\tau)$. In the first matching step the factorization formula thus takes the form

$$F_i(q^2) \simeq H_i(q^2)\, \xi(q^2) + \int_0^1 d\tau \ C_i(q^2;\tau)\, \Xi(\tau;q^2). \qquad (5.19)$$

The non-local form factor $\Xi(\tau;q^2)$ can be factorized further in a second matching step from $\text{SCET}_\text{I}$ to $\text{SCET}_\text{II}$ including the effects from hard-collinear fluctuations. This results in a convolution of a perturbative jet function $J(\tau;u,\omega;q^2)$ with leading twist distribution amplitudes given by

$$\Xi(\tau;q^2) = \int_0^\infty d\omega \int_0^1 du \ \phi_B(\omega)\, J(\tau;u,\omega;q^2)\, \phi_\eta(u). \qquad (5.20)$$

Combining (5.19) and (5.20), we see that the hard-scattering kernel from (5.17) can be identified as

$$T_i(u,\omega;q^2) = \int_0^1 d\tau \ C_i(q^2;\tau)\, J(\tau;u,\omega;q^2). \qquad (5.21)$$

In our analysis we calculate the leading twist distribution amplitudes of the $B_c$ and $\eta_c$ meson at leading power in the NR approximation and including perturbative (relativistic) effects to NLO in QCD. We then use our explicit NLO results of the form factors together with the known expressions for $H_i$, $C_i$ and $J$ to extract the overlap-contribution $\xi(q^2)$ in our NR set-up which may then be analyzed further concerning its factorization properties in $\text{SCET}_\text{II}$. This immediately leads us to the problem of endpoint singularities which arise in our calculation at NLO of the perturbative expansion. We find it instructive to demonstrate how these endpoint singularities enter our calculation before looking at the factorization of the heavy-to-light form factors in detail.

### 5.3.1 Endpoint singularities

The appearance of endpoint singularities is related to the issue of large logarithms which we already mentioned at the end of the last section. As these logarithms may spoil the convergence of the perturbation series, we are particularly interested in the resummation of such logarithms within the effective theory. The structure of formally large logarithms is particularly complicated in heavy-to-light decays due to the presence of various scales and degrees of freedom.

We encountered these logarithms in our explicit NLO calculation in form of $\ln \gamma$ where $\gamma = \mathcal{O}(M/m)$ is the large relativistic boost between the meson rest frames (cf. our results in Appendix B). We find that the origin of the leading double logarithms is related to two different mechanisms which we consider in detail in the remainder of this section: The first one gives rise to (standard) Sudakov logarithms, the second one is related to endpoint singularities.

**Sudakov logarithms**

Sudakov logarithms appear naturally in processes with (hard-)collinear and soft degrees of freedom.. In our calculation they arise for instance from the diagram in Figure 5.7 (in Feynman gauge). Rather than looking at the full diagram here, we profit from our reduction algorithm and consider an underlying (scalar) MI which allows for a more transparent presentation of the interesting aspects.

The MI to be considered here is

$$
\int [dk] \, \frac{1}{\mathcal{P}_1 \mathcal{P}_3 \mathcal{P}_6} \;\; \simeq \;\; \ln^2(4\gamma) - 2\mathrm{Li}_2(1 - s) - \ln^2 s + \pi^2 + \mathcal{O}(\varepsilon)
\tag{5.22}
$$

with the $\mathcal{P}_i$ given in (5.10). Notice that the integral contains a double logarithm in $\gamma$ and that we suppressed a prefactor $-1/(8\gamma m M)$ for simplicity, cf. (A.67). The integral may be calculated with Mellin-Barnes techniques as described in Section 2.4.4.

In order to understand the origin of the double logarithm, we disentangle the contributions from different momentum regions of the loop integration. Following the method of expansion by regions which we described in Section 2.4.3, the MI is found to receive leading contributions from the hard, hard-collinear and soft region.
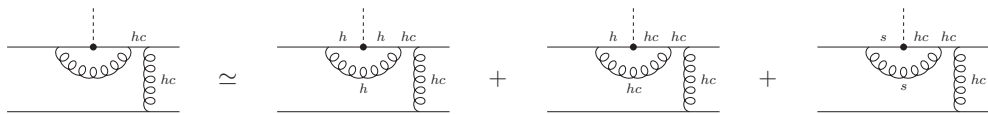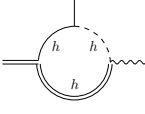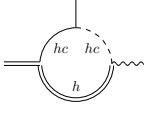


Figure 5.7: *Origin of Sudakov logarithms (in Feynman gauge).*

The hard momentum region with $k \sim (1, 1, 1)$ is found to give
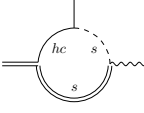
$$\simeq \frac{1}{\varepsilon^2} + \frac{1}{\varepsilon} \ln \frac{\mu^2}{16\gamma^2 m^2} + \frac{1}{2} \ln^2 \frac{\mu^2}{16\gamma^2 m^2} - 2\mathrm{Li}_2(1 - s) - \ln^2 s + \frac{\pi^2}{6} + \mathcal{O}(\varepsilon), \tag{5.23}$$

with double poles in $\varepsilon$ which arise in the limits $k_\perp \to 0$ and $k_+ \to 0$. The contribution from the hard-collinear region with $k \sim (1, \lambda, \lambda^2)$ becomes

$$\simeq -\frac{2}{\varepsilon^2} - \frac{2}{\varepsilon} \ln \frac{\mu^2}{4\gamma m^2} - \ln^2 \frac{\mu^2}{4\gamma m^2} + \mathcal{O}(\varepsilon), \tag{5.24}$$

where the singularities stem from $k_\perp \to \infty$ and $k_- \to 0$. Finally, the soft region with $k \sim (\lambda^2, \lambda^2, \lambda^2)$ generates poles for $k_\perp \to \infty$ and $k_+ \to \infty$ and reads

$$\simeq \frac{1}{\varepsilon^2} + \frac{1}{\varepsilon} \ln \frac{\mu^2}{m^2} + \frac{1}{2} \ln^2 \frac{\mu^2}{m^2} + \frac{5\pi^2}{6} + \mathcal{O}(\varepsilon). \tag{5.25}$$

Adding up these contributions, all singularities drop out and we reproduce (5.22).

From the viewpoint of QCD Factorization, the hard contribution from (5.23) is to be considered as part of a QCD $\to$ SCET$_\mathrm{I}$ matching calculation, the hard-collinear effects from (5.24) contribute in the SCET$_\mathrm{I}$ $\to$ SCET$_\mathrm{II}$ matching procedure and the soft contribution from (5.25) to the (perturbative) calculation of a SCET$_\mathrm{II}$ matrix element. Let us think of all regions to be $\overline{\mathrm{MS}}$-subtracted (the poles contain information about the anomalous dimensions of operators in the effective theory). We see that the first matching step in (5.23) is free of large logarithms if we choose the matching scale $\mu \sim M$. We may then evolve the scale down to $\mu \sim \mu_{hc}$ using RGEs in SCET$_\mathrm{I}$ which implicitly resum logarithms of the type $\ln M/\mu$. At the hard-collinear scale we perform the second matching step and we see that the choice $\mu \sim (Mm)^{1/2}$ guarantees the absence of large logarithms in (5.24). The procedure continues summing logarithms of the type $\ln \mu_{hc}/\mu$ with the help of corresponding RGEs in SCET$_\mathrm{II}$ and evolving the scale down to $\mu \sim m$. In the $B \to \pi$ case the SCET$_\mathrm{II}$ matrix elements have to be calculated with the help of a non-perturbative method. As the soft scale is still perturbative in our NR approach, the corresponding SCET$_\mathrm{II}$ matrix elements are calculable giving (5.25).

The aforementioned factorization and resummation procedure is of course oversimplifying as we considered a single integral instead of operators in the effective theory. However, it allowed us to emphasize an important feature concerning the resummation of Sudakov logarithms: We saw that we were able to choose the factorization scale $\mu$ such that there are no large logarithms in each matching calculation and we pointed out that the resummation of logarithms can be performed using standard RG-techniques varying $\mu$ between two well-separated scales which correspond to the *virtualities* of the respective modes. We will see in the following that part of the double logarithms in our explicit NLO results are of conceptually different origin.

**Non-factorizable logarithms**

In a second example we consider the pentagon diagram from Figure 5.8 (in Feynman gauge, see also the discussion in [108]). For simplicity, let us again focus on a related MI here given by

$$\text{(diagram)} \quad = \quad \int [dk] \, \frac{1}{\mathcal{P}_5 \mathcal{P}_6 \mathcal{P}_7} \quad \simeq \quad \frac{1}{2} \ln^2(2\gamma) + \frac{2\pi^2}{3} + \mathcal{O}(\varepsilon) \tag{5.26}$$

which may be calculated with Mellin-Barnes techniques. Notice that the MI gives rise to a double logarithm and that we dropped a prefactor $-1/(2\gamma m^2)$, cf. (A.76).

At leading power the MI receives contributions from the hard-collinear, collinear and soft momentum region. The hard-collinear contribution with $k \sim (1, \lambda, \lambda^2)$ is found to be divergent for $k_\perp \to 0$ and $k_+ \to 0$ and reads

$$\text{(diagram)} \quad \simeq \quad \frac{1}{\varepsilon^2} + \frac{1}{\varepsilon} \ln \frac{\mu^2}{2\gamma m^2} + \frac{1}{2} \ln^2 \frac{\mu^2}{2\gamma m^2} + \mathcal{O}(\varepsilon). \tag{5.27}$$

This looks very much like (5.24) but all poles are of IR origin in this case.

The collinear region with $k \sim (1, \lambda^2, \lambda^4)$ is found to be divergent for $k_\perp \to \infty$ and $k_- \to 0$ and similarly the soft region with $k \sim (\lambda^2, \lambda^2, \lambda^2)$ for $k_\perp \to \infty$ and $k_+ \to 0$. In contrast to what we have seen so far, it turns out that the longitudinal integrations along $k_-$ $(k_+)$ in the collinear (soft) region are *not* regularized in this case (notice that DR only influences the integration over transverse momenta in $d_\perp = 2 - 2\varepsilon$ dimensions). However, we may introduce an additional regularization procedure in order to render these contributions finite. Following [83,108], we apply an analytic continuation replacing $\mathcal{P}_6^{-1} \to (-\nu^2)^\delta \mathcal{P}_6^{-1-\delta}$ such that endpoint singularities for $k_- \to 0$ $(k_+ \to 0)$ show up as poles in $1/\delta$. We thus find
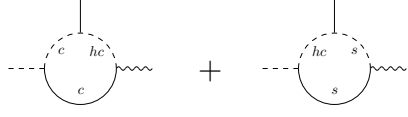
$$\text{(diagram)} \quad \simeq \quad - \left( \frac{1}{\varepsilon} + \ln \frac{\mu^2}{m^2} \right) \left( \frac{1}{\delta} + \ln \frac{\nu^2}{2\gamma m^2} \right) + \frac{\pi^2}{3} + \mathcal{O}(\varepsilon), \tag{5.28}$$

$$\text{(diagram)} \quad \simeq \quad - \frac{1}{\varepsilon^2} - \frac{1}{\varepsilon} \ln \frac{\mu^2}{m^2} - \frac{1}{2} \ln^2 \frac{\mu^2}{m^2}$$
$$+ \left( \frac{1}{\varepsilon} + \ln \frac{\mu^2}{m^2} \right) \left( \frac{1}{\delta} + \ln \frac{\nu^2}{m^2} \right) + \frac{\pi^2}{3} + \mathcal{O}(\varepsilon). \tag{5.29}$$



Figure 5.8: *Origin of non-factorizable logarithms (in Feynman gauge).*

Notice that the dependence on the ad-hoc parameters $\delta$ and $\nu$ disappears when we consider the sum of collinear and soft momentum regions



$$\simeq \; -\frac{1}{\varepsilon^2} - \frac{1}{\varepsilon}\ln\frac{\mu^2}{m^2} - \frac{1}{2}\ln^2\frac{\mu^2}{m^2} + \left(\frac{1}{\varepsilon} + \ln\frac{\mu^2}{m^2}\right)\ln(2\gamma) + \frac{2\pi^2}{3} + \mathcal{O}(\varepsilon) \quad (5.30)$$

and that we reproduce the full result from (5.26) by adding up (5.27) and (5.30).

To summarize, we have seen that we *cannot* disentangle collinear and soft effects in the considered integral as the respective contributions suffer endpoint singularities related to the integrations over longitudinal light-cone momentum fractions which are not regularized in DR (at fixed transverse momenta/virtuality). However, the sum of collinear and soft momentum region turns out to be unambiguously well-defined. We may now ask the question if we can factorize the perturbative hard-collinear effects in (5.27) from the remnant SCET$_{\rm II}$ matrix element in (5.30) summing all formally large logarithms into short-distance coefficient functions.

We repeat our analysis from the last section and think of the SCET$_{\rm I} \to$ SCET$_{\rm II}$ matching calculation in (5.27) and the SCET$_{\rm II}$ matrix element in (5.30) to be $\overline{\rm MS}$-subtracted. Similar to what we have seen in the last section, (5.27) is free of large logarithms choosing $\mu \sim (Mm)^{1/2}$. We then evolve the scale down to $\mu \sim m$ using RG-techniques which implicitly resum logarithms of the type $\ln\mu_{hc}/\mu$. However, in contrast to (5.25) the SCET$_{\rm II}$ matrix element (5.30) is found to contain a large logarithm $\ln(2\gamma)$ at the low scale $\mu \sim m$ (the term vanishes in our example for the specific choice $\mu_0 = m$ but is present in general for any variation of the scale with $\mu \sim m$). In other words, we do not resum *all* large logarithms with the help of standard RG-techniques in SCET$_{\rm II}$.

The remnant logarithms are related to the appearance of endpoint singularities as can be seen from the artificial decomposition into individual collinear and soft regions in (5.28) and (5.29). We see that they do not belong to the variation of the factorization scale $\mu$ but rather to the soft-collinear cross-talk *at fixed virtuality* $\mu^2 \sim m^2$. The low-energy SCET$_{\rm II}$ matrix element in (5.30) still depends on the high scale due to the fact that the meson rest frames are related by a large boost $\gamma = \mathcal{O}(M/m)$. We conclude that these logarithms *cannot* be factorized into short-distance coefficient functions and we therefore call them *non-factorizable*.

We emphasize in this context that we do not find contributions from soft-collinear messenger modes in our set-up. By looking at the scaling of soft-collinear momentum regions in the loop integrals we find that these modes always give power-suppressed contributions and that they are in particular not needed to describe the physics of endpoint-singularities. The reason for this is that the light quark mass $m$ provides a physical IR cut-off in our calculation such that messenger modes with virtualities smaller than $m^2$ cannot contribute to on-shell amplitudes.

### 5.3.2 Factorization of tree level result

For the following discussion it will be convenient to introduce a short-hand notation for the factorization formula (5.17)

$$F_i \simeq H_i\,\xi + \phi_B \otimes T_i \otimes \phi_\eta, \qquad (5.31)$$

where the symbol $\otimes$ represents the convolution integrals. We write the perturbative expansion of the form factors in the form

$$F_i = \sum_{k=1}^{\infty} \left(\frac{\alpha_s}{4\pi}\right)^k F_i^{(k)} \qquad (5.32)$$

and similarly for all other quantities in (5.31). Notice that the perturbative expansion of the form factor starts at $\mathcal{O}(\alpha_s)$ in our set-up according to our discussion in Section 5.2.1. Since the perturbative expansion of $H_i$ starts at $\mathcal{O}(1)$ and the one of $T_i$ at $\mathcal{O}(\alpha_s)$, the form factors take in LO the form

$$F_i^{(1)} = H_i^{(0)}\,\xi^{(1)} + \phi_B^{(0)} \otimes T_i^{(1)} \otimes \phi_\eta^{(0)} \qquad (5.33)$$

with the hard-scattering kernels given by (5.21) as $T_i^{(1)} = C_i^{(0)} \otimes J^{(1)}$. The jet function $J^{(1)}$ has first been computed by Beneke and Feldmann in [81] using a different definition of the soft-overlap contribution $\xi(q^2)$. Our convention corresponds to the one of Beneke and Yang in [76] from which we read off

$$H_+^{(0)} = -H_-^{(0)} = H_T^{(0)} = \frac{C_+^{(0)}(\tau)}{s-2} = -\frac{C_-^{(0)}(\tau)}{s} = \frac{C_T^{(0)}(\tau)}{s} = 1,$$

$$J^{(1)}(\tau; u, \omega) = -\frac{\hat{f}_M f_m}{N_c}\,\frac{\pi^2 C_F}{\gamma m}\,\frac{\delta(\tau - \bar{u})}{\omega\bar{u}}, \qquad (5.34)$$

where $\hat{f}_M$ ($f_m$) is the decay constant of the heavy (light) meson defined in HQET (QCD). In LO of the perturbative expansion we simply have $\hat{f}_M = f_M^{\mathrm{NR}}$, $f_m = f_m^{\mathrm{NR}}$.

In order to extract the overlap-contribution $\xi^{(1)}$ from (5.33) we have to calculate the distribution amplitudes of the $B_c$ and $\eta_c$ meson to LO in the perturbative expansion. As we treat the quarks in the static approximation at leading power in the NR expansion, we simply find

$$\phi_B^{(0)}(\omega) = \delta(\omega - m), \qquad \phi_\eta^{(0)}(u) = \delta(u - 1/2). \qquad (5.35)$$

The second term in (5.33) can now be calculated giving

$$\phi_B^{(0)} \otimes T_i^{(1)} \otimes \phi_\eta^{(0)} = -\frac{f_M^{\mathrm{NR}} f_m^{\mathrm{NR}}}{N_c}\,\frac{2\pi^2 C_F}{\gamma m^2} \begin{cases} s-2 & i = + \\ -s & \text{if} \quad i = - \\ s & i = T \end{cases} \qquad (5.36)$$

We may now isolate $\xi^{(1)}$ using our explicit LO results from (5.7) together with (5.33) and (5.34). We indeed find a universal contribution in this way which reads

$$\xi^{(1)} = \frac{f_M^{\mathrm{NR}} f_m^{\mathrm{NR}}}{N_c} \frac{\pi^2 C_F}{\gamma m^2} \; 10s. \tag{5.37}$$

We have shown in some detail how to extract the soft-overlap contribution $\xi(q^2)$ from our explicit perturbative calculation in Section 5.2. As the conceptually interesting aspects related to the physics of endpoint singularities and the appearance of non-factorizable logarithms only enter our calculation at NLO, we proceed with a similar analysis in the following section.

### 5.3.3   Factorization in NLO

At NLO of the perturbative expansion the extraction of the overlap-contribution is much more involved. We now start from

$$F_i^{(2)} = H_i^{(0)} \, \xi^{(2)} + H_i^{(1)} \, \xi^{(1)} \tag{5.38}$$
$$+ \; \phi_B^{(0)} \otimes T_i^{(2)} \otimes \phi_\eta^{(0)} + \phi_B^{(1)} \otimes T_i^{(1)} \otimes \phi_\eta^{(0)} + \phi_B^{(0)} \otimes T_i^{(1)} \otimes \phi_\eta^{(1)}$$

with $T_i^{(2)} = C_i^{(0)} \otimes J^{(2)} + C_i^{(1)} \otimes J^{(1)}$. Whereas the hard coefficient functions $H_i^{(1)}$ have already been computed in [81], the calculation of $C_i^{(1)}$ and $J^{(2)}$ has been performed recently [111,74,75,76]. In order to extract $\xi^{(2)}$ from (5.38), we still have to consider the corrections to the distribution amplitudes $\phi_B^{(1)}$ and $\phi_\eta^{(1)}$ and to perform the subsequent subtractions. In the following we present our results for the distribution amplitudes whereas we relegate the extraction of the overlap-contribution to [112].

**Light-cone distribution amplitude of $\eta_c$ meson**

We start with the calculation of the leading twist light-cone distribution amplitude (LCDA) of the "light" $\eta_c$ meson defined by [113,81]

$$\langle \eta_c(q) | \, \bar{c}(y) \gamma_\mu \gamma_5 c(x) \, | 0 \rangle \big|_{(x-y)^2=0} \simeq -i f_m \, q_\mu \int_0^1 du \, e^{i(uq\cdot y + \bar{u}q\cdot x)} \, \phi_\eta(u; \mu), \tag{5.39}$$

where we omitted an appropriate path-ordered exponential of gluon fields which makes the definition gauge-invariant. Notice that there is an additional leading twist two-gluon LCDA for flavour singlet mesons which we will not consider here.

The NR bound states are described by parton configurations with fixed momenta which correspond to the light-cone momentum fraction $u = 1/2$ for the $\eta_c$ meson, cf. (5.35). Relativistic effects from collinear gluon exchange lead to modifications: First, there is a correction from matching SCET$_{\mathrm{II}}$ to the NR theory. Second, there is the usual evolution under the change of the renormalization scale [36,37]. In particular, the support region for the parton momenta is extended to $0 < u < 1$.
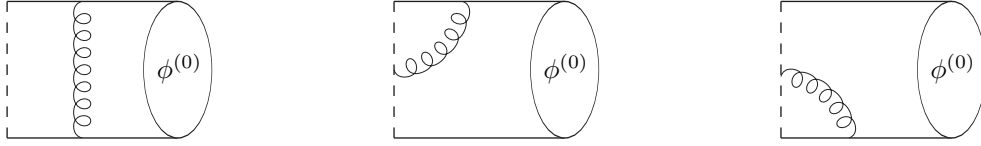
Figure 5.9: *Relativistic corrections to the light-cone distribution amplitudes. The dashes line indicates the Wilson-line.*

The first-order relativistic corrections arise from the diagrams in Figure 5.9. Apart from these 1-loop diagrams, we have to include the wave-function renormalization of the external quark lines. We first consider the local limit of the light-cone matrix element (5.39) which determines the relativistic corrections to the NR decay constant. In this case, the diagrams with the gluon attached to the Wilson-line are absent and we find

$$f_m = f_m^{\text{NR}} \left[ 1 - 6 \, \frac{\alpha_s C_F}{4\pi} + \mathcal{O}(\alpha_s^2) \right] \tag{5.40}$$

which coincides with the result in [114] for equal quark masses.

The NLO corrections to the leading twist distribution amplitude are found to be

$$\phi_\eta^{(1)}(u;\mu) = 4C_F \ln \frac{\mu^2}{m^2} \left[ \left( 1 + \frac{1}{1/2 - u} \right) u \, \theta(1/2 - u) + (u \leftrightarrow \bar{u}) \right]_+$$

$$- 4C_F \left\{ \left[ \left( 1 + \frac{1}{1/2 - u} \right) \ln(1 - 2u)^2 + \left( 1 - \frac{1/2}{(1/2 - u)^2} \right) \right] u \, \theta(1/2 - u) \right.$$

$$\left. + (u \leftrightarrow \bar{u}) \right\}_+ \tag{5.41}$$

where we have introduced plus-distributions defined by

$$\int_0^1 du \, [\ldots]_+ \, f(u) \equiv \int_0^1 du \, [\ldots] \left( f(u) - f(1/2) - f'(1/2) \, (u - 1/2) \right). \tag{5.42}$$

Notice that our result for the distribution amplitude obeys the evolution equation

$$\frac{d}{d \ln \mu} \, \phi_\eta(u;\mu) = \frac{\alpha_s C_F}{\pi} \int_0^1 dv \, V(u, v) \, \phi_\eta(v; \mu) + \mathcal{O}(\alpha_s^2), \tag{5.43}$$

where $V(u, v)$ denotes the familiar Brodsky-Lepage kernel [36,37]

$$V(u, v) = \left[ \left( 1 + \frac{1}{v - u} \right) \frac{u}{v} \theta(v - u) + \left( 1 + \frac{1}{\bar{v} - \bar{u}} \right) \frac{\bar{u}}{\bar{v}} \theta(u - v) \right]_+ \tag{5.44}$$

While writing this thesis an independent calculation of the leading-twist LCDAs of the $\eta_c$ and $J/\psi$ meson appeared in [115] where Ma and Si perform a similar analysis

factorizing perturbative effects from NRQCD matrix elements at leading power in the NR expansion. Our result is not in agreement with these findings which can already be seen by the fact that the distribution amplitude in [115] is not properly normalized to unity. We will have a closer look at the origin of this discrepancy in [112].

The factorization formula (5.38) contains the distribution amplitude $\phi_\eta^{(1)}$ in form of a convolution with the jet function $J^{(1)}$ from (5.34). We thus require the knowledge of the $1/\bar{u}$ moment which is found to be

$$\int_0^1 du\ \frac{\phi_\eta^{(1)}(u;\mu)}{\bar{u}} = C_F \left[ 2(3 - 2\ln 2)\ln\frac{\mu^2}{m^2} + 4\ln 2 - \frac{2}{3}\pi^2 + 12 \right]. \tag{5.45}$$

**Light-cone distribution amplitude of $B_c$ meson**

The calculation of the LCDA for the $B_c$ meson goes along the same lines as for the $\eta_c$ meson. However, important differences arise because the heavy $b$-quark is to be treated in HQET which modifies the divergence structure of the loop integrals. As a consequence, the evolution equations for the LCDA of heavy mesons [116,117] differ from that of light mesons [36,37].

We define the two-particle LCDAs of the $B_c$ meson following [118,81]

$$\langle 0|\bar{c}_\beta(z)b_\alpha(0)|B_c(p)\rangle\big|_{z^2=0} = -\frac{i\hat{f}_M(\mu)M}{4} \left[ \frac{1+\not{v}}{2} \left\{ 2\tilde{\phi}_+^B(t) + \frac{\tilde{\phi}_-^B(t) - \tilde{\phi}_+^B(t)}{t}\not{z} \right\} \gamma_5 \right]_{\alpha\beta} \tag{5.46}$$

with $p \simeq Mw$, $t \equiv w \cdot z$ and $\hat{f}_M$ the decay constant in HQET (we again omitted an appropriate Wilson-line in the definition). The Fourier-transformed expressions, which usually appear in factorization formulas, are given through

$$\tilde{\phi}_\pm^B(t) = \int_0^\infty d\omega\ e^{-i\omega t}\phi_\pm^B(\omega). \tag{5.47}$$

In the following we focus on the distribution amplitude $\phi_B(\omega) \equiv \phi_+^B(\omega)$ which enters the factorization formula (5.17). In the strict NR limit it simply corresponds to a delta-function, cf. (5.35). Similar to what we have seen in the case of the $\eta_c$ meson, we now have to take into account relativistic effects from soft gluon exchange according to analogous diagrams to those in Figure 5.9 which now extend the support region of the distribution amplitude to $0 < \omega < \infty$.

In the local limit we derive the corrections to the decay constant. We find

$$\hat{f}_M(\mu) = f_M^{\text{NR}} \left[ 1 + \frac{\alpha_s C_F}{4\pi} \left( 3\ln\frac{\mu}{m} - 4 \right) + \mathcal{O}(\alpha_s^2) \right]. \tag{5.48}$$

Notice that the decay constant of a heavy meson in HQET is scale-dependent.

The NLO corrections to the distribution amplitude read

$$
\phi_B^{(1)}(\omega;\mu) = 2C_F \ln \frac{\mu^2}{(\omega-m)^2} \left\{ \left[ \frac{\omega\theta(m-\omega) - m\theta(\omega-m)\theta(\Lambda-\omega)}{m(m-\omega)} \right]_+ + \frac{\theta(\omega-\Lambda)}{w-m} \right\}
$$

$$
- C_F\,\delta(\omega-m) \left( \frac{1}{2} \ln^2 \frac{\mu^2}{(\Lambda-m)^2} + \ln \frac{\mu^2}{m^2} + \frac{\pi^2}{12} \right)
$$

$$
+ 2C_F \left\{ \left[ \frac{(m+\omega)[\omega\theta(m-\omega) + m\theta(\omega-m)\theta(\Lambda-\omega)]}{m(m-\omega)^2} \right]_+ + \frac{(m+\omega)\theta(\omega-\Lambda)}{(w-m)^2} \right.
$$

$$
\left. -\delta(\omega-m) \left( \ln \frac{m}{\Lambda-m} + \frac{2m}{\Lambda-m} \right) - m\,\delta'(\omega-m) \left( 2\ln \frac{\Lambda-m}{m} + \frac{\Lambda}{m} + \frac{3}{2} \right) \right\}
$$

$$
\tag{5.49}
$$

with an analogous definition of plus-distributions as in (5.42). One remark is in order concerning the dependence of our results on an ad-hoc parameter $\Lambda > m$. In the computation of the LCDA we encounter IR singularities for $\omega = m$ (similar to the $\eta_c$ case for $u = 1/2$) which we regularize with the help of adequate plus-distributions. We rewrite for instance

$$
\frac{\theta(\omega-m)}{(w-m)^{1+2\varepsilon}} \quad \rightarrow \quad \left[ \frac{\theta(\omega-m)}{w-m} \right]_+
\tag{5.50}
$$

This is to be understood in the sense of a distribution which is convoluted with a kernel $f(\omega)$ that is assumed to be non-vanishing for $\omega = m$ and to scale as $1/\omega$ for large $\omega$ (as usual in application of QCD Factorization). The point to notice is that the (IR regular) plus-distribution gives rise to UV singularities in the convolutions as $f(\omega) \sim 1/\omega$ is replaced by $f(\omega) - f(m) \sim 1$ for large $\omega$. In order to avoid these artificial UV divergences we introduce an ad-hoc cutoff $\Lambda > m$ in the plus-distributions such that (5.50) is replaced by

$$
\frac{\theta(\omega-m)}{(w-m)^{1+2\varepsilon}} \quad \rightarrow \quad \left[ \frac{\theta(\omega-m)\theta(\Lambda-\omega)}{w-m} \right]_+ + \frac{\theta(\omega-\Lambda)}{w-m} - \frac{(\Lambda-m)^{-2\varepsilon}}{2\varepsilon_{\mathrm{IR}}}\delta(\omega-m) + \mathcal{O}(\varepsilon).
\tag{5.51}
$$

This expression is thus free of UV singularities whereas the IR divergence has been isolated in the local term. Notice that the dependence on the cutoff parameter drops out in the convolution with an arbitrary kernel $f(\omega)$. This can also be seen below in our expression for the $1/\omega$ moment of the LCDA in (5.56).

The distribution amplitude in (5.49) obeys the evolution equation

$$
\frac{d}{d\ln\mu}\,\phi_B(\omega;\mu) = \frac{\alpha_s C_F}{\pi} \int_0^\infty d\omega'\,\gamma_+(\omega,\omega';\mu)\,\phi_B(\omega';\mu) + \mathcal{O}(\alpha_s^2),
\tag{5.52}
$$

where the anomalous dimension $\gamma_+(\omega,\omega';\mu)$ is given by [116,117]

$$
\gamma_+(\omega,\omega';\mu) = \left( -\ln \frac{\mu}{\omega} + \frac{1}{2} \right)\delta(\omega-\omega') + \omega \left[ \frac{\theta(\omega'-\omega)}{\omega'(\omega'-\omega)} + \frac{\theta(\omega-\omega')}{\omega(\omega-\omega')} \right]_+
\tag{5.53}
$$

This can be verified most easily by integrating (5.52) over a test function $f(\omega)$ such that the dependence of the LCDA on the cutoff parameter $\Lambda$ drops out.

In contrast to the $\eta_c$ case, the normalization of the $B_c$ distribution amplitude is ill-defined. Imposing a hard cutoff $\Lambda_{\mathrm{UV}} \gg m$ and expanding to first order in $m/\Lambda_{\mathrm{UV}}$, we derive

$$\int_0^{\Lambda_{\mathrm{UV}}} d\omega\, \phi_B(\omega;\mu) \simeq 1 - \frac{\alpha_s C_F}{4\pi} \left[ \frac{1}{2} \ln^2 \frac{\mu^2}{\Lambda_{\mathrm{UV}}^2} + \ln \frac{\mu^2}{\Lambda_{\mathrm{UV}}^2} + \frac{\pi^2}{12} \right] + \mathcal{O}(\alpha_s^2) \qquad (5.54)$$

and similarly for the first moment

$$\int_0^{\Lambda_{\mathrm{UV}}} d\omega\, \omega\, \phi_B(\omega;\mu) \simeq \frac{\alpha_s C_F}{4\pi} \left[ 2 \ln \frac{\mu^2}{\Lambda_{\mathrm{UV}}^2} + 6 \right] \Lambda_{\mathrm{UV}} + \mathcal{O}(\alpha_s^2). \qquad (5.55)$$

The last two expressions provide model-independent properties of the distribution amplitude which have been studied within the operator product expansion in [119]. Our results are in agreement with these general findings. Notice, however, that our subleading terms in $m/\Lambda_{\mathrm{UV}}$ cannot be compared with [119] as we deal with massive light quarks here.

We finally quote our result for the $1/\omega$ moment which appears in the factorization formula (5.38) in form of the convolution with the jet function $J^{(1)}$ from (5.34)

$$\int_0^\infty d\omega\, \frac{\phi_B^{(1)}(\omega;\mu)}{\omega} = -\frac{C_F}{m} \left[ \frac{1}{2} \ln^2 \frac{\mu^2}{m^2} - \ln \frac{\mu^2}{m^2} + \frac{3\pi^2}{4} - 2 \right]. \qquad (5.56)$$

Notice the presence of a double Sudakov logarithm as in (5.25).

# Part IV

# Conclusion

# Conclusion

The dedicated study of charmless $B$ decays has become one of the most active and promising fields in particle physics. It aims at a precision determination of the flavour parameters in the Standard Model and may help to reveal the nature of CP violation. On the experimental side, the $B$ factories BaBar and Belle are continuously accumulating larger data samples and provide us with measurements of unprecedented precision. On the theory side, the main challenge consists in the quantitative control of the complicated hadronic dynamics.

QCD Factorization represents a model-independent framework to compute hadronic matrix elements from first principles. Based on a power expansion in $\Lambda_{\mathrm{QCD}}/m_b$, it allows for a clear separation of short- and long-distance effects in certain classes of $B$ decays. Whereas the development of Soft-Collinear Effective Theory provided the means to put factorization formulas onto a firmer basis, the implementation of higher-order QCD corrections has started only recently.

In this thesis we have mainly addressed the most challenging class of charmless $B$ decays: exclusive nonleptonic $B$ decays with its most prominent example $B \to \pi\pi$. This wide class of decays is of primary importance as most of the observables at the $B$ factories are related to it. Our calculation considers one class of the NNLO corrections to hadronic two-body decays within QCD Factorization. Whereas the (1-loop) spectator scattering contributions have been considered recently by various groups [25–27], we have presented the first calculation of the 2-loop vertex corrections which constituted the missing piece for a full NNLO analysis of the topological tree amplitudes in QCD Factorization.

The knowledge of the NNLO corrections is particularly important with respect to strong interaction phases and hence direct CP asymmetries. As strong phases arise first at $\mathcal{O}(\alpha_s)$ in QCD Factorization, they were known so far to LO accuracy only. As in any perturbative calculation the considered corrections are thus necessary to eliminate large scale ambiguities of the LO result. They may even drastically change the pattern of direct CP asymmetries in QCD Factorization.

We indeed found that the considered corrections can exceed the formally leading contributions whenever the latter are accompanied by small numerical coefficients. This is the case for the imaginary part of the colour-allowed tree amplitude which receives its dominant contribution from the considered 2-loop vertex corrections. The respective contribution to the colour-suppressed tree amplitude also turned out to be sizeable. However, in absolute terms our corrections are small. In other words,

we did not encounter any source of sizeable strong phases from the perturbative calculation. We further remark that we have observed an accidental cancellation between the individual NNLO contributions which resulted in a moderate correction to the NLO result for the imaginary part of the tree amplitudes.

The calculation of the real part of the topological tree amplitudes is more involved. We have presented a preliminary result for the colour-allowed tree amplitude which is based on certain technical simplifications. More importantly, we have already tackled the most challenging part of the calculation which consisted in the evaluation of a large set of 2-loop integrals. We could further verify that factorization holds at the considered order in perturbation theory which is a non-trivial statement as the formal all-order proof is still missing. We emphasize that this is the result of a highly complicated subtraction procedure which can also be considered as a very powerful cross-check of our calculation.

From the technical point of view we have presented a calculation of 2-loop hadronic matrix elements. Even in the wider sense of perturbative corrections to weak decays, there exist only very few calculations of this type. In the context of inclusive decays, 2-loop matrix elements have been considered for $B \to X_s \ell^+ \ell^-$ [120,121] and 3-loop matrix elements for $B \to X_s \gamma$ [122]. Concerning the exclusive modes 2-loop matrix elements have been calculated for $B \to K^* \gamma$ or $B \to \rho \ell^+ \ell^-$ [123]. However, our analysis represents the first calculation of 2-loop hadronic matrix elements for the more complicated nonleptonic decays which are mediated by a $b \to u\bar{u}d$ transition. For this class of decays 2-loop hadronic matrix elements have never been calculated so far, neither in the inclusive nor in the exclusive channel.

In our final analysis we examined the formal factorization properties of heavy-to-light form factors. The development of Soft-Collinear Effective Theory has led to a deeper understanding of the QCD dynamics in heavy-to-light transitions and the $B \to \pi$ form factor (at large recoil) has emerged as the central object in these studies. Rather than stating a complete separation of short- and long-distance effects, the factorization formula contains a classification into (non-calculable) symmetry conserving contributions, the so-called soft-overlap contribution, and perturbative symmetry breaking effects. Remnant short-distance effects in the soft-overlap cannot be factorized by standard means as this would lead to endpoint-divergent convolution integrals. The question arises if one can understand this non-factorization of soft and collinear effects from the viewpoint of the effective theory.

In order to address this question we have considered a simplified scenario. We investigated heavy-to-light form factors between non-relativistic bound states which can be addressed in perturbation theory. We have performed a NLO analysis of these form factors and looked for an interpretation in terms of the factorization formula. We showed that the soft-overlap contribution can be calculated in our set-up. We have addressed the question of the origin of formally large (Sudakov) logarithms and argued that one class of logarithms related to endpoint-singularities cannot be resummed with standard RG techniques. We in particular did not need to introduce soft-collinear messenger modes to describe the physics of the soft-overlap

contribution. As a byproduct of our analysis, we have calculated leading-twist light-cone distribution amplitudes for non-relativistic bound states which can be applied for the description of $B_c$ and $\eta_c$ mesons.

To summarize, the development of QCD Factorization and Soft-Collinear Effective Theory has substantially improved our understanding of QCD in $B$ meson decays. To date, the QCD Factorization predictions are in good overall agreement with the experimental measurements. In order to perform a precision study of $B$ decays, we have to reduce theoretical and experimental uncertainties as much as possible. This thesis has contributed to the former by calculating higher-order QCD corrections to exclusive charmless $B$ decays. Apart from the perturbative corrections, further improvements on the theory side concern the control of power corrections and precise determinations of the hadronic input parameters. We think that it will be exiting to confront these improved theoretical predictions with updated experimental data in the near future.

# Part V

# Appendix

# Appendix A

# Master Integrals

In the following we present the analytical results for all MIs that appeared in our calculations from Chapter 3, 4 and 5. The MIs are normalized according to

$$[dk] \equiv \frac{\Gamma(1-\varepsilon)}{i\pi^{d/2}} \, d^d k. \tag{A.1}$$

We give the results up to the order in $\varepsilon$ that was required in our calculations. For some simpler MIs, we obtain the results in a closed form in $\varepsilon$.

## A.1 Hadronic two-body decays I

In the calculation from Chapter 3 we found 14 MIs which are shown in Figure 3.3. The corresponding particle propagators $\mathcal{P}_i$ can be found in (3.6). Although the calculation in Chapter 3 requires the knowledge of the imaginary part only, we give the full results of the MIs here in view of our extension in Chapter 4.

**1–loop integrals**

Some 2-loop integrals can be written as products of the following 1-loop integrals

$$\bigcirc \qquad = \quad \int [dk] \, \frac{1}{\mathcal{P}_{13}} \qquad = \quad -(m^2)^{1-\varepsilon} \, \Gamma(1-\varepsilon)\Gamma(-1+\varepsilon) \tag{A.2}$$

$$-\bigcirc- \qquad = \quad \int [dk] \, \frac{1}{\mathcal{P}_1 \mathcal{P}_3} \qquad = \quad (um^2)^{-\varepsilon} \, e^{i\pi\varepsilon} \, \frac{\Gamma(\varepsilon)\Gamma(1-\varepsilon)^3}{\Gamma(2-2\varepsilon)} \tag{A.3}$$

$$
\underbrace{\phantom{xxx}}_{} \quad = \quad \int [dk]\, \frac{1}{\mathcal{P}_5 \mathcal{P}_{13}} \quad \equiv \quad (m^2)^{-\varepsilon} \left\{ \sum_{i=-1}^{3} c_i^{(22)}\, \varepsilon^i + \mathcal{O}(\varepsilon^4) \right\} \qquad \text{(A.4)}
$$

with

$$
c_{-1}^{(22)} = 1,
$$

$$
c_0^{(22)} = 2 + \frac{\bar{u}}{u} \ln \bar{u},
$$

$$
c_1^{(22)} = 4 + \frac{\pi^2}{6} - \frac{\bar{u}}{u} \left[ \mathrm{Li}_2(u) + \ln^2 \bar{u} - 2 \ln \bar{u} \right],
$$

$$
c_2^{(22)} = 8 + \frac{\pi^2}{3} - \frac{\bar{u}}{u} \left[ \mathrm{Li}_3(u) - 2\mathrm{S}_{1,2}(u) - 2 \ln \bar{u}\, \mathrm{Li}_2(u) - \frac{2}{3} \ln^3 \bar{u} + 2\mathrm{Li}_2(u) + 2 \ln^2 \bar{u} \right.
$$

$$
\left. - \left( 4 + \frac{\pi^2}{6} \right) \ln \bar{u} \right],
$$

$$
c_3^{(22)} = 16 + \frac{2\pi^2}{3} + \frac{7\pi^4}{360} - \frac{\bar{u}}{u} \left[ \mathrm{Li}_4(u) - 2\mathrm{S}_{2,2}(u) + 4\mathrm{S}_{1,3}(u) - 2 \Big( \mathrm{Li}_3(u) - 2\mathrm{S}_{1,2}(u) \Big) \ln \bar{u} \right.
$$

$$
+ 2 \ln^2 \bar{u}\, \mathrm{Li}_2(u) + \frac{1}{3} \ln^4 \bar{u} + 2\mathrm{Li}_3(u) - 4\mathrm{S}_{1,2}(u) - 4 \ln \bar{u}\, \mathrm{Li}_2(u) - \frac{4}{3} \ln^3 \bar{u}
$$

$$
\left. + \left( 4 + \frac{\pi^2}{6} \right) \Big( \mathrm{Li}_2(u) + \ln^2 \bar{u} - 2 \ln \bar{u} \Big) \right]. \qquad \text{(A.5)}
$$

**3–topologies**

$$
\underbrace{\phantom{xxx}}_{} \quad = \quad \int [dk][dl]\, \frac{1}{\mathcal{P}_1 \mathcal{P}_4 \mathcal{P}_9} \quad = \quad (um^2)^{1-2\varepsilon}\, e^{2i\pi\varepsilon}\, \frac{\Gamma(-1+2\varepsilon)\Gamma(1-\varepsilon)^5}{\Gamma(3-3\varepsilon)}
$$

$$
\text{(A.6)}
$$

**4–topologies**

$$
\underbrace{\phantom{xxx}}_{} \quad = \quad \int [dk][dl]\, \frac{1}{\mathcal{P}_1 \mathcal{P}_3 \mathcal{P}_8 \mathcal{P}_9}
$$

$$
= \quad (um^2)^{-2\varepsilon}\, e^{2i\pi\varepsilon}\, \frac{\Gamma(2\varepsilon)\Gamma(\varepsilon)\Gamma(1-2\varepsilon)^2 \Gamma(1-\varepsilon)^4}{\Gamma(2-2\varepsilon)\Gamma(2-3\varepsilon)} \qquad \text{(A.7)}
$$

$$
\underbrace{\phantom{xxx}}_{} \quad = \quad \int [dk][dl]\, \frac{1}{\mathcal{P}_1 \mathcal{P}_3 \mathcal{P}_6 \mathcal{P}_{10}} \quad \equiv \quad (m^2)^{-2\varepsilon}\, e^{2i\pi\varepsilon} \left\{ \sum_{i=-2}^{2} c_i^{(42)}\, \varepsilon^i + \mathcal{O}(\varepsilon^3) \right\}
$$

$$
\text{(A.8)}
$$

with

$$c_{-2}^{(42)} = \frac{1}{2},$$

$$c_{-1}^{(42)} = \frac{5}{2} - \ln u,$$

$$c_0^{(42)} = \frac{19}{2} - \frac{\pi^2}{6} + \mathrm{Li}_2(u) + \frac{1}{2}\Big(\ln u + \ln \bar u\Big)^2 - \frac{1}{2}\ln^2 \bar u - 5\ln u,$$

$$c_1^{(42)} = \frac{65}{2} - \frac{5\pi^2}{6} - 3\zeta_3 - \mathrm{Li}_3(u) - \mathrm{S}_{1,2}(u) + \Big(5 - \ln \bar u\Big)\mathrm{Li}_2(u) - \frac{1}{6}\Big(\ln u + \ln \bar u\Big)^3$$

$$+ \frac{1}{6}\ln^3 \bar u + \frac{5}{2}\Big(\ln u + \ln \bar u\Big)^2 - \frac{5}{2}\ln^2 \bar u + \frac{\pi^2}{6}\Big(\ln u + \ln \bar u\Big) - 19\ln u,$$

$$c_2^{(42)} = \frac{211}{2} - \frac{19\pi^2}{6} - \frac{13\pi^4}{120} - 15\zeta_3 + \mathrm{Li}_4(u) + \mathrm{S}_{2,2}(u) + \mathrm{S}_{1,3}(u) + \frac{1}{24}\Big(\ln u + \ln \bar u\Big)^4$$

$$- \frac{1}{24}\ln^4 \bar u - \frac{5}{6}\Big(\ln u + \ln \bar u\Big)^3 + \frac{5}{6}\ln^3 \bar u - \Big(5 - \ln \bar u\Big)\Big(\mathrm{Li}_3(u) + \mathrm{S}_{1,2}(u)\Big)$$

$$- \Big(5 - \frac{1}{2}\ln \bar u\Big)\ln \bar u\,\mathrm{Li}_2(u) + 19\Big(\mathrm{Li}_2(u) + \frac{1}{2}\ln^2 u + \ln u \ln \bar u\Big) - 2\zeta_3 \ln \bar u$$

$$+ \Big(8\zeta_3 - 65\Big)\ln u + \frac{5\pi^2}{6}\Big(\ln u + \ln \bar u\Big) - \frac{\pi^2}{12}\Big(\ln u + \ln \bar u\Big)^2. \tag{A.9}$$

$$\cdots\!\!-\!\!\bigcirc\!\!-\!\!\cdots \quad = \quad \int [dk][dl]\,\frac{1}{\mathcal{P}_4\mathcal{P}_7\mathcal{P}_{13}\mathcal{P}_{19}} \quad \equiv \quad (m^2)^{-2\varepsilon}\left\{\sum_{i=-2}^{2} c_i^{(43)}\,\varepsilon^i + \mathcal{O}(\varepsilon^3)\right\}$$
$$\tag{A.10}$$

with

$$c_{-2}^{(43)} = \frac{1}{2},$$

$$c_{-1}^{(43)} = \frac{5}{2},$$

$$c_0^{(43)} = \frac{19}{2} + \frac{\pi^2}{3} + \frac{u}{2\bar u}\ln^2 u - i\pi\,\frac{u}{\bar u}\ln u,$$

$$c_1^{(43)} = \frac{65}{2} + \frac{5\pi^2}{3} - \zeta_3 - \frac{u}{\bar u}\Big[2\mathrm{Li}_3(u) - 2\mathrm{Li}_2(u)\ln u + \frac{5}{6}\ln^3 u - \frac{5}{2}\ln^2 u - \frac{4\pi^2}{3}\ln u$$

$$- \ln^2 u \ln \bar u - 2\zeta_3\Big] - i\pi\,\frac{u}{\bar u}\Big[2\mathrm{Li}_2(u) + 2\ln u \ln \bar u - \frac{5}{2}\ln^2 u + 5\ln u - \frac{\pi^2}{3}\Big],$$

$$c_2^{(43)} = \frac{211}{2} + \frac{19\pi^2}{3} + \frac{5\pi^4}{36} - 5\zeta_3 + \frac{u}{\bar u}\Big[8\mathrm{Li}_4(u) - 4\mathrm{S}_{2,2}(u) + 4\mathrm{S}_{1,2}(u)\ln u + \frac{19}{24}\ln^4 u$$

$$-2\Big(5+\ln u+2\ln\bar u\Big)\mathrm{Li}_3(u)-\frac{5}{3}\ln^3 u\ln\bar u+\ln^2 u\ln^2\bar u+5\ln^2 u\ln\bar u$$

$$-\frac{25}{6}\ln^3 u+\frac{19}{2}\ln^2 u+2\Big(\zeta_3+\ln u\,\mathrm{Li}_2(u)\Big)\Big(5-\ln u+2\ln\bar u\Big)-\frac{47\pi^4}{90}$$

$$+\frac{\pi^2}{3}\Big(8\mathrm{Li}_2(u)-9\ln^2 u+8\ln u\ln\bar u+20\ln u\Big)\Big]+i\pi\frac{u}{\bar u}\Big[2\mathrm{Li}_3(u)-4\mathrm{S}_{1,2}(u)$$

$$+4\ln u\,\mathrm{Li}_2(u)-\Big(5+2\ln\bar u\Big)\Big(2\mathrm{Li}_2(u)-\frac{\pi^2}{3}\Big)-\frac{19}{6}\ln^3 u+5\ln^2 u\ln\bar u$$

$$-2\ln u\ln^2\bar u+\frac{25}{2}\ln^2 u-10\ln u\ln\bar u-\Big(19+\frac{\pi^2}{3}\Big)\ln u+2\zeta_3\Big]. \qquad\text{(A.11)}$$



$$=\quad\int[dk][dl]\,\frac{1}{\mathcal{P}_2\mathcal{P}_4\mathcal{P}_{13}\mathcal{P}_{19}}\quad\equiv\quad(m^2)^{-2\varepsilon}\left\{\sum_{i=-2}^{1}c_i^{(44)}\,\varepsilon^i+\mathcal{O}(\varepsilon^2)\right\}$$
$$\text{(A.12)}$$

with

$$c_{-2}^{(44)}=\frac{1}{2},$$

$$c_{-1}^{(44)}=\frac{5}{2}-\ln u+i\pi,$$

$$c_0^{(44)}=\frac{19}{2}-\frac{5\pi^2}{6}+\frac{1}{\bar u}\Big[\mathrm{Li}_3(u)-\ln u\,\mathrm{Li}_2(u)-\frac{1}{2}\ln^2 u\ln\bar u+\frac{1-2u}{2}\ln^2 u-\zeta_3$$

$$-\Big(5\bar u-\frac{\pi^2}{6}\Big)\ln u\Big]+i\pi\Big[5+\frac{1}{\bar u}\Big(\mathrm{Li}_2(u)+\ln u\ln\bar u-(1-2u)\ln u-\frac{\pi^2}{6}\Big)\Big],$$

$$c_1^{(44)}=\frac{65}{2}-\frac{25\pi^2}{6}-4\zeta_3+\frac{1}{\bar u}\Big[\frac{59\pi^4}{360}+2\mathrm{Li}_4(u)+3\mathrm{S}_{2,2}(u)-3\ln u\Big(\mathrm{Li}_3(u)+\mathrm{S}_{1,2}(u)\Big)$$

$$+\Big(3\ln\bar u+2(1+u)\Big)\Big(\mathrm{Li}_3(u)-\ln u\,\mathrm{Li}_2(u)\Big)+2\ln^2 u\,\mathrm{Li}_2(u)+\frac{5}{6}\ln^3 u\ln\bar u$$

$$-\frac{3}{4}\ln^2 u\ln^2\bar u-(1+u)\ln^2 u\ln\bar u-\frac{1-6u}{6}\ln^3 u-\frac{7\pi^2}{6}\mathrm{Li}_2(u)-19\bar u\ln u$$

$$+\frac{5(1-2u)}{2}\ln^2 u-\Big(\frac{1}{2}\ln^2 u+7\ln u\ln\bar u-2(2-5u)\ln u\Big)\frac{\pi^2}{6}+\Big(6\ln u$$

$$-3\ln\bar u-4\Big)\zeta_3\Big]+i\pi\Big[19+\frac{\pi^2}{3}+\frac{1}{\bar u}\Big(3\mathrm{Li}_3(u)+3\mathrm{S}_{1,2}(u)-6\zeta_3-\frac{5}{2}\ln^2 u\ln\bar u$$

$$-\Big(4\ln u-3\ln\bar u\Big)\mathrm{Li}_2(u)+\frac{3}{2}\ln u\ln^2\bar u+\frac{1-6u}{2}\ln^2 u-5(1-2u)\ln u$$

$$+2(1+u)\Big(\mathrm{Li}_2(u)+\ln u\ln\bar u\Big)+\Big(\ln u-3\ln\bar u-4\Big)\frac{\pi^2}{6}\Big)\Big]. \qquad\text{(A.13)}$$
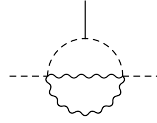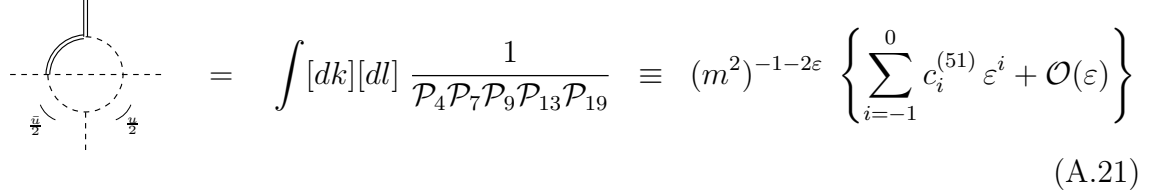
$$\int [dk][dl] \,\frac{1}{\mathcal{P}_2^2 \mathcal{P}_4 \mathcal{P}_{13} \mathcal{P}_{19}} \;\equiv\; (m^2)^{-1-2\varepsilon} \left\{ \sum_{i=-2}^{2} c_i^{(45)} \,\varepsilon^i + \mathcal{O}(\varepsilon^3) \right\} \tag{A.14}$$

with

$$c_{-2}^{(45)} = -\frac{1}{u},$$

$$c_{-1}^{(45)} = -\frac{1}{u}\Big( 2 - \ln u + i\pi \Big),$$

$$c_0^{(45)} = \frac{1}{u}\left[ \frac{\pi^2}{6} - 4 - \frac{1-2u}{2\bar{u}} \ln^2 u + 2\ln u - i\pi\Big( 2 - \frac{1-2u}{\bar{u}}\ln u \Big) \right],$$

$$c_1^{(45)} = \frac{1}{u}\left\{ \frac{\pi^2}{3} - 8 - 5\zeta_3 + \frac{1}{\bar{u}}\left[ (1-2u)\Big( \mathrm{Li}_3(u) - \ln u\,\mathrm{Li}_2(u) - \frac{1}{2}\ln^2 u\ln\bar{u} - \ln^2 u \Big) \right.\right.$$

$$+ \frac{1-6u}{6}\ln^3 u + \Big( 4\bar{u} - \frac{(1-10u)\pi^2}{6} \Big)\ln u + \zeta_3 \Big] - i\pi\Big[ 4 + \frac{1-6u}{2\bar{u}}\ln^2 u$$

$$\left.\left. - \frac{1-2u}{\bar{u}}\Big( \mathrm{Li}_2(u) + \ln u\ln\bar{u} + 2\ln u - \frac{\pi^2}{6} \Big) \Big] \right\},$$

$$c_2^{(45)} = \frac{1}{u}\left\{ \frac{2\pi^2}{3} + \frac{17\pi^4}{60} - 16 - 10\zeta_3 + \frac{1}{\bar{u}}\left[ 2(1+7u)\mathrm{Li}_4(u) - \frac{1-22u}{24}\ln^4 u \right.\right.$$

$$- 3(1+2u)\ln u\,\mathrm{Li}_3(u) + (2-u)\ln^2 u\,\mathrm{Li}_2(u) + \frac{(1-36u)\pi^2}{12}\ln^2 u + (3-4u)$$

$$\Big( \mathrm{S}_{2,2}(u) - \ln u\,\mathrm{S}_{1,2}(u) + \ln\bar{u}(\mathrm{Li}_3(u) - \ln u\,\mathrm{Li}_2(u)) - \frac{1}{4}\ln^2 u\ln^2\bar{u} - \zeta_3\ln\bar{u} \Big)$$

$$+ 2(1-2u)\Big( \mathrm{Li}_3(u) - \ln u\,\mathrm{Li}_2(u) + \frac{5}{12}\ln^3 u\ln\bar{u} - \frac{1}{2}\ln^2 u\ln\bar{u} - \ln^2 u \Big)$$

$$- \frac{(7-16u)\pi^2}{6}\Big( \mathrm{Li}_2(u) + \ln u\ln\bar{u} \Big) + \Big( 8\bar{u} - \frac{(1-10u)\pi^2}{3} + 4(1+u)\zeta_3 \Big)\ln u$$

$$+ \frac{1-6u}{3}\ln^3 u + 2\zeta_3 - \frac{17\pi^4}{40} \Big] + i\pi\Big[ \frac{1}{\bar{u}}\Big( 3(1+2u)\mathrm{Li}_3(u) - 2(2-u)\ln u\,\mathrm{Li}_2(u)$$

$$+ (3-4u)\Big( \mathrm{S}_{1,2}(u) + \ln\bar{u}\,\mathrm{Li}_2(u) + \frac{1}{2}\ln u\ln^2\bar{u} - \frac{\pi^2}{6}\ln\bar{u} \Big) + \frac{1-22u}{6}\ln^3 u$$

$$+ (1-2u)\Big( 2\mathrm{Li}_2(u) - \frac{5}{2}\ln^2 u\ln\bar{u} + 2\ln u\ln\bar{u} + 4\ln u \Big) - (1-6u)\ln^2 u$$

$$\left.\left. + \frac{(1-8u)\pi^2}{6}\ln u + \frac{\pi^2}{3} - 8\zeta_3 \Big) + 4\zeta_3 - 8 - \frac{2\pi^2}{3} \Big] \right\}. \tag{A.15}$$

The following MIs can be written in terms of the variable $\xi \equiv z^2/u$ and
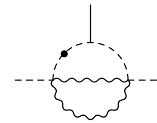
$$\eta \equiv \frac{1}{2}\left(1 - \sqrt{1+4\xi}\right),$$

$$\bar{\eta} \equiv 1 - \eta = \frac{1}{2}\left(1 + \sqrt{1+4\xi}\right). \tag{A.16}$$



$$= \int [dk][dl]\, \frac{1}{\mathcal{P}_1 \mathcal{P}_3 \mathcal{P}_{22} \mathcal{P}_{23}} \equiv (z^2 m^2)^{-2\varepsilon} \left\{ \sum_{i=-2}^{0} c_i^{(46)}\, \varepsilon^i + \mathcal{O}(\varepsilon) \right\} \tag{A.17}$$

with

$$c_{-2}^{(46)} = \frac{1}{2},$$

$$c_{-1}^{(46)} = \frac{5}{2} + \ln\xi + i\pi,$$

$$\begin{aligned}
c_0^{(46)} &= \frac{19}{2} - \frac{5\pi^2}{6} + 4\xi\left(\zeta_3 - \mathrm{S}_{1,2}(\eta) + \mathrm{Li}_3(\eta) - \ln\bar{\eta}\,\mathrm{Li}_2(\eta) + \frac{1}{2}\ln^2\xi\ln\bar{\eta} - \ln\xi\ln^2\bar{\eta} \right. \\
&\quad \left. - \frac{1}{12}\ln^3\xi + \frac{1}{2}\ln^3\bar{\eta}\right) - (1-2\eta)\left(2\mathrm{Li}_2(\eta) + 2\ln\xi\ln\bar{\eta} - \ln^2\bar{\eta}\right) + \bar{\eta}\ln^2\xi \\
&\quad + 5\ln\xi + \left(4\xi\ln\xi - 8\xi\ln\bar{\eta} + 4\eta\right)\frac{\pi^2}{6} + i\pi\left[5 - \xi\left(\ln\xi - 2\ln\bar{\eta}\right)^2 + 2\bar{\eta}\ln\xi \right. \\
&\quad \left. - 2(1-2\eta)\ln\bar{\eta}\right].
\end{aligned} \tag{A.18}$$



$$= \int [dk][dl]\, \frac{1}{\mathcal{P}_1 \mathcal{P}_3^2 \mathcal{P}_{22} \mathcal{P}_{23}} \equiv (z^2 m^2)^{-1-2\varepsilon} \left\{ \sum_{i=-2}^{0} c_i^{(47)}\, \varepsilon^i + \mathcal{O}(\varepsilon) \right\} \tag{A.19}$$

with

$$c_{-2}^{(47)} = -\xi,$$

$$c_{-1}^{(47)} = -\xi\left(\ln\xi + i\pi\right),$$

$$\begin{aligned}
c_0^{(47)} &= -\xi\left[4 - (1-2\eta)\left(2\mathrm{Li}_2(\eta) + 2\ln\xi\ln\bar{\eta} - \ln^2\bar{\eta}\right) + \bar{\eta}\ln^2\xi + 2\ln\xi - \frac{2\pi^2}{3}\bar{\eta} \right. \\
&\quad \left. + 2i\pi\left(1 + \bar{\eta}\ln\xi - (1-2\eta)\ln\bar{\eta}\right)\right].
\end{aligned} \tag{A.20}$$
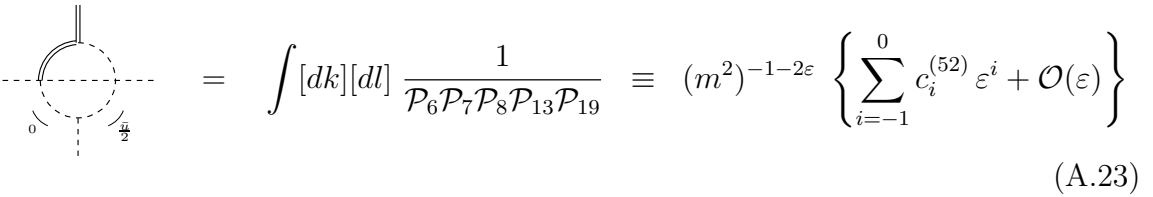
## 5–topologies

$$
\begin{aligned}
\text{(diagram)} \quad &= \quad \int [dk][dl]\, \frac{1}{\mathcal{P}_4\mathcal{P}_7\mathcal{P}_9\mathcal{P}_{13}\mathcal{P}_{19}} \equiv (m^2)^{-1-2\varepsilon} \left\{ \sum_{i=-1}^{0} c_i^{(51)}\, \varepsilon^i + \mathcal{O}(\varepsilon) \right\}
\end{aligned}
\tag{A.21}
$$

with

$$
\begin{aligned}
c_{-1}^{(51)} =\;& \zeta_3 + \mathrm{Li}_3(u) - \mathrm{S}_{1,2}(u) - \ln \bar{u}\, \mathrm{Li}_2(u) - \frac{1}{6}\Big( \ln u - \ln \bar{u} \Big)^3 - \frac{1}{6} \ln^3 \bar{u} \\
& - \Big( \ln u - \ln \bar{u} \Big)\frac{\pi^2}{6} + i\pi \left[ \frac{\pi^2}{3} - \mathrm{Li}_2(u) + \frac{1}{2}\ln^2 u - \ln u \ln \bar{u} \right]
\end{aligned}
$$

$$
\begin{aligned}
c_0^{(51)} =\;& -\frac{41\pi^4}{72} + 13\mathrm{Li}_4(u) - 6\mathrm{S}_{2,2}(u) - \mathrm{S}_{1,3}(u) - \Big( 11\ln u + 6\ln \bar{u} \Big)\mathrm{Li}_3(u) + \frac{3}{8}\ln^4 u \\
& + \Big( 11\ln u - \ln \bar{u} \Big)\mathrm{S}_{1,2}(u) - \frac{5}{6}\ln^3 u \ln \bar{u} + \frac{3}{2}\ln^2 u \ln^2 \bar{u} - \frac{1}{6}\ln u \ln^3 \bar{u} \\
& + \frac{1}{2}\Big( 5\ln^2 u + 12\ln u \ln \bar{u} - \ln^2 \bar{u} - 5\mathrm{Li}_2(u) \Big)\mathrm{Li}_2(u) - \zeta_3\Big( 11\ln u - 7\ln \bar{u} \Big) \\
& + \Big( 26\mathrm{Li}_2(u) - 4\ln^2 u + 16\ln u \ln \bar{u} + \ln^2 \bar{u} \Big)\frac{\pi^2}{12} + i\pi\Big[ 2\zeta_3 + 7\mathrm{Li}_3(u) - 2\mathrm{S}_{1,2}(u) \\
& - \Big( \ln u + 2\ln \bar{u} \Big)\mathrm{Li}_2(u) - \frac{3}{2}\ln^3 u + \frac{5}{2}\ln^2 u \ln \bar{u} - \ln u \ln^2 \bar{u} \\
& - \Big( 5\ln u - \ln \bar{u} \Big)\frac{\pi^2}{3} \Big].
\end{aligned}
\tag{A.22}
$$

$$
\begin{aligned}
\text{(diagram)} \quad &= \quad \int [dk][dl]\, \frac{1}{\mathcal{P}_6\mathcal{P}_7\mathcal{P}_8\mathcal{P}_{13}\mathcal{P}_{19}} \equiv (m^2)^{-1-2\varepsilon} \left\{ \sum_{i=-1}^{0} c_i^{(52)}\, \varepsilon^i + \mathcal{O}(\varepsilon) \right\}
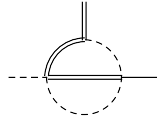\end{aligned}
\tag{A.23}
$$

with

$$
\begin{aligned}
c_{-1}^{(52)} =\;& \frac{1}{\bar{u}}\left[ \zeta_3 - \mathrm{S}_{1,2}(u) + i\pi\Big( \frac{\pi^2}{6} - \mathrm{Li}_2(u) \Big) \right] \\
c_0^{(52)} =\;& \frac{1}{\bar{u}}\left[ -\frac{29\pi^4}{180} - 2\mathrm{S}_{2,2}(u) - 5\mathrm{S}_{1,3}(u) + \frac{4\pi^2}{3}\mathrm{Li}_2(u) \right. \\
& \left. + i\pi\Big( 7\zeta_3 - 2\mathrm{Li}_3(u) - 5\mathrm{S}_{1,2}(u) \Big) \right]
\end{aligned}
\tag{A.24}
$$

**6–topologies**

The non-planar massless 6-denominator integral has been considered in [124–126]. Recently it has been formulated in terms of hypergeometric functions which can be expanded to arbitrary order in $\varepsilon$ with the help of the MATHEMATICA package HYPEXP [127]. Our result

$$
\begin{aligned}
\longrightarrow\!\!\!\!\!\!\!\!\!\!\!\!\!\!\!\!\!\!\!\!\!\!\!\!\!\!\!\!\!\!\!\!\!\!\!\!\!\!\!\! &= \int [dk][dl]\, \frac{1}{\mathcal{P}_1 \mathcal{P}_2 \mathcal{P}_3 \mathcal{P}_8 \mathcal{P}_9 \mathcal{P}_{10}} \\
&= (um^2)^{-2-2e}\, e^{2i\pi e} \left\{ \frac{1}{\varepsilon^4} - \frac{5\pi^2}{6\varepsilon^2} - \frac{27\zeta_3}{\varepsilon} - \frac{23\pi^4}{36} + \mathcal{O}(\varepsilon) \right\} \quad (A.25)
\end{aligned}
$$

is in agreement with the previous findings.

## A.2   Hadronic two-body decays II

Our analysis in Chapter 4 involves the calculation of the MIs from Figure 4.1. The corresponding particle propagators $\mathcal{P}_i$ can be found in (3.6). So far we have not yet calculated the MIs with an internal charm quark (wavy lines) which will be considered in [106] (these amount to four MIs out of 22).

**3–topologies**

$$
\begin{array}{ccc}
\text{} & = & \displaystyle\int [dk][dl]\, \frac{1}{\mathcal{P}_8 \mathcal{P}_{13} \mathcal{P}_{17}} \quad \equiv \quad (m^2)^{1-2\varepsilon} \left\{ \sum_{i=-2}^{2} d_i^{(31)} \varepsilon^i + \mathcal{O}(\varepsilon^3) \right\}
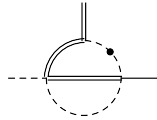\end{array}
\tag{A.26}
$$

with

$$
d_{-2}^{(31)} = \frac{1}{2},
$$

$$
d_{-1}^{(31)} = \frac{3}{2} - \frac{u}{4},
$$

$$
d_0^{(31)} = 3 + \frac{\pi^2}{3} - \frac{13u}{8} + \mathrm{Li}_2(u) - \frac{1-u^2}{2u}\ln \bar{u},
$$

$$
d_1^{(31)} = \frac{15}{4} + \pi^2 - \zeta_3 - \left(\frac{115}{16} + \frac{\pi^2}{6}\right)u + \mathrm{Li}_3(u) + 4\mathrm{S}_{1,2}(u) + \frac{1+6u-2u^2}{2u}\mathrm{Li}_2(u)
$$

$$
\qquad + \frac{1-u^2}{u}\ln^2 \bar{u} - \frac{13(1-u^2)}{4u}\ln \bar{u},
$$

$$
d_2^{(31)} = -\frac{21}{8} + 2\pi^2 + \frac{5\pi^4}{36} - 3\zeta_3 - \left(\frac{865}{32} + \frac{13\pi^2}{12} - \frac{\zeta_3}{2}\right)u + \mathrm{Li}_4(u) - 8\mathrm{S}_{2,2}(u)
$$

$$
\qquad + 16\mathrm{S}_{1,3}(u) + \frac{1+6u-2u^2}{2u}\mathrm{Li}_3(u) - \frac{4-12u-2u^2}{u}\mathrm{S}_{1,2}(u) + 3\mathrm{Li}_2^2(u)
$$

$$
\qquad - \frac{1-u^2}{u}\left[3\ln \bar{u}\,\mathrm{Li}_2(u) + \frac{4}{3}\ln^3 \bar{u} - \frac{13}{2}\ln^2 \bar{u} + \left(\frac{115}{8} + \frac{\pi^2}{3}\right)\ln \bar{u}\right]
$$

$$
\qquad + \frac{1}{4u}\left[13 + \left(24 + \frac{8\pi^2}{3}\right)u - 26u^2\right]\mathrm{Li}_2(u).
\tag{A.27}
$$

$$
\begin{array}{ccc}
\text{} & = & \displaystyle\int [dk][dl]\, \frac{1}{\mathcal{P}_8^2 \mathcal{P}_{13} \mathcal{P}_{17}} \quad \equiv \quad (m^2)^{-2\varepsilon} \left\{ \sum_{i=-2}^{2} d_i^{(32)} \varepsilon^i + \mathcal{O}(\varepsilon^3) \right\}
\end{array}
\tag{A.28}
$$

with

$$
d_{-2}^{(32)} = -\frac{1}{2},
$$

$$d_{-1}^{(32)} = -\frac{3}{2} - \frac{\bar{u}}{u}\ln\bar{u},$$

$$d_{0}^{(32)} = -\frac{9}{2} - \frac{\pi^2}{3} + \frac{1-2u}{u}\mathrm{Li}_2(u) + \frac{\bar{u}}{u}\Big(2\ln^2\bar{u} - 3\ln\bar{u}\Big),$$

$$d_{1}^{(32)} = \zeta_3 - \frac{27}{2} - \pi^2 - \frac{4(2-u)}{u}\mathrm{S}_{1,2}(u) + \frac{1-2u}{u}\Big(\mathrm{Li}_3(u) + 3\mathrm{Li}_2(u)\Big)$$
$$- \frac{\bar{u}}{u}\left[6\ln\bar{u}\,\mathrm{Li}_2(u) + \frac{8}{3}\ln^3\bar{u} - 6\ln^2\bar{u} + \Big(9 + \frac{2\pi^2}{3}\Big)\ln\bar{u}\right],$$

$$d_{2}^{(32)} = 3\zeta_3 - \frac{81}{2} - 3\pi^2 - \frac{5\pi^4}{36} - 3\mathrm{Li}_2^2(u) - \frac{12(2-u)}{u}\mathrm{S}_{1,2}(u)$$
$$+ \frac{1-2u}{u}\left[\mathrm{Li}_4(u) - 8\mathrm{S}_{2,2}(u) + 16\mathrm{S}_{1,3}(u) + 3\mathrm{Li}_3(u) + \Big(9 + \frac{2\pi^2}{3}\Big)\mathrm{Li}_2(u)\right]$$
$$+ \frac{\bar{u}}{u}\left[24\ln\bar{u}\,\mathrm{S}_{1,2}(u) - 6\ln\bar{u}\,\mathrm{Li}_3(u) + 12\ln^2\bar{u}\,\mathrm{Li}_2(u) + \frac{8}{3}\ln^4\bar{u} - 18\ln\bar{u}\,\mathrm{Li}_2(u)\right.$$
$$\left. - 8\ln^3\bar{u} + \Big(18 + \frac{4\pi^2}{3}\Big)\ln^2\bar{u} - \Big(27 + 2\pi^2 - 2\zeta_3\Big)\ln\bar{u}\right]. \tag{A.29}$$

The massive sunrise integral can be found in [128]. Our result for the equal mass case is in agreement with these findings and reads



$$= \int[dk][dl]\,\frac{1}{\mathcal{P}_{13}\mathcal{P}_{14}\mathcal{P}_{15}}$$

$$= (m^2)^{1-2\varepsilon}\left\{\frac{3}{2\varepsilon^2} + \frac{17}{4\varepsilon} + \Big(\frac{59}{8} + \frac{\pi^2}{2}\Big) + \Big(\frac{65}{16} + \frac{11\pi^2}{4}\Big)\varepsilon \right. \tag{A.30}$$
$$\left. + \Big(-\frac{1117}{32} + \frac{89\pi^2}{8} - 8\ln2\,\pi^2 + \frac{\pi^4}{10} + 28\zeta_3\Big)\varepsilon^2 + \mathcal{O}(\varepsilon^3)\right\}$$
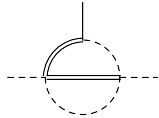
**4–topologies**



$$= \int[dk][dl]\,\frac{1}{\mathcal{P}_2\mathcal{P}_5\mathcal{P}_{13}\mathcal{P}_{17}} \equiv (m^2)^{-2\varepsilon}\left\{\sum_{i=-2}^{2}d_i^{(41)}\,\varepsilon^i + \mathcal{O}(\varepsilon^3)\right\} \tag{A.31}$$

with

$$d_{-2}^{(41)} = \frac{1}{2},$$

$$d_{-1}^{(41)} = \frac{5}{2} + \frac{\bar{u}}{u} \ln \bar{u},$$

$$d_{0}^{(41)} = \frac{19}{2} + \frac{\pi^2}{3} - \frac{\bar{u}}{u} \left[ \mathrm{Li}_2(u) + \frac{3}{2} \ln^2 \bar{u} - 5 \ln \bar{u} \right],$$

$$d_{1}^{(41)} = \frac{65}{2} + \frac{5\pi^2}{3} - \zeta_3 - \frac{\bar{u}}{u} \left[ \mathrm{Li}_3(u) - 3\mathrm{S}_{1,2}(u) - 3 \ln \bar{u}\, \mathrm{Li}_2(u) - \frac{3}{2} \ln^3 \bar{u} + 5\mathrm{Li}_2(u) \right.$$
$$\left. + \frac{15}{2} \ln^2 \bar{u} - \left( 19 + \frac{2\pi^2}{3} \right) \ln \bar{u} \right],$$

$$d_{2}^{(41)} = \frac{211}{2} + \frac{19\pi^2}{3} + \frac{5\pi^4}{36} - 5\zeta_3 - \frac{\bar{u}}{u} \left[ \mathrm{Li}_4(u) - 3\mathrm{S}_{2,2}(u) + 9\mathrm{S}_{1,3}(u) - 3 \ln \bar{u}\, \mathrm{Li}_3(u) \right.$$
$$+ 9 \ln \bar{u}\, \mathrm{S}_{1,2}(u) + \frac{9}{2} \ln^2 \bar{u}\, \mathrm{Li}_2(u) + \frac{9}{8} \ln^4 \bar{u} + 5\mathrm{Li}_3(u) - 15\mathrm{S}_{1,2}(u) - \frac{15}{2} \ln^3 \bar{u}$$
$$\left. - 15 \ln \bar{u}\, \mathrm{Li}_2(u) + \left( 19 + \frac{2\pi^2}{3} \right) \left( \mathrm{Li}_2(u) + \frac{3}{2} \ln^2 \bar{u} \right) - \left( 65 + \frac{10\pi^2}{3} - 2\zeta_3 \right) \ln \bar{u} \right]. \tag{A.32}$$

 $$= \int [dk][dl]\, \frac{1}{\mathcal{P}_5 \mathcal{P}_8 \mathcal{P}_9 \mathcal{P}_{13}} \equiv (m^2)^{-2\varepsilon} \left\{ \sum_{i=-2}^{2} d_i^{(42)} \varepsilon^i + \mathcal{O}(\varepsilon^3) \right\} \tag{A.33}$$

with

$$d_{-2}^{(42)} = \frac{1}{2},$$

$$d_{-1}^{(42)} = \frac{5}{2} + \frac{\bar{u}}{u} \ln \bar{u},$$

$$d_{0}^{(42)} = \frac{19}{2} + \frac{\pi^2}{2} - \frac{\bar{u}}{u} \left[ 2\mathrm{Li}_2(u) + 2 \ln^2 \bar{u} - 5 \ln \bar{u} \right],$$

$$d_{1}^{(42)} = \frac{65}{2} + \frac{5\pi^2}{2} + 4\zeta_3 - \frac{\bar{u}}{u} \left[ 4\mathrm{Li}_3(u) - 8\mathrm{S}_{1,2}(u) + 10\mathrm{Li}_2(u) - \frac{8}{3} \ln^3 \bar{u} \right.$$
$$\left. - 8 \ln \bar{u}\, \mathrm{Li}_2(u) + 10 \ln^2 \bar{u} - (19 + \pi^2) \ln \bar{u} \right],$$

$$d_{2}^{(42)} = \frac{211}{2} + \frac{19\pi^2}{2} + \frac{\pi^4}{2} + 20\zeta_3 - \frac{\bar{u}}{u} \left[ 8\mathrm{Li}_4(u) - 16\mathrm{S}_{2,2}(u) + 32\mathrm{S}_{1,3}(u) + \frac{8}{3} \ln^4 \bar{u} \right.$$
$$- 16 \ln \bar{u}\, \mathrm{Li}_3(u) + 32 \ln \bar{u}\, \mathrm{S}_{1,2}(u) + 16 \ln^2 \bar{u}\, \mathrm{Li}_2(u) + 20\mathrm{Li}_3(u) - 40 \ln \bar{u}\, \mathrm{Li}_2(u)$$
$$\left. - 40\mathrm{S}_{1,2}(u) - \frac{40}{3} \ln^3 \bar{u} + 2(19 + \pi^2)(\mathrm{Li}_2(u) + \ln^2 \bar{u}) - (65 + 5\pi^2 + 8\zeta_3) \ln \bar{u} \right]. \tag{A.34}$$

$$\text{(diagram)} \quad = \quad \int [dk][dl] \, \frac{1}{\mathcal{P}_5 \mathcal{P}_8 \mathcal{P}_{14} \mathcal{P}_{15}} \quad \equiv \quad (m^2)^{-2\varepsilon} \left\{ \sum_{i=-2}^{1} d_i^{(43)} \, \varepsilon^i + \mathcal{O}(\varepsilon^2) \right\}$$

(A.35)

with

$$d_{-2}^{(43)} = \frac{1}{2},$$

$$d_{-1}^{(43)} = \frac{5}{2},$$

$$d_0^{(43)} = \frac{1}{\bar{u}} \left[ \frac{19\bar{u}}{2} - 2\zeta_3 + 2\mathrm{Li}_3(u) + \bar{u} \, \mathrm{Li}_2(u) \right],$$

$$d_1^{(43)} = \frac{1}{\bar{u}} \left[ \frac{65\bar{u}}{2} - \frac{7\pi^4}{180} + 4\mathrm{S}_{2,2}(u) + 3\mathrm{Li}_2^2(u) + 4 \ln \bar{u} \, \mathrm{Li}_3(u) + (5 - 3u)(\mathrm{Li}_3(u) - \zeta_3) \right.$$

$$\left. - 2\bar{u} \ln \bar{u} \, \mathrm{Li}_2(u) + \left( 5\bar{u} - \frac{\pi^2}{3} \right) \mathrm{Li}_2(u) + \left( \frac{\pi^2}{3}\bar{u} - 4\zeta_3 \right) \ln \bar{u} \right].$$

(A.36)

$$\text{(diagram)} \quad = \quad \int [dk][dl] \, \frac{1}{\mathcal{P}_5 \mathcal{P}_8^2 \mathcal{P}_{14} \mathcal{P}_{15}} \quad \equiv \quad (m^2)^{-1-2\varepsilon} \left\{ \sum_{i=-2}^{2} d_i^{(44)} \, \varepsilon^i + \mathcal{O}(\varepsilon^3) \right\}$$

(A.37)

with

$$d_{-2}^{(44)} = -\frac{1}{2},$$

$$d_{-1}^{(44)} = \frac{1+u}{2u} + \frac{1+u^2}{2u^2} \ln \bar{u},$$

$$d_0^{(44)} = -2 - \frac{\pi^2}{6} + \frac{1 - 3u^2}{2u^2} \mathrm{Li}_2(u) - \frac{1+u^2}{u^2} \ln^2 \bar{u} + \frac{3(1 - 4u - u^2)}{2u^2} \ln \bar{u},$$

$$d_1^{(44)} = 2\zeta_3 + \frac{2(1+u)}{u} + \frac{(3+u)\pi^2}{6u} + \frac{1}{u^2} \left[ 2(3+u^2)\mathrm{S}_{1,2}(u) + 2(1 + 2u^2) \ln \bar{u} \, \mathrm{Li}_2(u) \right.$$

$$\left. - \frac{1 + 5u^2}{2} \mathrm{Li}_3(u) + \frac{4(1+u^2)}{3} \ln^3 \bar{u} + \frac{(1+u)(1+3u)}{2} \mathrm{Li}_2(u) \right.$$

$$\left. - (1 - 4u - u^2) \ln^2 \bar{u} + \left( 2(1+u^2) + (3+u^2)\frac{\pi^2}{6} \right) \ln \bar{u} \right],$$

$$d_2^{(44)} = -8 - \frac{2\pi^2}{3} + \frac{\pi^4}{180} + \frac{2(2-u)}{u} \zeta_3 + \frac{1}{u^2} \left[ \frac{1 - 3u^2}{2} \mathrm{Li}_4(u) - 2(3 - 5u^2)\mathrm{S}_{2,2}(u) \right.$$

$$\left. + 2(1 - 9u^2)\mathrm{S}_{1,3}(u) - 2(1 - 2u^2) \ln \bar{u} \, \mathrm{Li}_3(u) - 12(1+u^2) \ln \bar{u} \, \mathrm{S}_{1,2}(u) \right.$$
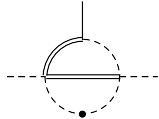
$$- 3u^2 \text{Li}_2(u)^2 - (5 + 7u^2) \ln^2 \bar{u} \, \text{Li}_2(u) - \frac{4(1 + u^2)}{3} \ln^4 \bar{u} - \frac{(1 + 5u)\bar{u}}{2} \text{Li}_3(u)$$

$$+ 2(3 - 6u - u^2) \text{S}_{1,2}(u) + 2(1 - 5u - 2u^2) \ln \bar{u} \, \text{Li}_2(u) + \frac{4(1 - 4u - u^2)}{3} \ln^3 \bar{u}$$

$$+ \left( 2(1 - 3u^2) + (3 - 5u^2)\frac{\pi^2}{6} \right) \text{Li}_2(u) - \left( 4(1 + u^2) + (5 + 3u^2)\frac{\pi^2}{6} \right) \ln^2 \bar{u}$$

$$+ \left( 2(1 - 4u - u^2) + (3 - 10u - u^2)\frac{\pi^2}{6} + 2(2 - u^2)\zeta_3 \right) \ln \bar{u} \bigg]. \tag{A.38}$$



$$\int [dk][dl] \, \frac{1}{\mathcal{P}_3 \mathcal{P}_6 \mathcal{P}_{14} \mathcal{P}_{15}} \equiv (m^2)^{-2\varepsilon} \left\{ \sum_{i=-2}^{1} d_i^{(45)} \varepsilon^i + \mathcal{O}(\varepsilon^2) \right\} \tag{A.39}$$

with

$$d_{-2}^{(45)} = \frac{1}{2},$$

$$d_{-1}^{(45)} = \frac{5}{2} + \frac{\bar{u}}{u} \ln \bar{u},$$

$$d_0^{(45)} = \frac{19}{2} + \frac{\pi^2}{6} + \frac{5\bar{u}}{u} \ln \bar{u} - \frac{1}{u} \left[ 2\text{S}_{1,2}(u) + \ln \bar{u} \, \text{Li}_2(u) + \text{Li}_2(u) + \bar{u} \ln^2 \bar{u} - \frac{\pi^2}{6} \ln \bar{u} \right],$$

$$d_1^{(45)} = \frac{65}{2} + \frac{5\pi^2}{6} - \frac{1}{u} \bigg[ 2\text{S}_{2,2}(u) + 3\text{S}_{1,3}(u) - \ln \bar{u} \, \text{Li}_3(u) - \frac{1}{2} \ln^2 \bar{u} \, \text{Li}_2(u) - \text{Li}_2(u)^2$$

$$+ (1 - 2u)\text{Li}_3(u) + 2(1 + 2u)\text{S}_{1,2}(u) + 2u \ln \bar{u} \, \text{Li}_2(u) - \frac{2\bar{u}}{3} \ln^3 \bar{u}$$

$$+ \left( 5 + \frac{\pi^2}{6} \right) \text{Li}_2(u) + \left( 5\bar{u} + \frac{\pi^2}{12} \right) \ln^2 \bar{u} - \left( 19\bar{u} + (2 - u)\frac{\pi^2}{3} - \zeta_3 \right) \ln \bar{u} \bigg]. \tag{A.40}$$



$$\int [dk][dl] \, \frac{1}{\mathcal{P}_3^2 \mathcal{P}_6 \mathcal{P}_{14} \mathcal{P}_{15}} \equiv (m^2)^{-1-2\varepsilon} \left\{ \sum_{i=-1}^{1} d_i^{(46)} \varepsilon^i + \mathcal{O}(\varepsilon^2) \right\} \tag{A.41}$$

with

$$d_{-1}^{(46)} = \frac{1}{u} \text{Li}_2(u),$$

$$d_0^{(46)} = \frac{1}{u} \left[ 4\text{S}_{1,2}(u) - \text{Li}_3(u) + \ln \bar{u} \, \text{Li}_2(u) - \frac{\pi^2}{6} \ln \bar{u} \right],$$

$$d_1^{(46)} = \frac{1}{u} \bigg[ 3\text{Li}_4(u) + 7\text{S}_{1,3}(u) - 4\text{S}_{2,2}(u) - \ln \bar{u} \, \text{Li}_3(u) - \frac{1}{2} \ln^2 \bar{u} \, \text{Li}_2(u) + \frac{\pi^2}{2} \text{Li}_2(u)$$

$$+ \frac{\pi^2}{12} \ln^2 \bar{u} + \zeta_3 \ln \bar{u} \bigg]. \tag{A.42}$$

The following MIs give rise to HPLs with parameter $-1$

$$\int [dk][dl]\, \frac{1}{\mathcal{P}_6 \mathcal{P}_{13}\mathcal{P}_{14}\mathcal{P}_{15}} \;\;\equiv\;\; (m^2)^{-2\varepsilon}\left\{\sum_{i=-2}^{1} d_i^{(47)}\,\varepsilon^i + \mathcal{O}(\varepsilon^2)\right\} \tag{A.43}$$

with

$$d_{-2}^{(47)} = \frac{1}{2},$$

$$d_{-1}^{(47)} = \frac{5}{2} + \frac{\bar{u}}{u}\ln\bar{u},$$

$$d_0^{(47)} = \frac{19}{2} + \frac{\pi^2}{6} + \frac{1}{\bar{u}}\Big[2\mathrm{Li}_3(u) - 2\zeta_3\Big] - \frac{1}{u}\Big[2\mathrm{Li}_2(u) + \bar{u}\ln^2\bar{u} - 5\bar{u}\ln\bar{u}\Big],$$

$$d_1^{(47)} = \frac{65}{2} + \frac{5\pi^2}{6} + \frac{1}{\bar{u}}\Big[6\mathrm{Li}_4(u) - 4\mathrm{S}_{2,2}(u) + 4\mathrm{Li}_2(u)^2 + 4\ln\bar{u}\,\mathrm{Li}_3(u) - 2(2+u)\zeta_3$$

$$- 8H(0,-1,0,1;u) - \frac{2\pi^2}{3}H(0,-1;u) + \frac{\pi^4}{60} - \frac{2(2+u)(1-2u)}{u}\mathrm{Li}_3(u)$$

$$- \Big(\frac{10\bar{u}}{u} + \frac{2\pi^2}{3}\Big)\mathrm{Li}_2(u) + \Big(\frac{19\bar{u}^2}{u} - \frac{2\bar{u}\pi^2}{3} - 4\zeta_3\Big)\ln\bar{u}\Big] + \frac{1}{u}\Big[4\ln\bar{u}\,\mathrm{Li}_2(u)$$

$$+ 4\mathrm{S}_{1,2}(u) + \bar{u}\Big(\frac{2}{3}\ln^3\bar{u} - 5\ln^2\bar{u}\Big) + (1+u)\Big(4H(-1,0,1;u) + \frac{\pi^2}{3}H(-1;u)\Big)\Big]. \tag{A.44}$$

$$\int [dk][dl]\, \frac{1}{\mathcal{P}_6^2 \mathcal{P}_{13}\mathcal{P}_{14}\mathcal{P}_{15}} \;\;\equiv\;\; (m^2)^{-1-2\varepsilon}\left\{\sum_{i=-2}^{1} d_i^{(48)}\,\varepsilon^i + \mathcal{O}(\varepsilon^2)\right\} \tag{A.45}$$
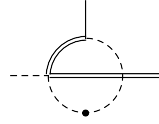
with

$$d_{-2}^{(48)} = \frac{1}{\bar{u}},$$

$$d_{-1}^{(48)} = -\frac{1+u}{u\bar{u}}\ln\bar{u},$$

$$d_0^{(48)} = \frac{1}{\bar{u}}\Big[4 + \frac{1+u}{u\bar{u}}\Big(2\mathrm{Li}_2(u) + \bar{u}\ln^2\bar{u} - 2\bar{u}\ln\bar{u} - \frac{u\pi^2}{3}\Big)\Big],$$

$$d_1^{(48)} = \frac{1}{\bar{u}^2}\bigg\{(3\ln 2 - 1)\frac{4\pi^2}{3} - 2(u+8)\zeta_3 + \frac{1+u}{u}\Big[4(1+u)\mathrm{Li}_3(u) - 4\ln\bar{u}\,\mathrm{Li}_2(u)$$

$$- 4\mathrm{S}_{1,2}(u) - \frac{2}{3}\bar{u}\ln^3\bar{u} + 4\mathrm{Li}_2(u) + 2\bar{u}\ln^2\bar{u} - \Big(4\bar{u} - \frac{2u\pi^2}{3}\Big)\ln\bar{u}$$

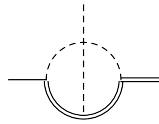$$- 4(1+u)H(-1,0,1;u) - \frac{(1+u)\pi^2}{3}H(-1;u)\Big]\bigg\}. \tag{A.46}$$

 $\displaystyle = \int [dk][dl]\, \frac{1}{\mathcal{P}_5 \mathcal{P}_{11} \mathcal{P}_{13} \mathcal{P}_{14}} \equiv (m^2)^{-2\varepsilon} \left\{ \sum_{i=-2}^{1} d_i^{(49)}\, \varepsilon^i + \mathcal{O}(\varepsilon^2) \right\}$

$$\text{(A.47)}$$

with

$$d_{-2}^{(49)} = \frac{1}{2},$$

$$d_{-1}^{(49)} = \frac{5}{2} + \frac{\bar{u}}{u} \ln \bar{u},$$

$$d_0^{(49)} = \frac{19}{2} + \frac{\pi^2}{3} + \frac{1}{\bar{u}} \Big[ 2\zeta_3 - \mathrm{Li}_3(u) - \mathrm{S}_{1,2}(u) + \mathrm{Li}_3(u-1) - \ln \bar{u}\, \mathrm{Li}_2(u-1)$$

$$- \frac{1}{2} \Big( \ln^2 \bar{u} + \pi^2 \Big) \ln(2-u) \Big] - \frac{1}{u} \Big[ (2-u)\mathrm{Li}_2(u) + \frac{3\bar{u}}{2} \ln^2 \bar{u} - 5\bar{u} \ln \bar{u} \Big],$$

$$d_1^{(49)} = \frac{65}{2} + \frac{5\pi^2}{3} - \frac{1}{\bar{u}} \Big[ 3\mathrm{Li}_4(u) - 4\mathrm{S}_{2,2}(u) + 12\mathrm{S}_{1,3}(u) + 2\ln \bar{u}\, \mathrm{Li}_3(u) + 2\ln \bar{u}\, \mathrm{S}_{1,2}(u)$$

$$+ 3\mathrm{Li}_2(u)^2 + \frac{\pi^2}{2}\mathrm{Li}_2(u) - 4\zeta_3 \ln \bar{u} - (3-u)\zeta_3 - \frac{161\pi^4}{720} + \frac{\pi^2}{3}\ln^2 2 - \frac{1}{3}\ln^4 2$$

$$- 7\zeta_3 \ln 2 - 8\mathrm{Li}_4(\tfrac{1}{2}) - 12\mathrm{Li}_4(u-1) - \Big( 4\ln^2 \bar{u} - u \ln \bar{u} + \frac{11\pi^2}{6} \Big) \mathrm{Li}_2(u-1)$$

$$+ 10\ln \bar{u}\, \mathrm{Li}_3(u-1) - \Big( \ln^3 \bar{u} - \frac{u}{2}\ln^2 \bar{u} + \frac{5\pi^2}{6}\ln \bar{u} - 7\zeta_3 - \frac{u\pi^2}{2} \Big) \ln(2-u)$$

$$- u\,\mathrm{Li}_3(u-1) - 2\mathcal{A}(u) + \frac{4 - 5u + 2u^2}{u}\mathrm{Li}_3(u) - \frac{6 - 12u + 5u^2}{u}\mathrm{S}_{1,2}(u)$$

$$- \frac{6 - 10u + 4u^2}{u} \ln \bar{u}\, \mathrm{Li}_2(u) \Big] + \frac{1}{u} \Big[ \frac{5\bar{u}}{3}\ln^3 \bar{u} - 5(2-u)\mathrm{Li}_2(u)$$

$$- \frac{15 - 16u}{2}\ln^2 \bar{u} + \Big( 19\bar{u} + (5-7u)\frac{\pi^2}{6} \Big) \ln \bar{u} \Big] - \frac{1}{2}\ln^2 \bar{u}, \qquad \text{(A.48)}$$

where we defined an auxiliary function $\mathcal{A}(u)$ which is given by the integral

$$\mathcal{A}(u) \equiv \int_0^u du' \frac{1}{2-u'}\, H(1,0,1;u'). \qquad \text{(A.49)}$$
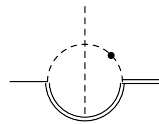
$$= \int [dk][dl]\, \frac{1}{\mathcal{P}_5^2 \mathcal{P}_{11}\mathcal{P}_{13}\mathcal{P}_{14}} \equiv (m^2)^{-1-2\varepsilon}\left\{\sum_{i=-2}^{2} d_i^{(410)}\,\varepsilon^i + \mathcal{O}(\varepsilon^3)\right\} \tag{A.50}$$
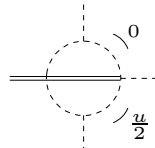
with

$$d_{-2}^{(410)} = \frac{1}{\bar{u}},$$

$$d_{-1}^{(410)} = \frac{1}{\bar{u}}\left[2 - \frac{1+u}{u}\ln\bar{u}\right],$$

$$d_0^{(410)} = \frac{1}{\bar{u}}\left[4 + \frac{2}{u}\mathrm{Li}_2(u) + \frac{3-u^2}{u(2-u)}\ln^2\bar{u} - \frac{2(1+u)}{u}\ln\bar{u} + \frac{(7-5u)\pi^2}{(2-u)6}\right],$$

$$d_1^{(410)} = \frac{1}{\bar{u}}\left\{8 + \frac{7\bar{u}\,\zeta_3}{2-u} + \frac{(7-5u)\pi^2}{(2-u)3} + \frac{2}{u}\left[(2-u)\mathrm{Li}_3(u) + 2\mathrm{Li}_2(u) - 2(1+u)\ln\bar{u}\right]\right.$$

$$\left. - \frac{2}{u(2-u)}\left[(6-3u-u^2)\mathrm{S}_{1,2}(u) + 2(3-2u)\ln\bar{u}\,\mathrm{Li}_2(u) + \frac{5-2u-u^2}{3}\ln^3\bar{u}\right.\right.$$

$$\left.\left. - (3-u^2)\ln^2\bar{u} + (5-u-2u^2)\frac{\pi^2}{6}\ln\bar{u}\right]\right\},$$

$$d_2^{(410)} = \frac{1}{\bar{u}}\left\{16 + \frac{14\bar{u}\,\zeta_3}{2-u} + \frac{2}{u}\left[(4-3u)\mathrm{Li}_4(u) - 2(3-2u)\mathrm{S}_{2,2}(u) + 2(2-u)\mathrm{Li}_3(u)\right.\right.$$

$$\left. + \left(4 + (5-3u)\frac{\pi^2}{6}\right)\mathrm{Li}_2(u) - 4(1+u)\ln\bar{u}\right] + \frac{2}{u(2-u)}\left[\frac{9-6u-u^2}{6}\ln^4\bar{u}\right.$$

$$+ (20-19u+3u^2)\mathrm{S}_{1,3}(u) - \frac{2+u-3u^2}{2}\mathrm{Li}_2(u)^2 + 2(5-4u)\ln^2\bar{u}\,\mathrm{Li}_2(u)$$

$$- 4(3-2u)\ln\bar{u}\,\mathrm{Li}_2(u) - (14-13u+u^2)\ln\bar{u}\,\mathrm{Li}_3(u) - 2(6-3u-u^2)\mathrm{S}_{1,2}(u)$$

$$+ (20-15u-u^2)\ln\bar{u}\,\mathrm{S}_{1,2}(u) - \frac{2(5-2u-u^2)}{3}\ln^3\bar{u} - (5-u-2u^2)\frac{\pi^2}{3}\ln\bar{u}$$

$$+ \left(2(3-u^2) + (5-3u-u^2)\frac{\pi^2}{3}\right)\ln^2\bar{u} + \frac{(17+47u-60u^2)\pi^4}{120} + \frac{u(7-5u)\pi^2}{3}$$

$$+ \bar{u}(2+u)\left(3\mathrm{Li}_4(u-1) - 2\ln\bar{u}\,\mathrm{Li}_3(u-1) + \frac{\ln^2\bar{u}+\pi^2}{2}\mathrm{Li}_2(u-1)\right)$$

$$\left.\left. - \bar{u}(3+u)\zeta_3\ln\bar{u}\right]\right\}. \tag{A.51}$$

$$\int [dk][dl] \, \frac{1}{\mathcal{P}_5 \mathcal{P}_{11}^2 \mathcal{P}_{13} \mathcal{P}_{14}} \equiv (m^2)^{-1-2\varepsilon} \left\{ \sum_{i=-1}^{1} d_i^{(411)} \varepsilon^i + \mathcal{O}(\varepsilon^2) \right\} \tag{A.52}$$

with

$$d_{-1}^{(411)} = \frac{1}{\bar{u}} \left[ \frac{\pi^2}{6} - \text{Li}_2(u) \right],$$

$$d_0^{(411)} = \frac{1}{\bar{u}} \left[ \zeta_3 - 2\text{Li}_3(u) + \text{S}_{1,2}(u) + 2\ln\bar{u}\,\text{Li}_2(u) - \frac{\pi^2}{3}\ln\bar{u} - \text{Li}_3(u-1) \right.$$

$$\left. + \ln\bar{u}\,\text{Li}_2(u-1) + \frac{1}{2}\ln^2\bar{u}\,\ln(2-u) + \frac{\pi^2}{2}\ln(2-u) \right],$$

$$d_1^{(411)} = \frac{1}{\bar{u}} \left[ \frac{35\pi^4}{144} + \frac{\pi^2}{3}\ln^2 2 - \frac{1}{3}\ln^4 2 - 7\zeta_3\ln 2 - 8\text{Li}_4(\tfrac{1}{2}) - 4\text{Li}_4(u) + 6\text{S}_{2,2}(u) \right.$$

$$+ 2\text{S}_{1,3}(u) - 2\ln^2\bar{u}\,\text{Li}_2(u) + 6\ln\bar{u}\,\text{Li}_3(u) - 2\mathcal{A}(u) - \frac{5\pi^2}{6}\text{Li}_2(u) + \frac{\pi^2}{3}\ln^2\bar{u}$$

$$- 6\zeta_3\ln\bar{u} - 6\text{Li}_4(u-1) + 6\ln\bar{u}\,\text{Li}_3(u-1) - 3\ln^2\bar{u}\,\text{Li}_2(u-1)$$

$$\left. - \frac{5\pi^2}{6}\text{Li}_2(u-1) + \left( \ln^3\bar{u} + \frac{5\pi^2}{6}\ln\bar{u} + 7\zeta_3 \right)\ln(2-u) \right]. \tag{A.53}$$

The auxiliary function $\mathcal{A}(u)$ can be found in (A.49).

**5–topologies**

$$\int [dk][dl] \, \frac{1}{\mathcal{P}_5 \mathcal{P}_8 \mathcal{P}_9 \mathcal{P}_{13} \mathcal{P}_{14}} \equiv (m^2)^{-1-2\varepsilon} \left\{ \sum_{i=0}^{0} d_i^{(51)} \varepsilon^i + \mathcal{O}(\varepsilon) \right\} \tag{A.54}$$

with

$$d_0^{(51)} = -\frac{1}{\bar{u}} \left[ \text{Li}_4(u) + 4\text{S}_{2,2}(u) - \frac{1}{2}\text{Li}_2^2(u) - \frac{\pi^2}{2}\text{Li}_2(u) + \frac{3\pi^4}{40} \right]. \tag{A.55}$$

$$\int [dk][dl] \, \frac{1}{\mathcal{P}_5 \mathcal{P}_8^2 \mathcal{P}_9 \mathcal{P}_{13} \mathcal{P}_{14}} \equiv (m^2)^{-2-2\varepsilon} \left\{ \sum_{i=-2}^{2} d_i^{(52)} \varepsilon^i + \mathcal{O}(\varepsilon^3) \right\} \tag{A.56}$$

with

$$d^{(52)}_{-2} = -\frac{1}{12\bar{u}^2},$$

$$d^{(52)}_{-1} = -\frac{1}{6\bar{u}^2}\Big[1 - 2\ln\bar{u}\Big],$$

$$d^{(52)}_0 = -\frac{1}{6\bar{u}^2}\Big[\frac{(8+3u)\pi^2}{6} - 7 - 6u + 6\mathrm{Li}_2(u) + 4\ln^2\bar{u} - 2(5-3u)\ln\bar{u}\Big],$$

$$d^{(52)}_1 = -\frac{1}{6\bar{u}^2}\Big[25 + 54u - \frac{16\pi^2}{3} + (11-3u)\zeta_3 + 6(1-2u)\mathrm{Li}_3(u) - 12(3+u)\mathrm{S}_{1,2}(u)$$

$$- 24\ln\bar{u}\,\mathrm{Li}_2(u) - \frac{16}{3}\ln^3\bar{u} - 6(2-u)\mathrm{Li}_2(u) + 8\ln^2\bar{u}$$

$$+ 2\Big(41 - 15u - \frac{(8+3u)\pi^2}{3}\Big)\ln\bar{u}\Big],$$

$$d^{(52)}_2 = -\frac{1}{6\bar{u}^2}\Big[\frac{2(35-12u)\pi^2}{3} - 67 - 330u + \frac{(179-93u)\pi^4}{90} - 38\zeta_3 + \frac{16}{3}\ln^4\bar{u}$$

$$+ 6(1-10u)\mathrm{Li}_4(u) - 12(1+5u)\mathrm{S}_{2,2}(u) + 24(7+3u)\mathrm{S}_{1,3}(u) - \frac{8(1+3u)}{3}\ln^3\bar{u}$$

$$- 24(1-2u)\ln\bar{u}\,\mathrm{Li}_3(u) + 48(3+u)\ln\bar{u}\,\mathrm{S}_{1,2}(u) - 6(1-2u)\mathrm{Li}_2^2(u)$$

$$+ 48\ln^2\bar{u}\,\mathrm{Li}_2(u) - 6(2-9u)\mathrm{Li}_3(u) + 24(2+3u)\mathrm{S}_{1,2}(u) + 12(3-u)\ln\bar{u}\,\mathrm{Li}_2(u)$$

$$+ 6\Big(4 - 9u - (1+3u)\frac{\pi^2}{3}\Big)\mathrm{Li}_2(u) - \frac{4}{3}\Big(69 + 9u - (8+3u)\pi^2\Big)\ln^2\bar{u}$$

$$- \frac{2}{3}\Big(645 - 171u - 4(5+3u)\pi^2 + 6(11-3u)\zeta_3\Big)\ln\bar{u}\Big]. \qquad (A.57)$$



$$= \int[dk][dl]\,\frac{1}{\mathcal{P}_2\mathcal{P}_5\mathcal{P}_7\mathcal{P}_8\mathcal{P}_{18}} \equiv (m^2)^{-1-2\varepsilon}\Big\{\sum_{i=-2}^{0} d^{(53)}_i\,\varepsilon^i + \mathcal{O}(\varepsilon)\Big\}$$

$$(A.58)$$

with

$$d^{(53)}_{-2} = \frac{1}{\bar{u}}\Big[\mathrm{Li}_2(u) - \frac{\pi^2}{6}\Big],$$

$$d^{(53)}_{-1} = \frac{1}{\bar{u}}\Big[2\mathrm{Li}_3(u) + 4\mathrm{S}_{1,2}(u) - 6\zeta_3\Big],$$

$$d^{(53)}_0 = \frac{1}{\bar{u}}\Big[2\mathrm{Li}_4(u) - 4\mathrm{S}_{2,2}(u) + 16\mathrm{S}_{1,3}(u) + 3\mathrm{Li}_2^2(u) + \frac{2\pi^2}{3}\mathrm{Li}_2(u) - \frac{23\pi^4}{60}\Big]. \quad (A.59)$$

**6–topologies**



$$
= \int [dk][dl]\, \frac{1}{\mathcal{P}_5 \mathcal{P}_8 \mathcal{P}_9 \mathcal{P}_{11} \mathcal{P}_{13} \mathcal{P}_{14}} \equiv (m^2)^{-2-2\varepsilon} \left\{ \sum_{i=-4}^{0} d_i^{(61)}\, \varepsilon^i + \mathcal{O}(\varepsilon) \right\}
\tag{A.60}
$$

with

$$
d_{-4}^{(61)} = \frac{1}{12\bar{u}^2},
$$

$$
d_{-3}^{(61)} = -\frac{1}{3\bar{u}^2} \ln \bar{u},
$$

$$
d_{-2}^{(61)} = \frac{1}{6\bar{u}^2} \left[ 4 \ln^2 \bar{u} - \frac{5\pi^2}{12} \right],
$$

$$
d_{-1}^{(61)} = \frac{1}{6\bar{u}^2} \left[ -\frac{89\zeta_3}{2} - \frac{16}{3} \ln^3 \bar{u} + \frac{5\pi^2}{3} \ln \bar{u} \right],
$$

$$
d_0^{(61)} = \frac{1}{6\bar{u}^2} \left[ -\frac{89\pi^4}{24} + 48 \ln \bar{u}\, \mathrm{Li}_3(u) + 24\mathrm{Li}_2^2(u) + \frac{16}{3} \ln^4 \bar{u} - \frac{10\pi^2}{3} \ln^2 \bar{u} + 130\zeta_3 \ln \bar{u} \right].
\tag{A.61}
$$

## A.3   Heavy-to-light form factors

The MIs in our calculation from Chapter 5 are shown in Figure 5.4. The corresponding propagators $\mathcal{P}_i$ can be found in (5.10) which involve two external momenta $w$ and $w'$ with $w^2 = w'^2 = 1$ and $\gamma \equiv w \cdot w' = \mathcal{O}(M/m)$. We extract the leading power of the MIs in $m/M$ and write $s \equiv M/(4\gamma m) = \mathcal{O}(1)$.

**1–topologies**

$$
\bigcirc = \int [dk]\, \frac{1}{\mathcal{P}_1}
$$

$$
= -(M^2)^{1-\varepsilon}\, \Gamma(1-\varepsilon)\Gamma(-1+\varepsilon) \tag{A.62}
$$

$$
\bigcirc = \int [dk]\, \frac{1}{\mathcal{P}_3}
$$

$$
= -(m^2)^{1-\varepsilon}\, \Gamma(1-\varepsilon)\Gamma(-1+\varepsilon) \tag{A.63}
$$

**2–topologies**

$$
\bigcirc = \int [dk]\, \frac{1}{\mathcal{P}_1 \mathcal{P}_3}
$$

$$
\simeq (M^2)^{-\varepsilon} \left\{ \frac{1}{\varepsilon} - \frac{1}{s-1}\ln s + 2 + \left[ 4 + \frac{\pi^2}{6} \right.\right. \tag{A.64}
$$

$$
\left.\left. + \frac{1}{s-1}\left( \mathrm{Li}_2(1-s) - \frac{1}{2}\ln^2 s - 2\ln s \right) \right] \varepsilon + \mathcal{O}(\varepsilon^2) \right\}
$$

$$
\bigcirc = \int [dk]\, \frac{1}{\mathcal{P}_3 \mathcal{P}_6}
$$

$$
\simeq (4\gamma m^2)^{-\varepsilon} \left\{ \frac{1}{\varepsilon} + 2 + 4\varepsilon + \mathcal{O}(\varepsilon^2) \right\} \tag{A.65}
$$

**3–topologies**

$$
\bigcirc = \int [dk]\, \frac{1}{\mathcal{P}_1 \mathcal{P}_3 \mathcal{P}_5} \tag{A.66}
$$

$$
\simeq -\frac{1}{8\gamma m M} \left\{ 2\ln^2(4\gamma) - 2\mathrm{Li}_2(1-s) - \ln^2 s + \frac{8\pi^2}{3} + \mathcal{O}(\varepsilon) \right\}
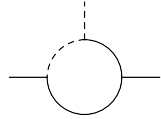$$

$$= \int [dk] \frac{1}{\mathcal{P}_1 \mathcal{P}_3 \mathcal{P}_6}$$

$$\simeq -\frac{1}{8\gamma mM} \left\{ \ln^2(4\gamma) - 2\text{Li}_2(1-s) - \ln^2 s + \pi^2 + \mathcal{O}(\varepsilon) \right\} \quad (\text{A.67})$$
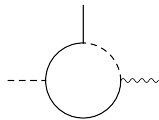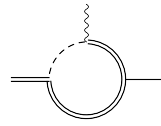
$$= \int [dk] \frac{1}{\mathcal{P}_1 \mathcal{P}_3 \mathcal{P}_7}$$

$$\simeq -\frac{1}{4\gamma mM} \left\{ 4\ln 2 \ln \gamma + 2\ln 2 \ln s + 2\text{Li}_2(1-2s) - 2\text{Li}_2(1-s) \right.$$

$$\left. + 7\ln^2 2 + \frac{\pi^2}{3} + \mathcal{O}(\varepsilon) \right\} \quad (\text{A.68})$$
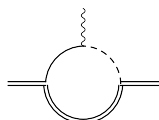
$$= \int [dk] \frac{1}{\mathcal{P}_1 \mathcal{P}_5 \mathcal{P}_7} \quad (\text{A.69})$$

$$\simeq -\frac{1}{4\gamma mM} \left\{ 2\ln^2(2\gamma) - 2\text{Li}_2(1-2s) - \ln^2(2s) + \frac{7\pi^2}{3} + \mathcal{O}(\varepsilon) \right\}$$

$$= \int [dk] \frac{1}{\mathcal{P}_3 \mathcal{P}_6 \mathcal{P}_7}$$

$$\simeq -\frac{1}{2\gamma m^2} \left\{ \ln 2 \ln \gamma + \frac{3}{2} \ln^2 2 + \frac{\pi^2}{6} + \mathcal{O}(\varepsilon) \right\} \quad (\text{A.70})$$
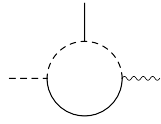
$$= \int [dk] \frac{1}{\mathcal{P}_3 \mathcal{P}_5 \mathcal{P}_6}$$

$$\simeq -\frac{1}{8\gamma m^2} \left\{ \ln^2(4\gamma) + \frac{5\pi^2}{3} + \mathcal{O}(\varepsilon) \right\} \quad (\text{A.71})$$
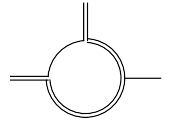
$$= \int [dk] \frac{1}{\mathcal{P}_2 \mathcal{P}_5 \mathcal{P}_6}$$

$$\simeq \frac{1}{2\gamma mM} \left\{ -2\ln(2\gamma) + \frac{1}{2s-1} \ln(2s) - 2 + \mathcal{O}(\varepsilon) \right\} \quad (\text{A.72})$$

$$\int [dk]\, \frac{1}{\mathcal{P}_4 \mathcal{P}_5 \mathcal{P}_7}$$

$$\simeq\; -\frac{1}{2\gamma m^2} \left\{ \ln 2 \ln \gamma + \frac{1}{2}\ln^2 2 + \frac{\pi^2}{6} + \mathcal{O}(\varepsilon) \right\} \tag{A.73}$$

$$\int [dk]\, \frac{1}{\mathcal{P}_8 \mathcal{P}_9 \mathcal{P}_{11}} \tag{A.74}$$

$$\simeq\; \frac{1}{4\gamma m M} \left\{ 2\mathrm{Li}_2(1 - 2s) - 2\mathrm{Li}_2(1 - s) + 2\ln 2 \ln s + \ln^2 2 + \mathcal{O}(\varepsilon) \right\}$$
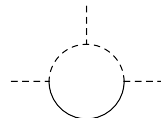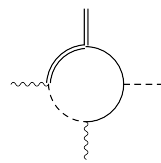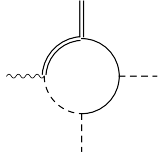
$$\int [dk]\, \frac{1}{\mathcal{P}_8 \mathcal{P}_9 \mathcal{P}_{12}}$$

$$\simeq\; -\frac{1}{4\gamma m M} \left\{ 2\mathrm{Li}_2(1 - 2s) + \ln^2(2s) + \frac{\pi^2}{3} + \mathcal{O}(\varepsilon) \right\} \tag{A.75}$$

$$\int [dk]\, \frac{1}{\mathcal{P}_5 \mathcal{P}_6 \mathcal{P}_7}$$

$$\simeq\; -\frac{1}{2\gamma m^2} \left\{ \frac{1}{2}\ln^2(2\gamma) + \frac{2\pi^2}{3} + \mathcal{O}(\varepsilon) \right\} \tag{A.76}$$

$$\int [dk]\, \frac{1}{\mathcal{P}_{11} \mathcal{P}_{12} \mathcal{P}_{15}}$$

$$=\; \frac{1}{2m^2} \left\{ 2\ln 2 - i\pi + \mathcal{O}(\varepsilon) \right\} \tag{A.77}$$
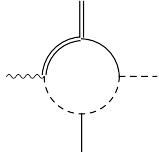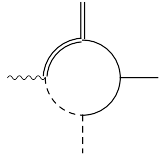
**4–topologies**

$$\int [dk]\, \frac{1}{\mathcal{P}_1 \mathcal{P}_3 \mathcal{P}_5 \mathcal{P}_6}$$

$$\simeq\; \frac{1}{4\gamma m^3 M}\, (m^2)^{-\varepsilon} \left\{ \frac{1}{2\varepsilon} - 1 + \mathcal{O}(\varepsilon) \right\} \tag{A.78}$$

$$= \int [dk] \, \frac{1}{\mathcal{P}_1 \mathcal{P}_3 \mathcal{P}_5 \mathcal{P}_7}$$

$$\simeq \frac{1}{4\gamma m^3 M} \, (m^2)^{-\varepsilon} \left\{ \frac{1}{\varepsilon} + 2\ln 2 - 2 + \mathcal{O}(\varepsilon) \right\} \tag{A.79}$$
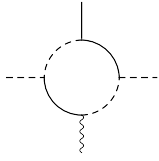


$$= \int [dk] \, \frac{1}{\mathcal{P}_1 \mathcal{P}_3 \mathcal{P}_6 \mathcal{P}_7}$$

$$\simeq \frac{1}{4\gamma^2 m^3 M} \left\{ \ln(4\gamma) + 1 + \mathcal{O}(\varepsilon) \right\} \tag{A.80}$$



$$= \int [dk] \, \frac{1}{\mathcal{P}_2 \mathcal{P}_4 \mathcal{P}_5 \mathcal{P}_7} \tag{A.81}$$
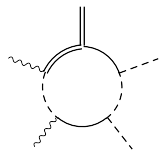
$$\simeq -\frac{1}{8\gamma^2 m^3 M} \, (m^2)^{-\varepsilon} \left\{ \frac{\ln(2\gamma)}{\varepsilon} - \frac{1}{2} \ln^2(4\gamma) + \ln^2 2 + \frac{\pi^2}{6} + \mathcal{O}(\varepsilon) \right\}$$



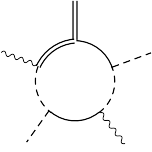$$= \int [dk] \, \frac{1}{\mathcal{P}_4 \mathcal{P}_5 \mathcal{P}_6 \mathcal{P}_7}$$

$$\simeq -\frac{1}{4\gamma^2 m^4} \, (m^2)^{-\varepsilon} \left\{ \frac{\ln(2\gamma)}{\varepsilon} - \ln^2 \gamma + \ln^2 2 - \frac{\pi^2}{6} + \mathcal{O}(\varepsilon) \right\} \tag{A.82}$$

**5–topologies**



$$= \int [dk] \, \frac{1}{\mathcal{P}_1 \mathcal{P}_3 \mathcal{P}_5 \mathcal{P}_6 \mathcal{P}_7}$$

$$\simeq -\frac{1}{8\gamma^2 m^5 M} \, (m^2)^{-\varepsilon} \left\{ \frac{3}{2\varepsilon} + \ln(16\gamma) - 2 + \mathcal{O}(\varepsilon) \right\} \tag{A.83}$$

$$= \int [dk] \, \frac{1}{\mathcal{P}_2 \mathcal{P}_4 \mathcal{P}_5 \mathcal{P}_6 \mathcal{P}_7} \tag{A.84}$$

$$\simeq \frac{1}{16\gamma^3 m^5 M} \, (m^2)^{-\varepsilon} \left\{ \frac{3\ln(2\gamma)}{\varepsilon} - \frac{5}{2} \ln^2 \gamma + 2(1 - \ln 2) \ln \gamma \right.$$

$$\left. + \ln^2 2 + 4\ln 2 + 2 - \frac{\pi^2}{6} + \mathcal{O}(\varepsilon) \right\}$$

# Appendix B

# Form factors in NLO

We summarize our NLO results for the transition form factors $F_+(q^2)$, $F_-(q^2)$ and $F_T(q^2)$ which can be defined in analogy to (1.27) for the $B_c \to \eta_c$ transition. All results are expressed in terms of pole masses $M \equiv m_b$ and $m \equiv m_c$ and correspond to the leading power in the HQE in $m/M$. The relation between the momentum tramsfer $q^2$ and the relativistic boost $\gamma = \mathcal{O}(M/m)$ can be found in (5.5). We further introduce $s \equiv M/(4\gamma m) = \mathcal{O}(1)$ and refer to (5.7) for the LO expressions.

$$
\begin{aligned}
\frac{F_+^{\text{NLO}}}{F_+^{\text{LO}}} = 1 + \frac{\alpha_s}{4\pi} \Bigg\{ & \left( \frac{11}{3} N_c - \frac{2}{3} n_f \right) \ln \frac{\mu^2}{2\gamma m^2} - \frac{10}{9} n_f + \mathcal{S}_+ \\
& + C_F \Bigg[ \frac{3s-2}{2(1+2s)} \ln^2 \gamma + \frac{3(9s+4-4\ln 2)}{2(1+2s)} \ln \gamma + 2\text{Li}_2(1-s) + \ln^2 s \\
& \quad + \frac{s(24s^2 - 20s + 5)}{(1+2s)(1-2s)^2} \ln(2s) - \frac{3s+7}{1+2s} \ln^2 2 + \frac{21s+10}{1+2s} \ln 2 \\
& \quad + \frac{(17s-8)\pi^2}{6(1+2s)} + \frac{170s^2 - 171s + 52}{18(1-2s)(1+2s)} \Bigg] \\
& + \left( C_F - \frac{N_c}{2} \right) \Bigg[ \frac{s}{1+2s} \ln^2 \gamma - \frac{2(s+(s-2)\ln 2)}{1+2s} \ln \gamma - \frac{2s^2}{1+2s} \ln^2 \left( \frac{s}{2} \right) \\
& \quad - \frac{2(4s^2+s-2)}{1+2s} \text{Li}_2(1-2s) + \frac{2(2s^2+s-2)}{1+2s} \text{Li}_2(1-s) \\
& \quad + \frac{2(s+(2+3s)(1-2s)^2 \ln 2)}{(1-2s)(1+2s)} \ln(2s) + \frac{2(5s^2-2s+2)}{1+2s} \ln^2 2 \\
& \quad + \frac{2(5s-2)}{1+2s} \ln 2 - \frac{(2s^2-s-2)\pi^2}{3(1+2s)} - \frac{2(85+134s)}{9(1+2s)} \Bigg] \Bigg\}, \quad \text{(B.1)}
\end{aligned}
$$

where $\mathcal{S}_+$ refers to the contribution from the flavour singlet diagrams which reads

$$
\mathcal{S}_+ = \frac{s}{1+2s} \ln \gamma - \frac{2(s-1)}{1+2s} \ln 2 + \frac{(s-1)\pi^2}{3(1+2s)}. \quad \text{(B.2)}
$$

$$\frac{F_-^{\mathrm{NLO}}}{F_-^{\mathrm{LO}}} = 1 + \frac{\alpha_s}{4\pi}\Bigg\{ \left(\frac{11}{3}N_c - \frac{2}{3}n_f\right)\ln\frac{\mu^2}{2\gamma m^2} - \frac{10}{9}n_f + \mathcal{S}_-$$

$$+ C_F\Bigg[\frac{3}{4}\ln^2\gamma + \frac{27}{4}\ln\gamma + 2\mathrm{Li}_2(1-s) + \ln^2 s - \frac{3}{2}\ln^2 2$$

$$+ \frac{24s^4 - 80s^3 + 125s^2 - 77s + 15}{2(1-s)^2(1-2s)^2}\ln s + \frac{3(18s^2 - 20s + 5)}{(1-2s)^2}\ln 2$$

$$+ \frac{17\pi^2}{12} - \frac{170s^2 - 57s + 13}{36(1-s)(1-2s)}\Bigg]$$

$$+ \left(C_F - \frac{N_c}{2}\right)\Bigg[\frac{1}{2}\ln^2\gamma - (1 + \ln 2)\ln\gamma - (1 + 4s)\mathrm{Li}_2(1-2s)$$

$$+ (1 + 2s)\mathrm{Li}_2(1-s) - s\ln^2(4s) - (3 - 2s)\ln^2 2$$

$$- \frac{s + 1 + (1-s)(1-2s)\ln 2}{(1-s)(1-2s)}\ln s - \frac{2(5s-1)}{1-2s}\ln 2$$

$$+ (1 - 2s)\frac{\pi^2}{6} - \frac{134}{9}\Bigg]\Bigg\} \tag{B.3}$$

with the flavour singlet contribution given by

$$\mathcal{S}_- = \frac{1}{2}\ln\gamma - \ln 2 + \frac{\pi^2}{6}. \tag{B.4}$$

$$\frac{F_T^{\mathrm{NLO}}}{F_T^{\mathrm{LO}}} = 1 + \frac{\alpha_s}{4\pi}\Bigg\{ \left(\frac{11}{3}N_c - \frac{2}{3}n_f\right)\ln\frac{\mu^2}{2\gamma m^2} - \frac{10}{9}n_f + \mathcal{S}_T$$

$$+ C_F\Bigg[-\ln\frac{\mu^2}{M^2} + \frac{3}{4}\ln^2\gamma + \frac{27}{4}\ln\gamma + 2\mathrm{Li}_2(1-s) + \ln^2 s - \frac{3}{2}\ln^2 2 + \frac{17\pi^2}{12}$$

$$- \frac{24s^3 - 28s^2 + 13s - 2}{2(1-s)(1-2s)^2}\ln s + \frac{54s^2 - 58s + 15}{(1-2s)^2}\ln 2 + \frac{170s - 103}{36(1-2s)}\Bigg]$$

$$+ \left(C_F - \frac{N_c}{2}\right)\Bigg[\frac{1}{2}\ln^2\gamma - (1 + \ln 2)\ln\gamma - (1 - 4s)\mathrm{Li}_2(1-2s)$$

$$+ (1 - 2s)\mathrm{Li}_2(1-s) + s\ln^2(4s) - (3 + 2s)\ln^2 2 - \frac{2s}{1-2s}\ln 2$$

$$+ \frac{s - 1 - (1-s)(1-2s)\ln 2}{(1-s)(1-2s)}\ln s + (1 + 2s)\frac{\pi^2}{6} - \frac{134}{9}\Bigg]\Bigg\} \tag{B.5}$$

and the flavour singlet contribution is found to be the same as in (B.4), i.e $\mathcal{S}_T = \mathcal{S}_-$. Notice that the tensor form factor $F_T(q^2)$ has a residual scale dependence of $\mathcal{O}(\alpha_s^2)$ in NLO due to the fact that the tensor current is not conserved.

# Bibliography

[1] S. L. Glashow, "Partial Symmetries Of Weak Interactions," Nucl. Phys. **22** (1961) 579.

[2] S. Weinberg, "A Model Of Leptons," Phys. Rev. Lett. **19** (1967) 1264.

[3] A. Salam, "Weak And Electromagnetic Interactions," Originally printed in *Svartholm: Elementary Particle Theory, Proceedings Of The Nobel Symposium Held 1968 At Lerum, Sweden*, Stockholm 1968, 367-377.

[4] M. Gell-Mann, "A Schematic Model Of Baryons And Mesons," Phys. Lett. **8** (1964) 214.

[5] M. Y. Han and Y. Nambu, "Three-triplet model with double SU(3) symmetry," Phys. Rev. **139** (1965) B1006.

[6] D. J. Gross and F. Wilczek, "Ultraviolet Behavior of Non-abelian Gauge Theories," Phys. Rev. Lett. **30** (1973) 1343.

[7] H. D. Politzer, "Reliable Perturbative Results for Strong Interactions?," Phys. Rev. Lett. **30** (1973) 1346.

[8] S. Weinberg, "Nonabelian Gauge Theories Of The Strong Interactions," Phys. Rev. Lett. **31** (1973) 494.

[9] H. Fritzsch, M. Gell-Mann and H. Leutwyler, "Advantages Of The Color Octet Gluon Picture," Phys. Lett. B **47** (1973) 365.

[10] W. M. Yao *et al.* [Particle Data Group], "Review of particle physics," J. Phys. G **33** (2006) 1, (URL:http://pdg.lbl.gov).

[11] G. Gabrielse, D. Hanneke, T. Kinoshita, M. Nio and B. Odom, "New Determination of the Fine Structure Constant from the Electron $g$ Value and QED," Phys. Rev. Lett. **97** (2006) 030802.

[12] N. Cabibbo, "Unitary symmetry and leptonic decays," Phys. Rev. Lett. **10** (1963) 531.

[13] M. Kobayashi and T. Maskawa, "CP Violation In The Renormalizable Theory Of Weak Interaction," Prog. Theor. Phys. **49** (1973) 652.

[14] J. Charles *et al.* [CKMfitter Group], "CP violation and the CKM matrix: Assessing the impact of the asymmetric $B$ factories," Eur. Phys. J. C **41** (2005) 1, (URL:http://ckmfitter.in2p3.fr).

[15] B. Aubert *et al.* [BABAR Collaboration], "Observation of CP violation in the $B^0$ meson system," Phys. Rev. Lett. **87** (2001) 091801.

[16] K. Abe *et al.* [Belle Collaboration], "Observation of large CP violation in the neutral $B$ meson system," Phys. Rev. Lett. **87** (2001) 091802.

[17] J. H. Christenson, J. W. Cronin, V. L. Fitch and R. Turlay, "Evidence For The $2\pi$ Decay Of The $K_2^0$ Meson," Phys. Rev. Lett. **13** (1964) 138.

[18] S. Kluth, "Tests of quantum chromo dynamics at $e_+e_-$ colliders," Rept. Prog. Phys. **69** (2006) 1771.

[19] M. Beneke, G. Buchalla, M. Neubert and C. T. Sachrajda, "QCD factorization for $B \to \pi\pi$ decays: Strong phases and CP violation in the heavy quark limit," Phys. Rev. Lett. **83** (1999) 1914.

[20] M. Beneke, G. Buchalla, M. Neubert and C. T. Sachrajda, "QCD factorization for exclusive, non-leptonic $B$ meson decays: General arguments and the case of heavy-light final states," Nucl. Phys. B **591** (2000) 313.

[21] M. Beneke, G. Buchalla, M. Neubert and C. T. Sachrajda, "QCD factorization in $B \to \pi K, \pi\pi$ decays and extraction of Wolfenstein parameters," Nucl. Phys. B **606** (2001) 245.

[22] C. W. Bauer, S. Fleming, D. Pirjol and I. W. Stewart, "An effective field theory for collinear and soft gluons: Heavy to light decays," Phys. Rev. D **63** (2001) 114020.

[23] C. W. Bauer, D. Pirjol and I. W. Stewart, "Soft-collinear factorization in effective field theory," Phys. Rev. D **65** (2002) 054022.

[24] M. Beneke, A. P. Chapovsky, M. Diehl and T. Feldmann, "Soft-collinear effective theory and heavy-to-light currents beyond leading power," Nucl. Phys. B **643** (2002) 431.

[25] M. Beneke and S. Jager, "Spectator scattering at NLO in non-leptonic $B$ decays: Tree amplitudes," Nucl. Phys. B **751** (2006) 160.

[26] N. Kivel, "Radiative corrections to hard spectator scattering in $B \to \pi\pi$ decays," arXiv:hep-ph/0608291.

[27] V. Pilipp, in preparation.

[28] A. V. Kotikov, "Differential equations method: New technique for massive Feynman diagrams calculation," Phys. Lett. B **254** (1991) 158.

[29] E. Remiddi, "Differential equations for Feynman graph amplitudes," Nuovo Cim. A **110** (1997) 1435.

[30] E. Remiddi and J. A. M. Vermaseren, "Harmonic polylogarithms," Int. J. Mod. Phys. A **15** (2000) 725.

[31] M. Beneke and V. A. Smirnov, "Asymptotic expansion of Feynman integrals near threshold," Nucl. Phys. B **522** (1998) 321.

[32] V. A. Smirnov, "Analytical result for dimensionally regularized massless on-shell double box," Phys. Lett. B **460** (1999) 397.

[33] J. B. Tausk, "Non-planar massless two-loop Feynman diagrams with four on-shell legs," Phys. Lett. B **469** (1999) 225.

[34] T. Binoth and G. Heinrich, "An automatized algorithm to compute infrared divergent multi-loop integrals," Nucl. Phys. B **585** (2000) 741.

[35] M. Neubert, "Heavy quark symmetry," Phys. Rept. **245** (1994) 259.

[36] A. V. Efremov and A. V. Radyushkin, "Factorization And Asymptotical Behavior Of Pion Form-Factor In QCD," Phys. Lett. B **94** (1980) 245.

[37] G. P. Lepage and S. J. Brodsky, "Exclusive Processes In Perturbative Quantum Chromodynamics," Phys. Rev. D **22** (1980) 2157.

[38] J. D. Bjorken, "Topics In $B$ Physics," Nucl. Phys. Proc. Suppl. **11** (1989) 325.

[39] M. J. Dugan and B. Grinstein, "QCD basis for factorization in decays of heavy mesons," Phys. Lett. B **255** (1991) 583.

[40] J. Chay and C. Kim, "Collinear effective theory at subleading order and its application to heavy-light currents," Phys. Rev. D **65** (2002) 114016.

[41] R. J. Hill and M. Neubert, "Spectator interactions in soft-collinear effective theory. ((U))," Nucl. Phys. B **657** (2003) 229.

[42] E. Eichten and B. Hill, "An effective field theory for the calculation of matrix elements involving heavy quarks," Phys. Lett. B **234** (1990) 511.

[43] H. Georgi, "An effective field theory for haevy quarks at low-energies," Phys. Lett. B **240** (1990) 447.

[44] L. L. Foldy and S. A. Wouthuysen, "On the Dirac theory of spin 1/2 particle and its nonrelativistic limit," Phys. Rev. **78** (1950) 29.

[45] N. Isgur and M. B. Wise, "Weak Decays Of Heavy Mesons In The Static Quark Approximation," Phys. Lett. B **232** (1989) 113.

[46] N. Isgur and M. B. Wise, "Weak transisiton form-factors between heavy mesons," Phys. Lett. B **237** (1990) 527.

[47] C. W. Bauer, D. Pirjol, I. Z. Rothstein and I. W. Stewart, "$B \to M_1 M_2$: Factorization, charming penguins, strong phases, and polarization," Phys. Rev. D **70** (2004) 054015.

[48] M. Beneke, G. Buchalla, M. Neubert and C. T. Sachrajda, "Comment on $B \to M_1 M_2$: Factorization, charming penguins, strong phases, and polarization'," Phys. Rev. D **72** (2005) 098501.

[49] C. W. Bauer, D. Pirjol, I. Z. Rothstein and I. W. Stewart, "On differences between SCET and QCDF for $B \to \pi\pi$ decays," Phys. Rev. D **72** (2005) 098502.

[50] M. Wingate, "$B$ physics on the lattice: Present and future," Mod. Phys. Lett. A **21** (2006) 1167.

[51] C. Davies, "Precision lattice QCD calculations and predictions of fundamental physics in heavy quark systems," J. Phys. Conf. Ser. **46** (2006) 107.

[52] A. Dougall, K. M. Foley, C. T. H. Davies and G. P. Lepage, "$B$ meson decays at high velocity from mNRQCD," PoS **LAT2005** (2006) 219.

[53] P. Ball and R. Zwicky, "New results on $B \to \pi, K, \eta$ decay formfactors from light-cone sum rules," Phys. Rev. D **71** (2005) 014015.

[54] P. Ball and R. Zwicky, "$|V_{ub}|$ and constraints on the leading-twist pion distribution amplitude from $B \to \pi\ell\nu$," Phys. Lett. B **625** (2005) 225.

[55] A. Khodjamirian, "$B \to \pi\pi$ decay in QCD," Nucl. Phys. B **605** (2001) 558.

[56] A. Khodjamirian, T. Mannel and P. Urban, "Gluonic penguins in $B \to \pi\pi$ from QCD light-cone sum rules," Phys. Rev. D **67** (2003) 054027.

[57] A. Khodjamirian, T. Mannel and B. Melic, "QCD light-cone sum rule estimate of charming penguin contributions in $B \to \pi\pi$," Phys. Lett. B **571** (2003) 75 [Phys. Lett. B **572** (2003) 171].

[58] A. Khodjamirian, T. Mannel, M. Melcher and B. Melic, "Annihilation effects in $B \to \pi\pi$ from QCD light-cone sum rules," Phys. Rev. D **72** (2005) 094012.

[59] F. De Fazio, T. Feldmann and T. Hurth, "Light-cone sum rules in soft-collinear effective theory," Nucl. Phys. B **733** (2006) 1.

[60] Y. Y. Keum, H. n. Li and A. I. Sanda, "Fat penguins and imaginary penguins in perturbative QCD," Phys. Lett. B **504** (2001) 6.

[61] Y. Y. Keum, H. N. Li and A. I. Sanda, "Penguin enhancement and $B \to K\pi$ decays in perturbative QCD," Phys. Rev. D **63** (2001) 054008.

[62] S. Descotes-Genon and C. T. Sachrajda, "Sudakov effects in $B \to \pi\ell\nu_\ell$ form factors," Nucl. Phys. B **625** (2002) 239.

[63] H. n. Li, S. Mishima and A. I. Sanda, "Resolution to the $B \to \pi K$ puzzle," Phys. Rev. D **72** (2005) 114005.

[64] H. n. Li and S. Mishima, "Implication of the $B \to \rho\rho$ data on the $B \to \pi\pi$ puzzle," Phys. Rev. D **73** (2006) 114014.

[65] A. Hocker and Z. Ligeti, "CP violation and the CKM matrix," arXiv:hep-ph/0605217.

[66] M. Beneke and M. Neubert, "QCD factorization for $B \to PP$ and $B \to PV$ decays," Nucl. Phys. B **675** (2003) 333.

[67] M. Bauer and B. Stech, "Exclusive $D$ Decays," Phys. Lett. B **152** (1985) 380.

[68] M. Bauer, B. Stech and M. Wirbel, "Exclusive nonleptonic decays of $D$, $D_s$, and $B$ mesons," Z. Phys. C **34** (1987) 103.

[69] C. W. Bauer, D. Pirjol and I. W. Stewart, "A proof of factorization for $B \to D\pi$," Phys. Rev. Lett. **87** (2001) 201806.

[70] J. Chay and C. Kim, "Nonleptonic $B$ decays into two light mesons in soft-collinear effective theory," Nucl. Phys. B **680** (2004) 302.

[71] M. Neubert and B. D. Pecjak, "Higher-order corrections to QCD factorization in $B \to \pi K, \pi\pi$ decays," JHEP **0202** (2002) 028.

[72] C. N. Burrell and A. R. Williamson, "Phenomenology of $B \to \pi\pi, \pi K$ decays at $O(\alpha_s^2 \beta_0)$ in QCD factorization," Phys. Rev. D **73** (2006) 114004.

[73] X. q. Li and Y. d. Yang, "Revisiting $B \to \pi\pi, \pi K$ decays in QCD factorization approach," Phys. Rev. D **72** (2005) 074007.

[74] T. Becher and R. J. Hill, "Loop corrections to heavy-to-light form factors and evanescent operators in SCET," JHEP **0410** (2004) 055.

[75] G. G. Kirilin, "Loop corrections to the form factors in $B \to \pi\ell\nu$ decay," arXiv:hep-ph/0508235.

[76] M. Beneke and D. Yang, "Heavy-to-light $B$ meson form factors at large recoil energy: Spectator scattering corrections," Nucl. Phys. B **736** (2006) 34.

[77] T. Feldmann and T. Hurth, "Non-factorizable contributions to $B \to \pi\pi$ decays," JHEP **0411** (2004) 037.

[78] C. M. Arnesen, Z. Ligeti, I. Z. Rothstein and I. W. Stewart, "Power corrections in charmless nonleptonic $B$ decays: Annihilation is factorizable and real,", arXiv:hep-ph/0607001.

[79] A. V. Manohar and I. W. Stewart, "The zero-bin and mode factorization in quantum field theory,", arXiv:hep-ph/0605001.

[80] J. Charles, A. Le Yaouanc, L. Oliver, O. Pene and J. C. Raynal, "Heavy-to-light form factors in the heavy mass to large energy limit of QCD," Phys. Rev. D **60** (1999) 014001.

[81] M. Beneke and T. Feldmann, "Symmetry-breaking corrections to heavy-to-light $B$ meson form factors at large recoil," Nucl. Phys. B **592** (2001) 3.

[82] C. W. Bauer, D. Pirjol and I. W. Stewart, "Factorization and endpoint singularities in heavy-to-light decays," Phys. Rev. D **67** (2003) 071502.

[83] M. Beneke and T. Feldmann, "Factorization of heavy-to-light form factors in soft-collinear effective theory," Nucl. Phys. B **685** (2004) 249.

[84] B. O. Lange and M. Neubert, "Factorization and the soft overlap contribution to heavy-to-light form factors,". Nucl. Phys. B **690** (2004) 249 [Erratum-ibid. B **723** (2005) 201].

[85] T. Becher, R. J. Hill and M. Neubert, "Soft-collinear messengers: A new mode in soft-collinear effective theory," Phys. Rev. D **69** (2004) 054017.

[86] M. Jamin and M. E. Lautenbacher, "Tracer: Version 1.1: A Mathematica Package For Gamma Algebra In Arbitrary Dimensions," Comput. Phys. Commun. **74** (1993) 265.

[87] P. Breitenlohner and D. Maison, "Dimensional Renormalization And The Action Principle," Commun. Math. Phys. **52** (1977) 11.

[88] P. Breitenlohner and D. Maison, "Dimensionally Renormalized Green's Functions For Theories With Massless Particles. 1," Commun. Math. Phys. **52** (1977) 39.

[89] P. Breitenlohner and D. Maison, "Dimensionally Renormalized Green's Functions For Theories With Massless Particles. 2," Commun. Math. Phys. **52** (1977) 55.

[90] A. J. Buras and P. H. Weisz, "QCD nonleading corrections to weak decays in dimensional regularization and 't Hooft-Veltman schemes," Nucl. Phys. B **333** (1990) 66.

[91] G. Passarino and M. J. G. Veltman, "One Loop Corrections For $e_+e_-$ Annihilation Into $\mu_+\mu_-$ In The Weinberg Model," Nucl. Phys. B **160** (1979) 151.

[92] F. V. Tkachov, "A Theorem On Analytical Calculability Of Four Loop Renormalization Group Functions," Phys. Lett. B **100** (1981) 65.

[93] K. G. Chetyrkin and F. V. Tkachov, "Integration By Parts: The Algorithm To Calculate Beta Functions In 4 Loops," Nucl. Phys. B **192** (1981) 159.

[94] T. Gehrmann and E. Remiddi, "Differential equations for two-loop four-point functions," Nucl. Phys. B **580** (2000) 485.

[95] S. Laporta, "High-precision calculation of multi-loop Feynman integrals by difference equations," Int. J. Mod. Phys. A **15** (2000) 5087.

[96] T. Huber and D. Maitre, "HypExp, a Mathematica package for expanding hypergeometric functions around integer-valued parameters," Comput. Phys. Commun. **175** (2006) 122.

[97] T. Gehrmann and E. Remiddi, "Two-loop master integrals for $\gamma^* \to$ 3jets: The planar topologies," Nucl. Phys. B **601** (2001) 248.

[98] U. Aglietti and R. Bonciani, "Master integrals with 2 and 3 massive propagators for the 2-loop electroweak form factor: Planar case," Nucl. Phys. B **698** (2004) 277.

[99] T. G. Birthwright, E. W. N. Glover and P. Marquard, "Master integrals for massless two-loop vertex diagrams with three offshell legs," JHEP **0409** (2004) 042.

[100] G. Bell, "NNLO vertex corrections in charmless hadronic $B$ decays: Imaginary part," in preparation.

[101] M. J. Dugan and B. Grinstein, "On the vanishing of evanescent operators," Phys. Lett. B **256** (1991) 239.

[102] S. Herrlich and U. Nierste, "Evanescent operators, scheme dependences and double insertions," Nucl. Phys. B **455** (1995) 39.

[103] K. G. Chetyrkin, M. Misiak and M. Munz, "$|\Delta F| = 1$ nonleptonic effective Hamiltonian in a simpler scheme," Nucl. Phys. B **520** (1998) 279.

[104] P. Gambino, M. Gorbahn and U. Haisch, "Anomalous dimension matrix for radiative and rare semileptonic B decays up to three loops," Nucl. Phys. B **673** (2003) 238.

[105] G. Buchalla, A. J. Buras and M. E. Lautenbacher, "Weak Decays Beyond Leading Logarithms," Rev. Mod. Phys. **68** (1996) 1125.

[106] G. Bell, "NNLO vertex corrections in charmless hadronic $B$ decays: Real part," in preparation.

[107] M. Gorbahn and U. Haisch, "Effective Hamiltonian for non-leptonic $|\Delta F| = 1$ decays at NNLO in QCD," Nucl. Phys. B **713** (2005) 291.

[108] G. Bell and T. Feldmann, Nucl. Phys. Proc. Suppl. **164** (2007) 189 [arXiv:hep-ph/0509347].

[109] M. Albrecht, G. Bell and G. Buchalla, in preparation.

[110] G. Bell, "A calculable model for heavy meson form factors" (in german), diploma thesis, RWTH Aachen 2003.

[111] M. Beneke, Y. Kiyo and D. s. Yang, "Loop corrections to sub-leading heavy quark currents in SCET," Nucl. Phys. B **692** (2004) 232.

[112] G. Bell and T. Feldmann, in preparation.

[113] V. M. Braun and I. E. Filyanov, "Conformal Invariance And Pion Wave Functions Of Nonleading Twist," Z. Phys. C **48** (1990) 239 [Sov. J. Nucl. Phys. **52** (1990 YAFIA,52,199-213.1990) 126].

[114] E. Braaten and S. Fleming, "QCD radiative corrections to the leptonic decay rate of the $B_c$ meson," Phys. Rev. D **52** (1995) 181.

[115] J. P. Ma and Z. G. Si, "NRQCD factorization for twist-2 light-cone wave-functions of charmonia," arXiv:hep-ph/0608221.

[116] B. O. Lange and M. Neubert, "Renormalization-group evolution of the B-meson light-cone distribution amplitude," Phys. Rev. Lett. **91** (2003) 102001.

[117] V. M. Braun, D. Y. Ivanov and G. P. Korchemsky, "The B-meson distribution amplitude in QCD," Phys. Rev. D **69** (2004) 034014.

[118] A. G. Grozin and M. Neubert, 'Asymptotics of heavy-meson form factors," Phys. Rev. D **55** (1997) 272.

[119] S. J. Lee and M. Neubert, "Model-independent properties of the B-meson distribution amplitude," Phys. Rev. D **72** (2005) 094028.

[120] H. H. Asatryan, H. M. Asatrian, C. Greub and M. Walker, "Calculation of two loop virtual corrections to $b \to s\ell^+\ell^-$ in the standard model," Phys. Rev. D **65** (2002) 074004.

[121] A. Ghinculov, T. Hurth, G. Isidori and Y. P. Yao, "The rare decay $B \to X_s\ell^+\ell^-$ to NNLL precision for arbitrary dilepton invariant mass," Nucl. Phys. B **685** (2004) 351.

[122] M. Misiak *et al.*, "The first estimate of $B(\bar{B} -- > X_s\gamma)$ at $\mathcal{O}(\alpha_s^2)$," arXiv:hep-ph/0609232.

[123] D. Seidel, "Analytic two-loop virtual corrections to $b \to \ell^+\ell^-$," Phys. Rev. D **70** (2004) 094038.

[124] R. J. Gonsalves, "Dimensionally Regularized Two Loop On-Shell Quark Form-Factor," Phys. Rev. D **28** (1983) 1542.

[125] W. L. van Neerven, "Dimensional Regularization Of Mass And Infrared Singularities In Two Loop On-Shell Vertex Functions," Nucl. Phys. B **268** (1986) 453.

[126] G. Kramer and B. Lampe, "Integrals for two loop calculations in massless QCD," J. Math. Phys. **28** (1987) 945.

[127] T. Gehrmann, T. Huber and D. Maitre, "Two-loop quark and gluon form factors in dimensional regularisation," Phys. Lett. B **622** (2005) 295.

[128] M. Argeri, P. Mastrolia and E. Remiddi, "The analytic value of the sunrise self-mass with two equal masses and the external invariant equal to the third squared mass," Nucl. Phys. B **631** (2002) 388.

# Acknowledgements

In the end I would like to thank everybody who helped this thesis coming into being.

First of all I would like to thank my advisor, Prof. Gerhard Buchalla, for being an outstanding teacher. I am grateful to his continuous help and guidance throughout my time in Munich. It was always a great pleasure to work with him. I certainly remember the many fruitful discussions we had and I highly value his permanent encouragement during my work.

Next I would like to thank Dr. Thorsten Feldmann for his exclusive support. The collaboration with him has been very pleasant and certainly very fruitful. I could in particular learn a lot about Soft-Collinear Effective Theory from him. I also would like to thank Thorsten for his assistance in arranging my stay at CERN.

I am grateful to Volker Pilipp and Matthäus Bartsch for numerous stimulating discussions. I also thank Gerhard, Thorsten, Volker and Matthäus for proofreading parts of the manuscript. I am indebted to Tobias Huber for discussions related to the calculation of loop-integrals.

Finally, I would like to thank my parents for their unconditional support. Last, but definitely not least, I thank Conchita for her patience and permanent encouragement.